Intraspecific Variation in the Armoured Dinosaurs (Dinosauria: Ankylosauria)

by

Michael Edward Burns

A thesis submitted in partial fulfillment of the requirements for the degree of

Doctor of Philosophy

in

Systematics and Evolution

Department of Biological Sciences
University of Alberta

Abstract

Here I assess sources of intraspecific morphological variability in the armoured dinosaurs (Dinosauria: Ornithischia: Ankylosauria), approached from the viewpoints of ontogenetic allometry, fossil bone histology, and individual variation. Juvenile specimens of *Pinacosaurus grangeri* Gilmore, 1933, demonstrate strong positive allometry in features of their forelimbs, a trend lacking in the hindlimb. This is likely related to an increase in weight-bearing of the anterior body with ontogeny. Although postcrania can provide useful taxonomic characters, the effects of ontogenetic allometry should be considered. Bone histology indicates that juvenile ankylosaurs experienced rapid growth, followed by a decline in growth rates. It is likely that this decline was more prolonged than in other dinosaurian taxa, possibly related to the mineralization of osteoderms later in ontogeny. Although it is not possible to construct a growth-dynamic curve for ankylosaurs given the current data, the rough ontogenetic stage of an individual may be assessed histologically. A specimen-based parsimony analysis is supported as a repeatable method to make falsifiable taxonomic hypotheses, including explicit *a priori* character weighting, and delimit species. It provides for a revision of Upper Cretaceous Nodosauridae, a group for which the degree of intraspecific morphological diversity has been difficult to distinguish from taxonomic variation. In addition to *Edmontonia* spp. and *Panoplosaurus mirus*, *Denversaurus schlessmani* Bakker, 1988, is likely valid. It also allows for most currently-known specimens to be referred to species. Endocranial anatomy is conservative and, although not useful at the species-level, may inform deeper evolutionary relationships within the Ankylosauria.

PREFACE

Chapter 2 of this thesis has been published as part of a collaboration among myself, T. Tumanova, and P.J. Currie. Nevertheless, I was lead on the project. T. Tumanova provided assistance at the PIN and provided background on the collection of specimens. P.J. Currie provided measurement data on ankylosaur specimens from a variety of collections and assisted in editing the manuscript.

This has been published as Burns, M.E., T.A. Tumanova, and P.J. Currie. 2014. Postcrania of juvenile *Pinacosaurus grangeri* (Ornithischia: Ankylosauria) from the Upper Cretaceous Alagteeg Formation, Alag Teeg, Mongolia: implications for ontogenetic allometry in ankylosaurs. Journal of Paleontology 89: 168–182. It was reviewed by K. Carpenter and J. Kirkland.

This thesis is dedicated to my supervisors, past and present.

ACKNOWLEDGEMENTS

I thank my supervisor, P. Currie, for allowing me to conduct this research as well as a great deal of guidance and support. Thanks also to committee members G. Erickson and R. Holmes for advice and assistance as well as examiners D. Brinkman and H. Proctor.

Thanks are also due to the many people that have provided access and assistance at their respective institutions. They include D. Evans (ROM), J. Mallon (CMN), C. Mehling (AMNH), L. Ivy (DMNH), B. Iwama (ROM), P. Larson (BHI), J. Sertich (DMNH), K Seymour (ROM), B. Strilisky (TMP), C. and K. Tsogtbaatar (MPC), M. Watabe (HMNS). I also benefitted greatly from discussions with V. Arbour, K. Carpenter, T. Ford, D. Fowler, S. Hayashi, T. Scheyer, R. Sullivan, D. Tanke, L. Witmer and countless others.

E. Koppelhus and all members of the University of Alberta Laboratory for Vertebrate Palaeontology provided advice and support. Special thanks, too, to T. Tumanova, who coauthored the manuscript that forms the basis of Chapter 2. Reviews by K. Carpenter and J. Kirkland greatly improved the quality of that manuscript. I thank E.N. Kurochkin and V.P. Tverdochlebov who began research at Alag Teeg and for collecting the material described in Chapter 2. J. Hudson discovered, excavated, and prepared BHI 6225. J.R. Krogstad assisted with the excavation and C. Smith assisted with preparation of BHI 6226.

Funding was provided by the Alberta Historical Resources Foundation, Alberta Lottery Fund, Dinosaur Research Institute, Jurassic Foundation, and University of Alberta Department of Biological Sciences,.

TABLE OF CONTENTS

LIST OF TABLES

Chapter 2

Chapter 3

Chapter 4

LIST OF FIGURES

Chapter 1

Chapter 2

Chapter 3

Chapter 4

Chapter 5

Institutional Abbreviations

AMNH – American Museum of Natural History, New York, New York, USA

BHI – Black Hills Geological Institute, Hill City, South Dakota, USA

CEUM – College of Eastern Utah Prehistoric Museum, Price, Utah, USA

CMN – Canadian Museum of Nature, Ottawa, Ontario, Canada

DMNH – Denver Museum of Nature and Science, Denver, Colorado, USA

DPMWA – Dorothy Page Museum, Wasilla, Alaska, USA

HMNS – Center for Paleobiological Research, Hayashibara Biochemical Laboratories, Inc., Okayama, Japan

INBR – Victor Valley Museum, Apple Valley, California, USA

IPB – Institut für Paläontologie, Rheinische Wilhelms Universität, Bonn, Germany

IVPP – Institute for Vertebrate Paleontology and Paleoanthropology, Beijing, China

MPC – Paleontological Center of the Mongolian Academy of Sciences, Ulaan Baatar, Mongolia

NMMNH – New Mexico Museum of Natural History and Science, Albuquerque, New Mexico, USA

PIN – Palaeontological Institute, Russian Academy of Sciences, Moscow, Russia

ROM – Royal Ontario Museum, Toronto, Ontario, Canada

SDNMH – San Diego Natural History Museum, San Diego, California, USA

SPM – State Museum of Pennsylvania, Harrisburg, Pennsylvania, USA

SMU – Shuler Museum of Paleontology, Southern Methodist University, Dallas, Texas, USA

TMP – Royal Tyrrell Museum of Palaeontology, Drumheller, Alberta, Canada

UALVP – University of Alberta Laboratory for Vertebrate Palaeontology, Edmonton, Alberta, Canada

USNM – National Museum of Natural History (Smithsonian), Washington DC, USA

ZPAL – Zoological Institute of Paleobiology, Polish Academy of Sciences, Warsaw, Poland

Other Abbreviations

α – allometric coefficient

a – astragalus

aa – anterior anastomosis of anterior nasal artery branches

ac – acetabulum

acr – acromion process

adp – anterodorsal process

ala – impression of anterior loop of the airway

anc – anterior corner of distal edge of band

ang – angular

asc – anterior semicircular canal

bc – fused bones of braincase

boc – basioccipital

br – bony ridge

buco – buccal osteoderm

c1, c2… – first cervical, second cervical, etc.

ca – coracoid articulation

cc – crus communis

cer – cerebral region

CGM –cyclical growth mark

ch – internal choanae

cha – chevron (haemal spine) articulation

CI – consistency index

cla – posterior loop of the airway

CN I–XI – cranial nerves (endocast) or foramina for cranial nerves (braincase)

cof – coracoid foramen

cor – coronoid process

db – smooth distal edge of band

dp – deltopectoral crest

dpf – descending process of the frontal

DPF – Dinosaur Park Formation

DPP – Dinosaur Provincial Park

dps – diapophysis

dr – dorsal rib

EFS – external fundamental system

en – external nare

ep – epiphysis cerebri

epf – pterygoid-ectopterygoid foramen

epp – ectopterygoid pad

exo – exoccipitals

FLB – fibrolamellar bone

fm – foramen magnum

gfs – glenoid fossa

grt – greater trochanter

hb – hindbrain

HCF – Horseshoe Canyon Formation

hf – femoral head

hh – humeral head

hy – hyoid

icn – anterior intercondylar notch

iocr – interosseous crest

isped – ischial peduncle

it – internal (medial) tuberosity

itf – infratemporal foramen

jf – jugular foramen

lac – lacrimal

LAG –line of arrested growth

lc – lateral condyle

lepc – lateral epicondyle

lii – labyrinth of the inner ear

lom – lateral osteodermal mass covering narial region

lsc – lateral semicircular canal

lsp – laterosphenoid

mb – medial brace

mc – medial condyle

md – mandible

mepc – medial epicondyle

most – mandibular osteoderm

MPT – most parsimonious tree

ms – medial suture

mx – maxilla

n – scapular neck

n/pmx – nasal-premaxillary suture

na – groove for the nasal artery

nas – neural arch sutural surface

nc – neural canal

ncs – neurocentral suture

np – notochordal prominence

o – orbit

oc – otic capsule

occ – occipital condyle

ocv – orbitocerebral vein

olf – olfactory bulb (or impression thereof in the braincase)

op – olecranon process

osq – osteoderm covering squamosal

ost – osteoderm

pac – postacetabular crest

paf – postacetabular fossa

PCA – principal components analysis

pd – predentary

pf – popliteal fossa

pla – impression of posterior loop of the airway

plc – posterolateral olfactory chamber

pmx – premaxilla

poap – postacetabuar process

poc – posterior corner of distal edge of band

pop – paroccipital process

pow – postocular wall

poz – postzygapophysis

prap – preacetabular process

PRC – People's Republic of China

prf – prefrontal

prz – prezygapophysis

psc – posterior semicircular canal

pt – pterygoid

pup – pubic peduncle

q – quadrate

qc – quadrate condyle

r – radius

rg – radial groove

rh – radial head

RI – retention index

rla – anterior loop of the airway

rp – rugose osteoderm projection

s1, s2… – first sacral, second sacral, etc.

sa – stapedial artery

SD – standard deviation of the mean

so – supraorbital ossification

soc – supraoccipital

sp – neural spine

stp – styloid process

tbp – tibial plateau

TL – tree length

tp – transverse process

u – ulna

unr – ulnar notch of the radius

v – vomer

vc – vascular canal foramina

ve – vestibule

vmg – ventral medial groove

vmr – ventral median ridge

CHAPTER 1

1.1 INTRODUCTION

The Ankylosauria Osborn, 1923, are a clade of herbivorous dinosaurs of the order Ornithischia and are generally divided into two families: the Ankylosauridae and the Nodosauridae (Coombs, 1971; 1978) (Fig. 1.1). The ankylosaurs are included within the Thyreophora, which also includes the Stegosauria. The sister clades Ankylosauria and Stegosauria are most readily distinguished from one another by having different types of armour, both divergent from the relatively uniformly shaped osteoderms of basal thyreophorans (Fig. 1.2). Stegosaurs show a reduction in the number of osteoderms covering the dorsum and their specialization into characteristic plates and spikes. Ankylosaurs, on the other hand, increased the number of osteoderms to the point of having an almost continuous sheet of larger osteoderms, small ossicles, and sections of osteoderms fused into half rings and/or a solid shield over the pelvis (Arbour et al., 2013; Burns and Currie, 2014) (Fig. 1.3).

Ankylosaurs first appear in the Early or Middle Jurassic Period (likely originating in Europe) and persisted until the Cretaceous-Paleogene extinction event. They have been found on every continent, including Antarctica, except Africa (Vickaryous et al., 2004). They were bulky herbivorous quadrupeds, with short, robust limbs, especially the forelimbs.

Built low to the ground relative to most other dinosaurs, they were most likely restricted to feeding on vegetation at or below 1 m off the ground (Mallon et al., 2013).

The teeth of ankylosaurs are relatively small and primitive (Fig. 1.4). The crowns are laterally compressed and phylliform, with one main apical cusp and several secondary cusps along the edge (Coombs, 1990). The tongue was likely large and powerful given the development of the hyoid (Carpenter, 2012). The presence of cheeks, at least in some taxa, is known thanks to the presence of a buccal osteoderm in this region in two nodosaurid specimens (Lambe, 1919; Chapter 4). This would indicate a reliance on oral processing, and other evidence indicates that they did not rely heavily on gastroliths for food processing (Molnar and Clifford, 2000). At least in one ankylosaurine, chewing was more complex than a simple up and down motion; rather the lower jaw protruded when the mouth was open and, after the mouth was closed, retracted (Rybczynski and Vickaryous, 2001; Ősi et al., 2014).

Little direct evidence exists for the diet of ankylosaurs. A small-bodied, primitive ankylosaur from Australia, *Minmi paravertebra*, preserves gut contents in the form of a cololite, a piece of organic matter preserved within the gut of a fossil organism similar, but not identical, to a coprolite, which has been expelled. The cololite indicates that, at least in this case, the animal ate soft vegetation (foliage, small stems and fruiting bodies). The broad, flaring pelvis of ankylosaurids and nodosaurids is highly derived with nearly horizontal ilia that, in some cases, make it wider than long (Carpenter et al., 2013), and several dorsal and caudal vertebrae and associated ribs often fused to the pelves to create rigid synsacra. This has been suggested to accommodate a relatively large or long hindgut, which would indicate that ankylosaurs may have been hindgut fermenters (DiCrioce et al., 2005).

The mineralization of ankylosaur osteoderms likely happened late in ontogeny as evidenced by juvenile specimens that lack osteoderms (Burns et al., 2011). There is a tendency in ankylosaur evolution for the osteoderms to fuse in certain regions of the body and diverge in shape from the primitive condition. Osteoderm ossification began in juveniles with the cervical and pectoral half rings (Fig. 1.5) and proceeded posteriorly in older individuals (Burns et al., 2011). Over the pelvis, osteoderms may fuse into pelvic shields (Fig. 1.6) depending on the taxon (Arbour et al., 2011). Although a mechanical protective function for ankylosaur osteoderms may seem favorable, it is likely that they had multiple functions. Even within a single individual, osteoderms of different shape and body placement were modified to serve specific roles (Burns and Currie, 2014). The osteoderms were covered by a thin scale of epidermal keratin (Fig. 1.7) as in modern crocodilians (Burns et al., 2013; Burns and Currie, 2014).

Over the approximate 180 years since the description of the first ankylosaur (*Hylaeosaurus armatus* Mantel, 1833), many generic and specific names have been proposed and rearranged in an environment of ever-changing higher taxa (Appendix 1). Some of these supra-generic categories have been proposed without justification and/or supporting evidence from the fossil record, further confounding the taxonomy. The split into Ankylosauridae and Nodosauridae of Coombs (1971, 1978) has held up to the discovery of new material and several phylogenetic analyses. The recently resurrected Struthiosaurinae is the only other formally-named clade within Ankylosauria that is currently valid (Kirkland et al., 2013).

1.1.1 Ontogenetic Allometry in Ankylosaur Assemblages

Dinosaurs changed considerably in terms of body size and proportions as they grew. These ontogenetic changes produced many of the "bizarre structures" (Padian and Horner, 2011) and vast morphological differences that form the basis for much of dinosaurian taxonomy. On the other hand, these degrees of ontogenetic allometry also mean that ontogenetic stages of one taxon may be as or more morphologically divergent from one another as different taxa. The use of taxonomic characters based on morphological proportions may further confound this problem. Whereas binary present/absent characters are often the least ambiguous, they may not always be applicable, especially at finer taxonomic levels. In addition, proportional characters are often used in a qualitative way (e.g., "prominent," "reduced," etc.) that limits their utility and repeatability.

Burns and Sullivan (2011) named *Ahshislepelta minor*, in part, on scapular proportions, as well as osteodermal characters. The osteoderms indicate that the animal was an ankylosaurid. On the other hand, the gracile postcrania are more similar to those of nodosaurids or juvenile ankylosaurids. By examining limb bones across taxa, the limb bone proportions for *Ahshislepelta minor* were expected given their lengths, and the development of the osteoderms and skeletal fusion indicated that the specimen was not a juvenile. Furthermore, quantifying the acromion overhang makes the hypothesis that it is a taxonomically-informative character falsifiable more easily in the face of new anatomical information.

1.1.2 Paleohistology and ontogeny

Ontogeny in fossil vertebrates may be assessed through bone microstructure, or paleohistology. The microstructure of vertebrate bone records many pieces of information about the life history of the organism including an ontogenetic signal, phylogenetically inherited traits, environmental conditions during the life (and post-mortem taphonomy) of the organism, the biomechanical history of the bone, lifestyle adaptations, etc. (Chinasmy-Turan, 2005). In order to address the effects of ontogeny on variation in ankylosaurs, this study (Chapter 3) is primarily concerned with the ontogenetic signal provided by fossil bone microstructure. Bone ontogeny, and by proxy the rough ontogeny of the whole individual, may be inferred from the microstructure of bone via extent of secondary remodeling, the density and/or orientation of vascularity, examining CGMs (=cyclical growth marks), or a combination thereof.

A generally followed rule (*Amprino's Rule*; Amprino, 1947) is that the degree of organization of bone tissue is positively correlated with the time needed to produce it (i.e., more organized tissues require longer periods to form). Primary tissues that are deposited quickly tend to have a woven-fibered matrix characterized by disorganized collagen, whereas more organized tissues incorporate collagen fibers that tend to be arranged in parallel. Primary bone may be deposited around existing vasculature, creating simple vascular canals in the matrix. If spaces around these vessels/nerves are infilled by concentric rings of lamellar bone, primary osteons develop. A tissue type commonly seen in dinosaur bone is termed a fibrolamellar complex (or FLB), characterized by a combination of woven-fibered matrix and intervening primary osteons surrounded by lamellar bone. In addition, during normal growth, bone is reabsorbed and redeposited as secondary tissue. Resorption cavities can be identified by having scalloped edges, created

by the activity of osteoclasts. Secondary osteons may form within these spaces and show cement lines around their margins, distinguishing them from primary osteons (Huttenlocker et al., 2013).

The density of vascularity in a histological section is generally positively correlated with the rate of bone deposition such that well-vascularized tissue is considered faster growing than more poorly-vascularized tissue (Amprino, 1947). In addition, the arrangement of vascular canals within the tissue is informative of relative growth rate (Fig. 1.8), Despite taxonomic changes in absolute growth rates for these different vascular orientations, the relative spectrum of higher growth rates associated with radial or laminar vasculature to lower rates associated with longitudinal vasculature is consistent (Castanet et al., 1996; Padian, 2013).

Finally, cyclical growth marks (CGMs) indicate fluctuations or even cessations of the deposition of bone. Annuli and LAGs (=lines of arrested growth) are thin hypermineralized bands that can be traced around the entire circumference of a bone with annuli, simply showing a relatively greater thickness than LAGs. They are separated by regions of bone deposited at a relatively constant rate. These marks are strongly correlated with annual cycles in extant vertebrates (Peabody, 1961; Hart, 1982; Hutton, 1986; Zug et al., 1986; de Buffrenil and Castanet, 2000; Snover & Hohn, 2004; Klein et al., 2009 Marangoni et al., 2009; Huttenlocker et al., 2013).

1.1.3 Intraspecific variation in Upper Cretaceous nodosaurs

A clade including the Upper Cretaceous nodosaurids *Edmontonia, Panoplosaurus*, and included junior synonyms is generally well-supported in

phylogenetic analyses. The alpha taxonomy for the group, however, has undergone considerable revision, a history discussed in detail in Chapter 4. The collection of new material since the last most recent taxonomic revision blurs the lines, morphologically, among species currently considered valid.

A similar problem existed for contemporaneous ankylosaurids and has recently been investigated in a similar manner. All Campanian North American ankylosaurid specimens were assigned to *Euoplocephalus tutus* by Coombs (1971, 1978), giving the species an unusually long stratigraphic range relative to other dinosaurs (Fig. 1.9). This scheme held for almost 40 years until *Dyoplosaurus acutosquameus* was revisited and considered distinct from *Euoplocephalus tutus* by Arbour et al. (2009). Subsequent revisions (Arbour and Currie, 2013; Penkalski, 2013; Penkalski and Blows, 2013) have hypothesized that ankylosaurid diversity was more similar to that of other dinosaurian groups (Fig. 1.10).

1.1.4 Objectives

In this thesis, the ontogeny, allometry, and intraspecific variation of armoured dinosaurs are examined. This includes photographing, thin sectioning, and measuring elements from ankylosaur specimens, concentrating on taxa with reasonable sample sizes and those represented by multi-individual assemblages. This approach includes, using several disparate ankylosaur taxa (Fig. 1.11), includes three components:

1. The first portion of the thesis will involve a description of material from Alag Teeg, Mongolia, consisting of juvenile to subadult specimens of the ankylosaurine *Pinacosaurus grangeri*. The sample size will allow for testing for allometry in the

postcrania within the assemblage and any allometry to be extrapolated to other taxa. Specimens with unexpected proportions can be further examined for taxonomically useful characters.

2. The second portion of the project relies on data collection from the Alag Teeg as well as "Lorrie's Site," a bonebed of Early Cretaceous *Gastonia* sp. With the possible exception of the type locality of *Gastonia burgei*, these represent the largest ankylosaur assemblages found to date. The goal is an analysis of ontogeny based on bone microstructure.
3. The third portion of the project involves a revision of Upper Cretaceous nodosaurids, incorporating into analyses several undescribed specimens, including four skulls at the Royal Tyrrell Museum and two at the Black Hills Institute. In addition to facilitating investigation of the range of intraspecific variation, this new material also necessitates a revision of the group's existing alpha taxonomy. Because even complete specimens have proven problematic in past reviews, a specimen-by-specimen parsimony analysis is employed here to aid in determining which characters actually provide the most useful taxonomic information. In addition, the detailed soft and hard tissue anatomy of the endocranium will be described based on a partial specimen with fortuitous preservation. This information is not used here as part of the taxonomic revision for the clade, but may be useful in future studies examining the deeper evolutionary relationships within the Ankylosauria.

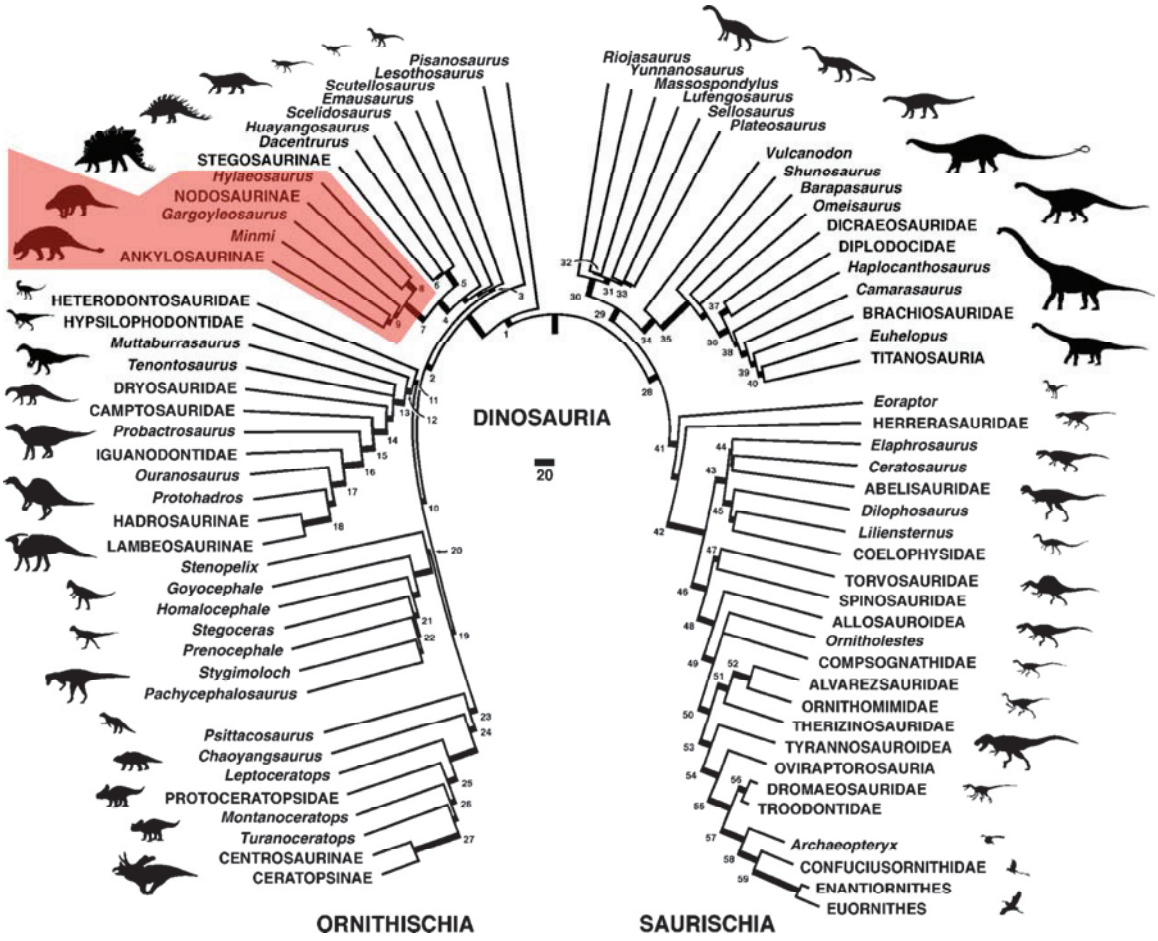

FIGURE 1.1. Phylogeny of the Dinosauria. The Thyreophora (node 3) appears on the left as a basal clade within Ornithischia. The Ankylosauria (node 7, highlighted), sister to the Stegosauria (node 5) is a derived clade within the Thyreophora, and includes the Ankylosauridae (node 9) and Nodosauridae (node 8). Modified from Sereno (1999; fig. 2).

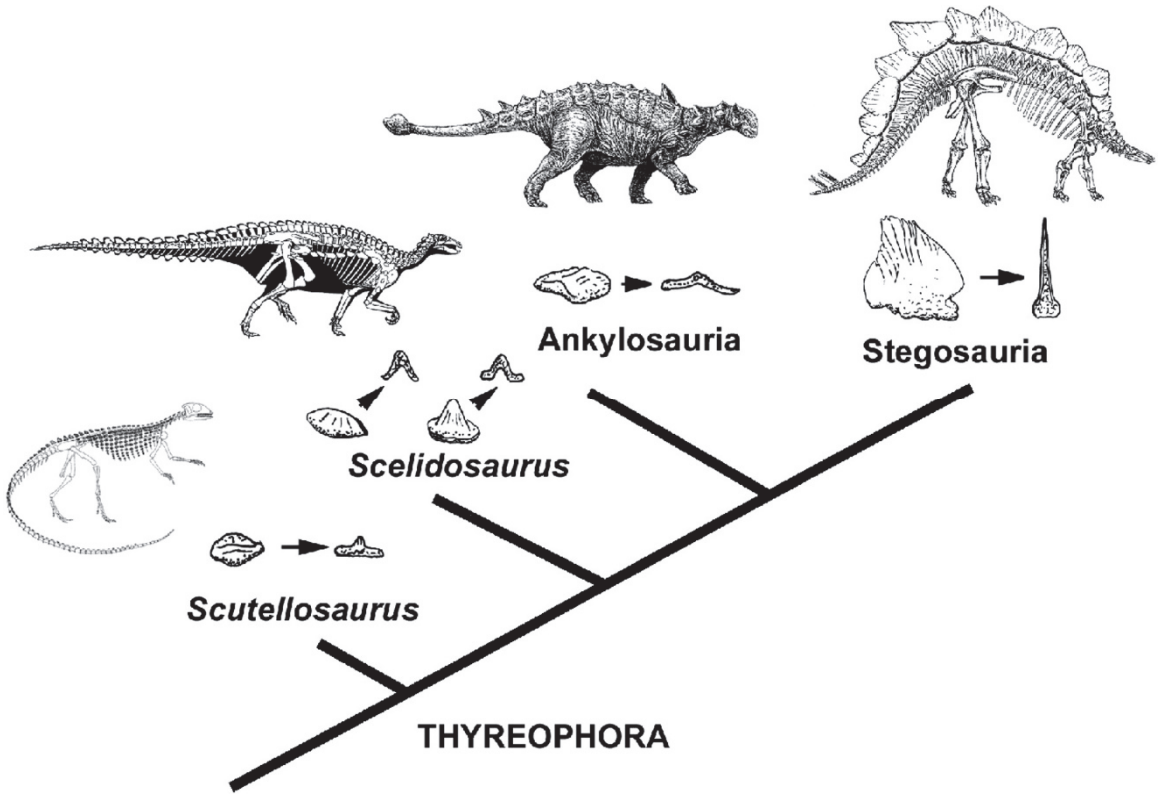

FIGURE 1.2. Phylogeny of the Thyreophora showing the evolution of osteoderms. Arrows point to cross sections through the osteoderms shown. Modified from Main et al. (2005; fig. 8). Reconstructions of *Scutellosaurus* from Colbert (1981), of *Scelidosaurus* from Greg Paul, of an ankylosaurine from Norman (1985), and of *Stegosaurus* from Ostrom and McIntosh (1966).

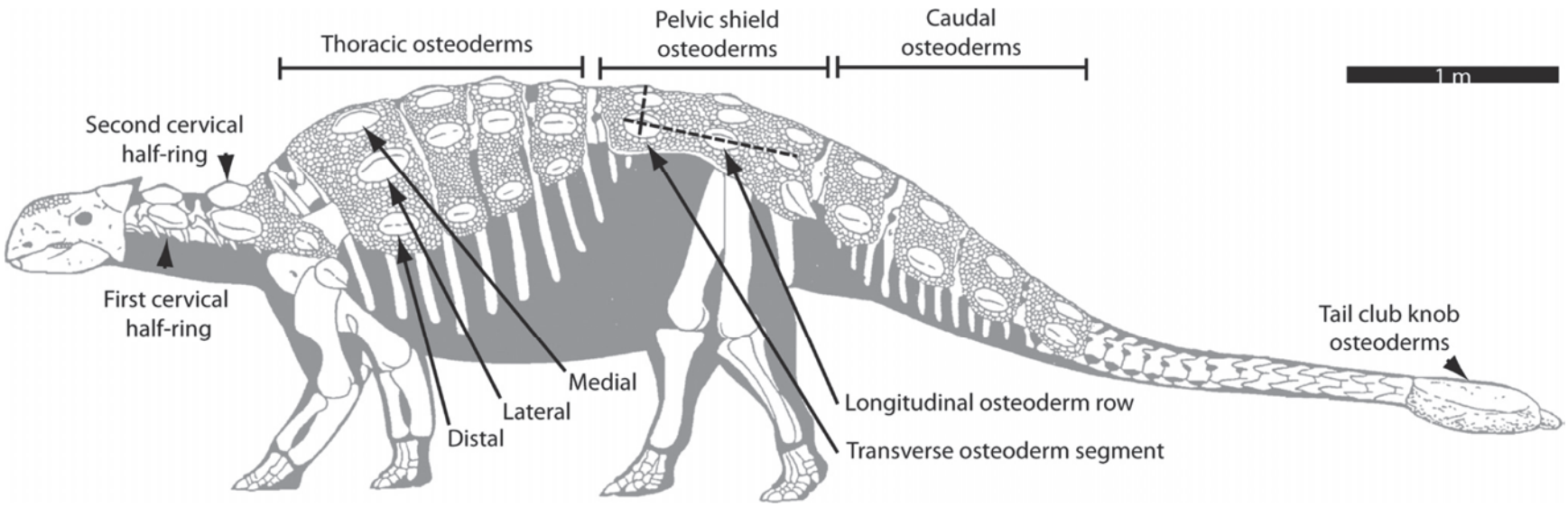

FIGURE 1.3. Ankylosaur osteoderms can be divided into distinct regions depending on placement along the dorsum of the body. Modified from Burns and Currie (2014; fig. 1) based on a reconstruction of *Ankylosaurus magniventris* by Ford (2013).

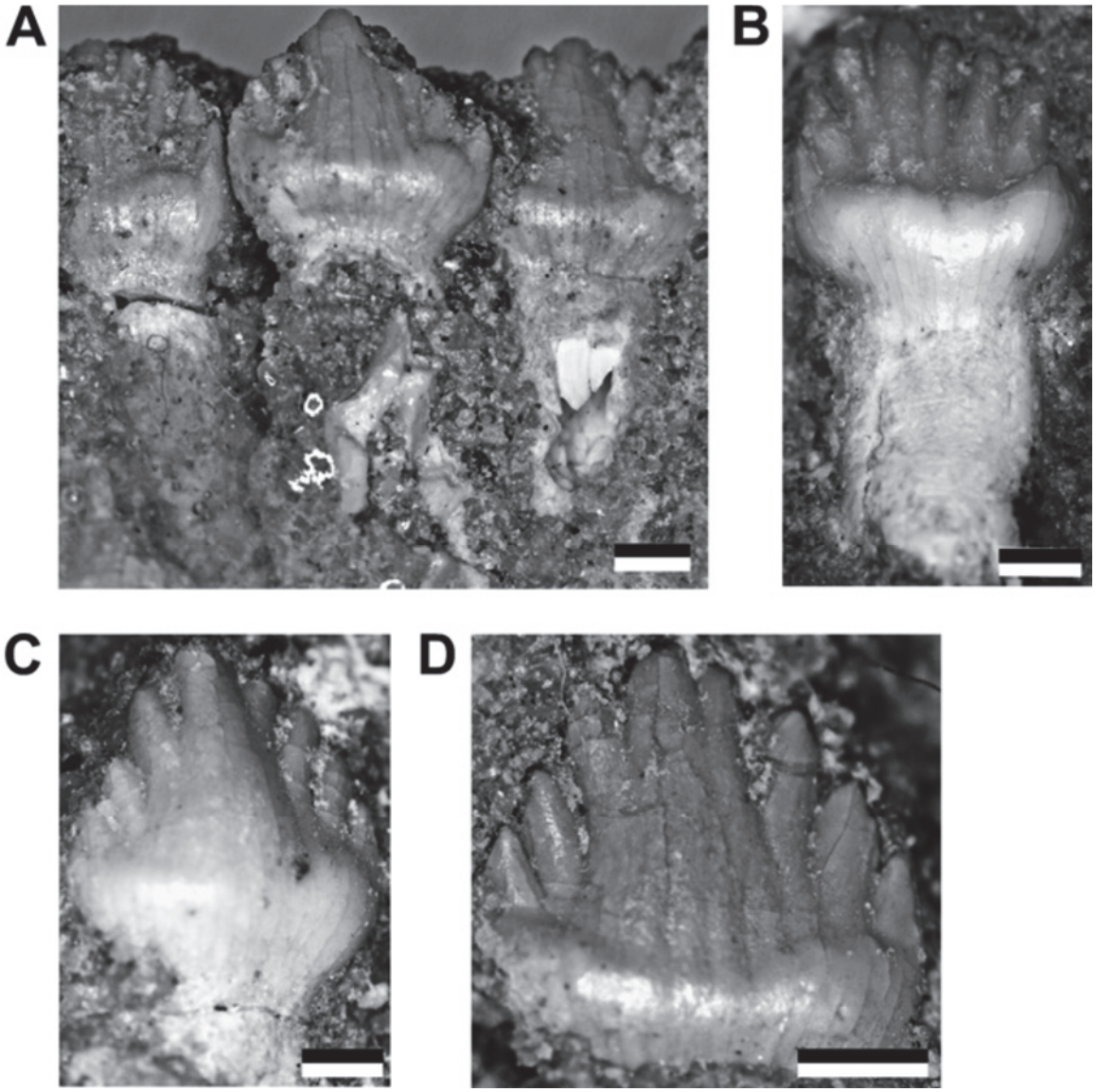

FIGURE 1.4. Mandibular teeth from a juvenile specimen of the ankylosaurine *Pinacosaurus grangeri*. Apical is up. Scale bars (lower right of each pane) equal 1 mm. Modified from Burns et al. (2011; fig. 7).

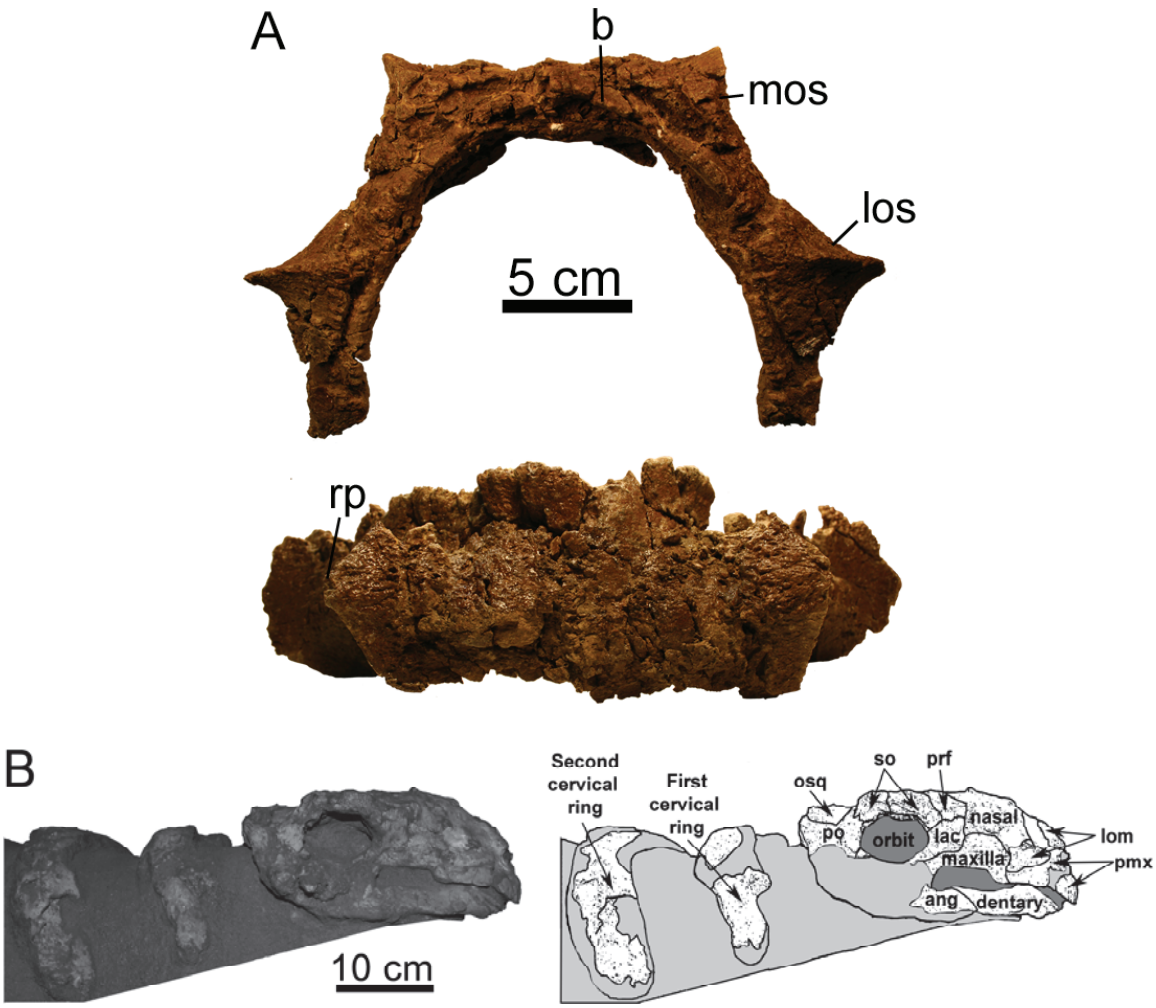

FIGURE 1.5. Cervical half rings in ankylosaurines. A, first cervical half ring from *Euoplocephalus tutus* (UALVP 31) in anterior and dorsal views (Modified from Arbour and Currie, 2013, fig. 13). B, juvenile *Pinacosaurus grangeri* skull and in situ cervical half-rings in right lateral view (anterior is to the right; natural orifices shaded dark) (Modified from Burns et al., 2011, fig. 6).

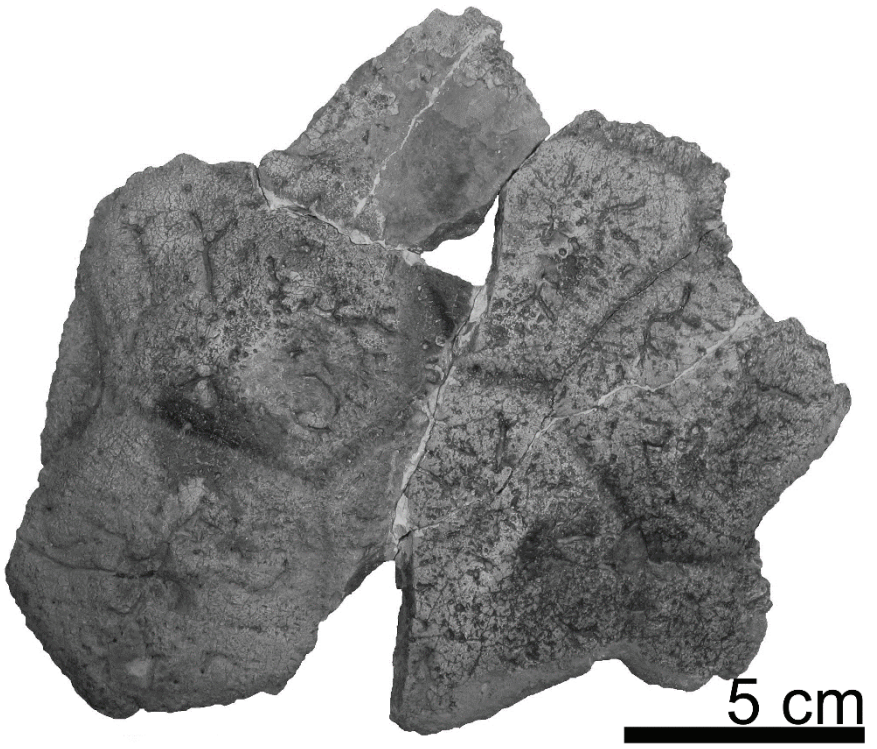

FIGURE 1.6. Fused mosaic of pelvic shield osteoderms (Category 3 pelvic shield sensu Arbour et al., 2011) from the holotype of the nodosaurid *Glyptodontopelta mimus* in dorsal view. Modified from Burns (2008, fig. 1).

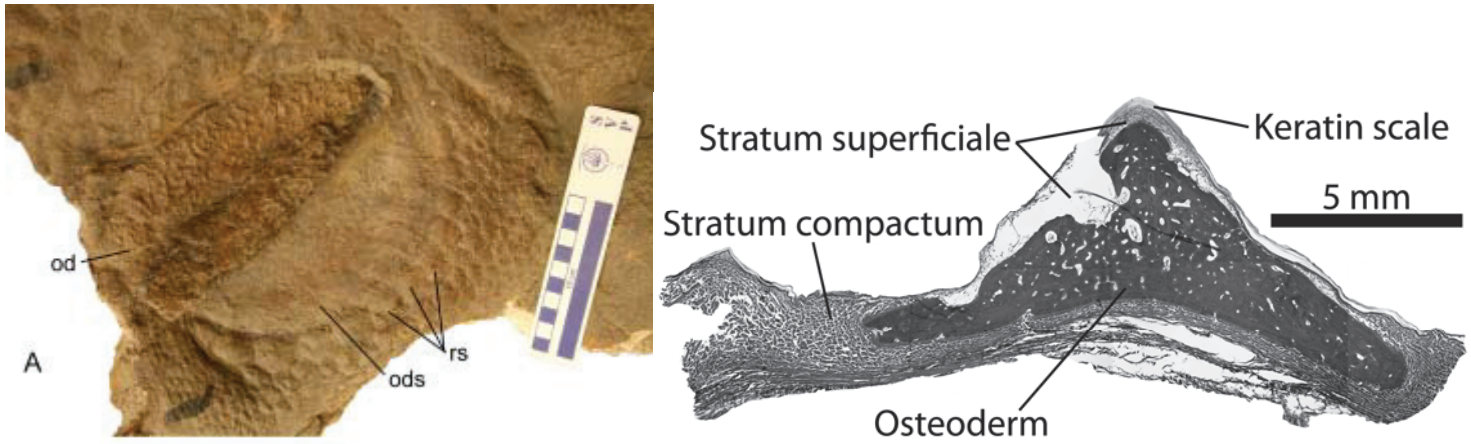

FIGURE 1.7. Thin keratin osteodermal coverings. A, in situ ankylosaur osteoderm exposed along its left side (od), but covered by impression of keratin scale on the right (ods) (Modified from Arbour et al., 2013, fig. 4). B, histological cross section of an osteoderm from a subadult *Alligator mississippiensis* showing the relationship of the thin keratin scale to the deeper osteoderm (Modified from Burns et al., 2013, fig. 2).

.

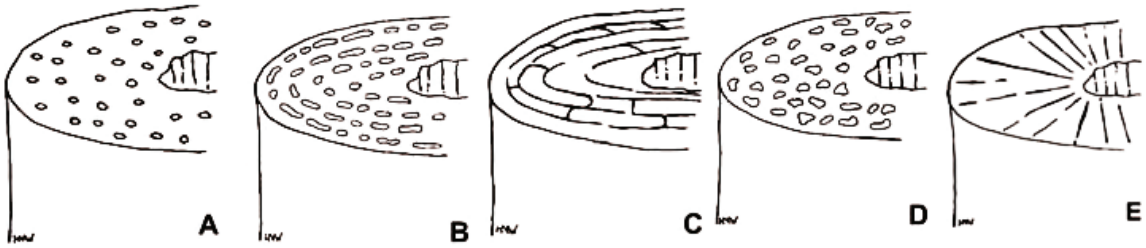

FIGURE 1.8. Classes of vascular orientations in cortical bone: A, longitudinal; B, laminar; C, plexiform; D, reticular; E, radial. Modified from Huttenlocker et al. (2013, fig. 2.4)

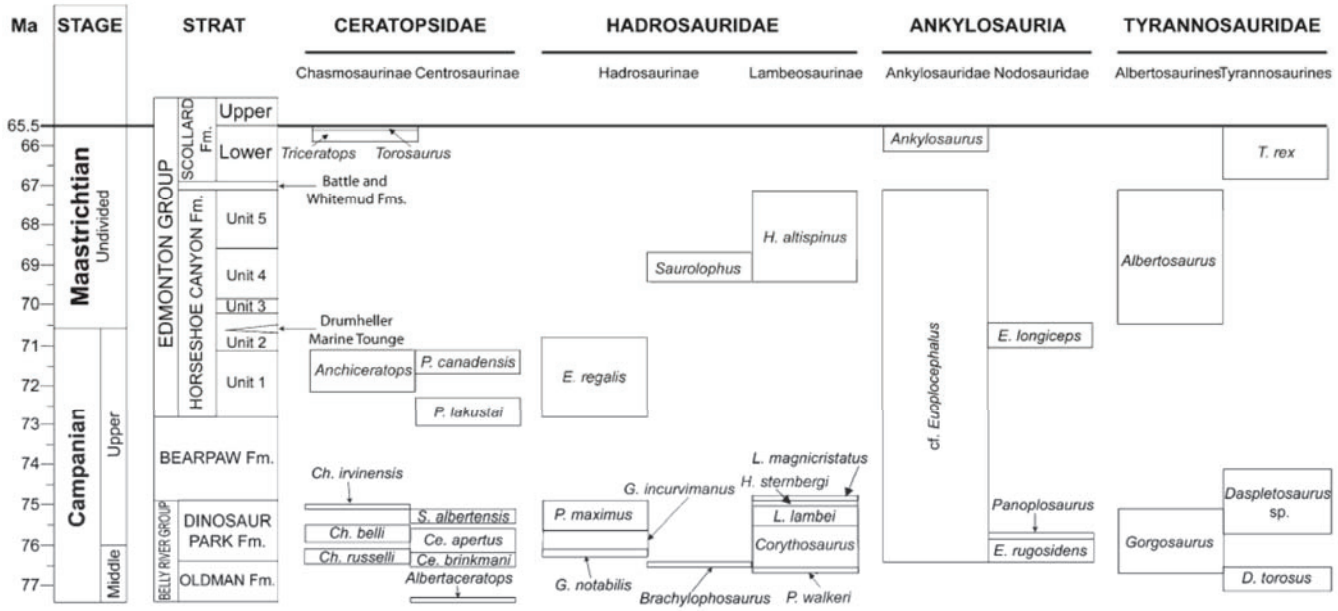

FIGURE 1.9. Lithostratigraphic section and outdated biostratigraphic distribution of selected dinosaur species in DPP demonstrating the relatively long range of *Euoplocephalus* (sensu lato) based on referred material prior to recent revisions by Arbour and Currie (2013), Penkalski (2013), and Penkalski and Blows (2013). Abbreviated taxa: ***Ce***., *Centrosaurus*; ***Ch***., *Chasmosaurus*; ***D***., *Daspletosaurus*; ***E. longiceps***, *Edmontonia longiceps;* ***E. regalis***, *Edmontosaurus regalis;* ***E. rugosidens***, *Edmontonia rugosidens;* ***G***., *Gryposaurus;* ***H***., *Hypacrosaurus;* ***L***., *Lambeosaurus;* ***P. canadensis***, *Pachyrhinosaurus candensis,* ***P. lakustai***, *Pachyrhinosaurus lakustai;* ***P. maximus***, *Prosaurolophus maximus;* ***P. walkeri***, *Parasaurolophus walkeri;* ***S***., *Styracosaurus;* ***T***., *Tyrannosaurus*. Modified from Arbour et al. (2009; fig. 7).

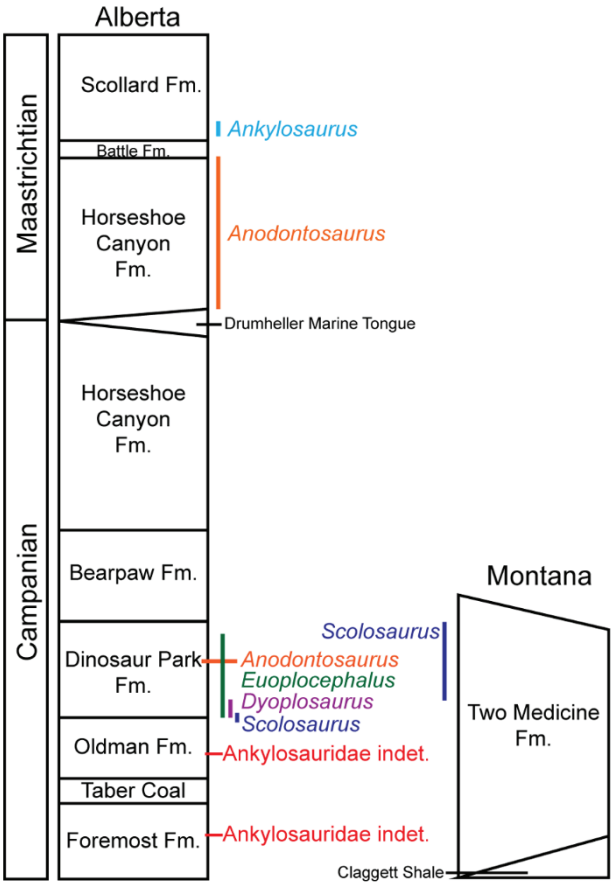

FIGURE 1.10. Revised current stratigraphic distribution of Upper Cretaceous ankylosaurine taxa in Alberta and Montana demonstrating the *Euoplocephalus* (sensu stricto) is confined to the Dinosaur Park Formation. Modified from Arbour and Currie (2013; fig. 15).

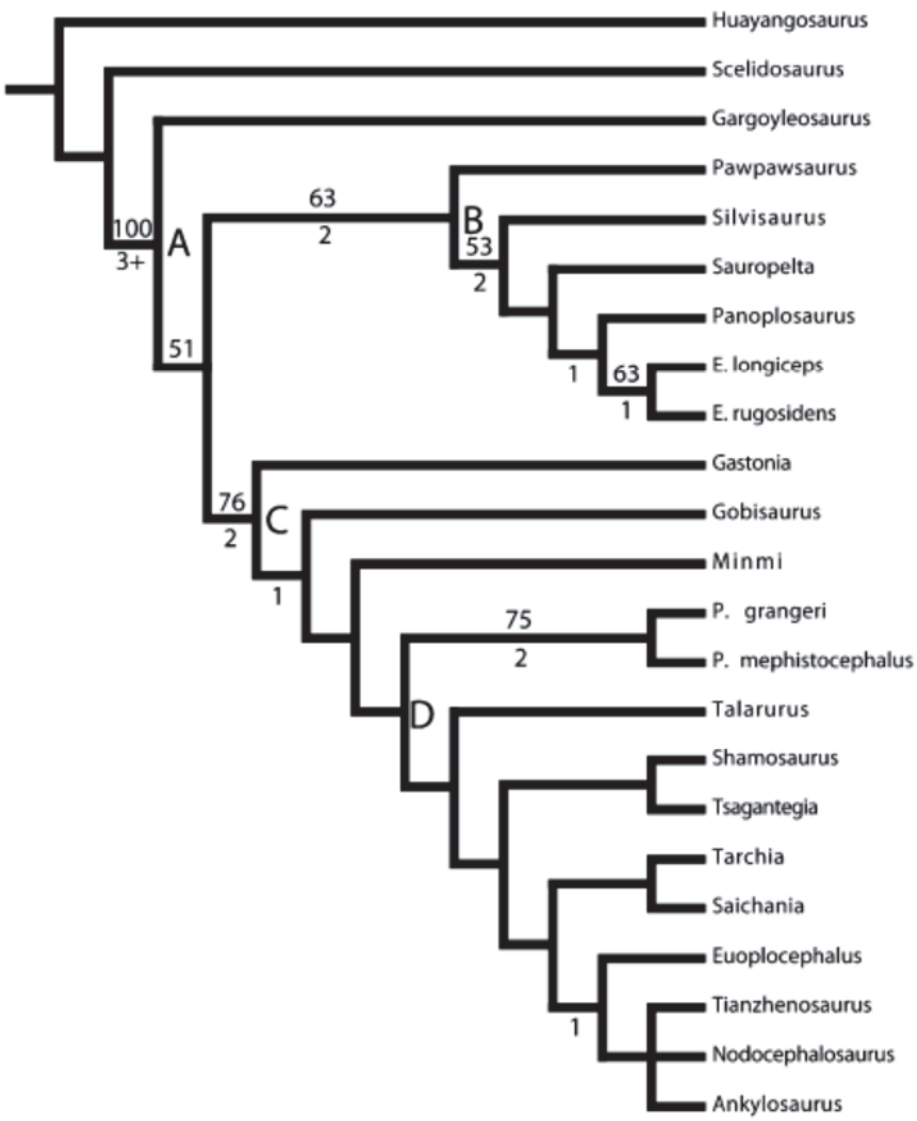

FIGURE 1.8. One phylogenetic hypothesis for the Ankylosauria noting taxa relevant to this study. Named clades are labelled as follows: A, Ankylosauria; B, Nodosauridae; C, Ankylosauridae; D, Ankylosaurinae. Numbers above branch are Bootstrap support values (only values >50% shown); numbers below branches are Bremer support values (symbol '+' represents "more than"). Modified from Burns et al. (2011; fig. 8).

CHAPTER 2

POSTCRANIA OF JUVENILE *PINACOSAURUS GRANGERI* (ORNITHISCHIA: ANKYLOSAURIA) FROM THE UPPER CRETACEOUS ALAGTEEG FORMATION, ALAG TEEG, MONGOLIA: IMPLICATIONS FOR ONTOGENETIC ALLOMETRY IN ANKYLOSAURS

2.1 INTRODUCTION

Originally described by Gilmore (1933) based on a specimen from the Djadokhta Formation at Bayan Zag, *Pinacosaurus* is one of the most commonly encountered dinosaur taxa in the Gobi Desert (Watabe and Suzuki, 2000; Currie et al., 2011). It has become the best known ankylosaur in terms of the number and preservational quality of specimens. In addition to Bayan Zag, the Djadokhta-age beds at Bayan Mandahu in Inner Mongolia have produced more than a dozen articulated partial skeletons of juveniles (Burns et al., 2011; Currie et al., 2011). From this site, the Chinese-Belgian expeditions (Godefroit et al., 1999) recovered a specimen identified as representative of a distinct species, *Pinacosaurus mephistocephalus* Godefroit, Pereda-Suberbiola, Li, and Dong, 1999, although *Pinacosaurus grangeri* Gilmore, 1933 can also be found at that site (Burns et al., 2011).

A third Djadokhta-age site is Alag Teeg, originally discovered in 1969 by the Soviet-Mongolian Paleontological Expedition and excavated in 1969 and 1970 (Tverdochlebov and Zybin, 1974). Several sources report that the expedition found several specimens of *P. grangeri* in 1969 (Tverdochlebov and Zybin, 1974; Maryańska, 1977; Fastovsky and Watabe, 2000; Currie et al., 2011), using a bulldozer to remove overburden and expose the fossil-bearing level.

Although most specimens collected were represented by isolated, disarticulated postcranial elements, some of the postcrania recovered were articulated. The Mongolian-Japanese Joint Paleontological Expedition also collected from Alag Teeg from 1993 to 1998, reporting about 30 individuals, although many were damaged or removed by fossil poachers (Watabe and Suzuki, 2000). Many specimens were preserved upright in life positions in the lower mudstone section at Alag Teeg, interpreted as the floodplain of a braided river system (Fastovsky, 2000). In 2001 and between 2003 and 2007, "Dinosaurs of the Gobi" (Nomadic Expeditions) found remains of over 40 *Pinacosaurus* specimens. These are housed in the Paleontological Center in Ulaan Baatar, and many were described by Currie et al. (2011), who suggested that the Alag Teeg specimens potentially might represent a different species than those from nearby sites like Bayan Zag because of their stratigraphically lower position.

Despite the attention given to the Alag Teeg locality by several institutions and expeditions for over forty years, a detailed description of the fossil material, which was restricted largely to manual and pedal elements, has only recently been published (Currie et al., 2011). The original material, first discovered by the Soviet-Mongolian Paleontological Expedition in 1969–1970, has escaped the attention of specialists and remained formally undescribed because of a general focus on cranial morphology over the years in ankylosaur research. This contribution remedies this by describing these specimens for the first time. The occurrence of many conspecifics in the same assemblage also allows for the assessment of postcranial variability within *Pinacosaurus*.

2.2 MATERIALS AND METHODS

Ankylosaur material at the PIN (Palaeontological Institute, Russian Academy of Sciences, Moscow, Russia) was collected from the Upper Cretaceous beds of the Alagteeg Formation at Alag Teeg, Mongolia (Fig. 2.1), by the Soviet-Mongolian Paleontological Expedition in 1969 and 1970. The collection comprises about 285 specimens, including ~160 vertebrae (disarticulated, except for three articulated series, including one of four cervicals, one of seven caudals, and another of 21 caudals), over 20 rib fragments, ~20 girdle elements, ~30 complete and fragmentary limb bones, ~30 isolated manual and pedal bones, and ~15 cervical half-ring fragments. This material, all of which is prepared, was examined via measurements, observations, and photographs. Only the most informative specimens (83 in total) were catalogued and form the basis of this chapter. Additional comparative material referable to *P. grangeri* from Alag Teeg, Bayan Zag, and Bayan Mandahu was examined at the HMNS (Center for Paleobiological Research, Hayashibara Biochemical Laboratories, Inc., Okayama, Japan), IVPP (Institute for Vertebrate Paleontology and Paleoanthropology, Beijing, China), MPC (Paleontological Center of the Mongolian Academy of Sciences, Ulaan Baatar, Mongolia) and ZPAL (Zoological Institute of Paleobiology, Polish Academy of Sciences, Warsaw, Poland).

Terminology for position and orientation of limb elements follows Currie et al. (2011). Statistical calculations and regression analyses were performed in Microsoft Excel. Uncorrected p-values were obtained in PAST (Hammer et al., 2001). Elements of the manus and pes have been described in detail from the collections of the MPC by Currie et al. (2011). MPC-D 100/1305 was recently referred by Carpenter et al. (2011) to *Saichania chulsanensis* Maryańska, 1977; however, its assignment to any ankylosaurid taxon is presently equivocal (Arbour and Currie, 2013) and the specimen number is used here without a taxonomic referral. References to *Saichania* here refer only to the holotype (MPC-D 100/151). In addition to examining the robustness of each element, specimens were compared with other ankylosaur taxa to see if

ontogenetic trends in growth can be separated from interspecific differences. Measurement data for all specimens used in regression and statistical analyses are available as Supplemental Data.

2.3 SYSTEMATIC PALEONTOLOGY

DINOSAURIA OWEN, 1842

ORNITHISCHIA SEELEY, 1887

THYREOPHORA NOPSCA, 1915

ANKYLOSAURIA OSBORN, 1923

ANKYLOSAURIDAE BROWN, 1908

ANKYLOSAURINAE BROWN, 1908

PINACOSAURUS GILMORE, 1933

Type species—*Pinacosaurus grangeri* Gilmore, 1933

Stratigraphic horizon—?Upper Santonian to Upper Campanian of Mongolia and PRC.

PINACOSAURUS GRANGERI GILMORE, 1933

=*Pinacosaurus ninghsiensis* Young, 1935:5, pls. 1–3 (original description).

=*Syrmosaurus viminocaudus* Maleev, 1952:131, figs. 1–3 (original description).

=*Syrmosaurus viminicaudus* Maleev: 1954:143, figs. 1–13, 16 (emended spelling).

Holotype—AMNH 6523, skull and mandible of an adult specimen, atlas, axis, and several associated osteoderms. Material is dorsoventrally crushed and has undergone expanding matrix distortion.

Type locality—Bayan Zag, Gobi Desert, Mongolia.

Stratigraphic horizon—Alagteeg and Djadokhta formations (Campanian, Upper Cretaceous).

New Referred Material—PIN 3144, basicranium, articulated, associated, and disarticulated postcranial elements, disarticulated cervical half ring segments.

2.4 CRANIAL DESCRIPTION

Basicranium—Although this description focuses on postcranial elements, the PIN collection includes one partial basicranium (Fig. 2.2) from Alag Teeg. The occipital condyle is 2.4 times wider than it is high, more similar to the condition in *Saichania* (MPC-D 100/151) than ZPAL MgD II/1, although this may be partially influenced by dorsoventral crushing. It incorporates the basioccipital and exoccipitals; the latter contribute to the dorsolateral corners of the occiput and form 75% of its dorsal width. The sutures separating the exoccipitals from the basioccipital are prominent as in ZPAL MgD II/1.

Conversely, the exoccipitals are excluded from the occipital condyle in *Euoplocephalus tutus* (Lambe, 1902; Vickaryous and Russell, 2003). There is no median basioccipital foramen on the ventral surface of the basioccipital between the basitubera and occiput. This foramen is absent in *Minotaurasaurus ramachandrani* Miles and Miles, 2009. It has not been reported for *Ankylosaurus magniventris* Brown, 1908 (Carpenter, 2004) or *Euoplocephalus tutus* (Vickaryous and Russell, 2003). It is present, however, in *Saichania* (Maryańska, 1977). The basisphenoid

bifurcates anteriorly into bilateral, anterolaterally directed basipterygoid processes. As preserved, the sutural contact between the basioccipital and basisphenoid is not visible.

2.5 AXIAL SKELETON DESCRIPTION

Cervical Vertebrae—Four articulated cervicals (PIN 3144/49/1–4; Fig. 2.3) were collected. Although the neural arches are attached to the centra, the neurocentral sutures are clearly visible. The amphiplatyan centra are consistently wider than long (by an average ratio of 1:0.88) as in *Ankylosaurus* (Coombs, 1986; Carpenter, 2004) and *Euoplocephalus* (juvenile and adult); in contrast, the centra in MPC-D 100/1305 become longer than wide posteriorly in the series (Carpenter et al., 2011). Ventrally, each has a median longitudinal ridge for attachment of the longitudinal ligament. The articular faces of any single centrum are not parallel in lateral view, but give the centrum a trapezoidal shape to accommodate the curved shape of the neck as in other ankylosaurs (Coombs, 1986; Carpenter et al., 2011). There are no horizontal bony laminae in the neural canals like those reported for *Saichania* (MPC-D 100/151) by Maryańska (1977). Each diapophysis is elliptical in cross section and projects laterally from the base of the prezygapophysis. The prezygapophyses are relatively as large as those figured for MPC-D 100/1305 (Carpenter et al., 2011, fig. 12). The neural spines are damaged in all four vertebrae, and there is no evidence of to suggest the cervical ribs were fused with any of the vertebrae.

Dorsal Vertebrae—The amphiplatyan anterior and posterior faces of each dorsal centrum (Fig. 2.4) are equal in width and height. The centra are constricted at midlength (to an average of 72% the widths of the anterior and posterior faces) into an hourglass shape when viewed ventrally. There are no horizontal grooves on the lateral surfaces of the centra as reported in MPC-D 100/1305 (Carpenter et al., 2011; Arbour and Currie, 2013). Such depressions are also

absent in *Euoplocephalus tutus* and *Talarurus plicatospineus* Maleev, 1952 (Arbour and Currie, 2013). Although dorsal neural arches are found at Alag Teeg, none are fused to the centra. Their sutures extend the entire length of the dorsal surface of a centrum. The prezygapophyses form a single median sagittal U-shaped structure (concave dorsally) similar to those of most ankylosaurs (Carpenter, 2004; Carpenter et al., 2011). The neural spines are vertically-oriented plates that are roughly rectangular in shape when viewed laterally. Like MPC-D 100/1305 (Carpenter et al., 2011), they do not show transversely-expanded distal ends as they do in *Ankylosaurus* (Carpenter, 2004). Each transverse process projects dorsolaterally, angles anteriorly, and is supported by two ventrally diverging struts that terminate on the parapophysis immediately dorsal to its articular surface. There is no evidence that dorsal ribs were fused to any of the neural spines. There is also nothing to suggest that ossified tendons were associated with the dorsals as in MPC-D 100/1305 (Carpenter et al., 2011).

Sacral Vertebrae—All sacral vertebrae (Fig. 2.5) are separate from each other, even in the largest Alag Teeg specimen (MPC-D 100/1333). Ventrally, each sacral centrum has a median longitudinal ridge but lacks a ventral groove, the latter of which is known in nodosaurs (e.g., *Edmontonia*, *Peloroplites*) and *Cedarpelta* (Carpenter et al., 2008). The neural canal excavates the dorsal surface of the centrum. The intervertebral articulations of the centra range from semi lunar to heart-shaped when viewed anteriorly or posteriorly. Lack of fusion of the synsacrum in these juvenile specimens makes it difficult to identify and differentiate dorsosacrals from dorsals, and sacrocaudals from free caudals.

Caudal Vertebrae—In ankylosaurines, the caudal series is divided into the free (= anterior) caudals and those (posterior) forming the handle of the tail club, although none from the latter series were identified in the PIN collection. The free centra (Fig. 2.6) in *P. grangeri* are amphiplatyan, and their heights, widths and lengths are roughly equidimensional. The neural

arches are not fused to the centra in any of the specimens collected from Alag Teeg. An anteroposteriorly elongate median groove occupies the ventral surface of each centrum. The chevrons (= haemal arches) are not fused to the centra, although their articular facets are visible on the posteroventral corners of the centra. Ossified tendons are not present on the free caudals.

Dorsal Ribs—Smaller dorsal ribs from Alag Teeg have distinct tubercula and capitulae, demonstrating that they were not fused to the vertebrae in young animals. Those ribs (PIN 3144/68 and 69) associated with a larger individual are medially broken at these articular surfaces, suggesting that they were fused to the vertebrae. Immediately distal to the articular surfaces, the ribs have T-shaped cross sections as in other derived ankylosaurs (Coombs, 1971). This cross-sectional shape changes distally along the rib until it is triangular and eventually elliptical.

2.6 APPENDICULAR SKELETON DESCRIPTION

Scapula—The scapula (Fig. 2.7.2) is medially concave to conform to the shape of the thorax. The constricted, neck-like region is poorly-developed as is characteristic for ankylosaurines, but in contrast with the distinct necks of derived nodosaurid scapulae. The acromion extends on average 40% the length of the scapula (although the range is from 30% to 50% with a standard deviation of 7.4% due to the ambiguities in determining the exact posteriormost extent of the acromion). In MPC-D 100/1305, the acromion extends one third the length of the scapula (Carpenter et al., 2011). It is formed by a lateral deflection of the dorsal border of the scapula but does not curve ventrally as in *Ahshislepelta minor* Burns and Sullivan, 2011.

Coracoid—None of the coracoids (Fig. 2.7.1) from Alag Teeg are coossified to scapulae. Posteroventrally, the coracoid contributes to half of the glenoid fossa. As is characteristic for most ankylosaurines (Carpenter et al., 2011), a ridge extends from the glenoid fossa to the anterodorsal process, giving the process a dorsolateral projection and imparting a sigmoidal curve to the anterior border of the coracoid. The glenoid foramen is situated anterior to the scapular contact dorsal to the glenoid fossa. The rounded anterior edges of the coracoids distinguishes them from those of MPC 100/1305, which have flat anterior edges (Arbour and Currie, 2013), although it is unknown whether this difference is taxonomic, ontogenetic, and/or individually variable.

Humerus—Proximally, each humerus (Fig. 2.8) is expanded mediolaterally to an average of 2.5 times the width of the shaft, forming a deltopectoral crest and medial process flanking the head. Distally, the humerus is expanded into the medial and lateral condyles to an average of 2.4 times the width of the shaft.

Godefroit et al. (1999) considered that the humeri were diagnostic for the two species of *Pinacosaurus* in that *P. mephistocephalus* had a better-developed deltopectoral crest that terminated distal to humeral mid-length. This is more similar to the condition in *Saichania chulsanensis* and *Shanxia tianzhenensis* Barrett, You, Upchurch, and Burton, 1998, according to Godefroit et al. (1999); however, the humeral shaft has a more rounded cross-section in *P. mephistocephalus*. Currie et al. (2011) noted that the deltopectoral crest in two humeri (MPC-D 100/1344 and MPC-D 100/1346) from Alag Teeg exhibited the condition reported for *P. mephistocephalus*. The character was considered non-diagnostic at the species level by Burns et al. (2011), who suggested it was possibly size-dependent.

Ulna—Proximally, the medial process of the ulna (Fig. 2.9), against which the radius articulates, is prominent as in other ankylosaurines (Maryańska, 1977; Carpenter et al., 2011).

The olecranon process is low and blunt as in MPC-D 100/1305 (Carpenter et al., 2011). The proximal articular surface comprises 66% of the total length of the ulna in *Saichania* and 50% in ZPAL MgD II/1, although the olecranon is more developed in PIN 614 than it is in ZPAL MgD II/1 (Maryańska, 1977). The shaft tapers distally to the radial (circumferential) articulation. This articulation conforms to the ulnar notch of the radius, and forms an anteroposteriorly-elongate oval in distal view.

Radius—The straight radius (Fig. 2.9) has an anteroposteriorly-elongate, oval (in proximal view) head with a cupped fovea for articulation with the humeral capitulum. The styloid process is underdeveloped as a blunt projection on the lateral side of the distal end of the radius. The distal articular surface is convex. The ulnar notch is a proximodistally-elongate groove on the medial surface of the distal end of the radial shaft.

Ilium—Godefroit et al. (1999) considered the ilium (Fig. 2.10) diagnostic at the species level in *Pinacosaurus*; it forms a horizontal shelf dorsal to the acetabulum in *P. mephistocephalus* but overhangs the acetabulum laterally in *P. grangeri*. Burns et al. (2011) tentatively retained the character because their revision focused on cranial characters. The Alag Teeg specimens match the morphology observed in ZPAL MgD II/1, although there is no published lateral figure of the ilium of *P. mephistocephalus* for comparison with that taxon. The alae of the ilia from the Alag Teeg specimens show no such ventral deflection lateral to the acetabulum. In fact, each of the two well-preserved specimens (PIN 3144/5 and 3144/9) has a dorsal deflection at the posterolateral corner of the ilium, leaving the acetabulum visible in lateral view. The same is observable on the ilium of PIN 614.

Ischium— Proximally, the ischium is expanded and forms the entire medial surface of the acetabulum, seen as a lateral concavity on the ischium. There is no evidence that the sacral

ribs were fused to the ischium as in *Ankylosaurus* (Carpenter, 2004). The distal end is anteroposteriorly expanded to 131% the anteroposterior diameter of the shaft.

Femur— The minimum circumference to length ratio (49%) in the Alag Teeg femora (Fig. 2.11) is similar to that reported for MPC-D 100/1305 (47%) by Carpenter et al. (2011). The articular surfaces and muscle attachment sites are not as rugose as they are in larger ankylosaur femora (e.g., MPC-D 100/1305; Carpenter et al., 2011). The greater trochanter is prominent along the lateral edge of the proximal end of the femur. It extends 23% the length of the femur as in other ankylosaurines (Carpenter et al., 2011). The shaft is anteroposteriorly compressed to a ratio of 1:0.45 (transverse/anteroposterior), although this is variable (SD=0.19). The fourth trochanter is visible on the posteromedial side of the shaft. The distal condyles are anteriorly separated by an intercondylar notch. The lateral condyle extends farther distally than the medial condyle, although the medial condyle is larger.

Tibiotarsus— Distally, the tibial shaft (Fig. 2.12) flares into lateral and medial condyles separated anteriorly by a sulcus. Astragali are preserved in articulation with the posteroventral, distal surfaces of two tibiae (PIN 3144/38 and 39). Their morphologies and positions are similar to those described for *P. grangeri* specimens from the MPC (Currie et al., 2011) and a juvenile North American ankylosaurine (Coombs, 1986). They articulate but are not fused to the tibiae, unlike in adult ankylosaurines (Coombs, 1979). No fibulae were recovered from Alag Teeg by the Soviet-Mongolian Expedition, but those in the collections of the MPC have been described by Currie et al. (2011).

2.7 DERMAL SKELETON DESCRIPTION

Cervical Half Rings—All cervical half rings from Alag Teeg are incomplete due to an apparent lack of complete mineralization at early ontogenetic stages. The preserved portions represent pieces of the transverse bands of the cervical half rings and have crenulated anterior and posterior edges. Distal portions of the bands (Fig. 2.13) have smooth edges that transition into rounded anterior corners. The posterior corner is angular, and separates a crenulated edge to the distal end of the band. Osteodermal projections extend from the external surface of the bands and have rugose, pitted textures contrasting with the smooth textures of the bands. The thickness of each band varies, being relatively thinner deep to the osteodermal projections, and thicker between them. This gives the band an undulating appearance in anterior or posterior views. The inter-osteodermal portions of the band are truncated by crenulated surfaces perpendicular to the band. Here, two portions of the band may have contacted one another in interdigitating sutures (as can be seen in other ankylosaurine cervical half rings) or interfaced with non-mineralized dermis. In two distal specimens (PIN 1344/74 and 75), the osteodermal projections have more rugose surface textures than other specimens, although this may be ontogenetically affected. These distal projections do not cover the distal end of the band as in other (more skeletally mature) ankylosaurs (Penkalski, 2001; Arbour et al., 2009), but they do extend with distal inclinations.

2.8 APPENDICULAR ALLOMETRY

Scapulae from the PIN Alag Teeg collection (Table 2.1) become allometrically dorsoventrally taller as their lengths increase. Height at the glenoid process has the highest coefficient of allometry ($\alpha = 1.29$, $R^2 = 0.93$, $p < 0.01$) followed by the articular surface for contact of the coracoid ($\alpha = 1.17$, $R^2 = 0.80$, $p = 0.13$), neck height ($\alpha = 1.14$, $R^2 = 0.92$, $p < 0.01$),

and posterior height ($\alpha = 1.02$, $R^2 = 0.88$, $p < 0.01$). The acromion shows negative allometry ($\alpha = -1.14$, $R^2 = 0.49$, $p = 0.26$) when compared with scapular length, although this trend is not significant. Coracoid height is negatively allometric ($\alpha = 0.59$, $R^2 = 0.68$, $p = 0.01$) to its length. Comparison of scapular blade length (y) with humerus length (Table 2.2) suggests that the scapular growth was negatively allometric within *Pinacosaurus* ($\alpha = 0.87$, $R^2 = 0.94$, $p < 0.01$), whereas the lengths of these two elements stay the same (are isometric) in specimens of all sizes but different taxa ($\alpha = 0.95$, $R^2 = 0.89$, $p < 0.01$). The results of comparisons between humerus length and scapular blade width of the neck are more equivocal because of variability (both within *Pinacosaurus* and between all taxa), but do confirm that shaft robustness is increasing in ontogenetic (but not interspecific) series.

Among the PIN humeri from Alag Teeg (Fig. 2.13), proximal and midshaft widths show size-dependence with respect to element length. Proximal width increases at a greater rate ($\alpha = 1.17$, $R^2 = 0.96$, $p < 0.01$) relative to humeral length than does midshaft width ($\alpha = 1.08$, $R^2 = 0.93$, $p < 0.01$). The distal humerus shows greater positive allometry ($\alpha = 1.41$, $R^2 = 0.88$, $p < 0.01$) than the proximal end. The deltopectoral crest shows no significant length-dependent trends with respect to crest length ($\alpha = 1.15$, $R^2 = 0.23$, $p = 0.85$) or its angle to the long axis of the humerus ($\alpha = 0.15$, $R^2 = 0.01$, $p = 0.64$). Few ankylosaur specimens have both femur and humerus, but comparison of humerus length with femur length suggests that the humeral growth was negatively allometric within specimens of all sizes but different taxa ($\alpha = 0.91$, $R^2 = 0.95$, $p < 0.01$).

The radius and ulna of PIN Alag Teeg specimens show significant allometric trends. In radii, the distal end has higher positive allometry ($\alpha = 1.14$, $R^2 = 0.87$, $p < 0.01$) than the proximal end ($\alpha = 1.12$, $R^2 = 0.83$, $p < 0.01$). The shaft has lower positive allometry than both ends ($\alpha = 1.07$, $R^2 = 0.68$, $p < 0.01$). Positive allometry in the ulna is strongest proximally ($\alpha = 1.49$, $R^2 =$

0.89, $p < 0.01$), likely due to the development of the olecranon process. The ulnar shaft shows higher positive allometry ($\alpha = 1.28$, $R^2 = 0.73$, $p < 0.01$) than the distal end ($\alpha = 1.03$, $R^2 = 0.27$, $p = 0.07$), although this latter relationship is not significant. Comparison of radius length with humerus length suggests that the radial growth was negatively allometric within *Pinacosaurus* ($\alpha = 0.89$, $R^2 = 0.90$, $p = 0.05$), whereas the lengths of these two elements stay the same (are isometric) in specimens of all sizes but different taxa ($\alpha = 0.99$, $R^2 = 0.95$, $p < 0.01$).

In PIN Alag Teeg specimens, hind limb element widths do not show strong length-dependent correlations like those of the forelimb. Both proximal ($\alpha = 1.03$, $R^2 = 0.76$, $p < 0.01$) and distal ends ($\alpha = 0.92$, $R^2 = 0.63$, $p = 0.01$) of the femur are roughly isometric. The femoral shaft diameter ($\alpha = 0.75$, $R^2 = 0.27$, $p < 0.01$) and circumference ($\alpha = 0.73$, $R^2 = 0.47$, $p = 0.01$) are both negatively allometric. In the tibia, there are no significant correlations between length and proximal ($\alpha = 0.59$, $R^2 = 0.07$, $p = 0.60$), midshaft ($\alpha = 0.54$, $R^2 = 0.12$, $p = 0.38$), or distal ($\alpha = -0.51$, $R^2 = 0.08$, $p = 0.60$) widths. The same is true for fibular proximal ($\alpha = -1.08$, $R^2 = 0.18$, $p = 0.54$), midshaft ($\alpha = -0.68$, $R^2 = 0.17$, $p = 0.54$), and distal ($\alpha = -1.70$, $R^2 = 0.37$, $p = 0.35$) widths.

Comparison of femur length with tibia length suggests that the tibial growth was negatively allometric in specimens of all sizes but different taxa ($\alpha = 0.86$, $R^2 = 0.96$, $p < 0.01$). Unfortunately, there are only four specimens in which both elements are preserved. Comparison of femur length with the length of the third metatarsal suggests that metatarsus growth was relatively isometric ($\alpha = 1.07$, $R^2 = 0.97$, $p < 0.01$).

2.9 DISCUSSION

2.9.1 Taxonomic Referral

Assignment of the Soviet-Mongolian ankylosaurine material described here is based on its occurrence in the bonebed at Alag Teeg. Several complete skulls collected from the same locality by the HMNS allow unequivocal referral to *P. grangeri* based on the current diagnosis from Burns et al. (2011). A description of the HMNS *P. grangeri* material from Alag Teeg is in preparation.

Currie et al. (2011) have suggested that due to their lower stratigraphic occurrence (Dashzeveg et al., 2005), the ankylosaurine specimens from Alag Teeg may represent a taxon distinct from those found at Bayan Zag. A problem when comparing *P. grangeri* specimens from different assemblages is the discrepancy in mean body size, which makes it difficult to distinguish between ontogenetic and possible taxonomically significant morphological variation. To date, there is little published data on the postcranial material from *P. grangeri*. Nevertheless, ZPAL MgD II/1 falls within the range of size variation of the Alag Teeg material. The large PIN 614 falls significantly outside of it. In addition, some material from Alag Teeg (possibly representing a single individual) is significantly larger than the remaining elements from the site.

Based on discrete cranial characters (Burns et al., 2011) all of the ankylosaurine material from Alag Teeg and ZPAL MgD II/1 is referable to *P. grangeri*.

2.9.2 Size Range of Alag Teeg *P. grangeri*

Arbour and Currie (2011) noted that two humeri and a scapula (found together and presumably representing one individual) were larger than other homologous elements in the MPC Alag Teeg collection. The scapula and humeri (MPC-D 100/1333) are larger than all others from Alag Teeg (at least 1.4 times larger). The same is true for the large coracoid (PIN 3144/23). Because the humeri are left and right, and the scapula and coracoid are from the same side (left),

this supports the idea that these large elements represent a single individual. Despite their size, the scapula and coracoid are unfused, as are several large neural spines in the PIN.

If all of the significantly larger elements from Alag Teeg do represent a single individual, then it would provide some of the first information on the timing of osteological fusion events in ankylosaurs. It is interesting that the neural arches are only preserved in articulation in the cervical vertebrae (although they are not fully coossified to the centra). There are no fully-fused neurocentral sutures on any of the dorsal, sacral, or free caudal vertebrae from Alag Teeg, although isolated arches have been recovered and demonstrate that their isolation is caused by lack of fusion and not breakage. In contrast, the neural arches of a juvenile North American ankylosaurid, referred to *Euoplocephalus* by Coombs (1986) were not found in association with the cervical centra. This might suggest that neurocentral closure began in the cervical series for *P. grangeri* and progressed in an anterior to posterior sequence. However, there are also examples of large unfused (not broken) neural arches from the cervical (PIN 3144/64), dorsal (PIN 3144/62), and caudal (PIN 3144/63) series. Evidence suggests the dorsal ribs and vertebrae were among the first elements to fully coosify during ontogeny. If most of the coosification is delayed ontogenetically, this would add support to the validity of taxa that may be relatively small in terms of body size, but show a skeletally mature pattern of coosification such as *Ahshislepelta* (Burns and Sullivan, 2011).

2.9.3 Growth in ankylosaurs

The length of the deltopectoral crest varies among specimens referred to *P. grangeri* and does not appear to exhibit any pattern that would warrant considering it entirely dependent on humeral length. As stated by Currie et al. (2011) and supported here, the deltopectoral crest in the Alag Teeg specimens is on average 51±2% the length of the humerus. In ZPAL MgD II-1 it

actually extends 64% the length of the humerus. Burns and Sullivan (2011) demonstrate that proximal humeral width is linked to humeral size across a wide range of taxa. In that case, only *Saichania* diverged noticeably from the overall trend. This, however, may be influenced by taphonomic crushing of the humerus in *Saichania*, which causes the deltopectoral crest to extend more laterally than anteriorly according to Carpenter et al. (2011). Perceived variability in deltopectoral crest length and angle may be due, in part, to difficulty measuring these features. Distally, the crest does not have a definite terminus but rather grades into the humeral shaft. Whatever the cause for this variation, humeral characters should be restricted to width measurements.

Overall, the widths of elements in the forelimbs in young *P. grangeri* show positive allometry and are strongly correlated with length. This suggests that forelimb characters can be useful for taxonomy and phylogenetic analyses for ankylosaurs because forms that diverge considerably from this overall trend should be readily apparent (e.g., proximal humeral width for *Saichania*). Because similarly strong correlations are not seen in hind limb elements, taxonomic characters should be restricted to those of the forelimb. At least in the early stages of growth, the forelimbs became more robust. In the zeugopodial elements, the allometric coefficient increases from proximal to distal in the radius but decreases proximal to distal in the ulna. This corresponds to an increase in robustness of the larger articulations in both elements (i.e., the olecranon of the ulna and distal end of the radius).

Although a digging function had been proposed (Maleev, 1954) to account for the robust structure of the ankylosaurian forelimb, Coombs (1978a) and Maryańska (1977) recognize that the manus is unsuitable for such an activity. Maryańska (1977) proposed, instead, a scenario of burrowing whereas Coombs (1978a) favoured a simple weight-bearing explanation. The forelimbs are shorter than the columnar hind limbs, and they are held in a flexed position. As a

result, the entire weight of the presacral part of the body would have been supported by the forelimbs. It is possible, then, that the allometry observed in the robust forelimbs is simply a response to increasing body mass as the animal grew, supporting the hypothesis of Coombs (1978a). The development of osteoderms on the forelimbs of other specimens, like those seen in MPC-D 100/1305, may exacerbate this trend in ontogenetically older individuals.

The articular surfaces of limb bones in juvenile *P. grangeri* are generally smooth and convex. For example, the proximal end of the radius is convex; the olecranon process is blunt, whereas it is a sharp, distinct projection in an adult ankylosaurine. Unlike mammals, sauropsid bones do not grow via secondary epiphyseal ossification centers (Chinsamy–Turan, 2005). The articular ends of developing long bones in dinosaurs are composed of uncalcified cartilage, which does not readily fossilize and is not preserved in the Alag Teeg specimens. The apparent articular ends of these immature bones represent the interface between calcified and uncalcified cartilage.

Ankylosaurid cervical half rings are usually interpreted as bands of fused, paired, smooth dermal elements with osteoderms fused to the external surface (Penkalski, 2001; Arbour et al., 2009). In the immature cervical half rings from Alag Teeg, however, osteodermal projections apparently emanate from the underlying band, becoming more rugose with an increase in their basal-apical height. Two distinct developmental processes (intramembranous ossification of the basal band and metaplastic mineralization of the dermis into the external osteoderms) have been hypothesized (Hayashi et al., 2012), but this will need to be tested histologically. Evidence from juvenile *P. grangeri* implies that development of the cervical half rings is dependent upon an intimate interaction between these two processes. A similar combination of processes is responsible for the development of cranial ornamentation in ankylosaurs (Vickaryous et al., 2001).

TABLE 2.1. Analyses of size-related differences in the postcrania of juvenile *Pinacosaurus grangeri* Gilmore, 1933 from Alag Teeg, Gobi Desert, Mongolia. Abbreviations: **α**, allometric coefficient (slope of regression line); **b**, regression line y-intercept; **Δx**, ratio of maximum to minimum x for samples used in analysis; **N**, number of samples. Only analyses with N ≥ 5 are included here.

y	x	N	Δx	α	b	R2	p
Height at glenoid	Scapula length	5	2.54	1.29	2.28	0.93	<0.01
Height at coracoid articulation	Scapula length	5	1.04	1.17	2.14	0.80	0.13
Height at neck	Scapula length	6	1.19	1.14	1.87	0.92	<0.01
Posterior height	Scapula length	6	1.19	1.02	1.10	0.88	<0.01
Acromion length	Scapula length	5	1.04	-1.14	-9.76	0.46	0.26
Coracoid height	Coracoid length	6	1.17	0.59	1.67	0.68	0.01
Proximal humerus width	Humerus length	8	1.16	1.17	1.61	0.96	<0.01
Midshaft humerus width	Humerus length	9	1.16	1.08	2.05	0.93	<0.01
Distal humerus width	Humerus length	9	1.16	1.41	2.91	0.88	<0.01
Angle deltopectoral crest to horizontal	Humerus length	5	1.16	-0.92	-7.33	0.08	0.64
Proximal radius width	Radius length	13	1.17	1.12	1.69	0.83	<0.01
Midshaft radius width	Radius length	14	1.18	1.07	2.23	0.68	<0.01

Distal radius width	Radius length	14	1.18	1.14	1.73	0.87	<0.01
Proximal ulna width	Ulna length	10	1.15	1.49	3.13	0.89	<0.01
Midshaft ulna width	Ulna length	13	1.15	1.28	1.66	0.73	<0.01
Distal ulna width	Ulna length	13	1.15	1.03	3.12	0.27	0.07
Proximal femur width	Femur length	10	1.07	1.03	1.26	0.76	<0.01
Midshaft femur width	Femur length	10	1.07	0.75	0.47	0.27	<0.01
Distal femur width	Femur length	9	1.05	0.92	0.74	0.63	0.01
Midshaft femur circumference	Femur length	9	1.07	0.73	-0.70	0.47	0.01
Proximal tibia width	Tibia length	7	1.05	0.59	1.15	0.07	0.60
Midshaft tibia width	Tibia length	7	1.05	0.54	-0.58	0.12	0.38
Distal tibia width	Tibia length	7	1.05	-0.51	-6.75	0.08	0.60

TABLE 2.2. Analyses of size-related differences in the postcrania of *Pinacosaurus* and other ankylosaur specimens of various taxa and body sizes. Abbreviations: **α**, allometric coefficient (slope of regression line); **b**, regression line y-intercept; **Δx**, ratio of maximum to minimum x for samples used in analysis; **N**, number of samples.

Taxa included	y	x	N	Δx	α	b	R2	p
Various	Humerus length	Scapula blade length	11	3.39	0.95	0.03	0.89	<0.01
Pinacosaurus	Humerus length	Scapula blade length	5	2.36	0.87	0.21	0.94	<0.01
Various	Humerus length	Femur length	38	5.81	0.91	0.11	0.95	<0.01
Pinacosaurus	Radius length	Humerus length	4	2.52	0.99	0.20	0.96	0.05
Various	Radius length	Humerus length	10	3.83	0.89	0.03	0.90	<0.01
Various	Tibia length	Femur length	11	5.71	0.86	0.24	0.96	<0.01
Various	Metatarsal III length	Femur length	25	5.67	1.07	0.79	0.97	<0.01

FIGURE 2.1. Locality map showing the productive Late Cretaceous Mongolian and Chinese ankylosaur localities, Alag Teeg, Bayan Mandahu, and Bayan Zag.

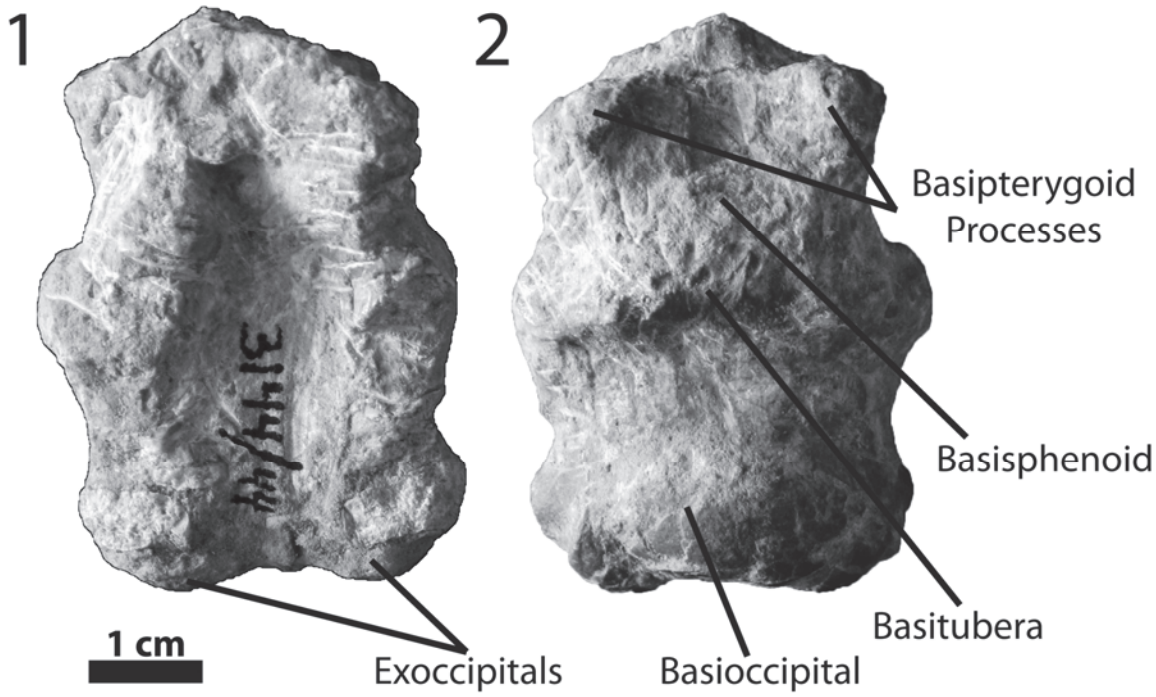

FIGURE 2.2. Basicranium of juvenile *Pinacosaurus grangeri*, Gilmore 1933, in, *1*, dorsal and, *2*, ventral views. Anterior is up.

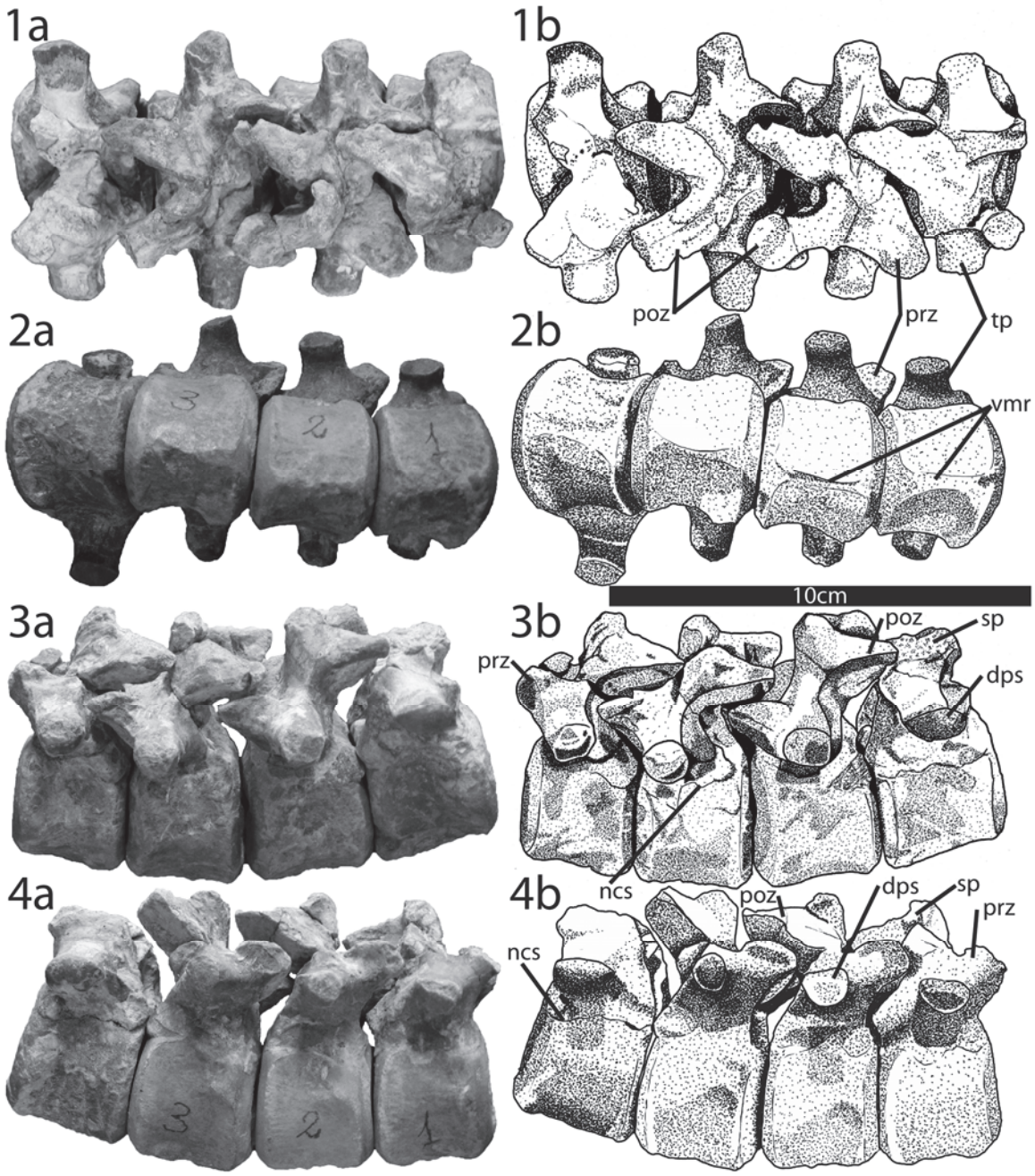

FIGURE 2.3. Articulated cervical vertebrae (?c3–c6) of juvenile *Pinacosaurus grangeri* in, *1*, dorsal, *2*, ventral, *3*, left lateral, and, *4*, right lateral views. Anterior is to the right in *1*, *2*, and *4* and to the left in *3*. Abbreviations: dps: diapophysis; ncs: neurocentral suture; poz, postzygapophysis; prz: prezygapophysis; sp: neural spine; tp: transverse process; vmr: ventral median ridge.

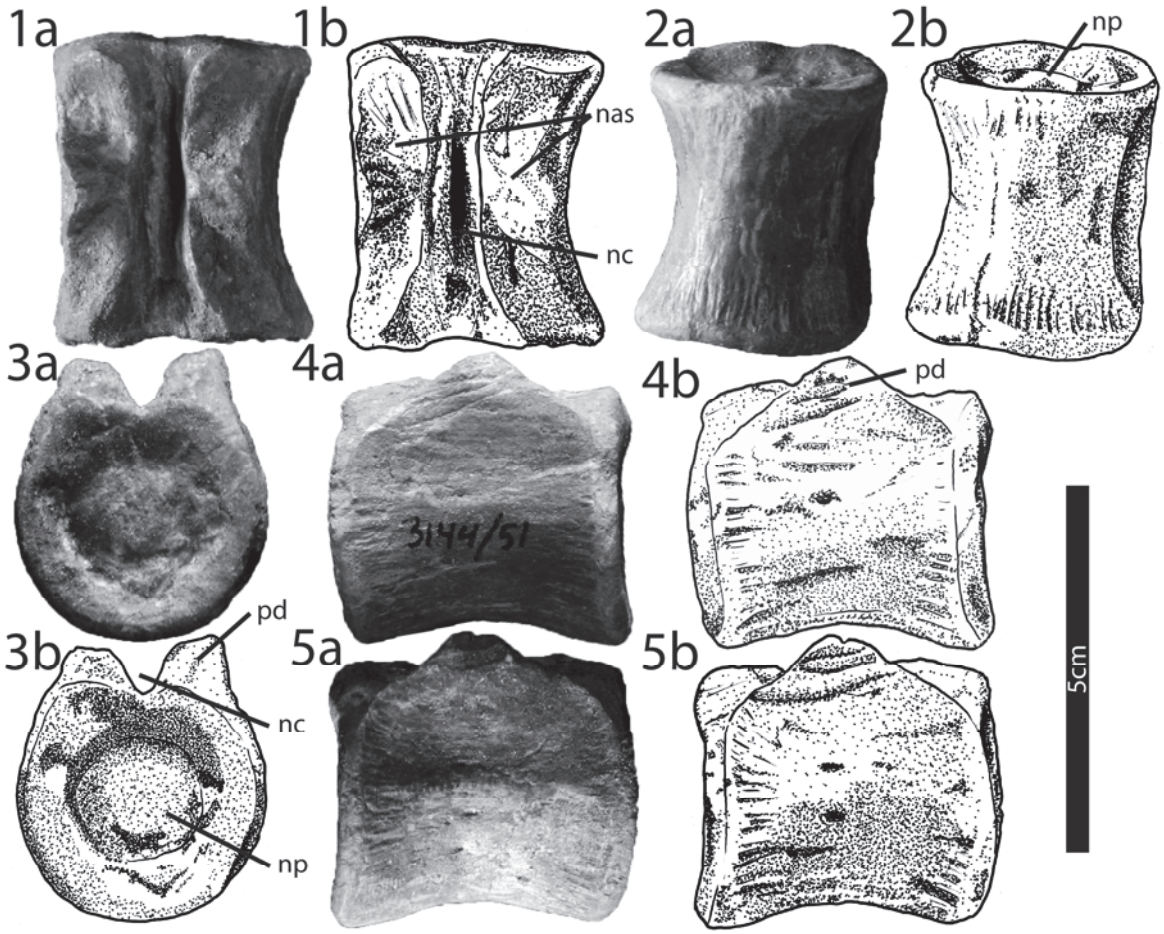

FIGURE 2.4 Dorsal centrum of juvenile *Pinacosaurus grangeri* in, *1*, dorsal, *2*, ventral, *3*, anterior or posterior, and, *4, 5*, lateral views. Orientation uncertain. Abbreviations: nas: neural arch sutural surface; nc: neural canal; np: notochordal prominence; pd: pedicle.

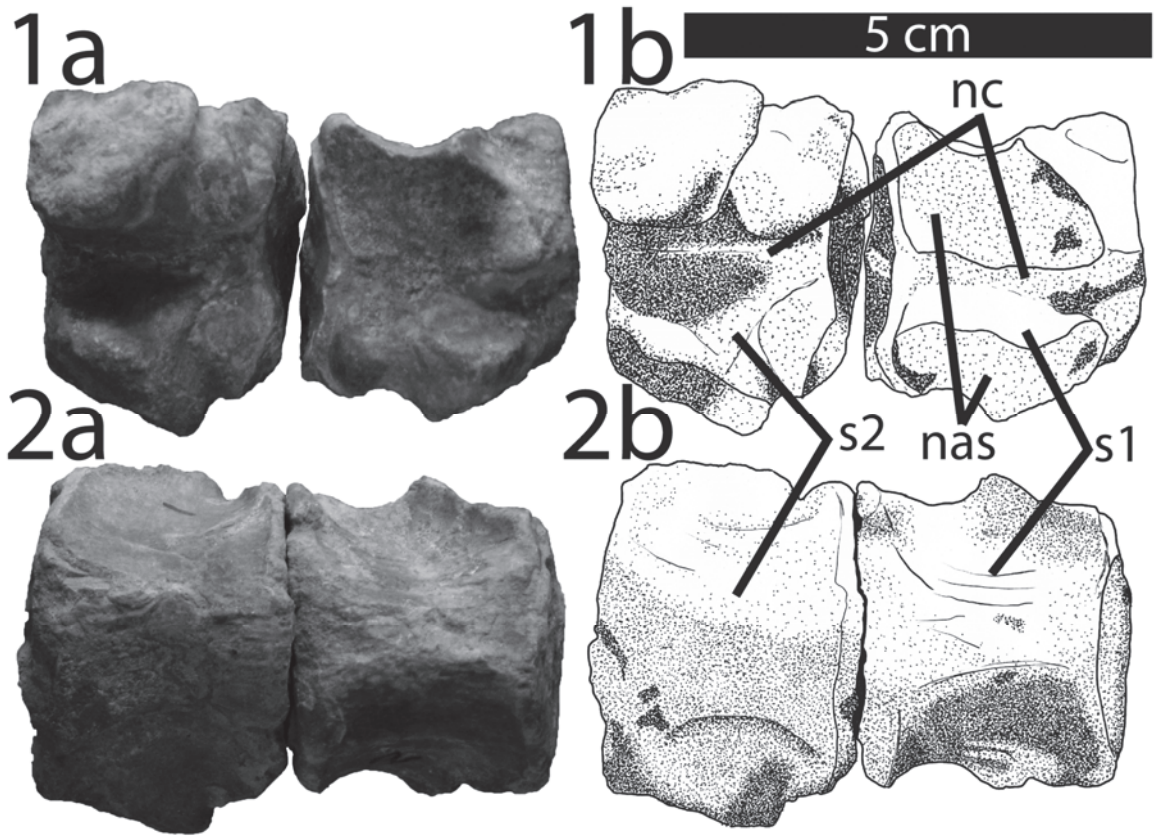

FIGURE 2.5. Sacral centra of juvenile *Pinacosaurus grangeri* in, *1*, dorsal, and, *2*, ventral views. Anterior is to the right. Abbreviations: nas: neural arch sutural surface; nc: neural canal; s1, s2: first, second sacral.

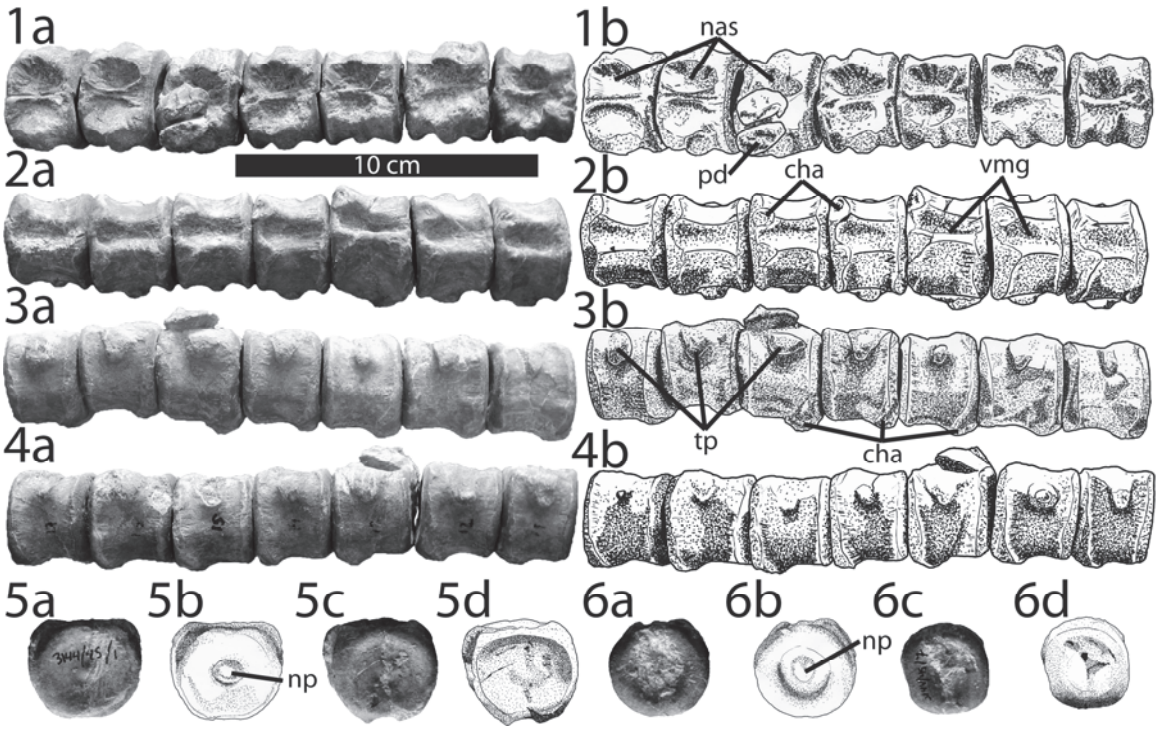

FIGURE 2.6. Articulated free caudal centra of juvenile *Pinacosaurus grangeri* in, *1*, dorsal, *2*, ventral, *3*, left lateral, and, *4*, right lateral views. Anteriormost centrum in, *5a, b*, anterior and, *5c, d*, posterior views. Posteiormost centrum in, *6a, b*, anterior and, *6c, d*, posterior views. Anterior is to the right in *1* and *4* and to the left in *2* and *3*. Dorsal is up in *5* and *6*. Abbreviations: cha: chevron (haemal spine) articulation; nas: neural arch sutural surface; np: notochordal prominence; pd: pedicle; tp: transverse process; vmg: ventral median groove.

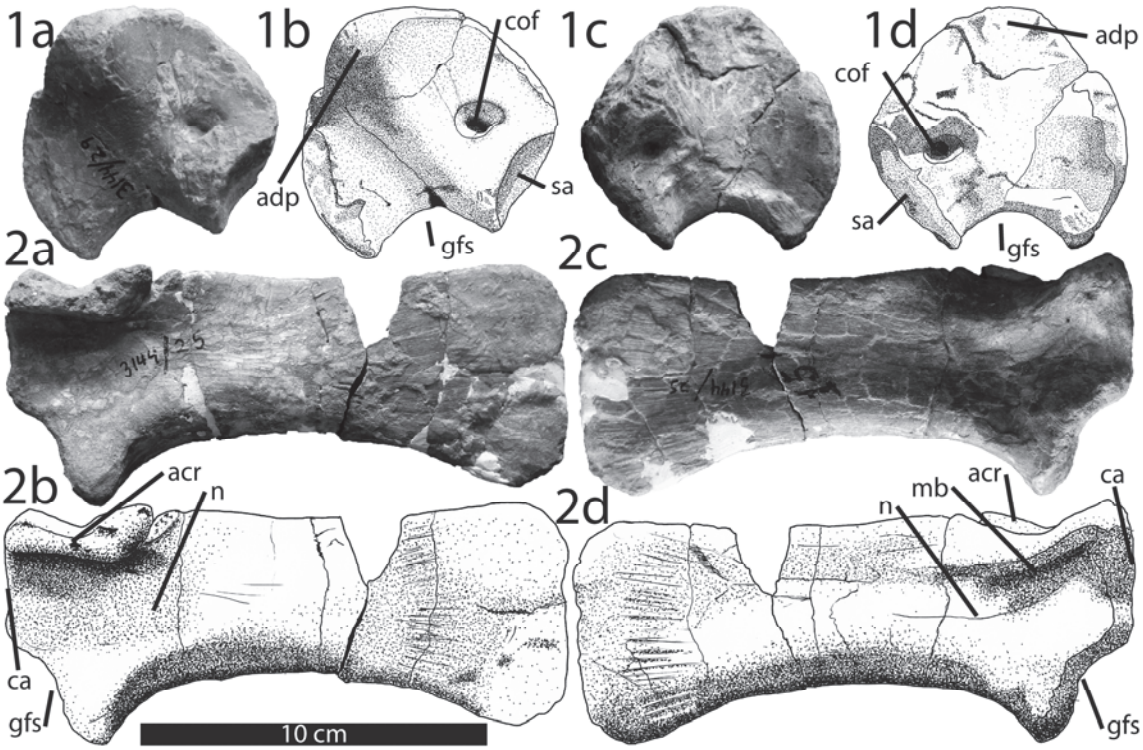

FIGURE 2.7. Left shoulder girdle elements of juvenile *Pinacosaurus grangeri*. Coracoid in, *1a, b*, lateral and, *1c, d*, medial views. Scapula in, *2a, b*, lateral and, *2c, d*, medial views. Anterior is to the right in *1a, b* and *2c, d* and to the left in *1c, d* and *2a ,b*. Abbreviations: acr: acromion process; adp: anterodorsal process; ca: coracoid articulation; cof: coracoid foramen; gfs: glenoid fossa; mb: medial brace; n: scapular neck; sa: scapular articulation.

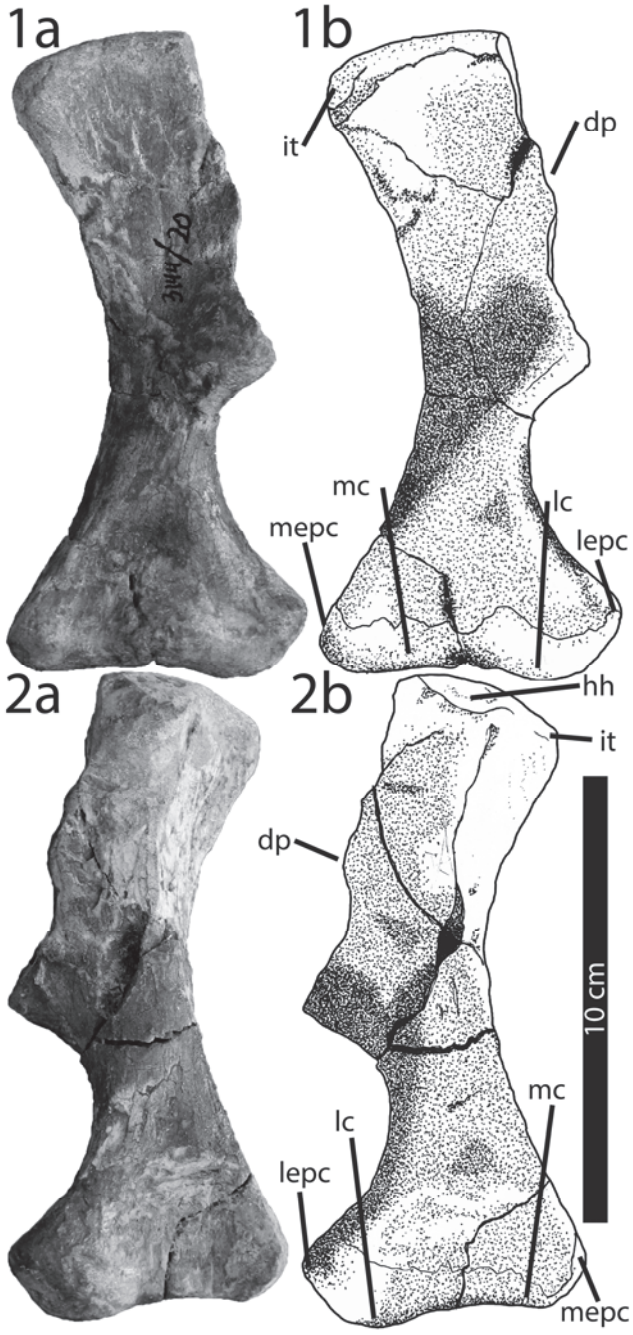

FIGURE 2.8. Left partial humerus of juvenile *Pinacosaurus grangeri* in, *1*, anterior and, *2*, posterior views. Note that the deltopectoral crest is largely broken off. Proximal is up. Abbreviations: dp: deltopectoral crest; hh: humeral head; it: internal (medial) tuberosity; lc: lateral condyle; lepc: lateral epicondyle; mc: medial condyle; mepc: medial epicondyle.

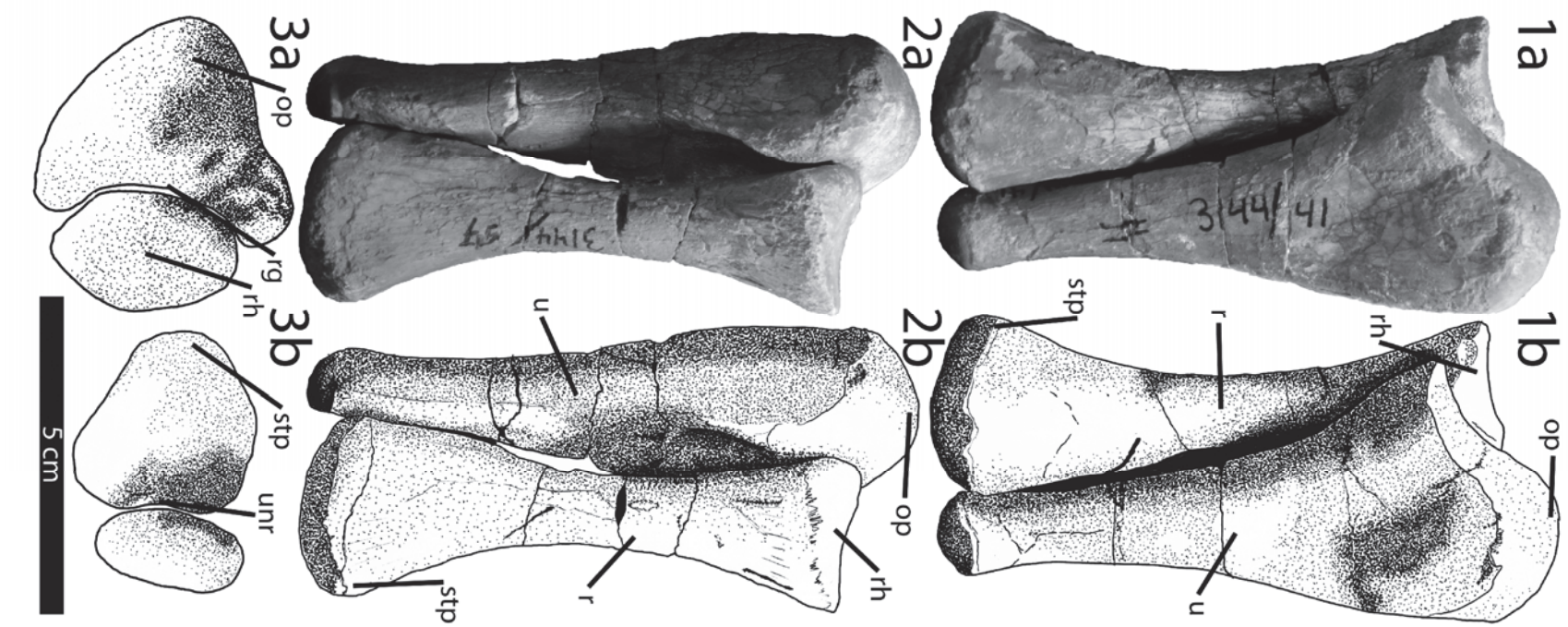

FIGURE 2.9. Right forelimb zeugopodial elements of juvenile *Pinacosaurus grangeri* in anterior (1), posterior (2), proximal (3a), and distal (3b) views. Proximal is up in 1 and 2. Anterior is up in 3. Abbreviations: op: olecranon process; r: radius; rg: radial groove of the ulna; rh: radial head; stp: styloid process; u: ulna; unr: ulnar notch of the radius.

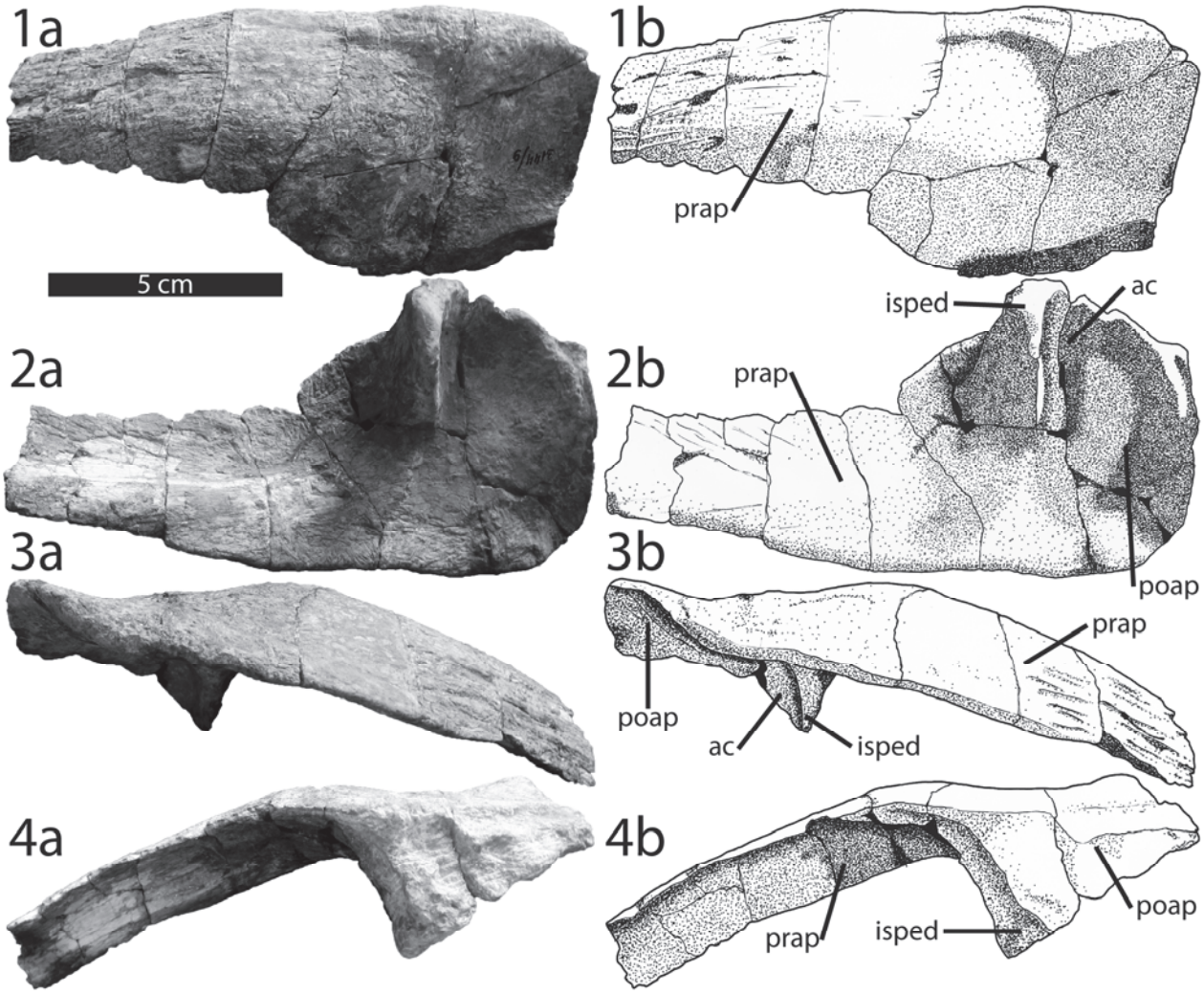

FIGURE 2.10. Right partial ilium of juvenile *Pinacosaurus grangeri* in, *1*, dorsal, *2*, ventral, *3*, lateral, and, *4*, medial views. Anterior is to the right in *1*, *2*, and *4* and to the left in *3*. Abbreviations: ac: acetabulum; isped: ischial peduncle; poap: postacetabular process; prap: preacetabular process.

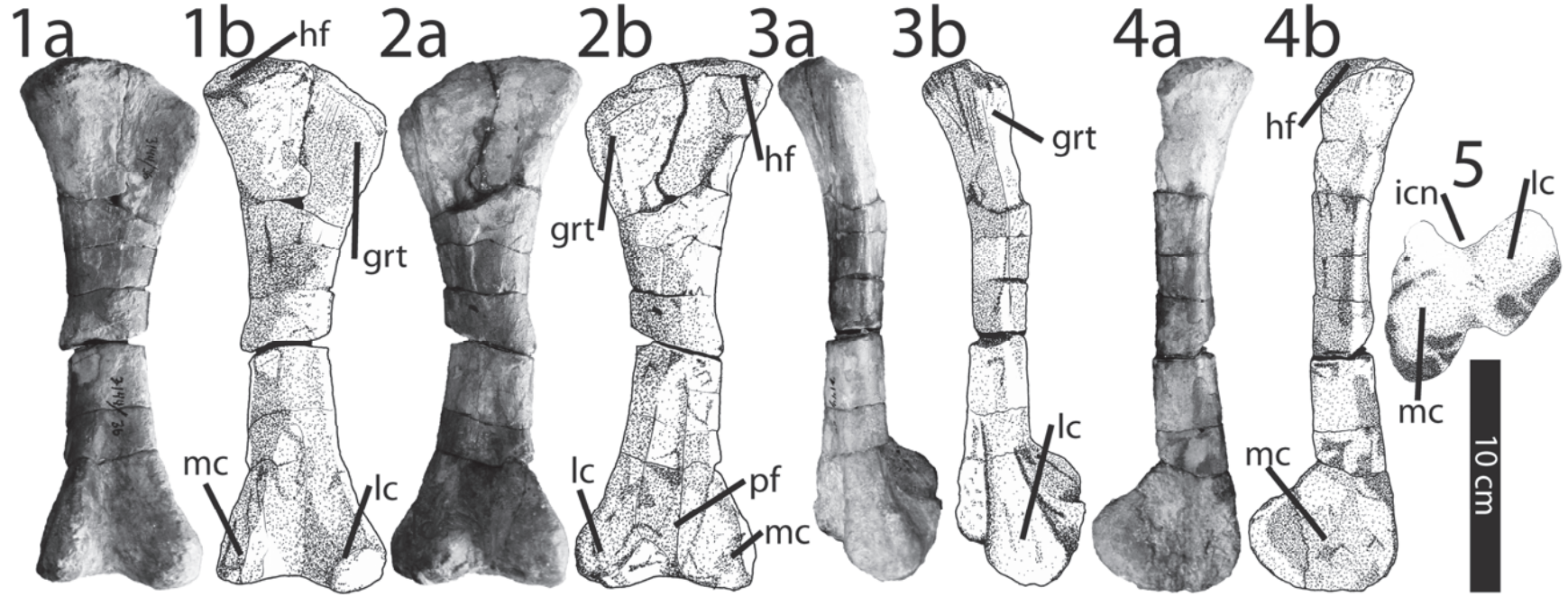

FIGURE 2.11. Left femur of juvenile *Pinacosaurus grangeri* in, *1*, anterior, *2*, posterior, *3*, lateral, *4*, medial, and, *5*, distal views. Proximal is up in *1–4*. Anterior is up in *5*. Abbreviations: grt: greater trochanter; hf: femoral head; icn: anterior intercondylar notch; lc: lateral condyle; mc: medial condyle; pf: popliteal fossa.

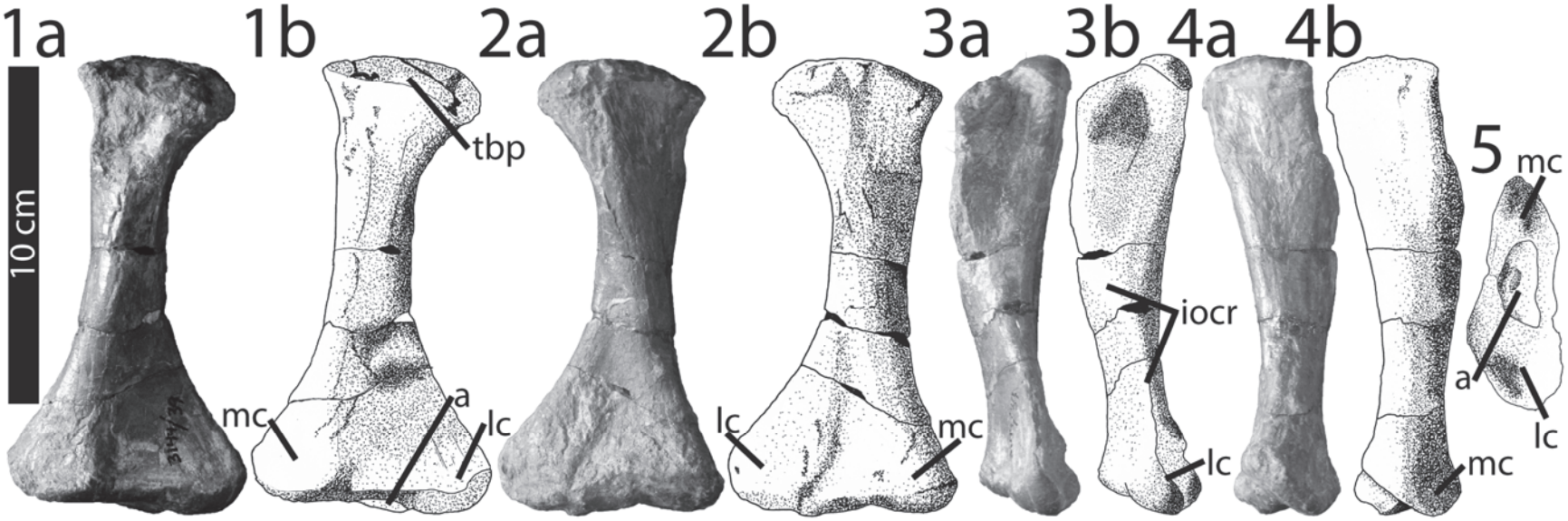

FIGURE 2.1. Left tibia of juvenile *Pinacosaurus grangeri* in, *1*, anterior, *2*, posterior, *3*, lateral, *4*, medial, and, *5*, distal views. Proximal is up in *1–4*. Anterior is to the right in *5*. Abbreviations: a: astragalus; iocr: interosseous crest; lc: lateral condyle; mc: medial condyle; tbp: tibial plateau.

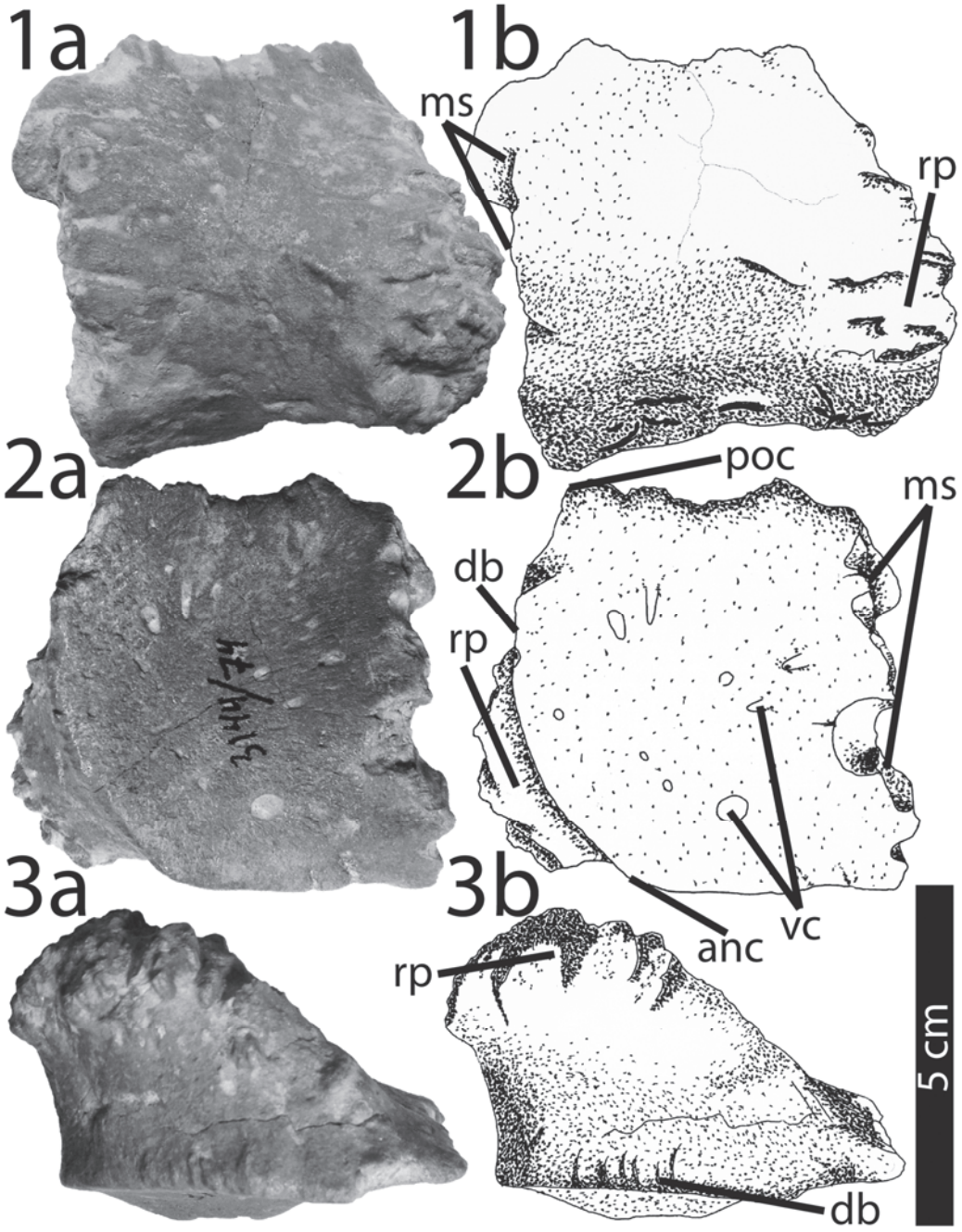

FIGURE 2.13. Right distal cervical half ring segment of juvenile *Pinacosaurus grangeri* in, *1*, external, *2*, basal, and, *3*, distal views. Anterior is up in *1*, *2*. External is up in *3*. Abbreviations: anc: anterior corner of distal edge of band; db: smooth distal edge of band; ms: medial suture; poc: posterior corner of distal edge of band; rp: rugose osteodermal projection; vc: vascular canal foramina

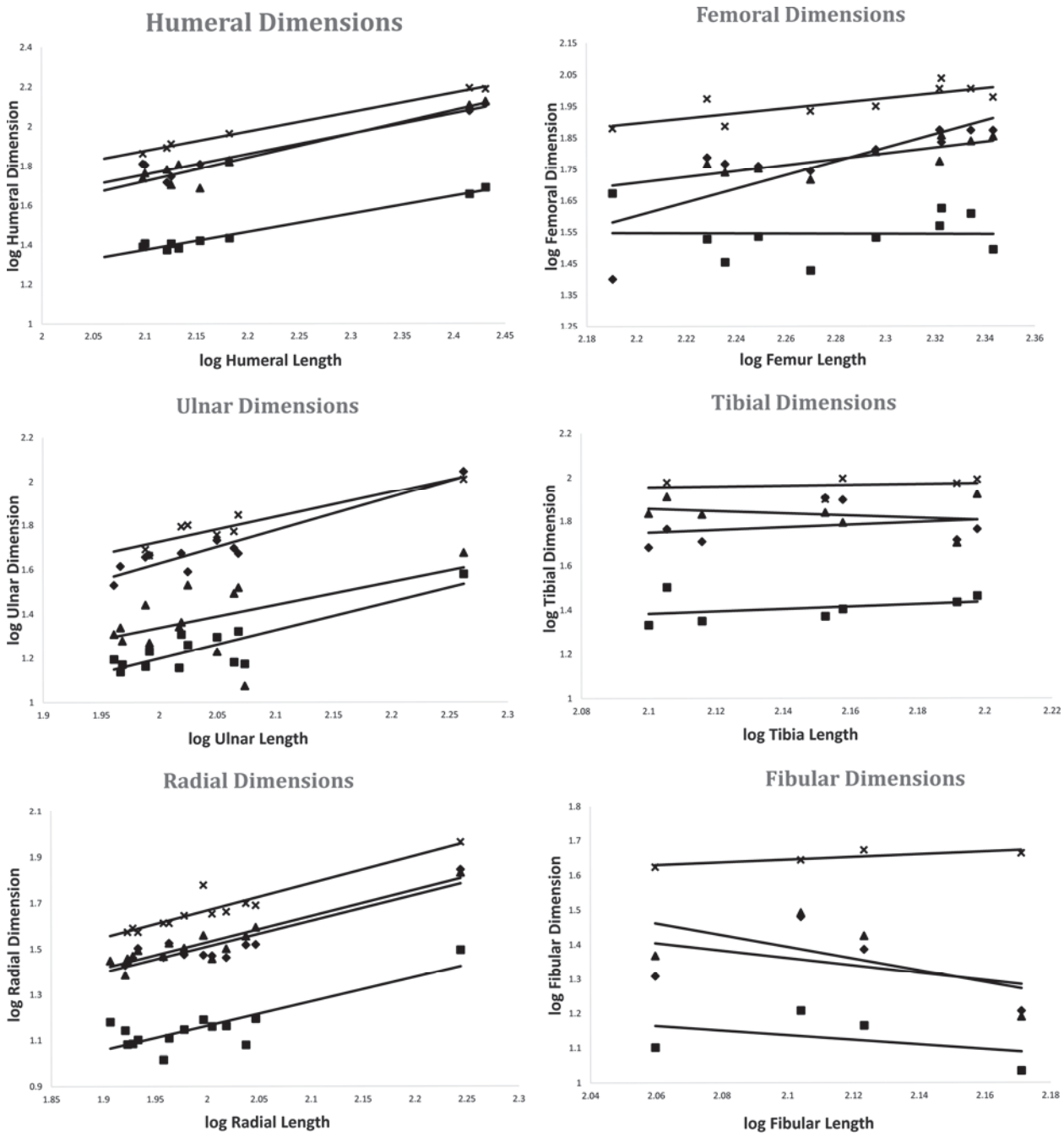

FIGURE 2.14. Bivariate log-log plots for postcranial dimensions in juvenile *Pinacosaurus grangeri* from Alag Teeg for forelimb (*1*, humerus, *2*, ulna, *3*, radius) and hind limb (*4*, femur, *5*, tibia, *6*, fibula) elements. Element length is plotted against maximum proximal width (diamonds), maximum midshaft width (squares), maximum distal width (triangles), and midshaft circumference (Xs). Slope, intercepts, and fit statistics are in Table 2.1.

CHAPTER 3

HISTOLOGICAL STUDY OF ANKYLOSAUR (ORNITHISCHIA: THYREOPHORA) ONTOGENY

3.1 INTRODUCTION

The Ankylosauria includes ornithischian dinosaurs best recognized by their possession of osteodermal armour covering most of the body. Whereas some aspects of ankylosaurian biology have been studied, such as tail-clubbing behaviour (Arbour and Snively, 2009) and feeding (Rybczynski and Vickaryous, 2001), their ontogeny is largely unknown. Whereas a rough framework for the phylogenetic relationships among ankylosaurs has been supported repeatedly (Vickaryous et al., 2004; Thompson et al., 2012; Burns and Currie, 2014), a high degree of uncertainty persists within the group's higher and lower taxonomy. It is likely that this poor understanding of ontogenetic variation is contributing, in part, to this uncertainty.

Most dinosaurs undergo considerable changes in absolute size and physical proportions during growth (Rozhdestvensky, 1965). Juvenile material has been collected for few of the known ankylosaur taxa, nevertheless size variability is rarely addressed in the descriptions of new taxa. It is possible that a lack of understanding of the morphological changes that take place during ontogeny has led to taxonomic over-splitting (e.g., Blows, 1996).

Although a component of dinosaur palaeontology for over 150 years, palaeohistology has only been studied in a systematic way during the last 30 years. In that time, large-scale, multi-element palaeohistological sampling on dinosaurian assemblages has led to an increased

understanding of the ages and growth rates of these animals (Chinsamy, 1993; Erickson and Tumanova, 2000; Sander and Tückmantel, 2003; Erickson et al., 2004; Horner and Padian, 2004; Lee and Werning, 2008). The bone histology of ankylosaurs is poorly known and investigations have been almost exclusively restricted to osteoderms (Scheyer and Sander, 2004; Burns, 2008; Hayashi et al., 2010). To date, only one study (Stein et al., 2013) has examined the long bone histology of ankylosaurs. Although providing information on the growth patterns of ankylosaurs based on sampling bones of varying sizes, the material used in Stein et al. (2013) represents various taxa from different geographic areas, stratigraphic ranges, and phylogenetic positions, thus bringing into question the veracity of their conclusions.

Here I systematically approach ankylosaurian limb bone histology from an ontogenetic perspective by sampling multiple elements of ankylosaur specimens preserved as bonebed assemblages at Alag Teeg in Mongolia and Lorrie's Site in Colorado. These new data add to an increasing understanding of the growth dynamics of armored dinosaurs. In addition, the ability to accurately assess the ontogenetic stage of ankylosaur specimens may allow for more accurate taxonomic reassessments, especially for those taxa diagnosed by possible ontogenetically and/or allometrically variable characters.

3.2 MATERIALS AND METHODS

Asia has produced many ankylosaur specimens from numerous genera, some of which include multiple species (Maryańska, 1977; Tumanova, 1983, 1993; Barrett et al., 1998; Godefroit et al., 1999; Vickaryous et al., 2001; Xu et al., 2001; Hill et al., 2003; Burns et al., 2011; Currie et al., 2011). Among these sites, the best known is the Djadokhta−age (Campanian)

locality Alag Teeg, which has produced numerous partial skeletons and disarticulated elements of the ankylosaurine *Pinacosaurus grangeri* over an intermittent 45-year history of collection by several institutions. Many specimens were preserved articulated and upright in the lower mudstone section representing the floodplain of a braided river system (Fastovsky, 2000). The Mongolian−Japanese Joint Paleontological Expedition collected more than thirty ankylosaurine specimens from the site (Fastovsky and Watabe, 2000; Watabe and Suzuki, 2000). To date, however, only three of the many blocks collected have been prepared. The Alag Teeg ankylosaur material can be identified as juvenile based on unfused neurocentral sutures and incompletely fused pelvic elements. Although a different taxon from the one known at Bayan Zag had been suggested based on stratigraphy (Currie et al., 2011), the Alag Teeg specimens are assigned to *Pinacosaurus* based on a posterior embayment of the nasal dermal ornamentation dorsal to external nares and paranasal apertures (which creates a shallow nasal vestibule) paranasal apertures that are unenclosed by the external nares, and a characteristic skull roof ornamentation composed of weakly-developed dermal elaborations and fused osteoderms (Burns et al., 2011). They are assigned to *Pinacosaurus grangeri* based on weakly-developed pyramidal dermal elaborations of the squamosals, a flat cranial roof posterior to orbits, and presence of a premaxillary notch (Burns et al., 2011). *Pinacosaurus* could represent either a derived (Kirkland, 1998; Carpenter, 2001; Vickaryous et al., 2004) or primitive (Hill et al., 2003; Burns et al., 2011) ankylosaurine. The ambiguity may be attributable to the relative dearth of identifiable adult specimens showing phylogenetically informative characters (Hill et al., 2003; Burns et al., 2011). Some material for this project was collected by the Mongolian−Japanese Joint Paleontological Expedition and accessioned at HMNS. Five additional femora from Alag Teeg, in the collections of the MPC, were also sampled histologically for this project (Table 1).

Specimens of *Gastonia* n. sp. (Table 2) were collected by the DMNH (Denver Museum of Nature and Science, Denver, Colorado, USA) from "Lorrie's Site" northwest of Arches National Park in Grand County, Utah (Kirkland and Madsen, 2007; Carpenter et al., 2008). The site is situated at the base of the Ruby Ranch Member (Cedar Mountain Formation), characterized by maroon mudstones with irregular spheres of carbonate nodules, suggesting a seasonal, semiarid palaeoclimate (Kirkland and Madsen, 2007). Although there is some debate as to the age of the base of the member, UPb dates place the upper portions of the Ruby Ranch Member in the late Aptian (Kirkland and Madsen, 2007). Ankylosaurs are unusually abundant and diverse throughout the member and include the giant nodosaurid *Peloroplites cedrimontanus* and the ankylosaurid *Cedarpelta bilbyhallorum* (Carpenter et al., 2001; Carpenter et al., 2008). The DMNH collections include 3566 catalogued fragmentary to complete elements. Partial to complete limb bones include 58 humeri, 30 radii, 24 ulnae, 57 femora, 76 tibiae, and 45 fibulae. Specimens were selected for sectioning to be representative of the entire size range represented by each element.

Specimens were documented through measurements, observations, and photographs. Samples for paleohistological analyses were taken from the diaphyseal midshaft. Thin sections of HMNS material were prepared at the IPB (Institut für Paläontologie, Rheinische Wilhelms Universität, Bonn, Germany). Samples from the MPC and DMNH were cut from the specimens at their respective institutions and further prepared at the UALVP palaeohistology laboratory. To preserve material, DMNH limb bones could not be cut completely, so billets were instead removed from the elements using an electric oscillating saw.

DMNH samples were stabilized via resin impregnation using Buehler EpoThin Low Viscosity Resin and Hardener. Thin sections were mounted to Plexiglas slides and prepared

petrographically to a thickness of 60–80 μm via grinding against a glass plate with silicon carbide powder (SiC400, SiC600, and SiC800) and polished using CeO_2 powder.Sections were examined at the UALVP on a Nikon Eclipse E600POL trinocular polarizing microscope with an attached Nikon DXM 1200F digital camera. Scans of the slides were taken with a Nikon Super Coolscan 5000 ED.

3.3 RESULTS

3.3.1 Juvenile *Pinacosaurus*

The limb bones of juvenile *Pinacosaurus grangeri* all share a similar histology consisting of a cortical matrix of fibrolamellar bone (FLB) of various vascular patterning and a medullary region composed of trabecular bone. Vascular orientation within the cortex varies. Most specimens display patterns of change from one orientation to another (moving from deep to superficial) and in some cases, namely in the radii, show isolated regions with radially-oriented vascular canals. Few of the sectioned specimens preserve cyclical growth marks (CGMs); however, a radius and fibula do, indicating that at least one specimen was at least three years old at the time of death. Many of the specimens also show significant crushing, making any CGMs preserved difficult to discern.

Humeri—Two humeri (Fig. 3.1) were sectioned from HMNS: 90-11-65 and 95-11-5. The medullary region consists of primary trabecular bone, but the level of porosity is difficult to estimate due to post-mortem crushing of this region in both specimens. The crushing also makes it difficult to follow and identify CGMs. The cortex is similarly crushed, but it is evident that it

consists entirely of primary FLB. From deep to superficial, there is an alternating pattern of reticular and circumferential vascular canals, although this is not the case everywhere (in places the orientation is more longitudinal). In HMNS 90-11-65, two CGMs can be roughly traced around the cross-section. These may represent annuli, because they have some measurable thickness, but may also simply represent the transition between two different zones of vascular orientation. HMNS 95-11-5, the larger specimen, has a relatively larger medullary area, and the cortex appears to have greater abundance of reticular FLB, although this specimen is more badly crushed.

Radii—The radii (Fig. 3.2), similar to the humeri, show a medullary region consisting of primary trabecular bone and cortices with no signs of remodeling. Unlike in the humeri, however, vascularity of the cortical FLB in the smaller radii is predominantly longitudinal. In HMNS 95-11-65, one region of radial vascularity is present, with reticular vascularity forming a transitional region between the longitudinal and radial bone. The larger radius (HMNS 00-11-1; Fig. 3.2B) shows more reticular FLB in the cortex, but still has a single region of radial FLB similar to HMNS 95-11-65. This reticular region may also have been present in HMNS 95-11-5, but is no longer visible due to more extensive crushing in this specimen. The large specimen (HMNS 00-11-1) also shows three LAGs. These LAGs, however, appear to split around the circumference of the section, although the point at which they do so is not visible due likely to crushing of the specimen.

Femora—The femora (Fig. 3.3) from Alag Teeg show medullary regions consisting of trabecular bone. Their cortices show a preponderance of longitudinally-oriented vascular canals in their cortical FLB, although in some isolated areas, vascularity takes on a more reticular appearance. Like the radii, several specimens have one region of predominantly radial vascular

orientation on the posterior surface. One of the femora from MPC-D 100/1322 has a greater contribution of reticular FLB, with only isolated patches of longitudinal canals. The largest femur sampled (HMNS 00-11-1) actually shows signs of faster deposition: a higher proportion of radial and reticular canals, as opposed to longitudinal canals. Canals open to the periosteal surface indicate that bone was still being deposited at this stage.

Fibulae—Two fibulae (Fig. 3.4) were sectioned and have trabecular medullary regions. Although somewhat crushed, the cortex of the smaller one (HMNS 95-11-25) has some intact areas that show alternation regions of circumferential and reticular FLB most similar to the histology seen in the humeri. The larger fibula (HMNS 08-6-49), although badly crushed does show one LAG in the outer cortex. Unlike in the radius, this LAG does not appear to split.

3.3.2 Subadult *Gastonia*

The long bone histological sections of *Gastonia* sp. show preservation of the primary growth record. The core is composed of secondary trabecular bone. The trabeculae tend to be relatively thinner than in *Pinacosaurus*, allowing for increased porosity in the medullary region. The primary cortical tissue consists of FLB preserving abundant CGMs in the form of LAGs, annuli, and zones. In some bones, the record of growth preserved correlates with element size, whereas in others, it does not.

Humeri— The humeri (Fig. 3.5) of *Gastonia* tend to show well-preserved annual growth records. DMNH 50110, the smallest humerus sampled, shows a broad zone of poorly vascularized, azonal, primary parallel-fibreed bone just deep to the periosteal surface. Element size and degree of secondary remodeling are proportional: the largest humerus (DMNH 57651;

Fig. 3.5D) exhibits dense Haversian remodeling throughout most of the cortext, with only a thin layer of primary periosteal bone. Consequently, no evidence of the primary growth record is preserved. Except for this largest specimen, the number of identifiable LAGs is correlated with element size despite encroachment by remodeling. Several of the humeri of intermediate size also exhibit annuli associated with LAGs, such as DMNG 53339 and 61109.

Radii— The radii (Fig. 3.6) of *Gastonia* show more remodeling than the humeri and, as a result, there is less of a correlation between element size and the number of LAGs preserved. The smallest radius retains only one definitive LAG. This appearsin the outermost cortex. Specimens of intermediate length range show from two to five LAGs, and the largest radius (DMNH 50302; Fig. 3.6A; almost twice as long as the next largest radius in the sample) preserves four. Also in the largest radius, the extent of remodeling is variable depending on position. In some areas, dense Haversian remodeling spans from the medullar cavity all the way to the periosteal surface. In other areas, primary bone including LAGs and annuli may be observed. Other specimens (such as DMNH 53084; Fig. 3.6D) show strong zonation, but not all CGMs may be confidently identified as LAGs.

Ulnae— The sectioned ulnae (Fig. 3.7) are similar to the radii in that the preservation of CGMs is more variable than in the humeri. Nevertheless, the largest ulna (DMNH 61129; Fig. 3.7E) also preserves the largest number of LAGs (6). The remainder show two or three lags each. The nature of CGMs is also more variable than in the other forelimb elements. Strong zonation is seen in some specimens, although these features cannot be confidently identified as annuli. Others show “bright lines” (*sensu* Stein et al., 2013) that may be analogous to LAGs; however, they are in places cross-cut by or deviate around other features of the primary tissue like vascular canals. Some of these are associated with changes in the size and/or density of osteocyte lacunae.

Femora— The femora (Fig. 3.8) show a great degree of zonation, making LAGs difficult to distinguish from annuli, regular changes in vascular orientation and other CGMs. The number of LAGs preserved is highly variable and is likely influenced by the degree of internal remodeling. For example, DMNH 50265 (Fig. 3.8A) preserves two LAGs, but also has a nearly avascular region of the outermost cortex composed of zonal parallel-fibreed bone that may indicate cessation of growth. The largest femur sampled, DMNH 50082, preserves the most extensive growth record of all elements sectioned from Gastonia, with seven definitive LAGs along with annuli and other CGMs.

Tibiae— All of the tibiae (Fig. 3.9) preserve some CGMs that are identifiable as annuli. Many of these are associated with bright lines, interpreted as LAGs or equivalent to LAGs (Stein et al., 2013). These lines are variously situated immediately superficial to or within the annuli. In some areas, annuli are observable without any associated LAGs. The number of LAGs in the tibiae are, however, variable and not strongly correlated with element size. The smallest tibia sectioned (DMNH 61133; Fig. 3.9E) preserves only two LAGs, although it is more vascularized than the other specimens.

Fibulae— The fibulae (Fig. 3.10) of *Gastonia* preserve a poorer record of growth than the other limb elements investigated here. These elements also tend to be poorly vascularized, showing only sparse longitudinally-oriented vascular canals. There is also no correlation between element size and degree of remodeling. The specimen that shows the most secondary bone in the cortex (DMNH 53858) is actually the smallest fibula examined. The largest fibula (DMNH 52077) retains some record of primary growth, although secondary remodeling has overprinted some of the cortex.

3.4 DISCUSSION

3.4.1 Bone histology and ontogeny in ankylosaurs

Juvenile and subadult ankylosaur long bones, represented here by *Pinacosaurus* and *Gastonia*, do not appear to exhibit unique tissue types for Dinosauria (Ricqlés, 1980; Horner et al. 1999, 2000, 2001; Padian et al. 2004; Hayashi et al., 2010). Stein et al. (2013) report heavily remodeled bone as making up the entire cross section of adult ankylosaur limb elements, in both nodosaurids and ankylosaurids. This is unlike the case in other dinosaurian groups that typically preserve greater relative amounts of primary bone in even the largest specimens, such as in sauropods (Curry, 1999) and tyrannosaurids (Erickson et al., 2004). The relatively small remnants of primary bone in large ankylosaur limb bones are restricted to the outermost cortex and/or isolated interstitial patches among secondary osteons (Stein et al., 2013). These demonstrate that the primary tissue was composed of poorly-vascularized fibrolamellar bone, or parallel-fibreed in some larger specimens, with longitudinal vascularization and Sharpey's fibres. A smaller specimen, a radius (48% maximum known size), showed a higher degree of vascularity with a reticular pattern (Stein et al., 2013). In *Stegosaurus*, primary bone tissue displays similar ontogenetic changes: from radial/reticular azonal FLB in small individuals to longitudinal FLB with LAGs to, in the largest individuals, FLB with LAGs and an EFS (Hayashi et al., 2009).

3.4.2 Individual Variation

Horner et al (2000) demonstrated considerable variability in the number of LAGs preserved within skeletal elements from a single individual in *Maiasaura*. In addition, the number of LAGs in modern *Alligator mississippiensis* limb elements is known to vary from element to element within a single individual (Woodward et al., 2014). Here, in juvenile *Pinacosaurus*, the lower number of specimens precludes making a similar comparison between elements within individuals.

Because the elements of *Gastonia* are from a bonebed assemblage that preserves no articulated material, it is unknown if more than one bone that I sectioned comes from the same individual. Nevertheless, whereas comments on histological variability among skeletal elements of an individual are not possible, variation in histology is observed within single elements based on position. Secondary remodeling occurs in larger elements unevenly around the circumference of the cortex. In some elements, this leads to the preservation of primary tissue in some regions of the cortex and its erasure by encroaching Haversian bone in others.

3.4.3 Growth Dynamics

Unless they reach somatic maturity in under one year, most if not all living vertebrates deposit some form of CGMs in their skeleton and these have been demonstrated to be deposited annually in living archosaurs (Peabody, 1961; Frylestam and Schantz, 1977; Hutton, 1986; Castanet et al., 1993; Klevezal, 1996; Tucker, 1997; Horner et al., 1999; de Bufrénil and Castanet, 2000; Castanet et al., 2004; Köhler et al., 2012). Although CGMs preserved in osteoderms have been used for skeletochronology in extant archosaurs (Hutton, 1986; Tucker, 1997), the same is not possible for ankylosaurs, in which osteoderms undergo extensive

remodeling to create their varied morphologies (Burns and Currie, 2014; Burns and Vavrek, 2014). Although CGMs have been reported in ankylosaur ossicles (Burns and Currie, 2014), they cannot be correlated with age estimates based on other sources (e.g., long bone histology). Stein et al. (2013) reported CGMs in the form of bright lines in adult ankylosaur limb bones, none of which could be unequivocally identified as LAGs.

Here, numerous CGMs are identified in the *Gastonia* sample, including LAGs and annuli. However, several factors preclude the construction of a growth dynamic curve based on the data available. First, complete cross-sections were not possible for the *Gastonia* sample and, although samples were cut from similar midshaft regions, the degree of diagenetic crushing has distorted histological features in many specimens. Second, accurate growth models require whole-animal mass estimates (or a reasonable proxy thereof), which, if it is to be accurate for quadrupeds, necessitates femoral and humeral measurements for a single individual (Campione and Evans, 2012). This is not possible with the disarticulated *Gastonia* material.

In *Apatosaurus*, LAGs were not deposited until an animal reached 91% adult size, before which azonal FLB dominated in the cortex (Curry, 1999). The hadrosaurid *Maiasaura* likely grew to 3m in its first year with onset of somatic maturity occurring by age 7 (Horner et al., 2000). The age which this decrease in growth rate occurs in *Psittacosaurus* has been estimated a 9 years (Erickson and Tumanova, 2000). Estimates for saurischian taxa include the small theropods *Coelophysis* (7–8 years; Chinsamy, 1990) and *Troodon* (3–8 years; Varricchio, 1993; Erickson et al., 2004), the sauropods *Janenschia* (26 years; Sander, 2000) and *Lapparentosaurus* (20 years, de Ricqlés, 1983), *Tyrannosaurus* (18.5 years; Erickson et al., 2004), and the Albertan tyrannosaurids *Albertosaurus*, *Daspletosaurus*, and *Gorgosaurus* (14–16 years; Erickson et al.,

2004). Relatively moderate growth trajectories are generally associated with relatively small ornithischians, such as the "hypsilophodontid" *Orodromeus* (Horner et al., 2009).

In juvenile *Pinacosaurus* specimens, the histological features of the limb bones indicate rapidly growing bone like that reported for other juvenile dinosaurs (Sander, 2000; Horner et al., 2000, 2001; Hayashi et al., 2009). None of the *Gastonia* elements sectioned, not even the largest for each element type, exhibit what may unequivocally referred to as an external fundamental system (EFS). Therefore, none of the specimens may be said to have reached somatic maturity by the time of death. Nevertheless, it is clear that secondary remodeling is extensive in the larger elements. This may mean that ankylosaurs exhibited a more prolonged period of growth rate change from a maximal rate in juveniles to a cessation of growth at maximal size. This is hypothesized to result in a shallower upper inflection of their growth dynamic curve unlike the prominent sigmoidal growth curve hypothesized for other dinosaurs such as tyrannosaurids (Erickson et al., 2004). Nevertheless, ankylosaurs, like *Stegosaurus*, still had higher maximal juvenile growth rates than the basal thyreophorans *Scutellosaurus*, in which the limb bones are characterized by slow-forming zonal parallel-fibreed to lamellar bone (Padian et al., 2004).

3.4.4 Timing of Osteoderm Development

Heterochrony between the mineralization of the endoskeleton and the dermal skeleton in ankylosaurs, like that seen in *Stegosaurus* (Hayashi et al., 2009), means that osteoderms and ossicles cannot be used as an independent source of exact age data in ankylosaurs at present. In *Stegosaurus*, osteoderm ossification is delayed relative to the rest of the skeleton (Hayashi et al., 2009). Based on the absence of osteoderms preserved with otherwise articulated juvenile

material in *Pinacosaurus*, a similar delay has been hypothesized for ankylosaurs as well (Burns and Currie, 2014).

In this study, the presence of extensively mineralized osteoderms is correlated with slower, more cyclical deposition of bone in the limbs. *Pinacosaurus* specimens show largely azonal, fast-growing bone and are devoid of osteoderms other than two incipient cervical half rings (Burns et al., 2011). The *Gastonia* specimens, on the other hand, are associated with fully-developed osteoderms and show more poorly-vascularized bone in their limb elements and more CGMs. The ontogenetically late mineralization of the osteoderms in ankylosaurs has been linked to the extensive remodeling seen early in ontogeny by Stein et al. (2013). In this scenario, similar to the mobilization of calcium from the limb bones during the laying down of the eggshell in modern crocodilians (Schweitzer et al., 2007), remodelling processes were driven by bone metabolism to release calcium for use in osteodermal mineralization. This would have led to the increased secondary remodelling seen here in the subadult stage, in which the limb bones would have reacted to increase mechanical loading. This may also indicate the period of gradually slowing growth hypothesized here for subadults. As remodeling increases in conjunction with the mineralization of the osteoderms, a corresponding decrease in the rate of deposition of primary bone at the periosteal surface is expected.

3.4.5 Structural Fibres

Stein et al. (2013) described diffusely oriented structural fibres within the cortical Haversian bone of large (>71% maximum size) ankylosaur limb bones. The fibres occur in bundles and tend to blur the otherwise crisp hypermineralized resorption lines demarcating the periphery of secondary osteons. In a smaller radius (48% maximum known size), these fibres are

present, but are more sparse than in the larger elements (Stein et al., 2013). Such structures were not observed here in either *Gastonia* or *Pinacosaurus*. It is possible that the incorporation of these fibres into the remodeled bone matrix served to enhance the strength of the Haversian bone, as hypothesized by Stein et al. (2013). The absence of this feature in *Gastonia*, however, which is known to have had fully developed osteoderms by the subadult stage, would not lend support to that hypothesis. Nevertheless, it is possible that these fibres are characteristic of the latest adult ontogenetic stages in ankylosaurs, associated with several generations of secondary osteons.

TABLE 3.1. Elements from juvenile specimens of *Pinacosaurus grangeri* from Alag Teeg histologically sampled. Length is in mm.

Inst.	Number	Element	Length	Side
HMNS	95-11-5	Humerus	150	
HMNS	95-11-5	Femur	180	
HMNS	95-11-5	Radius	100	
HMNS	95-11-25	Fibula		
HMNS	95-11-65	Humerus	131	
HMNS	95-11-65	Radius	85	
HMNS	00-11-1	Femur	220	R
HMNS	00-11-1	Radius	97	R
MPC-D	100/1322	Femur	198	R
MPC-D	100/1322	Femur	210	L
MPC-D	100/1322	Femur	216	L
MPC-D	100/1344	Femur	169	L
MPC-D	100/1344	Femur	186	R

TABLE 3.2. Elements of subadult *Gastonia* sp. from Lorrie's Site histologically sampled. LAGs refers to the maximum number of LAGs identifiable in each section. Length is in mm.

DMNH	Element	Length	Side	LAGs
50082	Femur	509	R	7
50215	Femur	414	L	2
53703	Femur	437	L	5
53705	Femur	390	L	3
50234	Fibula	210	R	1
50238	Fibula	227	R	0
52077	Fibula	248	L	2
53858	Fibula	195	L	1
56725	Fibula	239	R	0
53338	Humerus	297	R	4
53339	Humerus	326	R	5
57651	Humerus	364	R	
61109	Humerus	276	L	3
50302	Radius	304		4
50305	Radius	151		5
50328	Radius	154	R	4
53084	Radius	167		2
53283	Radius	140		1
50114	Tibia	243	L	6
50275	Tibia	294	L	4
51861	Tibia	252	R	1
57685	Tibia			4
61133	Tibia	206	R	2
50265	Ulna	150	L	3
50326	Ulna	195	R	2
51965	Ulna	184	L	3
53089	Ulna	173	L	3
61129	Ulna	218	L	6
50110	Humerus	234	R	3

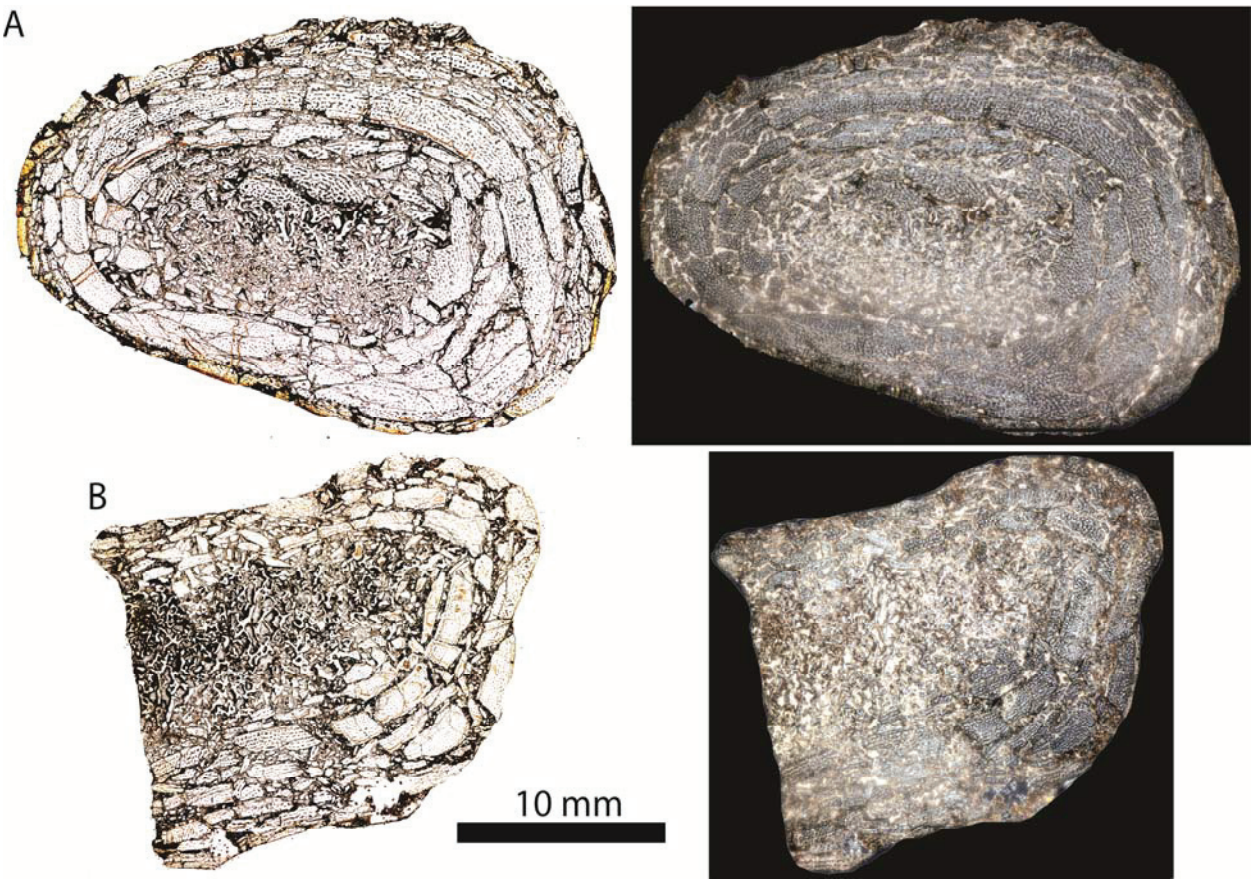

FIGURE 3.1. Thin sections thorugh humeri of *Pinacosaurus grangeri*: HMNS 95-11-5 (A) and 95-11-65 (B) in PPL and XPL. Some zonaton is seen in A in the form of alternating patterns of reticular and circumferential vascular canals in the FLB; however, no LAGs are discernable.

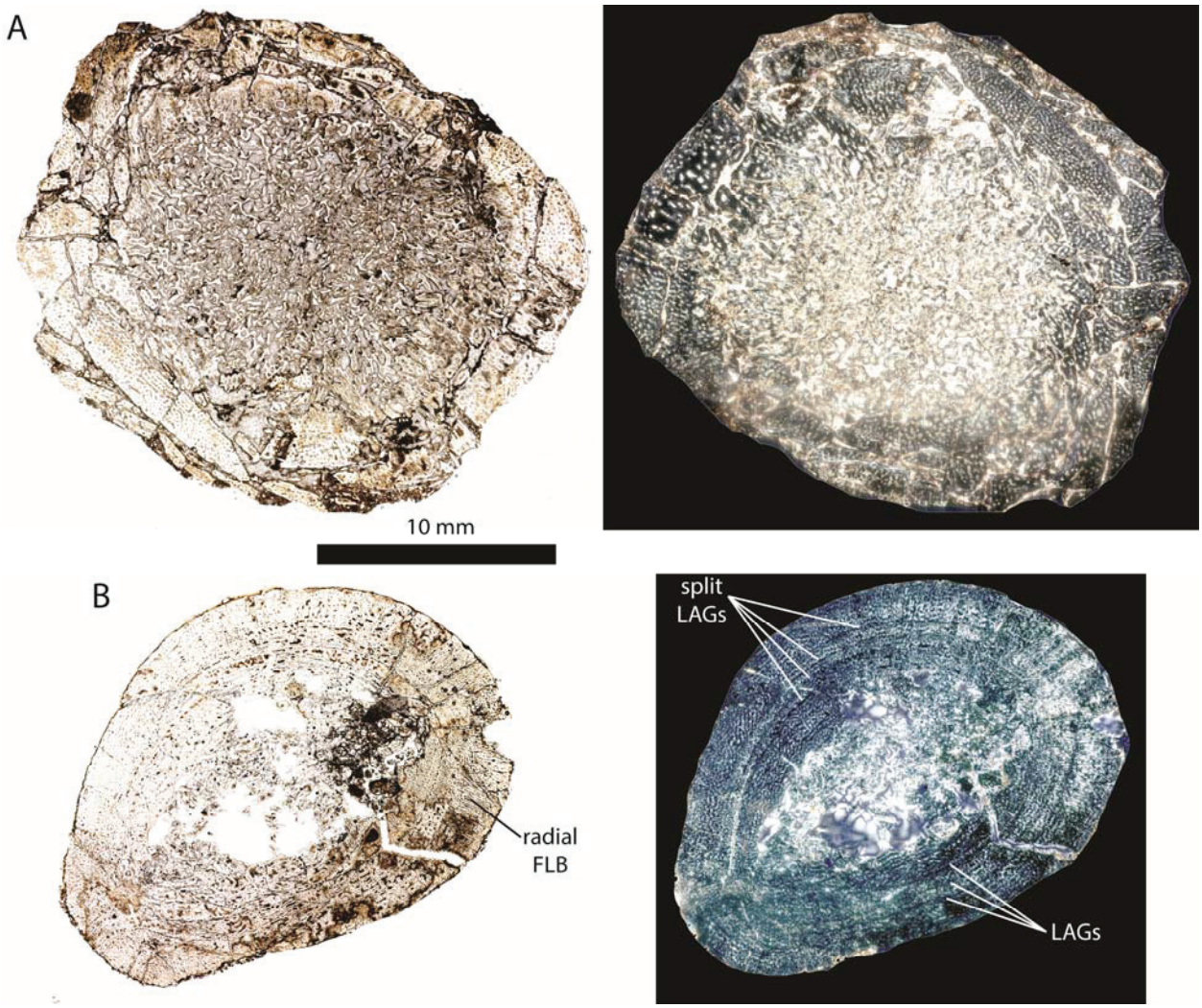

FIGURE 3.2. Thin sections through radii of juvenile *Pinacosaurus grangeri*, HMNS 95-11-25 (A) and 00-11-1 (B) in PPL and XPL. In B, a distinct region of radially-oriented vascular canals is evident. Three LAGs are also visible (lower right) but seem to split into more CGMs in other regions of the cross-section.

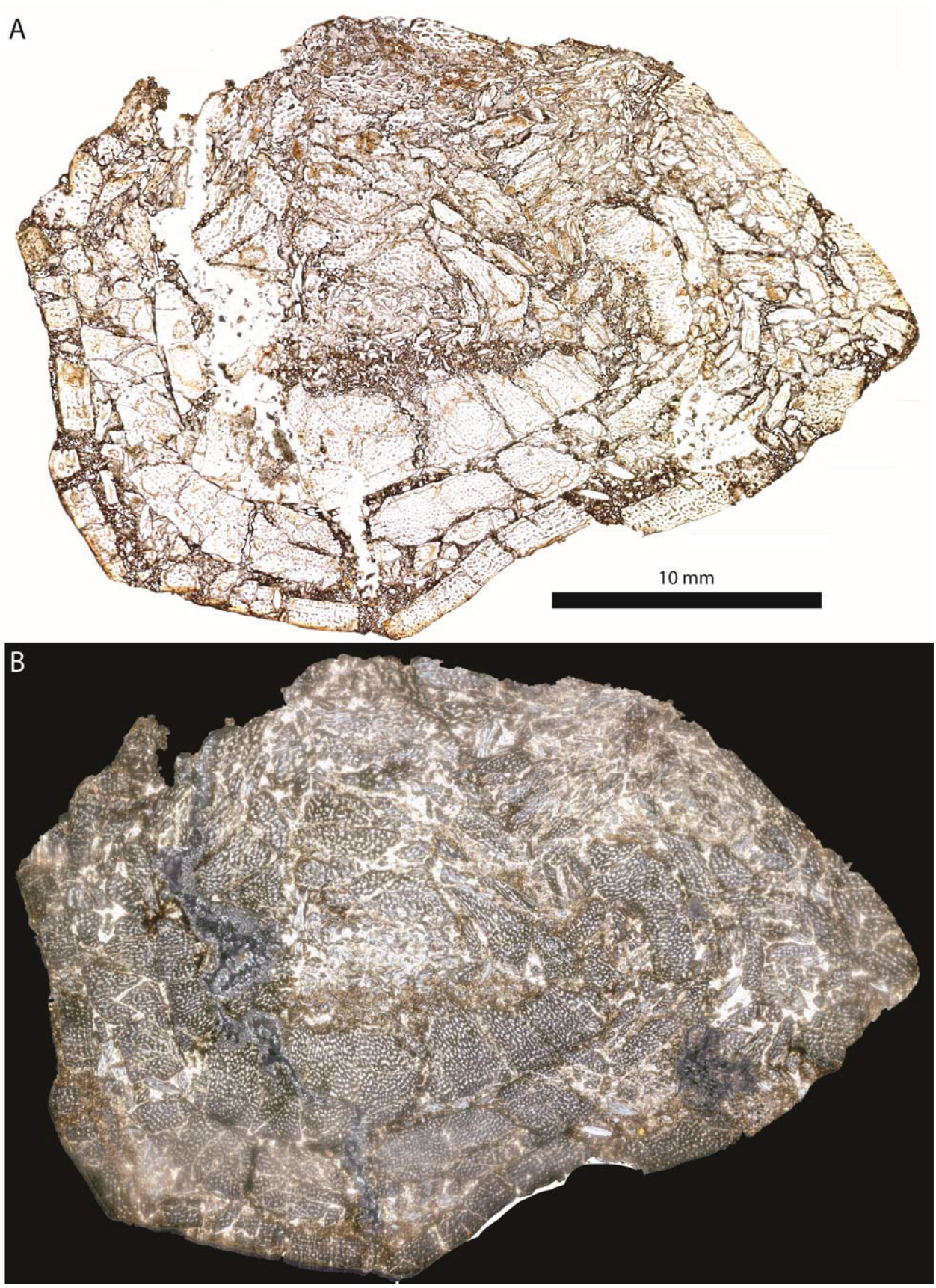
A
10 mm
B

FIGURE 3.3 (previous page). Thin section through femur of juvenile *Pinacosaurus grangeri* (HMNS 95-11-5) in PPL (A) and XPL (B) showing predominantly well-vascularized azonal FLB in the cortex.

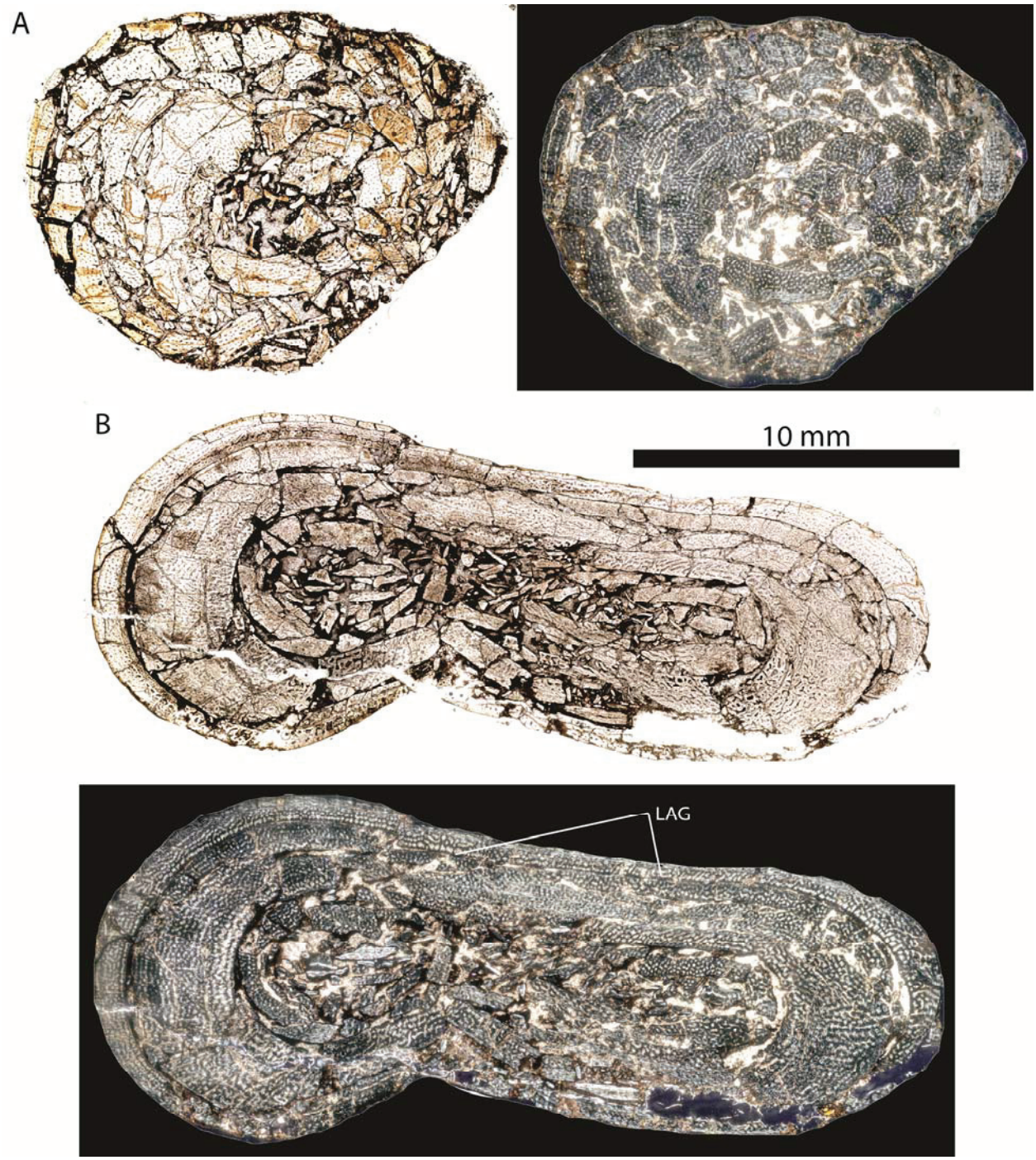

Figure 3.4. Thin section through fibulae of juvenile *Pinacosaurus grangeri* in PPL and XPL: HMNS 95-11-25 (A) and 08-6-49 (B). Zonation, including one LAG, is evident in B.

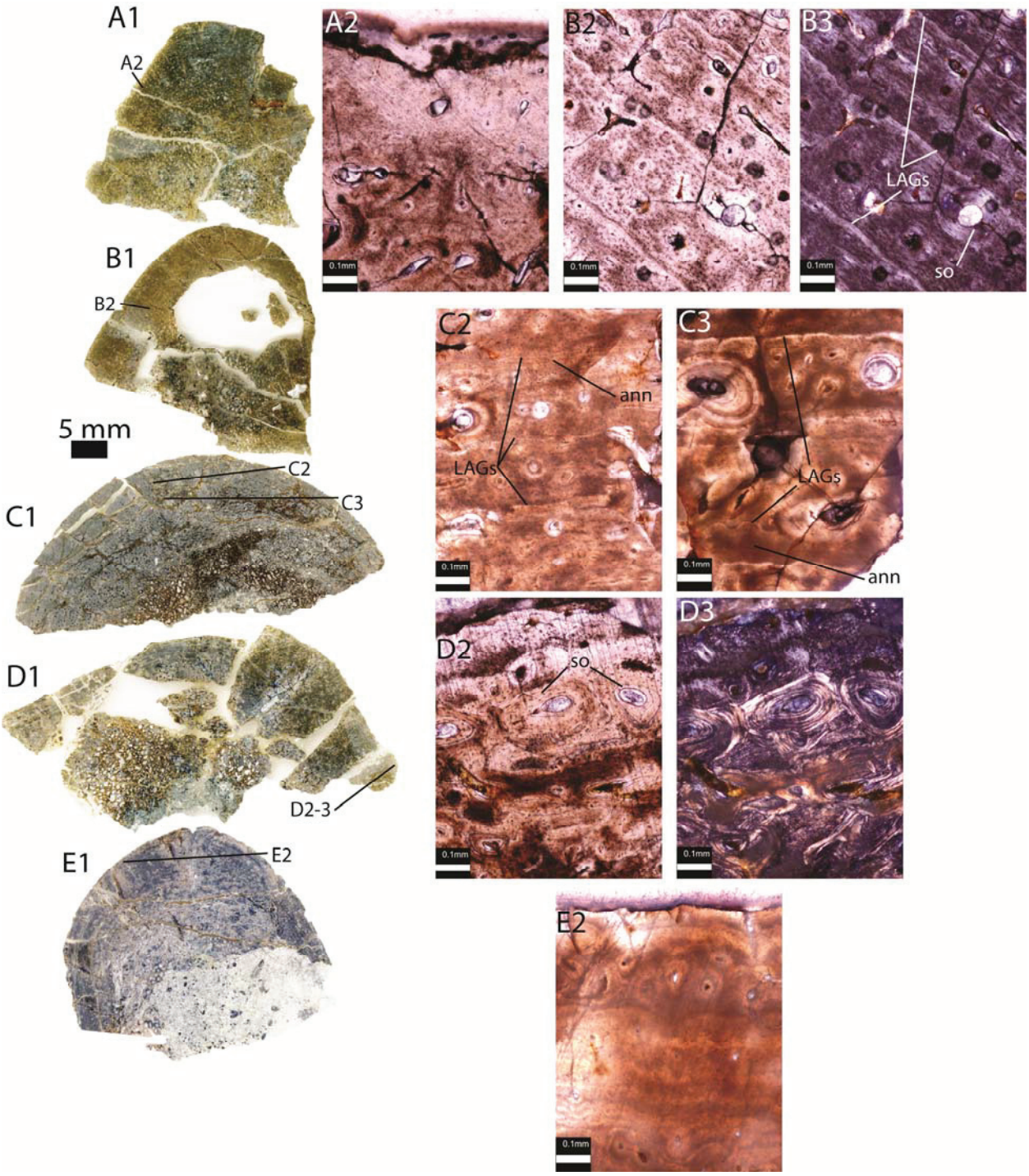
A1
A2
A2
B2
B3
LAGs
so
B1
B2
5 mm
C2
C3
C1
C2
ann
LAGs
C3
LAGs
ann
D1
D2-3
D2
so
D3
E1
E2
E2
0.1mm

Figure 3.5 (previous page). Thin sections through humeri of *Gastonia*. DMNH 50110 (A) with a broad zone of poorly vascularized azonal primary bone at the periosteal surface (A2). DMNH 53338 (B) with LAGs and some remodeling in the deep cortex (PPL in B2, XPL in B3). DMNH 53339 (C) showing some remodeling beginning to overprint LAGs and associated annuli in the superficial (C2) and deep (C3) cortex. DMNH 57651 (D) is almost entirely secondarily remodeled wiuth only a thin layer of primary periosteal bone (PPL in D2, XPL in D3). DMNH 61109 (E) shows zonal bone in the cortex, which is largely made up of annuli and other CGMs with few discernible LAGs (E2). Superficial is up.

Figure 3.6 (next page). Thin sections through radii of *Gastonia*. DMNH 50302 (A) retains LAGs and annuli in some areas of the cortex (A1) but is completely remodeled to the perisoteal surface in others (A2). DMNH 50305 (B) consists largely of primary bone in the cortex with LAGs (B2). DMNH 50328 (C) is simialr to DMNH 50305 with zonal primary bone in the cortex (C2). DMNH 53084 (D) preserves zonal bone without extensive LAGs. D2 shows some weak zonation and abudant Sharpey's fibres near the periosteal surface. DMNH 53283 (E) preserves only one potential LAG in the superficial cortex. Superficial is up.

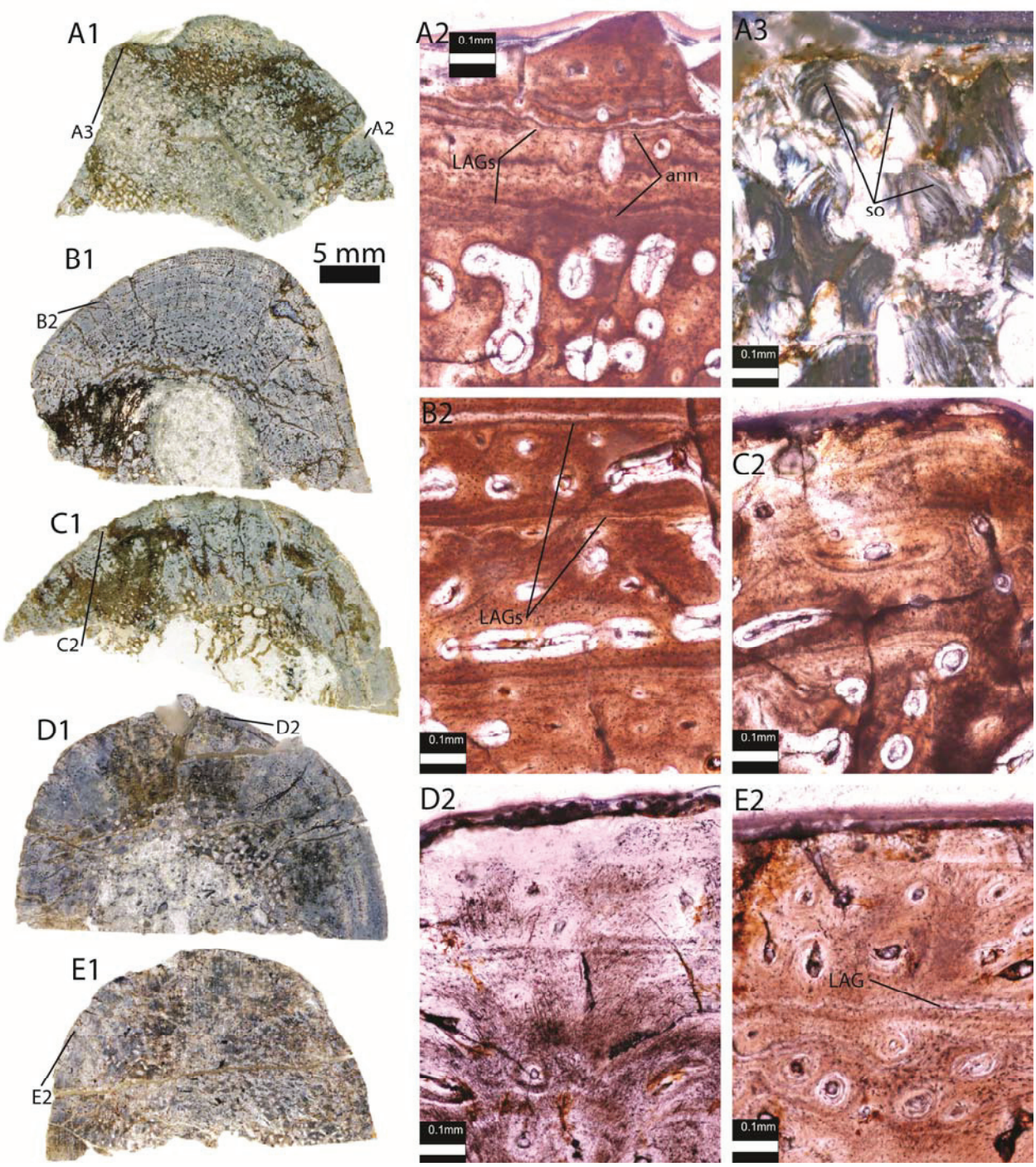
A1
A3
A2
5 mm
B1
B2
C1
C2
D1
D2
E1
E2
A2
0.1mm
LAGs
ann
A3
so
0.1mm
B2
LAGs
0.1mm
C2
0.1mm
D2
0.1mm
E2
LAG
0.1mm

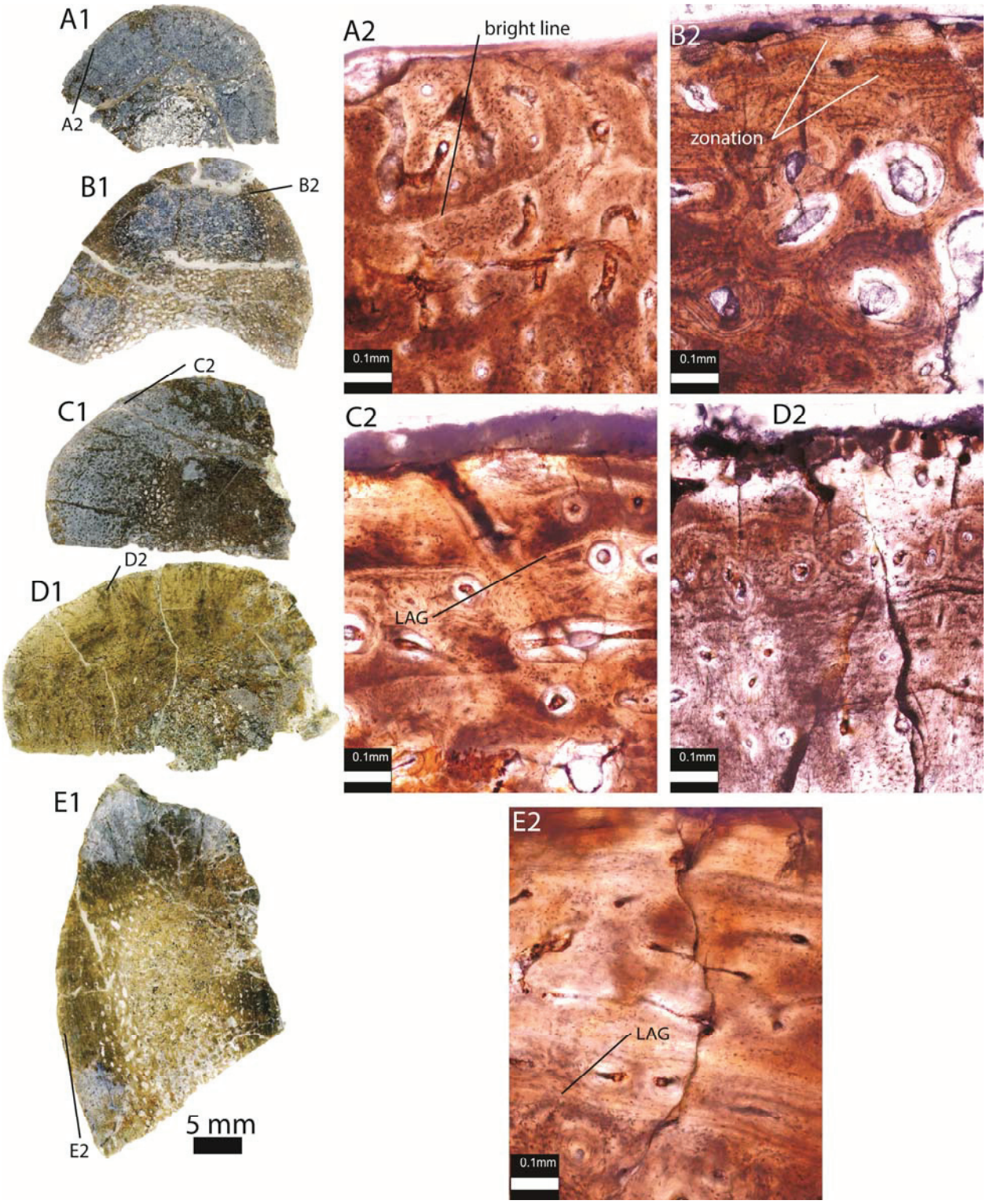
A1
A2
B1
B2
C1
C2
D1
D2
E1
E2
5 mm
A2
bright line
0.1mm
B2
zonation
0.1mm
C2
LAG
0.1mm
D2
0.1mm
E2
LAG
0.1mm

Figure 3.7 (previous page). Thin sections through ulnae of *Gastonia*. DMNH 50265 (A) with weak zonation in the form of a bright line (A2) near the perisoteal surface. DMNH 50326 (B) shows strong zonation at the perisoteal surface and extensive remodeling (B2). DMNH 51965 (C) also shows periosteal zonation, but retains LAGs deeper due to less extensie remodeling then in DMNH 50326. DMNH 53089 (D) has zonation in the superficial cortex (D2, also note the incorporation of extensive Sharpey's fibres in the primary matrix). DMNH 61129 (E) retains LAGs in the superficial cortex associated with visible changes in osteocyte lacunar density despite some secondary remodeling (E2).

Figure 3.8 (next page). Thin sections through femora of *Gastonia*. DMNH 50082 (A) showng several LAGs from superficial (A2) to deep (A5) and associated annuli (A6) near the periosteal surface. DMNH 50215 (B) consisting largely of azonal FLB with longitudinally orineted vascular canals (B2), but with a region of poorly-vascularized parallel-fibered bone near the periosteal surface (B3). DMNH 53703 (C) with several superficial (C2) and deep (C3) LAGs and annuli. DMNH 53705 (D) showing LAGs associated with annuli (D2). Superficial is up.

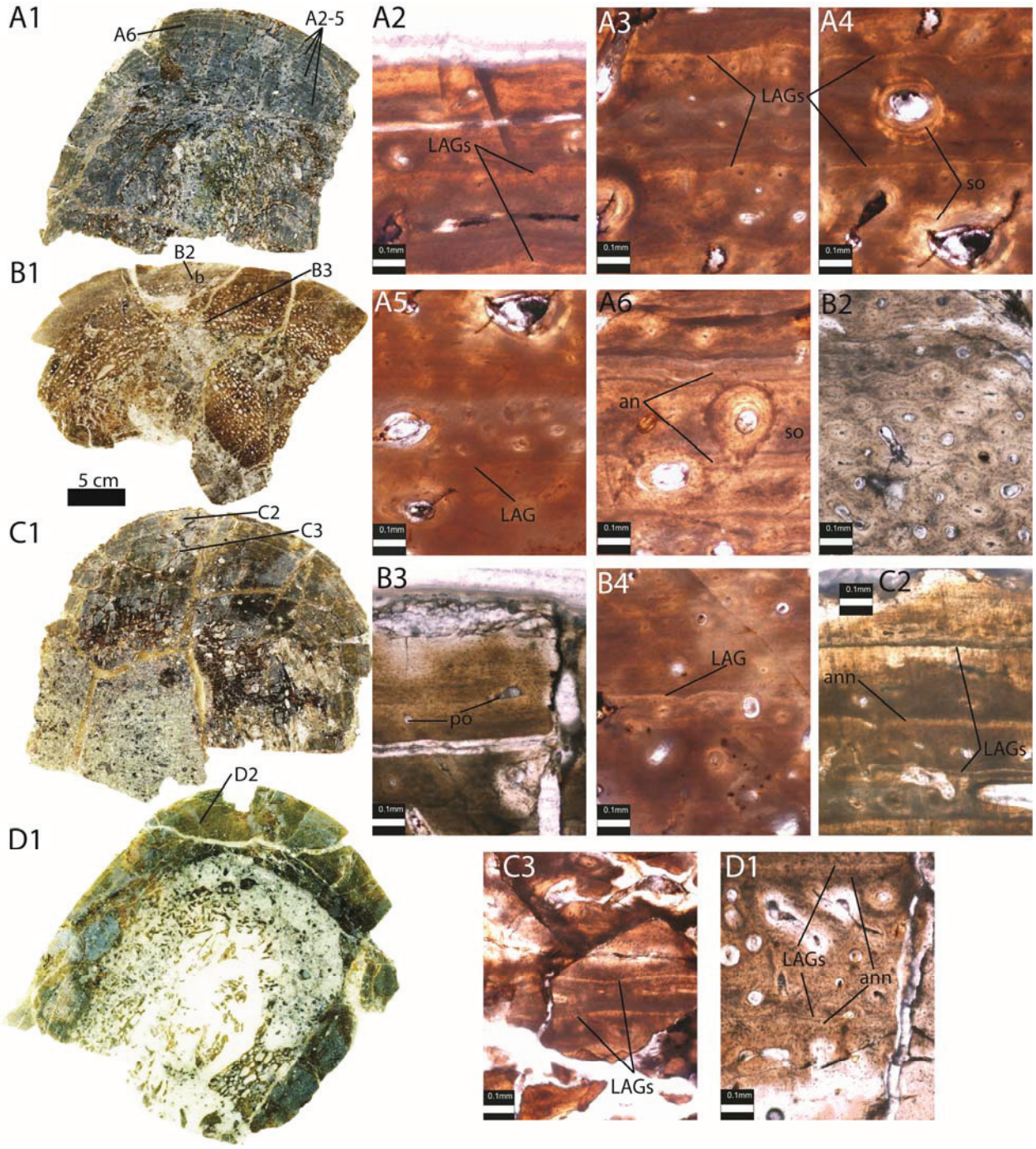
A1
A6
A2-5
B1
B2
b
B3
5 cm
C1
C2
C3
D1
D2
A2
LAGs
A3
LAGs
A4
so
A5
LAG
A6
an
so
B2
B3
po
B4
LAG
C2
ann
LAGs
C3
LAGs
D1
LAGs
ann
0.1mm

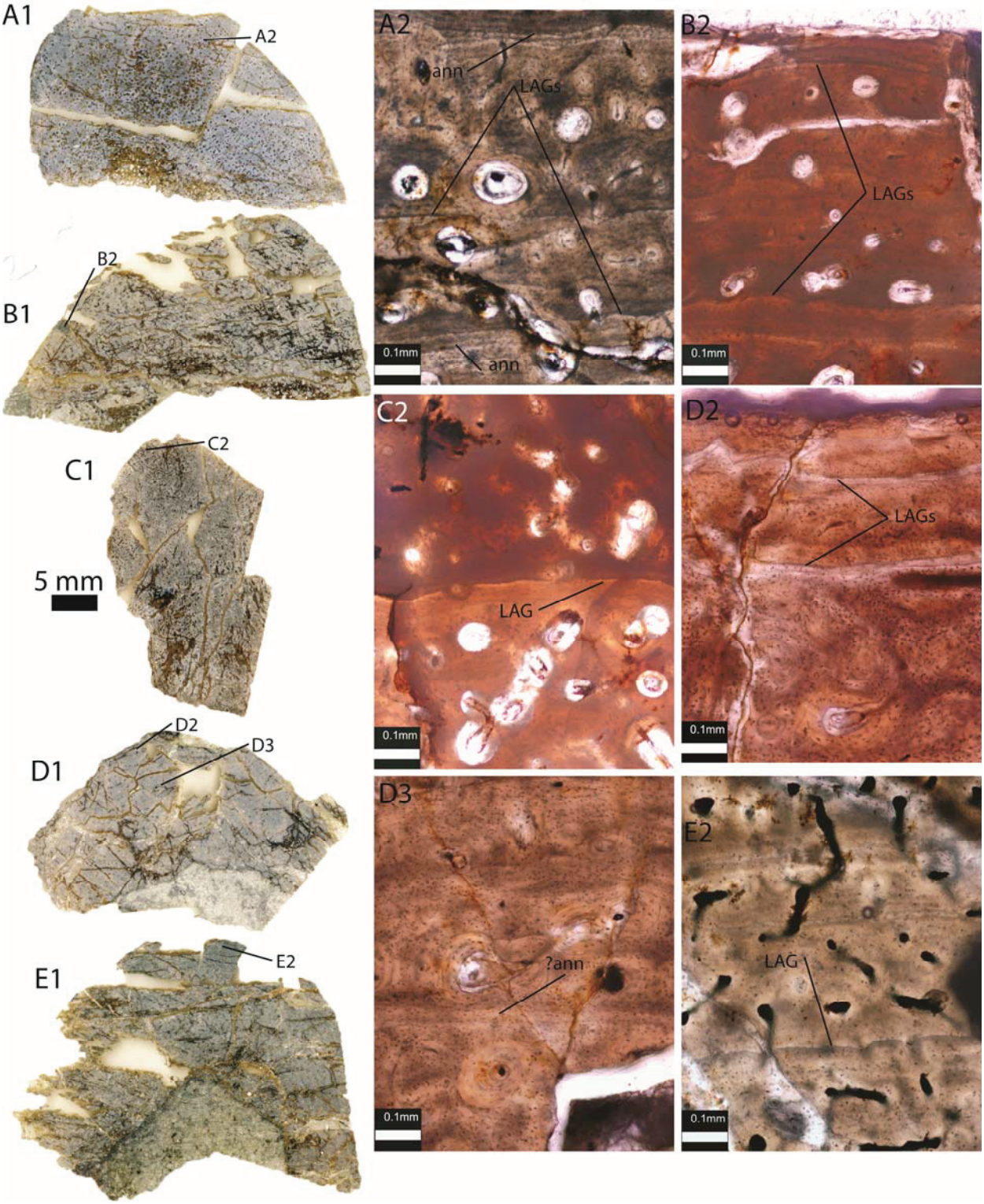
A1
A2
B2
B1
C2
C1
5 mm
D2
D3
D1
E2
E1
A2
ann
LAGs
ann
0.1mm
B2
LAGs
0.1mm
C2
LAG
0.1mm
D2
LAGs
0.1mm
D3
?ann
0.1mm
E2
LAG
0.1mm

Figure 3.9 (previous page). Thin sections through tibiae of *Gastonia*. DMNH 50114 (A) has extensively developed LAGs and annuli throughout the cortext (A2). DMNH 50275 (B) shows a similar development of LAGs (B2). DMNH 51861 (C) is more badly crushed than the other samples, but does preserve on LAG (C3). DMNH 57685 (D) showing LAGs near the periosteal surface (D2) and annuli lacking definite LAGs in the deeper cortex (D3). DMNH 61133 (E), better vascularized than the other tibiae with some reticular vascular canals, shows some zonation and LAGs within the primary bone (E2). Superficial is up.

Figure 3.10 (next page). Thin sections through fibulae of *Gastonia*. DMNH 50234 (A) showing LAGs and annuli in the outer cortex (A2) with some secondary remodeling. DMNH 50238 (B) is largely secondarily remodeled but retains some zonation (B2) at the periosteal surface. DMNH 52077 (C) preserves LAGs and annuli in the outer cortex (C2) with secondary osteons only beginning to encroach upon and overprint the primary bone. DMNH 53858 (D) is almost entirely remodeled, but preserves some primary zonal bone at the periosteal surface (D2). DMNH 56725 (E) has been comepletely remodeled and consists entirely of dense Haversian bone (E2). Superficial is up.

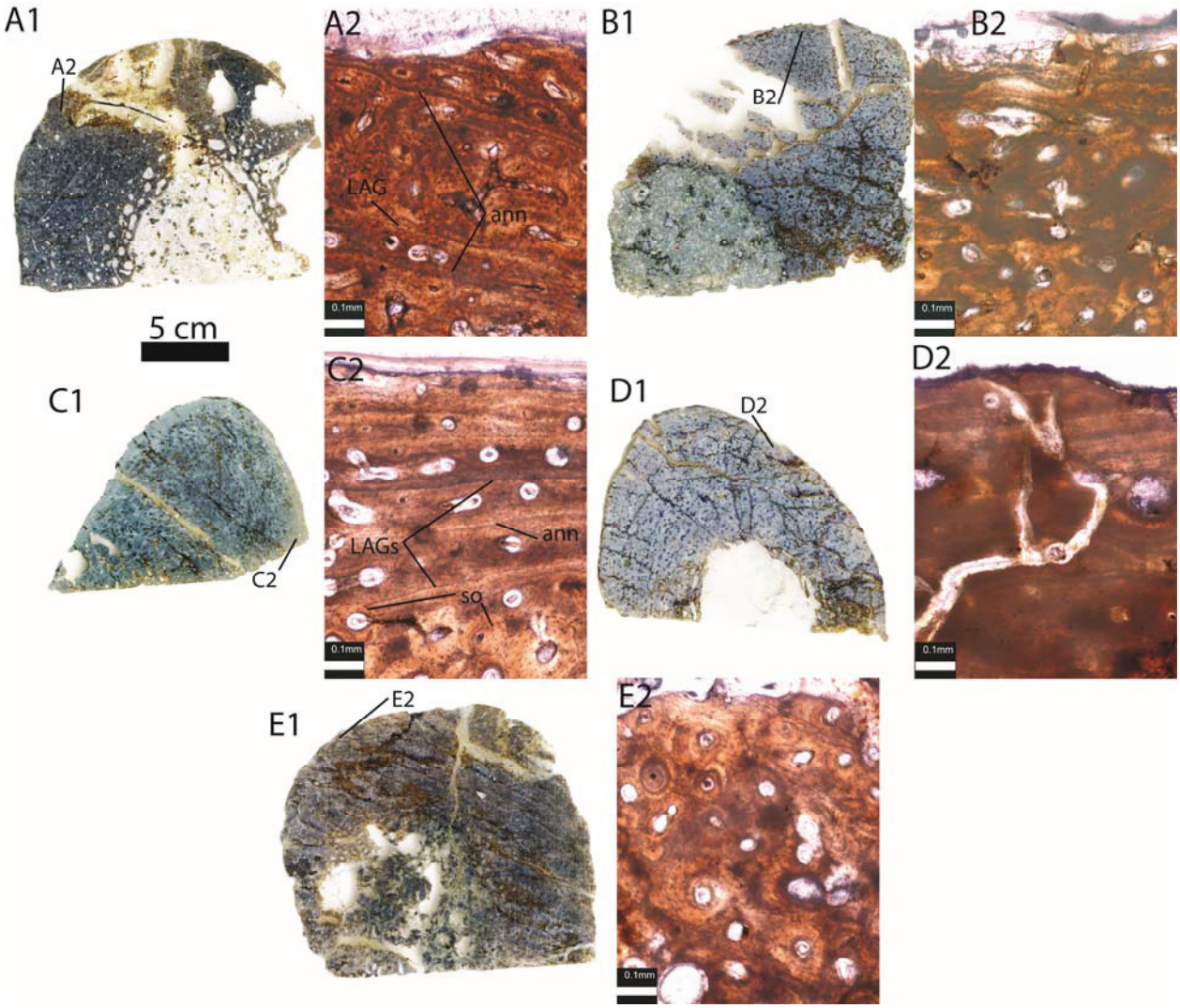
A1
A2
5 cm
A2
LAG
ann
0.1mm
B1
B2
B2
0.1mm
C1
C2
C2
LAGs
ann
so
0.1mm
D1
D2
D2
0.1mm
E1
E2
E2
0.1mm

CHAPTER 4

A TAXONOMIC REVISION OF THE LATE CRETACEOUS NODOSAURIDAE

4.1 INTRODUCTION

Armoured dinosaurs (ankylosaurids and nodosaurids) of the Late Cretaceous are often less commonly preserved than contemporaneous ceratopsians and hadrosaurs. In Dinosaur Provincial Park (DPP), the number of articulated remains and significant cranial material of ankylosaurs is half that of hadrosaurs but roughly equal to ceratopsians; however, disarticulated ceratopsian remains in bonebed assemblages make them the most common dinosaur taxa in DPP (Eberth and Getty, 2005; Ryan and Evans, 2005). Ankylosaur bonebeds are rare, and generally include ankylosaurids (Burns et al., 2011). Although the large-bodied nodosaurid *Peloroplites* is known from a bonebed assemblage (Carpenter et al., 2008), derived Upper Cretaceous nodosaurid specimens tend to be discovered as isolated individuals.

The nodosaurid genera *Edmontonia* and *Panoplosaurus* (including their junior synonyms) include relatively large-bodied (total length 6–7 m; Vickaryous et al., 2004) forms from the Upper Cretaceous of Canada and the United States. They are often well-supported in phylogenetic analyses as belonging to their own clade within Nodosauridae (Lee, 1996; Kirkland, 1998; Carpenter et al., 1998; Carpenter, 2001; Hill et al., 2003; Vickaryous et al., 2004) and are represented by numerous well-preserved and nearly complete cranial and postcranial specimens. Many of the specimens of these two genera are contemporaneous or nearly so (Fig. 4.1), although they have only been found as isolated individuals. In addition to their similar stratigraphic occurrence, these taxa also likely overlap geographically.

The first ankylosaur taxon named from North America was actually a Late Cretaceous nodosaurid, *Paleoscincus costatus* (Leidy, 1856) based on a tooth from the Campanian of Montana. Its defining characters have since been recognized as diagnostic for Nodosauridae (Coombs, 1978, 1990). *Panoplosaurus mirus* Lambe, 1919, was named on the basis of a complete skull and partial articulated postcranium (CMN 2759) from the Dinosaur Park Formation (DPF) of DPP. From the younger Horseshoe Canyon (HCF of Alberta, Sternberg (1928) named *Edmontonia longiceps* (CMN 8531). Gilmore (1930) named *Paleoscincus rugosidens* (USNM 11868) shortly thereafter.

Nodosaurus textilis, the sole species of the type genus of the Nodosauridae, was named by Marsh (1889) on the basis of a partial postcranial skeleton and several osteoderms from the Frontier Formation of Wyoming. *Niobrarasaurus coleii*, originally named by Mehl (1936) as *Hierosaurus coleii*, was revised by Carpenter et al. (1995) and given its new genus. It is known from a single partial skeleton recovered from the Niobrara Chalk Formation of Kansas, representing one of the few ankylosaurs found in marine strata (most are found in terrestrial sediments; Vickaryous et al., 2004).

Russell (1940) described a skull and partial skeleton from the DPF of DPP (ROM 1215), which remains possibly the most complete and well-preserved nodosaur specimen collected. He assigned it to Gilmore's (1930) *Paleoscincus rugosidens*, but synonymized it with *Edmontonia* as *Edmontonia rugosidens*. Russell (1940) still recognized the validity of *Panoplosaurus* and *Paleoscincus*.

Coombs (1971, 1978), in his revision of the Ankylosauria, synonymized all of the Late Cretaceous nodosaurids with *Panoplosaurus*, as *Panoplosaurus longiceps*, *Panoplosaurus mirus*, and *Panoplosaurus rugosidens* (which included *Paleoscincus rugosidens*). By this time, the

genus *Paleoscincus* had also grown to include *Paleoscincus africanus* Brown, 1910 (Judith River Formation, Montana), *Paleoscincus asper* Lambe, 1902 (Oldman or DPF, Alberta), and *Paleoscincus latus* Marsh, 1892 (Lance Formation, Wyoming). Coombs (1971) assigned *Paleoscincus asper* to *Euoplocephalus tutus* and considered all others *nomina dubia*, referring them to Nodosauridae indet. Coombs (1971) also illustrated the problematic skull proportions by plotting the crania against one another via various cranial proportions, noting that the holotypes of *Panoplosaurus mirus* and *Edmontonia longiceps* lie at opposite ends of a continuum bridged by the remaining referred specimens and *Edmontonia rugosidens* with no clear breaks to aid in taxonomic delineation.

Another skull (DMNH 468), from the Lower Hell Creek Formation of South Dakota, initially mentioned by Carpenter and Breithaupt (1986), was named by Bakker (1988) as *Denversaurus schlessmani*. Bakker (1988) argued that the diversity and evolutionary rates of Late Cretaceous nodosaurs had previously been underestimated, and that they more closely resembled those of ceratopsians and hadrosaurs, offering another revision of the Late Cretaceous nodosaurids that has yet to find common acceptance. In fact, with the exception of ROM 1794, which had an affinity to *Edmontonia longiceps*, and AMNH 5361 and 5665, which were placed in *Edmontonia (Chassternbergia)* sp. 1, Bakker's (1988) nested classification scheme suggested a species (or subspecies in some cases) for each specimen, although they were not all named. In it, *Panoplosaurus mirus* was placed in the Panoplosaurinae Nopcsa, 1928, and ROM 1215 was placed in its own (unnamed) species separate from *Panoplosaurus mirus*. The remaining specimens were classified in Edmontoniinae. *Edmontonia* was divided into the subgenera *Edmontonia* and *Chassternbergia*. The former included *Edmontonia longiceps* and ROM 1714 (although Bakker (1988) mentioned only an affinity for *Edmontonia (Edmontonia) longiceps*), a

postorbital region from a skull from the lower DPF of Alberta. The latter included *Edmontonia (Chassternbergia) rugosidens*, AMNH 5665 (a complete skull), and AMNH 5381 (the latter two as *Edmontonia (Chassternbergia)* sp. 1), both skulls also from the lower DPF of Alberta. All of these Late Cretaceous nodosaurids were placed in the Family Edmontoniidae.

A further revision by Carpenter (1990) presents a classification that has since gained the most recognition (Vickaryous, 2004). At the same time, Coombs (1990) came to similar conclusions based on an examination of teeth. Carpenter's (1990) classification did not differ significantly from Bakker's (1988) but corrected much of the redundant taxonomy and synonymized *Denversaurus* with *Edmontonia*, as *Edmontonia* sp., which also included AMNH 3076, a weathered skull from the Aguja Formation of Texas. A partial skull (DPMWA 90-25) from the late Campanian/early Maastrichtian Matanuska Formation of Alaska was assigned to *Edmontonia* sp. by Gangloff (1995) (not equivalent to *Edmontonia* sp. sensu Carpenter, 1990), who noted that the specimen possessed a combination of characters considered diagnostic for both *Edmontonia* and *Panoplosaurus* (Carpenter, 1990). In addition, Gangloff (1995) agreed with Coombs (1990) that ROM 1215 represented a specimen of *Edmontonia*, not *Panoplosaurus*.

In 2000, Ford named *Glyptodontopelta mimus* and *Edmontonia australis*, both based solely on osteoderms from the Late Cretaceous Ojo Alamo Formation (Naashoibito Member) of the San Juan Basin, New Mexico. Ford (2000) sought to organize the use of osteoderms in ankylosaur systematics and presented a revised classification for Ankylosauria. It largely followed Carpenter's (1990) arrangement although *Denversaurus schlessmani* was considered valid and as Nodosauridae *incertae sedis* as was *Animantarx ramaljonesi*. *Glyptodontopelta mimus* was included in Ankylosauridae, grouped with *Stegopelta landernensis* and the holotype of what would become *Aletopelta coombsi* Ford and Kirkland, 2001 (SDNHM 33909), in the

subfamily Stegopeltinae. In a review of this material, Burns (2008) synonymized *Edmontonia australis* and *Glyptodontopelta mimus*, maintaining the latter as the valid name and removing it to Nodosauridae incertae sedis. Stegopeltinae was considered a redundant taxon because Ford and Kirkland (2001) had classified *Aletopelta coombsi* as an ankylosaurid (Burns, 2008).

Antarctopelta oliveroi Salgado and Gasparini, 2006, known from James Ross Island, represents the only formally-named Late Cretaceous ankylosaur from the southern hemisphere. The holotype was recovered from marine sediments at the base of the Gamma Member of the Santa Marta Formation (Salgado and Gasparini, 2006). Although a pelvic shield consisting of fused polygons is shared by *Aletopelta coombsi*, (possibly) *Antarctopelta ramaljonesi*, *Nodosaurus textilis*, and the early Cretaceous nodosaurid *Sauropelta edwardsorum*, this likely represents convergence or parallelism and is not necessarily an indicator of monophyly (Arbour et al., 2011).

4.1.1 Nodosaurid phylogeny

Several phylogenetic analyses have been conducted on the Ankylosauria (Lee, 1996; Kirkland, 1998; Carpenter et al., 1998; Carpenter, 2001; Vickaryous et al., 2001; Hill et al., 2003; Vickaryous et al., 2004). Thompson et al. (2012) conducted the most recent global parsimony analysis to date, greatly expanding character and taxon sampling; alternative codings for some taxa and characters were proposed by Arbour and Currie (2013a). In the analysis, Nodosauridae was expanded to include many taxa formerly considered basal ankylosaurs and/or "polacanthids." These taxa were united with the nodosaurids on the basis of a narrow posterior skull margin (narrower than at the orbits), doming of the skull roof over the parietals, and

presence of four or fewer phalanges in pedal digit IV, although none of these characters are unambiguous (Thompson et al., 2012).

The resulting inclusion of the "polacanthid" taxa into the Nodosauridae in Thompson et al. (2012) meant a loss of the higher resolution found for the nodosaurids in most prior analyses. Nevertheless, several trends emerged. *Antarctopelta* is recovered as the basalmost nodosaurid, suggesting its occurrence in the Late Cretaceous of Antarctica may be the result of vicariance. The monophyly of nodosaurs nested deep to *Antarctopelta*, however, was not supported by any unambiguous synapomorphy. *Edmontonia+Panoplosaurus* was recovered as the most derived clade of nodosaurids. The close relationship between *Animantarx* and *Edmontonia* of prior analyses was not supported. A monophyletic Struthiosaurinae (sensu Kirkland et al., 2013) was also not recovered. *Denversaurus* was a priori considered a junior synonym of *Edmontonia longiceps*. Thompson et al. (2012) suggested that the low phylogenetic resolution may have been the product of characters that failed to accurately capture the variation within the Nodosauridae.

Here, I revise the clade including *Denversaurus*, *Edmontonia*, and *Panoplosaurus*, incorporating all assignable specimens currently known. Because the observed variability, due to anatomy and diagenetic distortion of many of the specimens, had proven difficult in previous revisions (Bakker, 1988; Carpenter, 1990), diagnostic characters from those revisions are tested here, via a specimen-by-specimen parsimony analysis, in light of new material.

4.2 MATERIALS AND METHODS

4.2.1 Material Examined

Late Cretaceous nodosaurid specimens were examined in the collections of AMNH, BHI, CMN, DMNH, ROM, TMP, UALVP, and USNM throughout the course of this project. The holotype of *Pawpawsaurus* (SMU 73203) was examined via a cast (UALVP 54698). A specimen from Alaska (DPWMA 90-25) was also examined via a cast (TMP 93.11.1). This material was documented via measurements (Tables 4.1–4.5), observations, and photographs. In addition to *Pawpawsaurus*, outgroup taxa included *Emausaurus* and *Scelidosaurus*, the latter two of which were both coded using descriptive information and figures from the literature. Material for *Glyptodontopelta* had been examined previously by me at the NMMNH, SMP, and USNM. Material for *Antarctopelta* and *Niobrarasaurus* were not analyzed, although they are included here in the systematic palaeontology section for completeness.

4.2.2 Quantitative analyses

Measurement data from the crania (Table 4.1) of Late Cretaceous nodosaurid specimens, and *Pawpawsaurus* as an outgroup, were used for PCA and Neighbor Joining analyses in PAST. Because of the inability of these analyses to deal with missing data, the number of taxa included was reduced to 12 including the outgroup. These data were then corrected for specimen size by dividing each measurement by the largest value prior to analysis (Table 4.2).

4.2.3 Character Specimen Matrix and Maximum Parsimony Analyses

The full character specimen matrix (Table 4.3), created in Mesquite 2.75 (build 564), consists of 42 morphological characters (26 (=63%) of which are parsimony informative), three outgroup taxa, and 17 ingroup Late Cretaceous nodosaurid specimens. Overall, 42% of the data

were missing (evenly spread with an average of 42% per character and taxon). To determine character polarity for the ingroup, outgroup taxa included the Early Jurassic thyreophorans *Emausaurus* and *Scelidosaurus*, and Early Cretaceous (late Albian) nodosaurid *Pawpawsaurus*. Safe taxonomic reduction was performed in TAXEQ3 (Wilkinson, 2001) to determine which if any taxa could be safely removed from the matrix without a resulting change in tree topology. All characters were treated as unordered and equally weighted.

Maximum parsimony analyses were conducted in TNT 1.1 via a traditional (=heuristic) search using 1000 replicates and the tree bisection reconnection swapping algorithm (also used for Bremer, bootstrap, and jackknife searches). From the returned fundamental trees, 50% majority rule consensus trees were used for interpretation because strict consensus trees lacked resolution. Bremer supports were calculated retaining suboptimal trees by 50 steps. Bootstrap and jackknife values were calculated using 1000 replicates, a majority rule cutoff value of 50%, and, for the latter, a resampling probability of 0.36. Trees were edited and analyzed in Mesquite version 2.75 (build 564) for Windows and MacClade v. 4.08a for Mac OSX.

4.3 RESULTS

4.3.1 *A Priori* Character Analysis

Anterior snout width—The relative width of the anterior snout was here assessed relative to the overall greatest skull width. Bakker described only ROM 1215 as having the primitive condition of a relatively narrow anterior snout. Indeed, *Pawpawsaurus* has the lowest anterior width to total width ratio (28%) indicating that this is the primitive condition for derived nodosaurids. TMP 81.3.3, however, has a lower ratio (30%) than ROM 1215 (35%). Plotting this

ratio revealed no natural breaks, but dividing them into two groups (excluding *Pawpawsaurus*) on either side of the mean of 46% produced a separation with significantly different means ($p<0.01$). Therefore, this character was scored for derived nodosaurids based on this ratio relative to the mean of 46%.

Ectopterygoid-pterygoid foramen—Bakker (1988) described differences in a foramen piercing the ectopterygoid pad in nodosaur specimens. Russell (1940) noted its presence on ROM 1215 (Fig. 4.2), in which it occurs on the smooth medial surface of the ectopterygoid. In other derived nodosaurids, this foramen is present instead on the anteroventral part of the ectopterygoid pad. Although it cannot be assessed in all specimens due to crushing, it has not been found on the medial surface of the ectopterygoid in any specimen other than ROM 1215 and is, therefore, uninformative, although it is retained here for parsimony analysis.

Encroachment of ornamentation on the anterior infratemporal bar— In lateral view the anterior rim of lateral temporal fenestra was characterized for *Panoplosaurus mirus* and ROM 1215 as being obscured completely by osteodermal encroachment (Bakker, 1988). This character can be seen in other specimens including *Edmontonia longiceps* and *Pawpawsaurus campbelli*. In *Edmontonia rugosidens* and ROM 1215, the rim is partly visible. The distribution of this character within derived nodosaurids may be more complex than previously intimated and it was not used as part of Carpenter's (1990) revision. It is possible that this character is actually ontogenetically variable, although this would need to be tested via juvenile nodosaurid specimens. It is retained here for parsimony analysis.

Internarial bridge— A wider portion of the ornamented premaxillae and nasals between the external nares (Fig. 4.3) was cited by Bakker (1988) as diagnostic for *Panoplosaurus*+ROM 1215. In terms of absolute width, this bridge is narrower in *Pawpawsaurus* than in derived

nodosaurids (mean 84 mm, SD=±26 mm); however, it is of only intermediate width in *Panoplosaurus* (78 mm) and ROM 1215 (55 mm). As a percentage of anterior snout width, the relative width of the internarial bridge in *Panoplosaurus* is high (70%) but low in ROM 1215 (52%), although both fall within the range of variation of other specimens (mean=60%, SD=±16%). The only real outliers are TMP 83.25.2 at 95% and CMN 8879 at 32%. Because it would not be informative, this character was not used.

Mid-snout region— *Panoplosaurus mirus* has been described as having a plumper mid snout region versus *Edmontonia* spp., which shows an hourglass constriction (Bakker, 1988; Carpenter, 1990). This was tested here by measuring the angle of taper of the edges of the snout and as a ratio between maximum and minimum skull widths. As preserved, *Denversaurus schlessmani* actually has the greatest width ratio (87%) and TMP 98.98.1 the smallest (28%). The angle of the snout relative to the median sagittal plane varies bilaterally in many specimens, although a low angle in *Pawpawsaurus campbelli* (13°) indicates a tapering snout is the primitive condition. The same angle for *Denversaurus schlessmani* (20°) falls between *Edmontonia longiceps* (17°) and *Edmontonia rugosidens* (30°), the latter of which shares the highest angle with AMNH 5381. Because there are no obvious quantitative breaks, this character has been simplified to refer to the lateral line of the snout as viewed dorsally from the postorbital prominence to the anterolateral corner of the premaxilla. In DPMWA 90-25, *Panoplosaurus mirus*, ROM 1215, and TMP 83.25.2 this edge is flat to convex, whereas it is concave in all other specimens for which this region is preserved.

Posterior displacement of orbit— There are no natural breaks in a plot of antorbital versus postorbital skull lengths with respect to derived nodosaurs. *Pawpawsaurus* and TMP 98.98.1 all have shorter postorbital lengths irrespective of different antorbital lengths. TMP

98.67.1 has an unusually long antorbital length. The holotype of Denversaurus, however, clusters with other derived nodosaurs with respect to both dimensions. Nevertheless, whereas some specimens may be differentiated by absolute antorbital or postorbital length, the ratio between these two measurements produces no morphological outliers. When measured in this way, TMP 98.98.1 shows more posterior displacement of the orbit than *Denversaurus*. Bakker's (1988) discussion of this character notes that the posterior displacement of the orbit is taken to be in relation to the quadratojugal flare, not necessarily the skull overall. However, whereas this may be true, the placement of the orbit relative to this flare is dependent upon the reconstruction (=retrodeformation) of *Denversaurus* and is therefore, impossible to assess in the actual specimen.

Protrusion of postorbital boss— Here, the protrusion of the postorbital boss was measured as a ratio between the skull width across the bosses and the width of the anterior end of the snout. *Pawpawsaurus* has the greatest protrusion (3.36), suggesting that this is the primitive state for Nodosauridae. *Denversaurus* shows the least protrusion (1.60) and *Panoplosaurus* average protrusion (2.48). When plotted, this ratio presents no natural breaks.

Quadrate elongation—Bakker (1988) noted that the ratio of the quadrate length to the width of the paroccipital process was shorter in *Panoplosaurus*, ROM 1215, and ROM 1794 (mean 50%) than in other specimens (mean 59%). The difference between these means is on the margin of significance ($p=0.053$), but the character was coded for the specimens as delineated by Bakker (1988) because the character could be assessed more readily than most.

4.3.2 Neighbor Joining and Principle Components Analysis

Neighbor joining (Fig. 4.4) and Principle Components (PCA) analyses (Figs. 4.5, 4.6) show a high degree of variability in cranial proportions across specimens and taxa. The holotype of *Panoplosaurus mirus* (CMN 2759) is most similar to *Pawpawsaurus campbelli*, although the PCA indicates that the difference between the two is greater than among any of the ingroup specimens. TMP 83.25.2 and TMP 84.0.32 are also proportionally more similar to CMN 2759 than to other specimens based on the minimum spanning tree of the PCA biplot (Fig. 4.5, 4.6), although they still show a higher degree of variation. The holotype of *Denversaurus schlessmani* (DMNH 468) is intermediate between the holotypes of *Panoplosaurus mirus* and *Edmontonia* spp., but is more similar to the latter cluster. The holotype of *Edmontonia longiceps* (CMN 8531) clusters most closely with ROM 1215. The largest grouping clusters near the holotype of *Edmontonia rugosidens* (USNM 11868), which is most similar to TMP 81.3.3 and CMN 8879. This group also includes TMP 97.9.1 and TMP 2000.12.158.

4.3.3 Maximum Parsimony Analyses

The maximum parsimony analysis of the full character specimen matrix returned 147 MPTs of TL=61 steps. Safe taxonomic reduction performed in TAXEQ3 indicated that only DPMWA 90-25 could be safely removed from the data matrix as long as the index taxon ROM 1215 was retained. A subsequent run of the reduced matrix in TAXEQ3 suggested that removal of any other specimens would result in an altered tree topology. The data matrix was reanalyzed in TNT. For the reduced character specimen matrix, the maximum parsimony analysis also returned 147 MPTs of TL=61 steps. The 50% majority rule consensus tree (Fig. 4.7; CI=0.70,

RI=0.71) shows low support (<50% bootstrap/jackknife and <1 Bremer support values) for almost all branches. Nevertheless, groupings around holotype specimens aid in delineating taxa.

The holotype of *Edmontonia longiceps* (CMN 8531) is located in a basal grade with AMNH 3076, TMP 98.98.1, and UALVP 16249. *Edmontonia rugosidens* may be identified as a monophyletic group basal to *Denversaurus schlessmani*+*Panoplosaurus mirus*. The species includes AMNH 5665 and AMNH 5381, both considered *Edmontonia rugosidens* by Bakker (1988) and Carpenter (1990) as well as TMP 2000.12.158. *Denversaurus schlessmani* is represented as a monophyletic group by the holotype (DMNH 468) and BHI 6225. *Panoplosaurus mirus*, also monophyletic, consists of the holotype (CMN 2759), DPMWA 90-25, ROM 1215, TMP 83.25.2, and TMP 98.67.1. ROM 1215 and TMP 83.25.2 had been considered *Panoplosaurus* by Bakker (1988) and Carpenter (1990). Both BHI 6332 and ROM 20892 also fall out within *Panoplosaurus mirus*. However, due to the extreme transverse crushing of BHI 6332 (other specimens tend to be dorsolaterally crushed) and the fragmentary nature of ROM 20892, they are here conservatively assigned to Panoplosaurinae indet.

4.4 SYSTEMATIC PALAEONTOLOGY FOR LATE CRETACEOUS NODOSAURIDS

REPTILIA LAURENTI, 1768

DINOSAURIA OWEN, 1842

ORNITHISCHIA SEELEY, 1888

THYREOPHORA NOPCSA, 1915

EURYPODA SERENO, 1986

ANKYLOSAURIA OSBORN, 1923

= Ancylosauria Huene, 1914

= Thyreophora Nopcsa, 1915

= Apraedentalia Huene, 1948

= Apraedentalidae Huene, 1956

NODOSAURIDAE MARSH, 1890

= Acanthopholidae Marsh, 1890

= Acanthopholididae Nopcsa, 1902

= Acanthopholinidae von Huene, 1956

= Acanthopholinae Nopcsa, 1923

= Edmontoniidae Bakker, 1988

= Edmontoniinae Russell, 1940

= Hylaeosauridae Nopcsa, 1917

= Hylaeosauridae Nopcsa, 1917

= Nodosaurinae Abel, 1919 (Nopcsa, 1923)

= Palaeoscincidae Nopcsa, 1918

= Polacanthidae Wieland, 1911

= Polacanthinae Lapparent and Lavocat, 1955

PANOPLOSAURINAE NOPCSA, 1928

Definition—All Late Cretaceous nodosaurids more closely related to *Panoplosaurus* than to *Pawpawsaurus*.

DENVERSAURUS BAKKER, 1988

Type species—*Denversaurus schlessmani* Bakker, 1988.

Included species—Type species only.

Revised diagnosis—As for type and only known species.

DENVERSAURUS SCHLESSMANI BAKKER, 1988

Figs. 4.8–4.10

Holotype—DMNH 468; skull (Fig. 4.8).

Type locality—Corson County, South Dakota, USA.

Type horizon—Lower Hell Creek Formation.

Distribution—upper Maastrichtian (Upper Cretaceous), Montana and South Dakota, USA.

Revised diagnosis—Differs from *Edmontonia rugosidens* and *Panoplosaurus mirus* in ratio of the width of the anterior end of the snout to maximum skull width being greater than 46%. Differs from *Edmontonia rugosidens* in presence of anteroventrally narrow dermal ossification along the posterior border of the skull roof (shared with other panoplosaurines); anterior rim of lateral temporal fenestra obscured completely in lateral view by osteodermal encroachment (shared with other panoplosaurines). Differs from *Panoplosaurus mirus* in

maximum adult skull width being greater than 300 mm (shared with *Edmontonia* spp.); lateral edge of the snout in dorsal view, between the postorbital prominence and anterolateral corner of the premaxillary beak, concave (shared with *Edmontonia* spp.); lateral margin of medial cervical/pectoral osteoderms angular (shared with *Edmontonia* spp.).

Referred specimens—BHI 6225 (Figs. 4.9–4.10).

Comments—Carpenter (1990) considered *Denversaurus schlessmani* to be a junior synonym of *Edmontonia* and maintained that it had affinities to *Edmontonia rugosidens*, but conservatively regarded it as *Edmontonia* sp. Since then, this scheme has generally been followed by other workers, and *Denversaurus schlessmani* has not been considered a valid taxon. Although the combination "*Edmontonia schlessmani*" has been used in print informally by Carpenter et al. (2013), the original combination of Bakker (1988) is retained here for simplicity.

EDMONTONIA STERNBERG, 1928

= *Chassternbergia* (Bakker, 1988) Olshevsky, 1991

= *Edmontia* (Hunt and Lucas, 1992)

= *Panoplosaurus* (Lambe, 1919) (partim)

Type species—*Edmontonia longiceps* Sternberg, 1928

Included species—*Edmontonia longiceps* Sternberg, 1928; *Edmontonia rugosidens* (Gilmore, 1930) Russell, 1940

Distribution—Campanian–Maastrichtian (Upper Cretaceous), Aguja Formation, DPF, HCF, and Two Medicine Formation, Alberta, Canada, to Texas, USA.

Revised diagnosis—Differs from other panoplosaurs in cranial osteoderms over rostral region completely fused, not separated by grooves. Differs from *Panoplosaurus* in lateral edge of the snout in dorsal view, between the postorbital prominence and anterolateral corner of the premaxillary beak, concave (shared with *Denversaurus*); lateral margin of medial cervical/pectoral osteoderms angular (shared with *Denversaurus*).

EDMONTONIA LONGICEPS STERNBERG, 1928

Figs. 4.11–4.25

= *Panoplosaurus longiceps* (Sternberg, 1928)

Holotype—CMN 8531; skull, right mandible, 11 dorsal vertebrae, synsacrum, nine caudal vertebrae, four cervical ribs, 26 dorsal ribs, left humerus, right and left radius, left ulna, ilia, ischia, right femur, right tibia, right and left fibula, osteoderms (Figs. 4.11–4.23)

Type locality—UTM 12U 367696E 5727158N, Red Deer River, Alberta, Canada.

Type horizon—Campanian–Maastrichtian (Upper Cretaceous), HCF.

Distribution—Campanian–Maastrichtian (Upper Cretaceous), Aguja Formation, DPF, and HCF, Alberta, Canada, to Texas, USA.

Revised diagnosis—Differs from *Edmontonia rugosidens* in anterolateral projection of distal pectoral spines; presence of prevomer foramen; presence of anteroposteriorly narrow dermal ossification along the posterior border of the skull (shared with *Denversaurus schlessmani* and *Panoplosaurus mirus*); anterior rim of lateral temporal fenestra completely

obscured in lateral view by osteodermal encroachment (shared with *Denversaurus schlessmani* and *Panoplosaurus mirus*).

Referred specimens—AMNH 3076, TMP 98.98.1 (Figs. 4.24–4.25).

Comments—Carpenter (1990) referred no additional material beyond the holotype to *Edmontonia longiceps*. AMNH 3076 was instead referred to *Edmontonia* sp. (=*Denversaurus schlessmani*). Although it is displayed behind glass and not accessible for study, it was coded as best as possible for inclusion in analysis here, although it is not possible to figure the specimen.

EDMONTONIA RUGOSIDENS (GILMORE, 1930) RUSSELL, 1940

Figs. 4.26–4.35

= *Chassternbergia rugosidens* (Bakker, 1988) Olshevsky, 1991

= *Paleoscincus* sp. Matthew, 1922

= *Paleoscincus rugosidens* Gilmore, 1930

= *Panoplosaurus rugosidens* (Gilmore, 1930)

Holotype—USNM 11868;.skull, right mandible, five cervical vertebrae, ten dorsal vertebrae, synsacrum, 11 caudal vertebrae, 17 ribs, partial right ilium, ischia, right pubis, osteoderms (Figs. 4.26–4.31).

Type locality—UTM 12U 378177E 5424854N, Milk River, Blackfeet Indian Reservation, Glacier County, Montana.

Type horizon—Campanian (Upper Cretaceous), Two Medicine Formation.

Distribution—Campanian (Upper Cretaceous), DPF and Two Medicine Formation.

Revised diagnosis—Differs from *Edmontonia longiceps* in anterior rim of lateral temporal fenestra at least partially visible in lateral view; anterior projection of distal lateral spines; highest point of skull roof above orbits (shared with *Panoplosaurus mirus*).

Referred specimens—AMNH 5381 (Figs. 4.32–4.34), AMNH 5665, TMP 2000.12.158 (Fig. 4.35).

Comments—AMNH 5381 and 5665 were considered by Bakker (1988) to have an affinity with *Edmontonia rugosidens* (=*Edmontonia (Chassternbergia) rugosidens*) but to be specifically distinct as *Edmontonia (Chassternbergia)* sp. 1. Carpenter (1990) assigned AMNH 5665 to *Edmontonia rugosidens*. Currently this specimen is in an inaccessible display case and not available for detailed study. Previous descriptions are used here for comparative purposes and Carpenter's (1990) referral of the specimen to *Edmontonia rugosidens* is followed.

PANOPLOSAURUS LAMBE, 1919

= *Edmontonia* Russell, 1940 (partim)

= *Edmontonia rugosidens* (Gilmore, 1930) (partim)

Type species—*Panoplosaurus mirus* Lambe, 1919

Included species—Type species only.

Revised diagnosis—As for type and only known species

PANOPLOSAURUS MIRUS LAMBE, 1919

Figs. 4.36–4.51

Holotype—CMN 2759; skull, mandibles, atlas, axis, cervical vertebrae, dorsal vertebrae, partial synsacrum, caudal vertebrae, cervical ribs, dorsal ribs, intersternal plate, xiphisternals, left scapulocoracoid, left humerus, manus, tibia, fibula, pes elements, osteoderms (Figs. 4.36–4.45).

Type locality—Quarry Q008 (#69, Sternberg, 1950; GSC 2), UTM 12U 463938E 5620734N, Dinosaur Provincial Park, Alberta, Canada.

Type horizon—upper Campanian (Upper Cretaceous), lower DPF.

Distribution—upper Campanian to ?lower Maastrichtian (Upper Cretaceous) of Alberta and Alaska.

Revised diagnosis—Differs from all other panoplosaurs in groove on ventral margin of vomer; lateral edge of the snout in dorsal view, between the postorbital prominence and anterolateral corner of the premaxillary beak flat to convex; lateral margin of medial cervical/pectoral osteoderms rounded. Differs from *Edmontonia* spp. in cranial osteoderms over rostral region: separated by distinct (3-4 mm wide) grooves (shared with *Denversaurus schlessmani*).

Referred specimens: DPMWA 90-25 (Fig. 4.46), ROM 1215 (Figs. 4.47–4.50), TMP 83.25.2 (Fig. 4.51), TMP 98.67.1 (Fig. 4.52).

Comments—Bakker (1988) considered ROM 1215 as representative of a second species of *Panoplosaurus*, *Panoplosaurus* sp. 1. The referral to *Panoplosaurus mirus* of ROM 1215 and TMP 83.25.2 agrees with the taxonomic assignments of Carpenter (1990). DPMWA 90-25 was originally described as a specimen of *Edmontonia* sp. (Gangloff, 1995) based on having anteriorly parallel maxillary tooth rows and a keeled vomer, although the latter is broken.

PANOPLOSAURINAE INCERTAE SEDIS

Figs. 4.53–4.54

Referred material—BHI 6332 (Fig. 4.53), ROM 20892 (Fig. 4.54).

Comments—BHI 6332 shows an extreme amount of mediolateral crushing in contrast to most other panoplosaurine specimens that show dorsoventral crushing or less severe mediolateral shear.

NODOSAURIDAE INCERTAE SEDIS

ANTARCTOPELTA SALGADO AND GASPARINI, 2006

Type species—*Antarctopelta oliveroi* Salgado and Gasparini, 2006.

Included species—Type species only.

Diagnosis—As for type and only known species.

ANTARCTOPELTA OLIVEROI SALGADO AND GASPARINI, 2006

Holotype—MLP 86-X-28-1; fragment of left dentary, teeth, two cervical vertebrae (and a latex cast prepared from a natural mould of three articulated cervical vertebrae), fragments of dorsal ribs, two dorsal centra representing part of the presacral rod, partial synsacrum, eight incomplete caudal vertebrae, partial left scapula, right ilium fragment, left femur fragment, five metatarsals, two phalanges, osteoderms.

Type locality—UTM 21E 457251E 2914683S, locality D6-1, Santa Marta Cove, North James Ross Island, Antarctica.

Type horizon—Upper Cretaceous (upper Campanian), Marambio Group (Santa Marta Formation, lower part of the Gamma Member) of the Santa Marta Formation

Distribution—Known only from the type locality.

Diagnosis—cervical centra short (length about 70% height) with anterior articular faces higher than posterior; relatively slender transverse processes of anterior caudals; dorsoventrally depressed centra of posteriormost caudals with articular faces anteriorly inclined and laterally expanded; transverse processes of posterior caudals well developed (transverse processes length about 40% of centrum width), dorsoventrally depressed, and positioned within the anterior half of the centrum; at least six morphotypes of postcranial osteoderms including 1-narrow and spine-shaped, 2-ovoid plate-like with a rugose external surface texture, 3-plate-like with a smooth external surface texture, 4-polygonal with a rugose external surface texture, 5-shield-shaped with an external keel, and 6-ossicles (less than 5 mm in diameter) (Salgado and Gasparini, 2006).

GLYPTODONTOPELTA FORD, 2000

Type species—*Glyptodontopelta mimus* Ford, 2000

Included species—Type species only.

Diagnosis—As for type and only known species.

GLYPTODONTOPELTA MIMUS FORD, 2000

= *Edmontonia australis* Ford, 2000

Holotype—USNM 8610; portion of pelvic shield, several isolated thoracic and pelvic osteoderms, and osteoderm fragments from the cervical/pectoral half rings.

Type locality—Barrel Springs Arroyo (=De-na-zin Wash), about 1.5 km southwest of Ojo Alamo Store, San Juan County, New Mexico, USA.

Type horizon—lower Maastrichtian (Upper Cretaceous), Ojo Alamo Formation (Naashoibito Member).

Distribution—upper Campanian to lower Maastrichtian, San Juan Basin, New Mexico, USA.

Revised diagnosis—Differs from Late Cretaceous North American nodosaurids (*Denversaurus schlessmani, Edmontonia* spp., and *Panoplosaurus mirus*) in the dorsal surface of the osteoderms possess a distinctive dendritic pattern consisting of vascular furrows radially directed away from the keel coupled with randomly distributed small pits and pores; rectangular medial cervical osteoderms with rounded edges and a keel medial in position (Burns, 2008).

Referred specimens—NMMNH P-14266, 20880, 22753, 25063, 27420, 27450, 27849, SMP VP-1147, 1319, 1580, 1640, 1731, 1825, 1826, 1831, 1832, 1863, 2026, 2067, 2077, 2109, USNM 8611.

Comments—Previously, *Glyptodontopelta mimus* had be considered restricted to the Naashoibito Member; however, a review of additional material suggests the genus also occurs in the upper Campanian Fossil Forest member of the Fruitland Formation (Burns and Lucas, 2015).

NIOBRARASAURUS CARPENTER, DILKES, AND WEISHAMPEL, 1995

Type species—*Niobrarasaurus coleii* (Mehl, 1936)

Included species—Type species only.

Diagnosis—As for type and only known species.

NIOBRARASAURUS COLEII (MEHL, 1936)

= *Hierosaurus coleii* Mehl, 1936

= *Nodosaurus coleii* (Mehl, 1936)

Holotype—MU 650 VP; skull fragments, teeth, cervical vertebrae, dorsal vertebrae, dorsal ribs, partial synsacrum, caudal vertebrae, chevrons, partial right scapulocoracoid, right humerus, right radius and ulna, fragments of left radius and ulna, metacarpals, right femur, right tibia and fibula, right pes, fragments of left femur, fragments of left tibia and fibula, osteoderms.

Type locality—14S 394197E 4289588N est., Gove County, Kansas, USA.

Type horizon—Coniacian–lower Campanian (Upper Cretaceous), Niobrara Chalk Formation (Smoky Hill Chalk Member).

Distribution—Known only from the type locality.

Diagnosis—Cranial ornamentation of the rostral region composed of two pairs of elongate plates; secondary palate extending further posteriorly than in other nodosaurids; caudal neural spines short and terminating in an expanded knob; anterior caudal transverse processes project posteriorly; humerus differs from *Denversaurus schlessmani*, *Edmontonia* spp., and *Panoplosaurus mirus* in a shallower olecranon fossa; deltopectoral crest undifferentiated from

the humeral head; bicipital crest less pronounced than in *Sauropelta edwardsorum* but more so than in *Denversaurus schlessmani*, *Edmontonia* spp., and *Panoplosaurus mirus*; olecranon process more pronounced than in *Stegopelta landernensis* but less so than in *Sauropelta edwardsorum*; femur differs from that of *Hoplitosaurus marshi* in not being sigmoidal in lateral view (Carpenter et al., 1995).

4.5 DESCRIPTIVE RESULTS AND A POSTERIORI CHARACTER ANALYSIS

Because many of the specimens used herein have been described in previous studies (Coombs, 1971, 1978; Bakker, 1988; Carpenter, 1990), their work will not be repeated here. The description here instead focuses on characters that may or may not be taxonomically useful as indicated by previous studies and tested here. Characters are also analyzed in terms of their taxonomic utility versus variability within taxa. Because it is generally conservative and not visible on many specimens due to preservation, a detailed anatomy of the braincase and other endocranial hard and soft tissue anatomy is presented elsewhere (Chapter 5).

4.5.1 The Skull

Maximum adult skull width is variable among panoplosaurs and is likely ontogenetically plastic. Nevertheless, *Denversaurus schlessmani* and *Edmontonia rugosidens* individuals tend to have wider skulls than those of *Panoplosaurus mirus*. Adult skull width is more variable for *Edmontonia longiceps* specimens. In AMNH 3076 and UALVP 16249 the skull is narrower than 300 mm, whereas it is wider in the holotype of *Edmontonia longiceps* (Fig. 4.11) and TMP 98.98.1 (Fig. 4.24).

When viewed dorsally, the lateral edges of the snout in most panoplosaurs and in *Pawpawsaurus* are concave, forming an hourglass shape. In *Panoplosaurus*, however, these margins are flat to convex, contributing to the "plum-snouted" condition (Figs. 4.36, 4.46, 4.47, and 4.51) for the genus recognized by Bakker (1988). The exception to this is TMP 98.67.1 (Fig. 4.52), in which the snout retains a more primitive hourglass shape. Carpenter (1990) noted variation in skulls referred to *Panoplosaurus*, from the short and deep skull of the holotype (CMN 2759; Fig. 4.36) to the more elongate skulls of ROM 1215 (Fig. 4.47) and TMP 85.25.2 (Fig. 4.51). Unable to find differences in the postcrania, however, Carpenter (1990) suggested that the condition in the holotype was the result of ontogenetic variation or sexual dimorphism. Although the source is not tested here, the hypothesis that this is representative of variation within the taxon is supported.

Primitively in nodosaurids, the highest point of the skull roof is situated posterior to the orbits. This condition is variable in some panoplosaurs referable to *Edmontonia longiceps*, although in the holotype (Fig. 4.11) the highest point is actually located anterior to the orbits. In *Denversaurus schlessmani*, *Edmontonia rugosidens*, and *Panoplosaurus mirus*, this point is consistently located between the orbits.

The location of the orbit relative to the length of the skull is highly variable. In *Pawpawsaurus campbelli* and most specimens of *Edmontonia longiceps*, with the exception of UALVP 16249, the ratio of antorbital to postorbital skull length is greater than 2, indicating a more posterior orbit. The same condition is seen in the *Edmontonia rugosidens* specimen TMP 2000.12.158, whereas a more anterior orbit (antorbital to postorbital skull length less than 2) is seen in the holotype and AMNH 5381. In *Panoplosaurus mirus*, only the holotype shows a more posterior orbit. Bakker diagnosed *Denversaurus schlessmani* in part based on a more posteriorly-

placed orbit. Carpenter (1990), however noted that this was not based on the morphology of the skull, which is dorsoventrally crushed and sheared anteroposteriorly, but rather on Bakker's (1988) reconstruction. Whereas the holotype of *Denversaurus schlessmani* (Fig. 4.8) does indeed have a more posteriorly placed orbit, the variability of this character within taxa indicates that it is not taxonomically useful.

The antorbital and supratemporal fenestrae are secondarily closed in all nodosaurs. In addition, cranial sutures are obliterated due to the development of osteodermal ornamentation, which includes individual plates often demarcated by sulci, over the dermatocranium. A single, subcircular plate occurs between the orbits in all panoplosaurs specimens, although this is not a feature of *Pawpawsaurus campbelli* which retains several smaller elements in this region more similar to the condition known in ankylosaurids. A mediolaterally elongate plate is present at the posterior terminus of the skull in *Denversaurus schlessmani*, *Edmontonia longiceps*, *Panoplosaurus mirus*, and *Pawpawsaurus campbelli* but is absent in *Edmontonia rugosidens*.

The degree to which osteodermal encroachment occurs over the anterior temporal bar is also variable in nodosaurids. In *Pawpawsaurus campbelli,* the bar is completely obscured. This state is retained in *Denversaurus schlessmani* and *Edmontonia longiceps*. In *Edmontonia rugosidens*, the bar is partially visible in all specimens except for AMNH 5665, in which the primitive condition is retained. The bar is also completely obscured in most specimens of *Panoplosaurus mirus* with the exception of ROM 1215 (Fig. 4.47).

Some of the pattern of sculpturing on the skull roof may also be diagnostic, but also likely varies due to other factors. *Pawpawsaurus campbelli* primitively has bulbous ornamentation on the skull roof, more similar to the condition seen in ankylosaurids. In almost all specimens referable to *Edmontonia* spp., cranial sculpturing consists of flat plates that are

completely fused, and not separated by discernable sulci or grooves. In the holotype of *Edmontonia longiceps*, however, whereas the plates partially obscure the sulci, the contacts between adjacent plates are still discernable (Fig. 4.11). In *Denversaurus schlessmani* and *Panoplosaurus mirus*, these plates are separated by distinct (3-4 mm wide) grooves (Figs. 4.9, 4.46, 4.47, 4.51, 4.52). In the holotype of *Panoplosaurus mirus* (Fig. 4.36), however, their condition is more similar to that of the holotype of *Edmontonia longiceps* (Fig. 4.11), in that they are still discernable but have expanded to obscure the wider grooves seen in other specimens.

Two specimens of *Panoplosaurus*, DPMWA 90-25 (Fig. 4.46) and ROM 1215 (Fig. 4.47), are united by the presence of a triangular plate over the rostral region immediately posterior to the nasal plate. Due to the preservation of DPMWA 90-25, however, there are no other diagnostic characters known for this specimen.

Premaxilla— The length of the premaxillary palate, measured anteroposteriorly, is consistently greater than its width in primitive nodosaurids as well as almost all panoplosaurines. In the holotype of *Panoplosaurus mirus*, however, the opposite is true. Premaxillary teeth are present in primitive nodosaurids, but are not known in any specimen of panoplosaurs. Osteodermal sculpturing occurs on *Pawpawsaurus campbelli* and is present in all panoplosaurs. The premaxilla supports a single median ossification that is also common to all nodosaurs (although the extent to which this ossification also overlies the nasals is unknown). In some specimens, such as the holotypes of *Pawpawsaurus campbelli* and *Panoplosaurus mirus* (Fig. 4.36), this sculpturing forms conspicuous ventrally-directed projections at the anterolateral corners of the premaxillary beak. At the anterior terminus of the premaxillary beak, a ventrally concave notch is apparent in anterior view in *Pawpawsaurus campbelli*. This feature is absent in all panoplosaurines for which this part of the skull is preserved.

In some nodosaurids, there is an oval, anteroposteriorly elongate prevomer foramen situated along the midline of the premaxillary palate and its absence or presence has taxonomic utility. It is present primitively in *Pawpawsaurus campbelli*, which also has a diagnostic posteriorly concave U-shaped ridge anterior to the prevomer foramen that is absent in panoplosaurs. The prevomer foramen is retained in *Edmontonia longiceps* but lost in the more derived *Denversaurus schlessmani*, *Edmontonia rugosidens*, and *Panoplosaurus mirus*.

The relative width of the anterior terminus of the snout is more variable than previously thought. The primitive condition, seen in *Pawpawsaurus campbelli* and basal thyreophorans, is one of a narrower anterior skull (ratio of the width of the anterior end of the snout to maximum skull width less than 46%). Some specimens of *Edmontonia longiceps* (TMP 98.98.1 (Fig. 4.24) and UALVP 16249) show a wide snout (ratio greater than 46%), although the snout of the holotype is narrow. Both specimens of *Edmontonia rugosidens* for which this character is assessable (the holotype and TMP 2000.12.158 (Fig. 4.35)) show a narrow snout. Both specimens of *Denversaurus schlessmani* show a wide snout. Finally, in *Panoplosaurus mirus*, some specimens (the holotype, ROM 1215 (Fig. 4.47), and TMP 98.67.1 (Fig. 4.52)) show the narrow condition, although the snout is wide in TMP 83.25.2 (Fig. 4.51). Tentatively, this may represent an ambiguous apomorphy for *Denversaurus schlessmani*, but more specimens are required to test this.

Maxilla— The maxillary tooth rows in all nodosaurs are deeply emarginated from the lateral edges of the skull and are laterally concave, forming an hourglass-like shape in ventral view. The degree of convergence of the anterior maxillary tooth rows is variable among taxa. In *Pawpawsaurus campbelli*, they are nearly parallel (<10° from median sagittal plane). This state is retained in most panoplosaurs, and in some the tooth rows are actually convergent. Some

specimens, however, show strongly divergent (>20° from median sagittal plane) anterior maxillary tooth rows. These include TMP 83.25.2 (*Panoplosaurus mirus*; Fig. 4.51), TMP 2000.12.158 (*Edmontonia rugosidens*; Fig. 4.35), and UALVP 16249 (*Edmontonia longiceps*), so it is doubtful that this character has any taxonomic significance. The maxillae also contribute to the bony secondary palate. This feature is absent in *Pawpawsaurus campbelli* and *Sauropelta edwardsorum* (Lee, 1996) and is, therefore likely diagnostic for the Panoplosaurinae.

Vomer— The vomer in all nodosaurid specimens for which it is preserved extends dorsally from the skull roof ventrally at least to the level of the maxillary tooth rows, partially subdividing the oral cavity into two lateral compartments when the mouth is closed. Along its ventral margin, the vomer may be keeled (Fig. 4.26) or laterally swollen and grooved (Figs. 4.47, 4.51). The latter condition was recognized by Carpenter (1990) as a diagnostic character for *Panoplosaurus mirus*. It is retained here as an apomorphy for the genus; however, this condition is also seen in TMP 2000.12.158 (Fig. 4.35), which is here regarded as *Edmontonia rugosidens*. *Denversaurus schlessmani* and *Edmontonia longiceps* show the primitive condition of having a keeled vomer.

Pterygoid and Ectopterygoid— In nodosaurids, the ectopterygoids form thickened pads at the posterior terminus of the maxillary tooth rows. In ROM 1215, a pterygoid-ectopterygoid foramen occurs on the medial surface (Fig. 4.2). Because this region is often poorly preserved, diagenetically distorted, and/or not visible, this is a difficult character to assess for most other panoplosaur specimens. Nevertheless, it is located on the anteroventral surface of the pad in ROM 20892, referable to *Panoplosaurus mirus* along with ROM 1215, TMP 2000.12.158, referable to *Edmontonia rugosidens* and the holotype of *Edmontonia longiceps*. A pterygoid-ectopterygoid pad is absent in *Pawpawsaurus campbelli*; however, *Pawpawsaurus campbelli* has

a relatively large pterygoid foramen on the anteroventral aspect of the anterior flange of the pterygoid that is absent in panoplosaurs. Based on these few specimens, it appears that the occurrence of this foramen of the ectopterygoid pad is apomorphic for panoplosaurs, but that its location is somewhat labile.

Quadrate— The shaft of the quadrate in nodosaurids extends anteroventrally, as opposed to simply ventrally as in primitive thyreophorans like *Scelidosaurus harrisonii*. Due to the fact that diagenetic crushing has distorted most panoplosaurines skulls, this character is only assessable in two specimens: the holotype of *Panoplosaurus mirus* and BHI 6332. In all nodosaurs, a rounded ornamental ossification projects ventrolaterally from the quadratojugal region. In ankylosaurids, this ossification is more prominent and wedge-shaped.

Mandible— All ankylosaurs, including nodosaurs, possess a secondary closure of the mandibular fenestra caused, in part, by the fusion of an osteoderm to the ventrolateral corner of the mandible. This osteoderm contributes to the shape of the ventral border of the mandible, which is variable in nodosaurids. Generally, this margin is sinuous, following the shape of the maxillary tooth row, a condition known in *Pawpawsaurus campbelli* and most panoplosaurs. In the holotype of *Edmontonia longiceps* (Fig. 4.11) and ROM 1215 (Fig. 4.48), however, this margin is flat.

Teeth— There are no consistent taxonomic differences among teeth for panoplosaurines in which they are known, as has been noted previously (Coombs, 1990). The crowns are compressed labiolingually and have a number of cusps. The notches between cusps grade into grooves that extend to the base of the crown. The number of cusps is variable among and within taxa. *Edmontonia longiceps* (holotype, CMN 8531) has 8–11. The same is true of AMNH 5381 (*Edmontonia rugosidens*), although AMNH 5665 (*Edmontonia rugosidens*) has 9–10 according

to Coombs (1990). The base of the crown is characterized by a well-defined cingulum or swelling, and the root is peg-like and circular in cross section.

4.5.2 Axial skeleton

Cervical— One cervical vertebra is known from the holotype of *Edmontonia longiceps* (CMN 8531; Fig. 4.12) and a series of three cervical vertebrae are visible in the holotype of *P. mirus* (CMN 2759), in which they are fused into a syncervical as part of a block that also preserves some cervical and gular osteoderms in situ (Fig. 4.37). Presumably, a complete cervical series is preserved in the latter but is obscured. The same is true for AMNH 5665, in which a complete articulated series is present but obscured by the articulated cervical and pectoral osteoderms and inaccessible as currently displayed, although it was described by Carpenter (1990).

Dorsal— Two dorsal vertebrae are known from *Edmontonia rugosidens* (AMNH 5381; Fig. 4.33) and at least seven from the holotype of *Edmontonia longiceps* (CMN 8351; Fig. 4.13). The neural spines are rectangular in lateral view, project dorsally, and are posteriorly offset from the centrum. The transverse processes extend dorsolaterally. In AMNH 5381, dorsal ribs are coossified to the transverse processes; however, they are not in CMN 8351. It is not known if this is ontogenetically-variable. In *Edmontonia longiceps*, the posteriormost five dorsal ribs contact the ilium laterally. Those ribs that are anterior partially underlie the ilium, contact along its ventral surface, whereas that of the posteriormost sacrodorsal contacts just the medial edge of the blade of the ilium. Only the posteriormost four dorsal vertebrae, though, are fused into the presacral rod of the synsacrum (Fig. 4.18A).

Sternal Elements— The sternum (Fig. 4.17) in panoplosaurines is known in *Edmontonia longiceps* (holotype, CMN 8531), *Edmontonia rugosidens* (AMNH 5665), and *Panoplosaurus mirus* (ROM 1215; Fig. 4.49) and consists of two unfused, bilateral, paddle-like elements and, posteriorly, a number of paired xiphisternal ossifications. The sternal elements described here for *Edmontonia longiceps* were considered fibulae by Carpenter (1990); however, they show an expansion that more closely resembles the condition of the sternals in ROM 1215 than the fibula of CMN 2759 (holotype, *Panoplosaurus mirus*), which shows no such expansion. The preservation of the relatively thinner and more delicate xiphisternals in CMN 8531 also lends support to the sternal plates having been preserved, as well. The paddle-like elements, medially, are sub-oval and each has a shaft that extends posterolaterally. This is unlike the condition in ankylosaurines, in which the sternals fuse medially into a quadrangular element (Vickaryous et al., 2004) but is similar to the condition in *Sauropelta edwardsorum* (Coombs and Maryańska, 1990). The medial margin of the sternal is more triangular in *Edmontonia longiceps* and more rounded in *Panoplosaurus mirus*. The xiphisternal plates are among the thinnest postcranial bones and contact one another medially. The medial side is characterized by several foramina of varying sizes, and the lateral side is smooth and convex. At present, in dinosaurs these elements are only known from nodosaurs, with the possible exception of ornithomimisaurs (Nicholls and Russell, 1981; Godfrey and Currie, 1994).

Synsacrum— The synsacrum is preserved for CMN 2759 (holotype *Panoplosaurus mirus*; Fig. 4.44A) and CMN 8351 (holotype *Edmontonia longiceps*; Fig. 4.16A), in which is articulated with the right ilium and associated in situ osteoderms. Carpenter (1990) tentatively agreed with Sternberg (1921), who reported four true sacrals in *Panoplosaurus mirus*. The morphology of the transverse process of the first sacral is different than in the other three sacrals,

which have more robust transverse processes that extend laterally and coalesce to form the sacroiliac joint. In *Edmontonia longiceps*, the rib of the posteriormost sacrodorsal just contacts the medial edge of the ilium. In a recent review of pelvic morphology and evolution in ankylosaurs, Carpenter et al. (2013) confirm that panoplosaurines have four true sacral vertebrae. The synsacrum of AMNH 5665 (*Edmontonia rugosidens*) was described by Carpenter (1990) as being more robust than that of *Edmontonia longiceps*, but this has not been tested quantitatively here.

Caudal— Series of caudal vertebrae are known from the holotypes of *Edmontonia longiceps* (CMN 8351; Figs. 4.15, 4.16), *E. rugosidens* (USNM 11868; Fig. 4.27), and *Panoplosaurus. mirus* (CMN 2759; Fig. 4.39) as well as a referred specimen of *Edmontonia rugosidens* (AMNH 5381; Fig. 4.33). In *Edmontonia longiceps*, the anteriormost caudal is coossified into a post sacral rod of the synsacrum (Fig. 18A; Carpenter et al., 2013). In most vertebrae, transverse processes extend laterally from the dorsolateral corners of the centra. In others, namely those of the holotype of *Edmontonia rugosidens* (Fig. 4.27A, C, E), they extend ventrolaterally, although this is not the case in the referred specimen (AMNH 5381; Fig. 4.33F). One specimen (Fig. 4.16D) from the holotype of *Edmontonia longiceps* (USNM 11868), however, shows both conditions contralaterally, indicating that, at least in some cases, this character may be the result of diagenetic processes or individual variation. A notochordal prominence is present in some specimens (USNM 11868, holotype *Edmontonia rugosidens*; Fig. 4.27) but not in others (AMNH 5381, *Edmontonia rugosidens*; Fig. 4.33; CMN 2759, holotype *Panoplosaurus mirus*; Fig. 4.39).This prominence is individually variable, as indicated by its faint presence on one caudal centrum of CMN 8351 (holotype *Edmontonia longiceps*; Fig. 4.16B). It is possible that this feature is ontogenetically variable.

4.5.3 Appendicular Skeleton

Scapulocoracoid— The scapulocoracoid was described for AMNH 5665 (*Edmontonia rugosidens*) by Carpenter (1990) but is partially reconstructed and is not accessible at present. This element is known from the right side for *Panoplosaurus mirus* in ROM 1215 (Fig. 4.50A). It is medially concave to accommodate the curvature of the thorax. The coracoid and scapula are coossified in ROM 1215 but not in AMNH 5665, although the latter is the larger individual. The coracoid is ovoid in shape, elongate anteroventrally from its contact with the scapula. In ankylosaurines, a ridge extends from the glenoid fossa to the anterodorsal process (Carpenter et al., 2011); however, this is absent in panoplosaurs. The coracoid of AMNH 5665 is more quadrangular (Carpenter, 1990, fig. 12.10A). The glenoid foramen is anterior to the scapular contact and dorsal to the glenoid fossa. The constricted, neck-like region of the scapula is well-developed, unlike in ankylosaurines. The prominent, knob-like acromion process protrudes from the lateral surface of the scapular neck. The posteroventral corner of the coracoid and anteroventral corner of the scapula contribute to the glenoid fossa in roughly equal proportions.

Humerus— In general, the humeri of panoplosaurines are more gracile than those of ankylosaurines (Vickaryous et al., 2004); however, they are more robust than those of more basal nodosaurids. The posteromedial head is medially offset from the midline axis of the elements and is located proximal to an internal (medial) tuberosity (=medial process). The deltopectoral crest is located on the lateral side and is larger than the internal tuberosity. The anterior surface of the proximal humerus is characterized by a shallow, triangular fossa. The medial condyle is smaller than the lateral condyle. The medial epicondyle is angular, giving it a rectangular appearance in anteroposterior view. The lateral epicondyle is more extensive and rounded.

Carpenter (1990) noted no differences in the humerus among panoplosaurs, an observation supported here.

Radius— The radius is known only from the holotype of *Edmontonia longiceps* (CMN 8351). The proximal articulation is expanded relative to the shaft into a cup-like fossa to accommodate the radial condyle of the humerus. Distally, the radius is expanded and extends ventrally into a blunt styloid process on the lateral side.

Ulna— The ulna is known for *Edmontonia longiceps* (holotype, CMN 8351) and *Panoplosaurus mirus* (ROM 1215), although it is anteroposteriorly crushed in the former making comparison difficult. The olecranon process occupies 1/3 the length of the ulna in ROM 1215. It is shorter in CMN 8531 due to crushing.

Manus— Manual elements of *Edmontonia rugosidens* (AMNH 5381) were described and illustrated by Carpenter (1990) and an articulated manus is known for *Panoplosaurus mirus* (holotype CMN 2759; Figs. 4.40–4.42). If complete, the manus of *Panoplosaurus mirus* would have a phalangeal formula of 2:3:3:0:0; however, as noted by Carpenter (1990) this would make it the only quadrupedal dinosaur to reduce the manus to three digits, and it is possible the fourth digit was not preserved. The manus of *Edmontonia rugosidens* is tetradactyl (Carpenter, 1990) and it is pentadactyl in *Sauropelta edwardsorum*. In *Panoplosaurus mirus*, MC I has a less constricted midshaft and MC II is less robust than their counterparts in *Edmontonia* spp. However phalanx I-1 is more robust in *Panoplosaurus mirus*.

Pelvis— A nearly complete partially articulated pelvis is known for *Edmontonia longiceps* (holotype, CMN 8351; Fig. 4.18) and *Edmontonia rugosidens* (AMNH 5381). For the holotype *Edmontonia rugosidens* (USNM 11868) there is a fragment of the preacetabular process of the ilium (Fig. 4.28), a complete right and proximal left ischium (Fig. 4.29), and a fragment of

the pubis. The ilium fragment of *Edmontonia rugosidens* is from the right side and likely from the anteriormost portion of the preacetabular process. Three dorsal ribs are coossified to it, identifying this as the medial portion of the ventral surface. Also, in *Edmontonia longiceps,* only the ribs of the anterior sacrodorsal vertebrae underlie the blade of the ilium, so it is likely from the anterior portion.

The ischium articulates with the ischial peduncle of the ilium and forms the majority of the medial wall of the acetabulum, with the ilium contributing to the dorsal wall. The shaft extends ventrally for two thirds of its length and, distally, projects anteroventrally. The shaft is more anteroposteriorly expanded in *Edmontonia longiceps* than in *Edmontonia rugosidens*. The distal anteroventral flexion is identical in both at 32° from the ventrally-projecting shaft.

Femur— The femur is known from the holotype of *Edmontonia longiceps*, although it is anteroposteriorly crushed. The greater trochanter projects laterally from the lateral side of the femur distal to the contralateral femoral head in contrast to the condition in *Sauropelta edwardsorum*, in which the greater trochanter is located more proximally (Carpenter, 1990). The head extends medially from the plane of the femoral shaft at 53°.

Tibia— Both tibiae are preserved in the holotype of *Panoplosaurus mirus*. The right tibia is nearly complete, missing only the medial corner of the tibial plateau, and is articulated with the fibula. The left tibia is missing the midshaft area, although both ends are preserved. The medial side of the tibia is straight, whereas the lateral side is curved, laterally concave, to accommodate the fibula. Proximally, the medial condyle is rounded whereas the lateral condyle is more rectangular. Distally, the medial malleolus is evident as a bulge on the medial side of the distal end of the tibia and is more prominent on the anterior side.

Fibula— The fibula of the holotype of *Panoplosaurus mirus* is preserved in articulation with the tibia and is nearly straight. Articulating proximally with the posterolateral corner of the tibia, it curves anteriorly to articulate with the anterolateral corner of the tibia distally. Carpenter (1990) described the fibulae of *Edmontonia longiceps* as being more curved than those of *Panoplosaurus mirus*; however, these elements are reinterpreted here as sternal elements. One end of each element is broadly expanded and more closely resembles the sternals of ROM 1215 than the fibula of CMN 2759, which shows no such expansion at either end.

Pes— The anatomy of the pes is poorly known in panoplosaurines. One metatarsal and three pedal phalanges are associated with the holotype of *Panoplosaurus mirus*. The metatarsal is a straight element, with little midshaft constriction. The unguals are more proximodistally elongate than the manual unguals. Carpenter (1990) notes no differences between these and the unguals of *Edmontonia* spp.

4.5.4 Integumentary Skeleton

Nodosaurids are distinguished from ankylosaurids in part by the presence of three half rings over the cervical and pectoral regions, as opposed to two. There are differences among panoplosaurs in terms of the morphology of the osteoderms that comprise these structures. The following description relies on the holotype specimens for *Edmontonia longiceps, Edmontonia rugosidens,* and *Panoplosaurus mirus*. In the latter, the lateral margins of the osteoderms are rounded, whereas they are angular in *Edmontonia* spp. The medial osteoderms of the first and second cervical half rings in *Panoplosaurus mirus* (Fig. 4.45) show this rounded condition. In *Edmontonia* spp., the lateral and distal osteoderms are anteroposteriorly elongate with higher keels that do not overhang the posterior border of the osteoderm (Fig. 4.38C). The cervical half

ring osteoderms of *Edmontonia* spp. have keels that terminate posteriorly in spines that project beyond the border of the base of the osteoderm in some cases. In *Edmontonia longiceps* (Fig. 4.21), the medial osteoderm of the first cervical half ring is trapezoidal, with a transverse anterior border and a posterior border that extends posterolaterally. The lateral osteoderm is square with a longitudinally-oriented keel that overhangs the basal border of the osteoderm posteriorly. The distal osteoderm is smaller and triangular. In *Edmontonia rugosidens* (Fig. 4.30A), the medial osteoderm is not preserved. The lateral osteoderm is pentagonal, with the posterior edges projecting posteriorly along with the median keel, unlike the straight posterior border in *Edmontonia. longiceps*. The distal osteoderm has a tear-drop shape and a posterolaterally extending keel ending in a point overhanging the posterolateral border of the osteoderm.

In *Panoplosaurus mirus*, medial osteoderms of the second cervical half ring (Fig. 4.45B) may be distinguished from those of the first by a more posterolaterally bulging posterolateral corner. The keel parallels the midline, but, posteriorly, diverges laterally. In *Edmontonia longiceps* (Fig. 4.22A, B), the osteoderms are more laterally skewed. The medial border of the medial osteoderm is parallel to the midline, but those of the lateral and distal osteoderms extend posterolaterally. Distal to the distal osteoderm, is a ventrally-projecting spine (Fig. 4.22C, D). These spines are not preserved in the holotype of *Edmontonia rugosidens* but are present in AMNH 5665 (Carpenter, 1990, fig. 21.4). In this taxon (Fig. 4.30B), the medial osteoderms are pentagonal, and anteroposteriorly constricted medially. The lateral osteoderm is similar to the distal osteoderm of the first cervical half ring but has a more prominently overhanging posterior extension of the median keel. The distal osteoderm forms a laterally-projecting spine.

The pectoral half ring is partially preserved in the holotypes of *Edmontonia longiceps* (Fig. 4.23) and *Edmontonia rugosidens* (Fig. 4.30C) as well as AMNH 5665. In *Edmontonia*

longiceps, the medial osteoderms are rhomboidal with a median keel that parallels the midline. In *Edmontonia rugosidens*, the medial osteoderms are more similar to those of the second cervical half ring in the same taxon in that they are polygonal; however, the median keels diverge more strongly posterolaterally. They also show a medial anteroposterior constriction similar to those of the second cervical half ring. The distal spines of the pectoral half-ring are also taxonomically useful for panoplosaurs. In the holotype of *Edmontonia longiceps*, they project laterally. They are, however, not preserved in other specimens referable to *Edmontonia longiceps*. In *Edmontonia rugosidens* (the holotype (Fig. 4.31A) and AMNH 5665) they project anteriorly. In *Panoplosaurus mirus* they are unknown, although the preservation of articulated osteoderms in this region in the holotype and the extensive suite of osteoderms known in ROM 1215 indicates that this is likely due to their absence and not lack of preservation.

Posterior to the pectoral half ring in *Edmontonia rugosidens* (the holotype (Fig. 4.31B) and AMNH 5665) a pair of coossified thoracic spines projects from the lateral side of the body, a larger anterior spine and smaller posterior spine. These spines are not preserved in other panoplosaurine specimens.

The presence of osteoderms that are wider than long had been noted by Carpenter (1990) as diagnostic for *Edmontonia longiceps*. When subjected to measurement, the osteoderms of the holotype of *Edmontonia longiceps* are, on average, not distinguishable in this regard from other specimens for which a considerable sample of osteoderms are known. The presence of this osteoderm type in the pelvic region may be diagnostic for *Edmontonia longiceps*; however, it is also possible that these osteoderms are merely not preserved in other specimens.

Humeral osteoderms are preserved in the holotype specimen of *Panoplosaurus mirus*. A block of the thoracic region in ventral view (Fig. 4.38) includes distal cervical osteoderms, throat

osteoderms, and smaller osteoderms and skin impressions posteriorly, although there is no evidence for keratinized skin overlying the osteoderms as in ROM 813 (Arbour et al., 2013). Humeral osteoderms are preserved as a row oriented transverse to the midline of the body, suggesting the animal had died with its right arm tucked underneath the body. These osteoderms are ovoid with strongly offset keels and are surrounded by rosettes of smaller osteoderms.

4.6 DISCUSSION

4.6.1 Taxonomy and Taxonomic Method

Various authors have demonstrated how different aspects of phylogeny can be quantified and integrated (Stuessy, 1983, 1987, 1997, 2009a, b; Estabrook, 1986; Felsenstein, 2004; Hörandl & Stuessy, 2010). In studies on dinosaur taxa, the use of individual specimens as operational taxonomic units in parsimony analyses has recently proven useful for the delineation of species and the taxonomic referral of specimens for diplodocoid sauropods (Upchurch et al., 2004; Tschopp et al., 2015). A cladogram is a useful tool for formulating phylogenetic hypotheses, but is merely one depiction/hypothesis for all possible evolutionary inferences (Fig. 4.55).

One issue in the present analysis is the apparent paraphyly of *E. longiceps* and, more generally, of *Edmontonia* itself (Fig. 4.7). Arguments have been proposed both against (e.g., Schmidt-Lebuhn, 2012) and in favor of (e.g., Hörandl & Stuessy, 2010) use of paraphyletic groups in taxonomy. A purely dichotomous cladistic approach would dictate that a speciation event results in two new species with the ancestral species going extinct. Nevertheless, panoplosaurine taxa are closely related and partially overlap temporally and geographically.

Therefore, the restriction of dichotomy creates what is probably a false model for the evolutionary relationships of these animals. In addition, adhering to such a restriction would lead to two possible taxonomic decisions. First, all panoplosaurines could be included within a single species, removing all categorizing utility that taxonomy provides. Second, all specimens referred herein to *Edmontonia longiceps* could be considered separate taxa. This is better but still removes most of the utility and leads to a preponderance of even more named single-specimen species.

It is likely that, although speciation events did occur, exemplified by the divergence of *Denversaurus schlessmani* and *Panoplosaurus mirus*, that *Edmontonia* spp. did not go extinct and are instead represented on a cladogram by a morphocline. A similar morphocline is seen in *Panoplosaurus mirus* (Fig. 4.7). Specimens of *Edmontonia longiceps* do have characters in common (see Systematic Palaeontology for Late Cretaceous Nodosaurids), but they are overshadowed in the analysis by other variable but equally weighted characters. A more traditional alpha taxonomic approach would weight these characters implicitly a priori to constrain the monophyly of these specimens as a terminal taxon for analysis. Here, character weighting is explicit and taxonomic decisions may be easily tested and revised in light of new anatomical data.

4.6.2 Character Evolution

Bakker (1988) noted that *Edmontonia* was a more basal taxon compared to *Denversaurus* and *Panoplosaurus*, and this hypothesis is supported here. Additionally, the hypothesis that *Edmontonia longiceps* is more basal than *Edmontonia rugosidens* (Bakker, 1988) is also

supported. There are a few overall character trends observable from primitive to more derive panoplosaurs.

Although potentially taxonomically variable, there does not seem to be an overall trend in maximum adult skull width. There does, however, seem to be a trend in greater development of dermal sculpturing in more derived panoplosaurs. The highest part of the skull moves from posterior to the orbits to above the orbits, potentially indicating a greater doming of the dermal sculpturing on this portion of the skull roof. The temporal regions of derived specimens have a greater degree of dermal encroachment over the anterior temporal bar. The increase in sculpturing leads to a snout with more straight or convex edges, as opposed to concave edges forming an hourglass shape in dorsal view in more primitive forms. Individual dermal plates in this region tend to be better delineated by sulci in derived forms. The anteroposteriorly narrow dermal ossification along the posterior border of the skull is lost only in *E. rugosidens*, although the significance of this loss, if any, is unclear. Postcranially, the lateral margins of the cervical and pectoral half ring osteoderms tend to become more rounded.

The ventral extent of the vomer and its development into a thickened pendulous structure in derived panoplosaurs is interesting. The vomer often extends past the maxillary tooth rows, indicating that the oral cavity was at least partially divided into two contralateral chambers. Such a condition has not been reported in other vertebrates. The loss of a prevomer foramen is also associated with the derived condition.

4.6.3 Stratigraphy and Panoplosaurine Diversity

In a recent taxonomic revision of Upper Cretaceous North American ankylosaurids by Arbour and Currie (2013), genera roughly correlated with their stratigraphic distributions, adding support to the taxonomic hypothesis. The same, unfortunately, does not seem to be the case for panoplosaurines, largely due to the presence of specimens in Alaska and Texas that do not represent distinct species and that are from formations with poor temporal resolution. As a result, the stratigraphic distribution of panoplosaurines (Fig. 4.56) appears to be more complex than that of contemporaneous North American ankylosaurids.

Denversaurus is the youngest panoplosaurine and is restricted to the upper Maastrichtian (Upper Cretaceous) of Montana and South Dakota USA. The holotype and most of the referred specimens of *Panoplosaurus mirus* are known from the upper Campanian DPF at DPP; however, DPWMA 90-25 was collected in Alaska from Member 3 of the 2 km-thick upper Matanuska Fm. (Jones, 1963; Gangloff, 1995), potentially extending the upper stratigraphic boundary for this taxon into the lower Maastrichtian.

The holotype of *Edmontonia longiceps* was collected in the HCF of Alberta, but the referred specimen TMP 98.98.1 occurs in the older DPF. The full extent of the stratigraphic distribution of *Edmontonia longiceps*, however, is dependent upon the age of the referred specimen (AMNH 3076) from the Aguja Fm. of Texas. The formation's extent is estimated to range from 80.5 Ma (Sullivan and Lucas, 2006) to 70 Ma (Woodward, 2005) or even 68.5 Ma (Sankey, 2010). Two samples of volcanic ash from the upper shales of the formation have been dated to 72.6 Ma +/- 1.5 Ma and 76.9 Ma +/- 1.2 Ma (Breyer et al., 2007; Befus et al., 2008). *Edmontonia rugosidens* potentially has, at present, the most restricted stratigraphic distribution. It is known only from the Campanian DPF and Two Medicine Formation.

With the exceptions of AMNH 3076 from Texas and DPMWA 90-25 from Alaska, panoplosaurine taxa appear to have distributions mirroring contemporaneous ankylosaurids. *Denversaurus,* restricted to the upper Maastrichtian, is roughly contemporaneous with *Ankylosaurus*. *Edmontonia rugosidens* and *Panoplosaurus mirus* are largely restricted to the lower DPF similar to *Dyoplosaurus* (known only from the holotype from the lowermost DPF) and *Euoplocephalus*, although the occurrence of *Edmontonia rugosidens* in the Two Medicine Formation may mean that its range extends further back. If so, its range may be more consistent with that of *Scolosaurus*, also known to occur in the DPF and Two Medicine Formation. *Edmontonia longiceps* has a similar distribution to *Anodontosaurus*, occurring in the DPF and HCF.

Until recently (Arbour et al., 2009; Arbour and Currie, 2013; Penkalski, 2013; Penkalski and Blows, 2013), most North American ankylosaurid specimens had been placed into the genus *Euoplocephalus* (*sensu lato*), due in part to holotype specimens of synonymized taxa lacking good cranial material, creating a wastebasket taxon that extended from 76 to 67 Ma (Arbour and Currie, 2013). Panoplosaurine taxonomy seems to have experienced the opposite, with holotype specimens including complete skulls and in cases extensive postcranial material, culminating in the revision of Bakker (1988) in which almost every specimen was assigned its own taxon. The revision of Carpenter (1990) has been the most widely accepted and is the most applicable in the light of new material, with the exception of the validity of *Denversaurus*. The accurate delineation of panoplosaurine taxa has important paleobiogeographic and biostratigraphic implications for the diversity of dinosaurs in the North American Upper Cretaceous. It is possible that there is a finer stratigraphic and/or geospatial distribution of panoplosaurine

specimens within DPP, but this will need to be tested by ground-truthing the occurrences of all known specimens.

TABLE 4.1. Cranial quantitative data (in mm unless otherwise specified) for Late Cretaceous nodosaurid specimens, and the holotype (SMU 73203) of the outgroup taxon *Pawpawsaurus campbelli*, used in a priori character analyses. Unless otherwise specified, length refers to an anteroposterior dimension, width to a mediolateral dimension, and height to a dorsoventral dimension. Abbreviations: **% POboss offset**, ratio of anterior snout width to width across the postorbital bosses; **Ant:Post L**, ratio of anterior to posterior skull length (both to the midpoint of the orbit); **Antorbital H**, maximum skull height anterior to orbits; **Antorbital L**, length from anteriormost point on skull to the midpoint of the orbit; **A-P L post dermal band**, maximum anteroposterior length of the dermal bony band at the posterior edge of the skull roof; **Dentary H**, maximum height of the dentary; **Dentary L**, maximum length of the dentary; **Dentary tooth row L**, length of the dentary tooth row; **Foramen Magnum D**, average diameter of the foramen magnum; **H pterygoid ramus**, maximum height of the pterygoid ramus of the quadrate; **L**, maximum skull length; **Mandible H**, maximum height of the mandible; **Mandible L**, maximum length of the mandible; **Mandible tooth count**, tooth count of one mandible; **Max TR Div (ant)**, width between anterior termini of maxillary tooth rows; **Max TR Div (post)**, width between posterior termini of maxillary tooth rows; **Maxillary tooth count**, tooth count of one maxilla; **Maxillary tooth row Ang**, angle (in degrees) between the anterior and posterior portions of one maxillary tooth row; **Maxillary tooth row L**, maximum length of one maxillary tooth row; **Min Max TR W**, ratio between the minimum and maximum skull widths; **Min. Snout W**, minimum width of the snout when viewed dorsally; **Occ H**, height of the occipital condyle; **Occ W**, width of the occipital condyle; **Offset POboss**, difference between anterior snout width to width across the postorbital bosses divided by 2; **Orbit Circ**, circumference of the orbit; **Orbit H**, height of the orbit; **Orbit L**, length of the orbit; **Pmx palate L**, maximum length of the premaxillary

palate; **Pmx palate W**; maximum length of the premaxillary palate; **Postorbital H**, maximum skull height posterior to the orbits; **Postorbital L**, length from posteriormost point on skull to the midpoint of the orbit; **Quadrate H**, maximum height of the quadrate; **Quadrate W**, maximum width of the quadrate; **Snout taper**, angle (in degrees) of the lateral edge of the skull (anterior to the orbits) to the median sagittal plane; **Vomer W**, maximum width of the vomerine keel; **W**, maximum skull width; **W @ orbits**, skull width across the midpoint of the orbits; **W @ POboss**, skull width across the postorbital bosses; **W @ QJ boss**, skull width across the quadratojugal bosses; **W ant snout**, skull width at the anterior terminus; **W between ant. Max teeth**, width between the anteriormost maxillary teeth; **W between post. Max teeth**, width between the posteriormost maxillary teeth; **W btw Narial**, width across internarial bridge; **W PoP**, width across paroccipital processes; **W PoP of Qu**, maximum width of the paroccipital process of the quadrate; **W:L**, ratio of maximum skull width to maximum skull length.

Specimen	L	Antorbital H	Postorbital H	Antorbital L	Postorbital L	Ant:Post L	W	W:L	Min. Snout W	W btw Narial	W ant snout	W @ POboss	Offset POboss	% POboss offset	W @ orbits	W @ QJ boss	Snout taper	Pmx palate W	Pmx palate L	Maxillary tooth row L	Maxillary tooth row Ang	Max TR Div (ant)	Max TR Div (post)
Pawpawsaurus	245	91	132	164	80	2.0	203	0.83	86	35	56	190	67	3.4	169	200	13	50	52	74	139	1.8	60
AMNH 5381	469			289	180	1.6					132					322		111					
AMNH 5665		136	175		151		431		199	99		431			296	402	15			181	160	13.2	61
BHI 6225					193		390		186		196	393	99	2.0	350								
BHI 6332	502	194	263	331	171	1.9													125	158			
CMN 2759	350	117	199	231	127	1.8	282		119	78	113	290	89	2.6	276	276		106					
CMN 8531	447	104	155	265	130	2.0	311	0.70	179	53	118	282	82	2.4	276	263		102		151			
CMN 8879	430			311	119	2.6	314	0.73	167	58	178				314		14	128			137	38.0	75
DMNH 468	488			354	134	2.6	220	0.45	191	83	129	206	39	1.6	171	220							
ROM 1215	408	126	171	271	137	2.0	303	0.74	184	55	105	303	99	2.9	271		16	102	128	95	151	7.0	67
TMP 00.12.158	536	219	178	364	172	2.1	336	0.63	128	83	153	354	101	2.3	322		7	114	111	140	137	28.9	71
TMP 81.3.3	433	280	260	265	168	1.6	392	0.90	144	74	117	382	133	3.3	304		11						
TMP 83.25.2	443			280	163	1.7	277	0.63	152	137	144	337	96	2.3	279		16	124	103	102	154	40.2	45
TMP 84.0.32	364	228	221	280	84	3.3	302	0.83	138	100	119	295	88	2.5	292		26	94	81	108	132	4.6	78
TMP 93.11.1							215		120						215		15			121	158	-7.6	55
TMP 97.9.1	477			317	160	2.0	353	0.74	171	81	138	352	107	2.6	328		15	140	134	127	149	1.9	58
USNM 11868	455			293	162	1.8	332	0.73	167	68	133	332	100	2.5	312	312		140	125	128			

Specimen	W between ant. Max teeth	W between post. Max teeth	Min Max TR W	Vomer W	Orbit L	Orbit H	Orbit Circ	Occ W	Occ H	Foramen Magnum D	Quadrate H	Quadrate W	W PoP of Qu	W PoP	H pterygoid ramus	Mandible L	Mandible H	Dentary L	Dentary tooth row L	Dentary H	Maxillary tooth count	Mandible tooth count	A-P L post dermal band
Pawpawsaurus	34	73	32	6.1	35	31	91	31	28	22	21	52	23	54						14		18	
AMNH 5381				6.6	43	42		60	52	38	125	105	57	32		312	129						
AMNH 5665	54	159	54	7.3	41	51	158	60	35					146		352	107						
BHI 6225					88					34													
BHI 6332					74	47		50	52														
CMN 2759					50	45		57	40	31	124	110	48	103		270	150					27	
CMN 8531	65			12.3	61	34		57	48	31	134	85	42	85	55	313	120			141		16	23
CMN 8879	45		31																		36		
DMNH 468								59	59					132									
ROM 1215	60	119	60	17.6	48	35	155	44	25	33	99	95	81	299	103	272	129	56	16	13	19		
TMP 00.12.158	43	106	26	12.5	57	48	168	55	51	33	167	147			52								
TMP 81.3.3			35	8.0	52	49	160	60	49	40	123.	122			56	372	119						
TMP 83.25.2	67	117	61	20.1			167	55	46	29		92			43							40	
TMP 84.0.32	71	135	47	13.7	64	47	172	56	38	30	102	91	26	85	43	287	118					34	
TMP 93.11.1	40	70	38																				
TMP 97.9.1	71	142	59	7.2	62	67	180	60	47	31	108	113			58	352	139	236	163	82	17		58
USNM 11868	62	135	57		68	19		59	42	35	122	98	46	102	93	353	121	243	140	86	16		

TABLE 4.2. Cranial quantitative data for Late Cretaceous nodosaurid specimens, and the holotype (SMU 73203) of the outgroup taxon *Pawpawsaurus campbelli*, used in multivariate analyses. Data represent raw measurement data (in mm on the left) and size-corrected data (right) created by dividing each measurement by the largest value. Abbreviations are from Table 1.

Specimen	L	Antorbital L	Postorbital L	W	Min. Snout W	W btw Narial	W ant snout	W @ orbits
Pawpawsaurus	245	164	80	203	86	35	56	169
CMN 2759	350	231	127	282	119	78	113	276
CMN 8531	447	265	130	311	179	53	118	276
CMN 8879	430	311	119	314	167	58	178	314
DMNH 468	488	354	134	220	191	83	129	171
ROM 1215	408	271	137	303	184	55	105	271
TMP 00.12.158	536	364	172	336	128	83	153	322
TMP 81.3.3	433	265	168	392	144	74	117	304
TMP 83.25.2	443	280	163	277	152	137	144	279
TMP 84.0.32	364	280	84	302	138	100	119	292
TMP 97.9.1	477	317	160	353	171	81	138	328
USNM 11868	455	293	162	332	167	68	133	312

Specimen	L	Antorbital L	Postorbital L	W	Min. Snout W	W btw Narial	W ant snout	W @ orbits
Pawpawsaurus	0.46	0.45	0.47	0.52	0.45	0.25	0.32	0.51
CMN 2759	0.65	0.63	0.74	0.72	0.62	0.57	0.63	0.84
CMN 8531	0.83	0.73	0.76	0.79	0.94	0.39	0.67	0.84
CMN 8879	0.80	0.85	0.69	0.80	0.87	0.42	1.00	0.96
DMNH 468	0.91	0.97	0.78	0.56	1.00	0.61	0.72	0.52
ROM 1215	0.76	0.75	0.80	0.77	0.97	0.40	0.59	0.83
TMP 00.12.158	1.00	1.00	1.00	0.86	0.67	0.61	0.86	0.98
TMP 81.3.3	0.81	0.73	0.98	1.00	0.75	0.55	0.65	0.93
TMP 83.25.2	0.83	0.77	0.95	0.71	0.79	1.00	0.81	0.85
TMP 84.0.32	0.68	0.77	0.49	0.77	0.72	0.73	0.67	0.89
TMP 97.9.1	0.89	0.87	0.93	0.90	0.90	0.59	0.78	1.00
USNM 11868	0.85	0.81	0.94	0.85	0.88	0.50	0.75	0.95

TABLE 4.3. Character-specimen matrix used in parsimony analysis of Late Cretaceous Nodosauridae and three outgroup taxa, *Emausaurus, Pawpawsaurus*, and *Scelidosaurus*. Some cranial and dental characters are modified from Vickaryous et al. (2004) and some new characters are based on Bakker (1988) and Carpenter (1990).

	1	2	3	4	5	6	7	8	9	10	11	12	13	14	15	16	17	18	19	20	21	22	23	24	25	26	27	28	29	30	31	32	33	34	35	36	37	38	39	40	41	42
Scelidosaurus	0	?	0	?	?	0	0	?	0	0	?	?	0	0	0	0	?	0	0	0	0	0	0	0	0	1	0	0	0	0	?	?	?	?	?	0	0	0	?	?	?	0
Emausaurus	0	0	0	0	?	0	?	0	?	?	?	?	?	?	?	0	?	0	0	0	0	0	0	0	0	1	0	0	0	0	?	?	?	0	?	0	0	0	?	?	?	0
Pawpawsaurus	0	0	0	1	1	1	1	1	1	1	1	2	1	1	1	1	?	1	1	0	1	1	1	1	1	?	?	1	?	2	0	0	0	?	?	?	0	1	0	1	1	0
AMNH 3076	?	?	?	1	?	1	1	?	?	?	?	?	?	?	?	?	?	1	1	1	1	1	1	?	?	?	?	?	?	?	?	0	0	?	?	?	0	4	?	1	1	?
AMNH 5381	1	?	1	1	0	?	1	?	1	?	?	?	1	?	1	1	?	1	1	1	0	1	1	?	1	?	1	?	?	1	?	1	0	?	?	?	0	4	?	0	?	?
AMNH 5665	1	?	1	?	?	1	1	?	1	1	1	?	1	?	1	1	1	1	1	1	?	1	?	1	1	?	1	1	0	2	?	1	0	?	1	1	0	4	0	?	?	?
BHI 6225	?	?	?	?	?	?	?	1	1	1	?	?	?	?	1	?	?	1	1	1	1	?	1	?	?	?	?	?	?	?	?	1	0	?	1	?	0	2	?	?	?	1
BHI 6332	?	?	1	1	0	?	?	?	1	?	1	?	?	1	1	0	?	1	1	1	1	?	?	1	?	?	?	?	?	2	?	?	?	0	?	?	0	?	?	0	?	?
CMN 2759	1	1	1	1	0	1	1	1	1	1	1	2	?	1	1	1	?	1	1	1	1	1	1	1	1	?	1	1	1	2	?	0	1	?	0	0	0	3	0	1	0	0
CMN 8531	2	?	1	1	0	1	1	?	1	1	1	?	1	?	1	1	?	1	1	1	1	1	1	1	1	?	1	0	0	2	2	1	0	?	1	2	0	3	?	1	1	0
DMNH 468	?	?	1	1	?	1	1	?	1	1	1	?	?	?	1	1	?	1	1	1	1	1	1	1	?	?	?	?	0	2	?	?	0	?	?	?	0	2	?	1	0	1
DPMWA 90-25	?	?	?	1	?	?	1	?	1	?	?	?	1	?	?	?	?	?	1	?	?	?	1	1	?	?	?	?	?	?	?	?	1	?	?	?	1	2	0	?	?	?
ROM 1215	1	0	1	1	0	1	1	?	1	1	1	2	1	?	1	1	?	1	1	1	1	1	1	1	1	?	1	0	1	1	1	0	1	1	0	0	1	2	0	0	0	0
ROM 20892	?	?	?	?	?	?	?	?	?	?	?	?	1	?	1	0	?	1	1	1	1	1	?	?	?	?	?	?	?	2	2	0	?	?	?	?	?	2	?	?	?	?
TMP 00.12.158	1	?	1	1	0	?	1	?	1	?	1	2	1	?	1	1	?	1	1	1	0	1	1	?	?	?	?	?	?	1	1	2	1	0	?	?	?	0	?	1	1	0	0
TMP 83.25.2	?	?	1	1	0	?	1	?	1	?	1	2	1	?	1	1	?	1	1	1	1	1	1	?	?	?	?	?	?	1	2	?	0	1	?	?	?	0	?	1	0	0	1
TMP 98.67.1	?	?	?	?	?	?	1	?	1	?	?	?	?	?	?	?	?	1	1	1	?	?	1	?	1	?	1	?	?	?	?	0	0	?	0	?	0	?	?	0	?	0
TMP 98.98.1	0	0	1	1	0	?	1	?	1	?	1	2	1	?	?	?	?	1	1	1	1	1	1	1	1	?	1	1	?	?	?	0	0	?	?	?	0	4	?	1	?	1
UALVP 16249	0	0	1	1	0	?	1	1	1	1	?	2	1	?	1	1	?	1	1	1	1	1	1	?	?	?	?	?	?	2	?	1	0	?	?	?	0	?	1	0	1	1
USNM 11868	?	?	1	1	0	?	1	?	1	?	1	2	1	?	1	1	?	1	1	1	?	1	1	?	1	?	1	1	?	1	?	1	0	?	1	1	0	?	0	0	0	0

TABLE 4.4. Limb bone measurements (mm) for some Late Cretaceous nodosaurid specimens. Abbreviations: **C**, midshaft circumference; **DW**, maximum distal width; **L**, maximum proximodistal length; **M**, manual; **MC**, metacarpal; **MPh**, manual phalanx; **MT**, metatarsal; **MW**, maximum midshaft width; **P**, pedal; **PW**, maximum proximal width; **S**, side; **Spec**., specimen number.

Spec.		**S**	**L**	**PW**	**MW**	**DW**	**C**
AMHH 5381	humerus	L	563	329	89	219	288
CMN 2759	fibula	L	315	17	40	70	106
	humerus	L	440	244	71	195	201
	M ungual I-2	L	50	38	36	22	99
	M ungual II-3	L	52	47	42	31	101
	M ungual III-3	L			42	31	101
	MC I	L	97	53	31	45	
	MC II	L	110	48	35	51	97
	MC III	L	117	69	37	43	104
	MPh I-1	L	51	42	37	41	
	MPh II-1	L	26	55	52	49	129
	MPh II-2	L	27	47	49	48	117
	MPh III-1	L	28	53			
	MPh III-2	L	22	45	48	47	
	MT		134	43	35	67	118
	P ungual		82	58	50	28	117
	P ungual		81	54	52	29	120
	tibia	L	381	47	70	147	191
	tibia	R		39	64	157	193
CMN 8531	femur	R	661	244	109	221	283
	humerus	L	485	195	106	225	266
	radius	L	291	112	34	62	164
	radius	R	287	53	33	65	181
	tibia	R		106			
	ulna	L	323	194	74	53	207
TMP 98.98.1	fibula	R	133	128	50	66	133
	humerus	R	586	290	89	194	305
	radius	R	425	233	109	81	251
	ulna	R			69	157	193

TABLE 4.5. (next page). Vertebral measurements (mm) for some Late Cretaceous nodosaurid specimens. Abbreviations: **AH**, anterior centrum height; **AW**, anterior centrum width; **Cd**, caudal; **Cv**, cervical; **D**, dorsal; **H**, total height; **L**, total centrum anteroposterior length; **MW**, middle centrum width; **NCH**, neural canal height; **NCW**, neural canal width; **NSH**, neural spine height measured from top of centrum; **PH**, posterior centrum height; **PW**, posterior centrum width; **S**, side; **S1–4**, sacrals; **Spec**., specimen number.

Spec.	S	L	H	AW	MW	PW	AH	PH	NCH	NCW	NSH
AMNH 5381	Cd	59	217	93	83	107	80	90	44	21	127
	D	263	306	136	93	121	115	110	35	23	201
	D	93	304	116	61	130	132	115	51	19	189
	D	81	302	109	75	109	107	104	31	21	181
	D	89		117	86	130	100	114	40	32	
	D	74		104	153	53	109	119	37		
CMN 2759	Cd	58		92	83	95			40	25	
	Cd	51		84	64	83	65	68		23	
	Cv1	89	77	72			47		28	48	40
	Cv2	53	114								51
	Cv3	63	113			87		49			76
	DS1			87		87					
CMN 8531	Cd	44	202	80	78	93	82	112	35	18	96
	Cd	41		87	81	93	70	76	19	22	77
	Cd	55	195	102	94	98	75	91	39	25	104
	Cd	48		89	84	92	74	80	22	15	74
	Cd	63	179	107	96	103	75	80	17	17	96
	Cd	43	202	99	86	102	85	103	32	21	100
	Cd1					99					
	Cv	53	187	98	89	111	79	89	31	48	106
	D	75		106	87	107	69	104	23	39	
	D	87	240	88	55	85	98	99	30	19	168
	D	84	252	82	61	98	91	94	28	28	172
	D	73	257	83	55	91	97	91	25	21	166
	D	74	247	109	76	117	102	99	29	29	163
	D	80	260	103	78	118	98	94	35	26	161
	D	73		122	96	118					
	D	82		115	91	112					
	D	92		100	88	102					
	S1			126		154					
	S2			154		151					
	S3			151		111					
	S4	74		112	92	97					

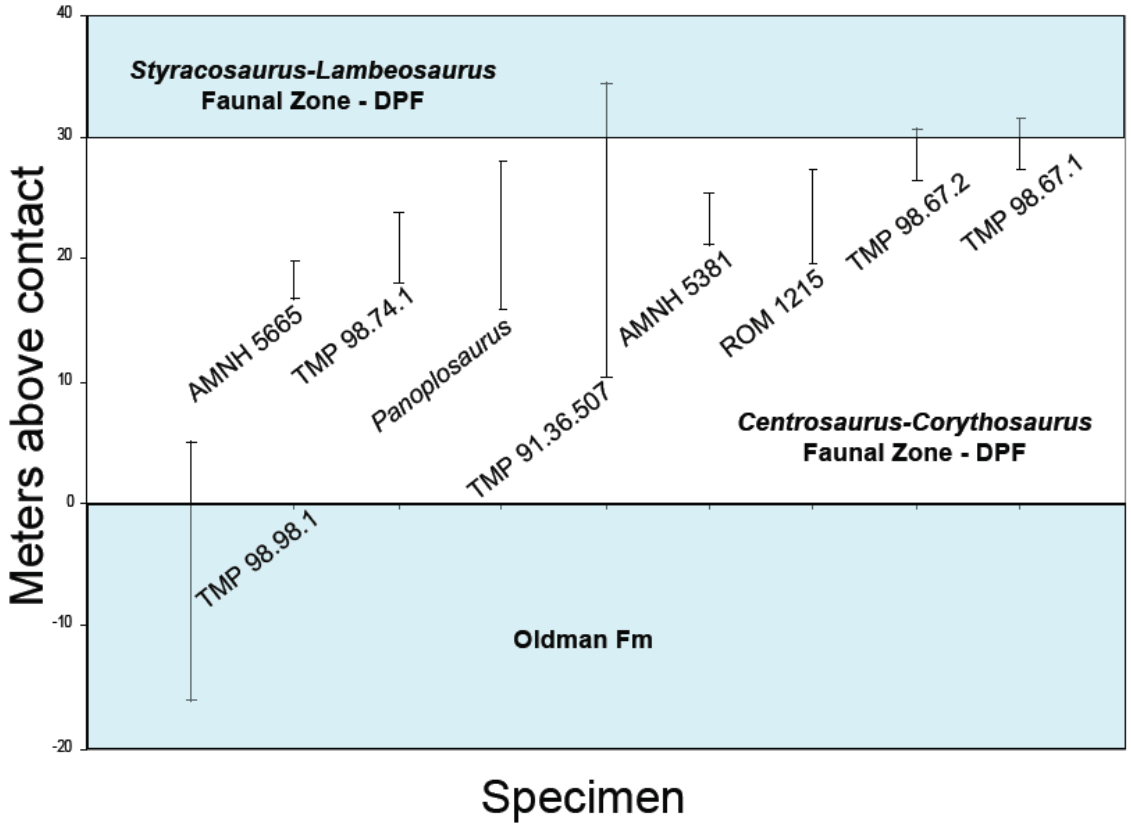

FIGURE 4.1. Vertical distance (m) relative to Oldman Formation/DPF contact of nodosaur crania from DPP. *Panoplosaurus* is the holotype (CMN 2759) of *Panoplosaurus mirus*. Because the exact stratigraphic positions of all specimens were ground-truthed, these values were estimated using contact data from Eberth (2005, fig. 3.3) and specimen provenance information from Currie and Koppelhus (2005, CD-ROM Supplement) and Stenberg (1950) in Google Earth 7.1.2.2041. Error bars = standard deviation of the mean. Faunal Zones are from Ryan and Evans (2005).

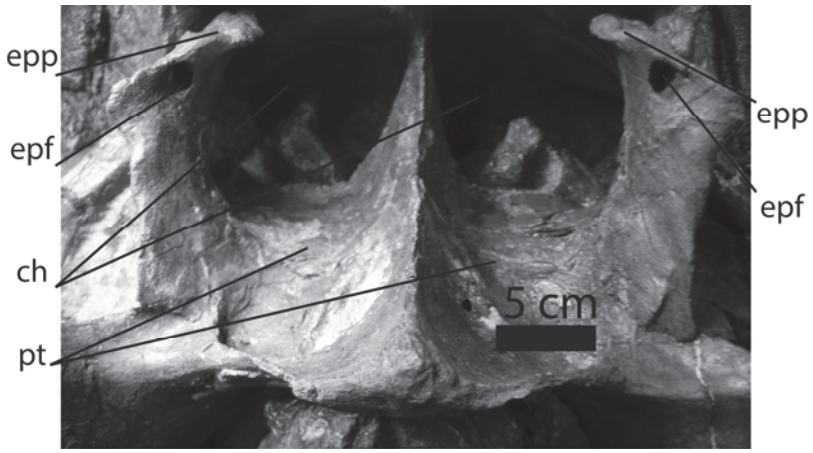

FIGURE 4.2. Ectopterygoid-pterygoid foramen on the medial surface of the ectopterygoid pad. Posterior palate of ROM 1215 in ventral view, anterior is up.

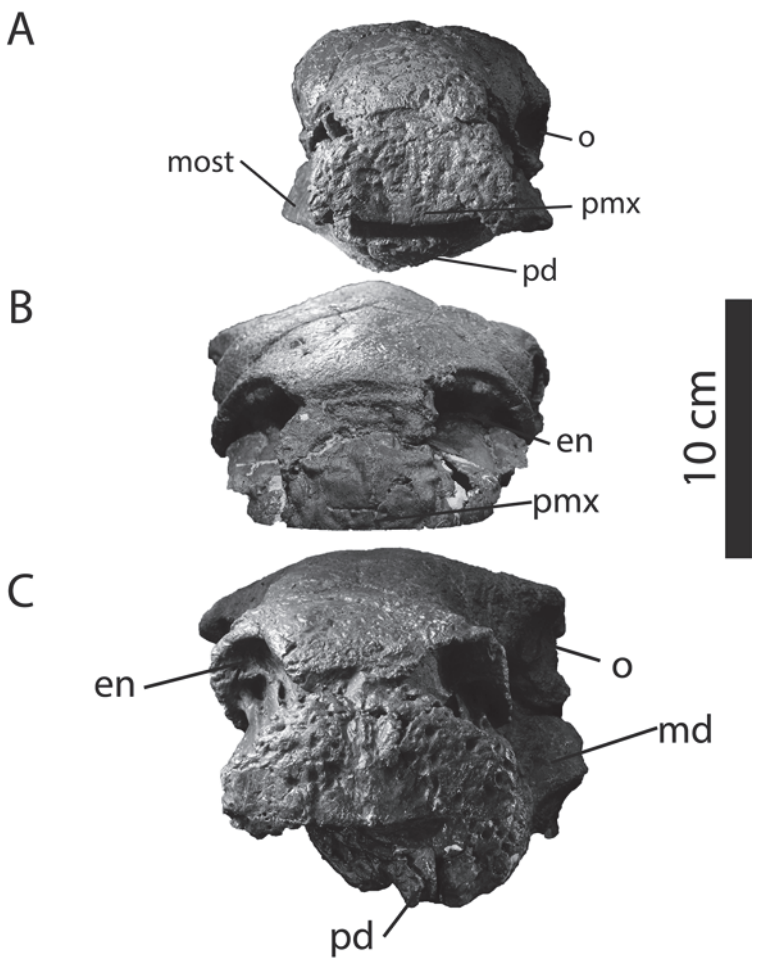

FIGURE 4.3. Variation of the width of the internarial bar in Late Creaceous North American nodosaurids. Skulls of CMN 2759 (A), ROM 1215 (B), and AMNH 5381 (C), in anterior view, dorsal is up.

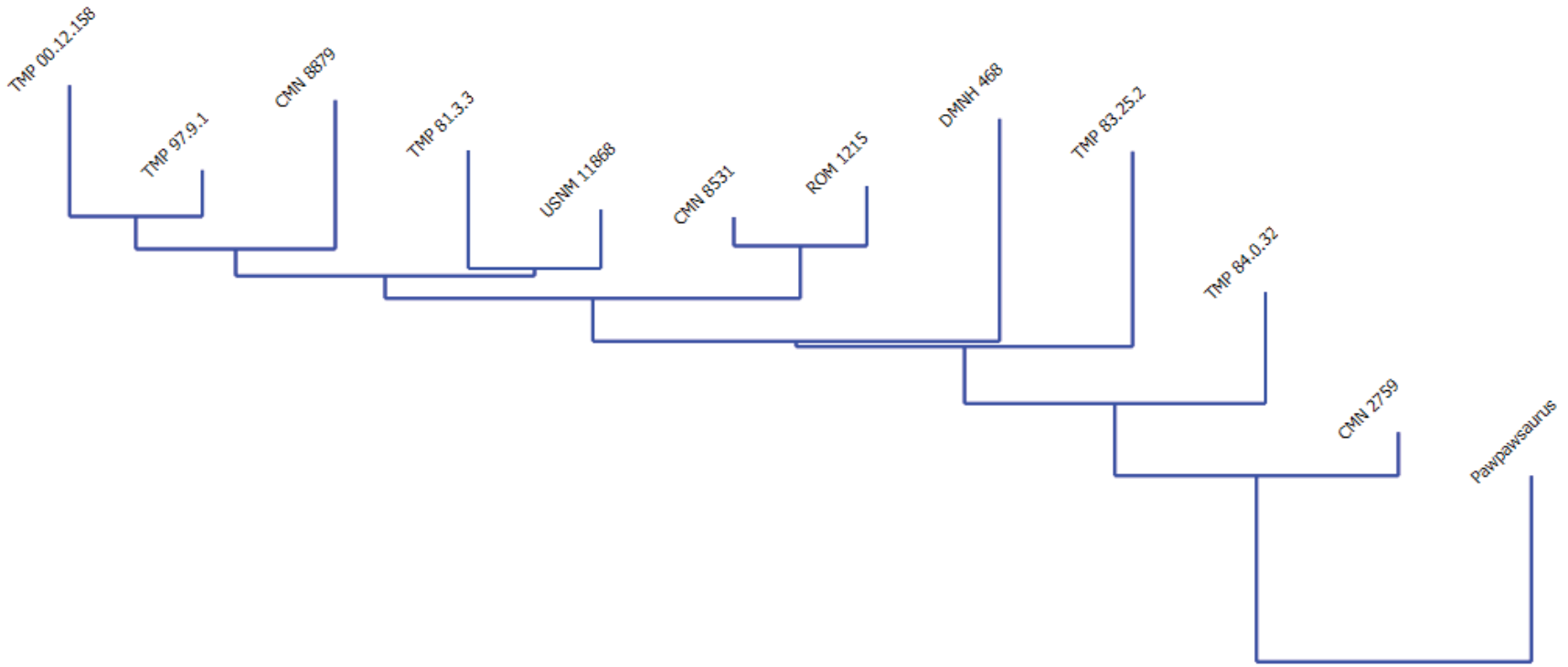

FIGURE 4.4. Result of neighbor joining analysis on size-corrected measurement data (Table 2) for Late Cretaceous nodosaurid specimens, and the holotype (SMU 73203) of the outgroup taxon *Pawpawsaurus campbelli*.

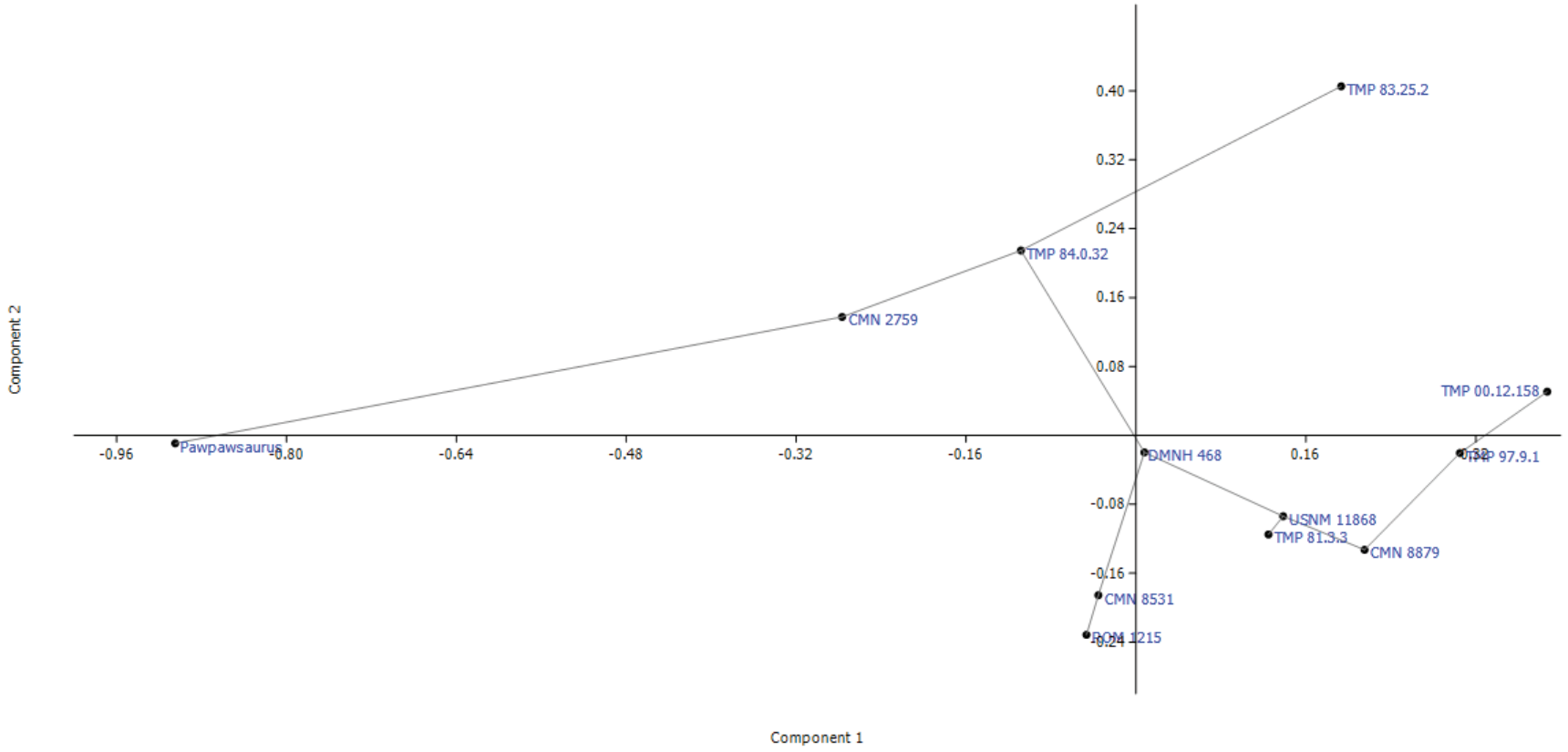

FIGURE 4.5. Result of Principal Components Analysis on size-corrected measurement data (Table 2) for Late Cretaceous nodosaurid specimens, and the holotype (SMU 73203) of the outgroup taxon *Pawpawsaurus campbelli*, with the minimum spanning tree.

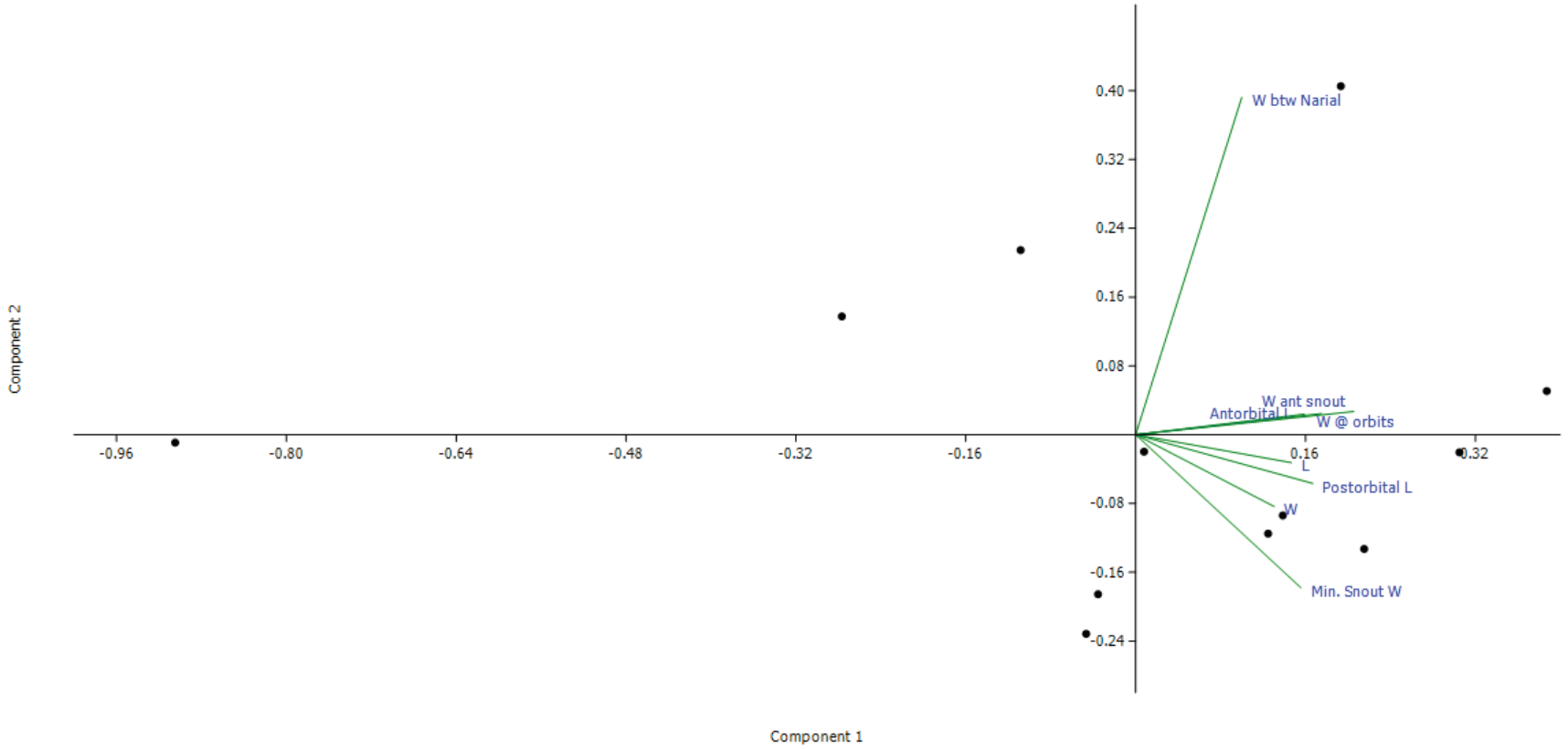

FIGURE 4.6. Principal Components Analysis biplot based on size-corrected measurement data (Table 2) for Late Cretaceous nodosaurid specimens, and the holotype (SMU 73203) of the outgroup taxon *Pawpawsaurus campbelli*, with the minimum spanning tree. Anterior snout width has largest coordinate on the horizontal axis and the width of the narial bridge has the largest coordinate on the vertical axis. Abbreviations are from Table 1.

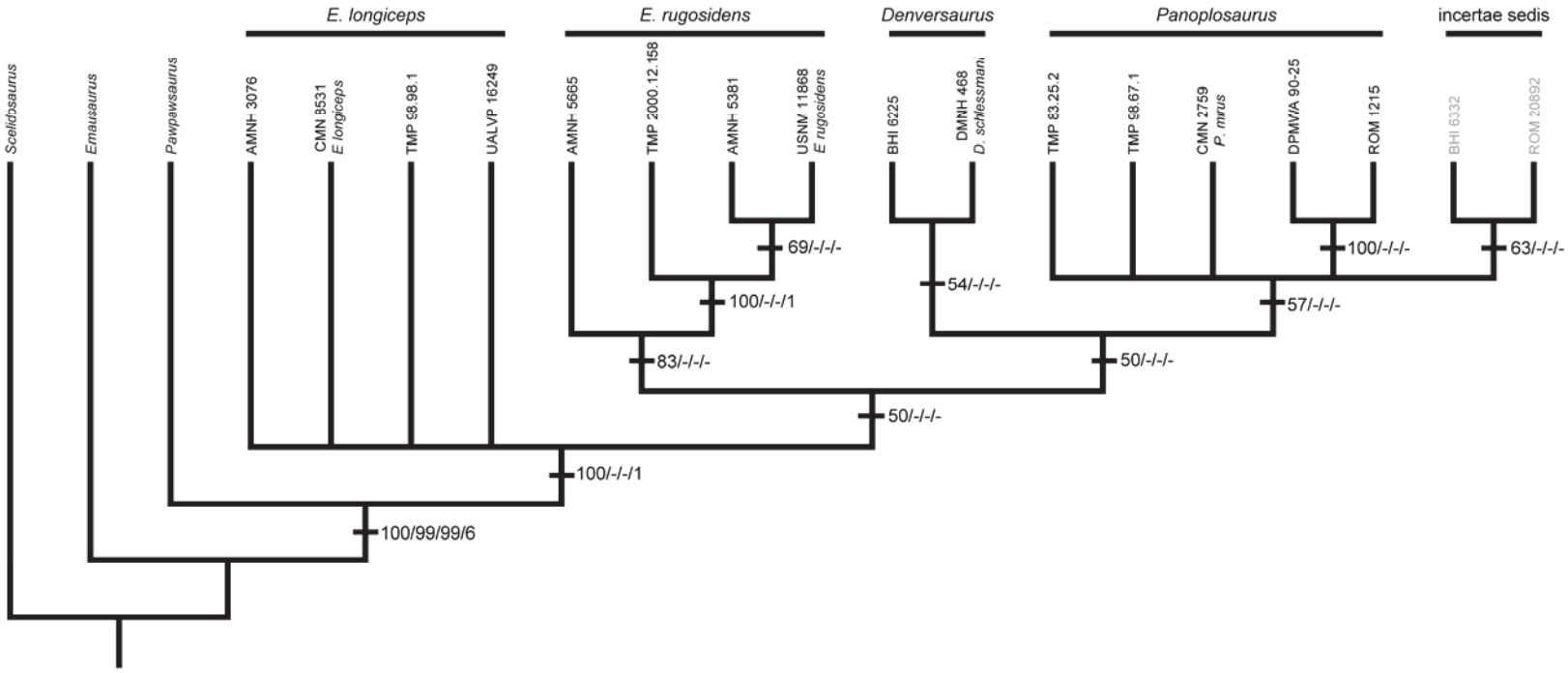

FIGURE 4.7. 50% majority rule consensus of 147 most parsimonious tress based on a traditional (=heuristic) search (tree bisection reconnection swapping algorithm) of 1000 replicates in TNT 1.1 of 42 morphological characters (all equally weighted and unordered; 26 (=63%) parsimony informative), three outgroup taxa (*Emausaurus*, *Pawpawsaurus*, and *Scelidosaurus)*, and 17 ingroup Late Cretaceous nodosaurid specimens. Tree edited in Mesquite version 2.75 (build 564) for Windows. Numbers on branches represent majority rule percentages, bootstrap, jackknife, and Bremer support values. Dashes (-) indicate bootstrap/jackknife values below 50% or Bremer support values below 1. Holotypes are indicated by the species name at each terminal node. Taxa along the top indicate the resultant taxonomy of Panolposaurinae followed in this study.

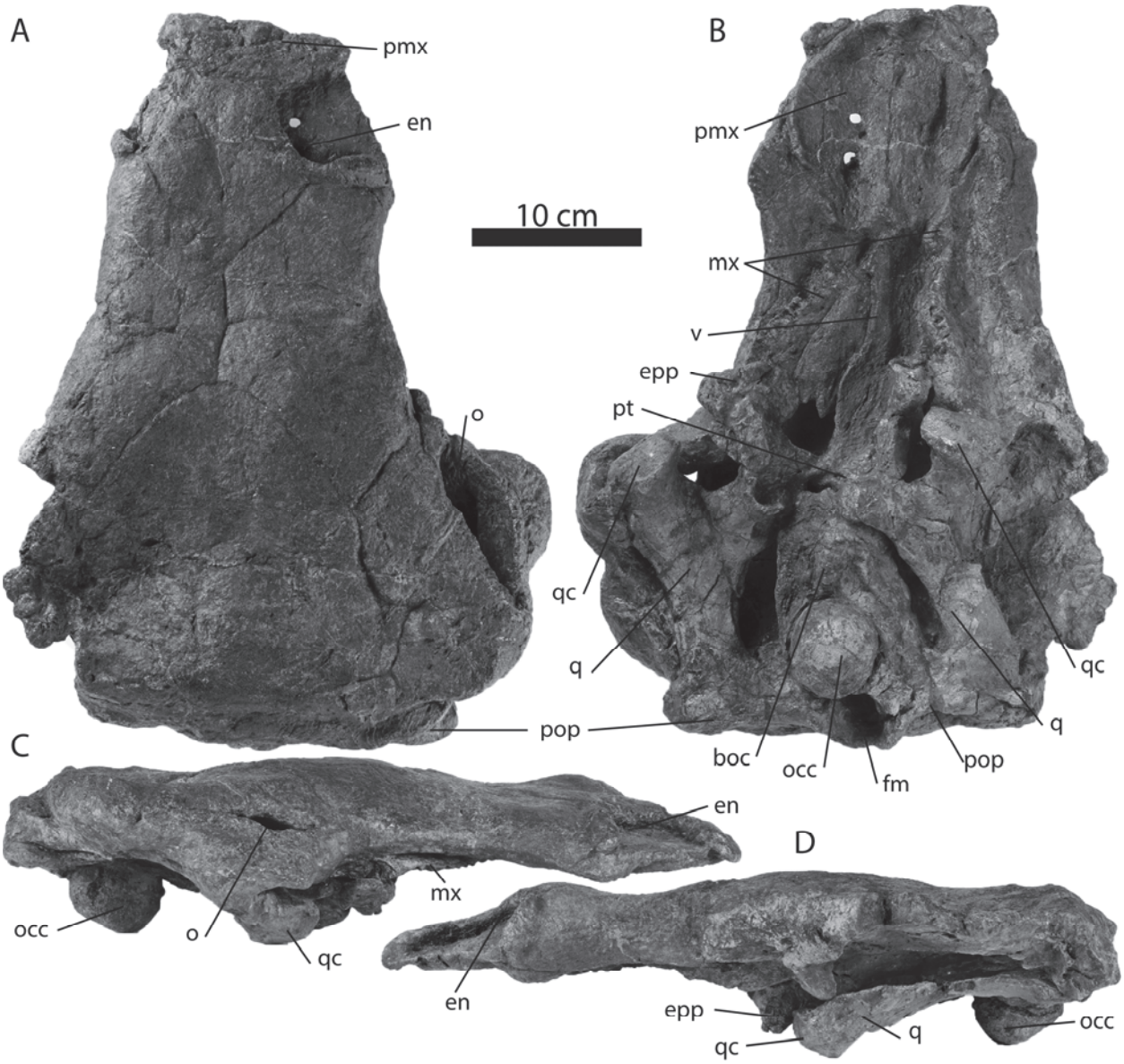

FIGURE 4.8. Skull of *Denversaurus schlessmani* (holotype, DMNH 468) in dorsal (A), ventral (B), right lateral (C), and left lateral views. Anterior is up in A and B. Dorsal is up in C and D.

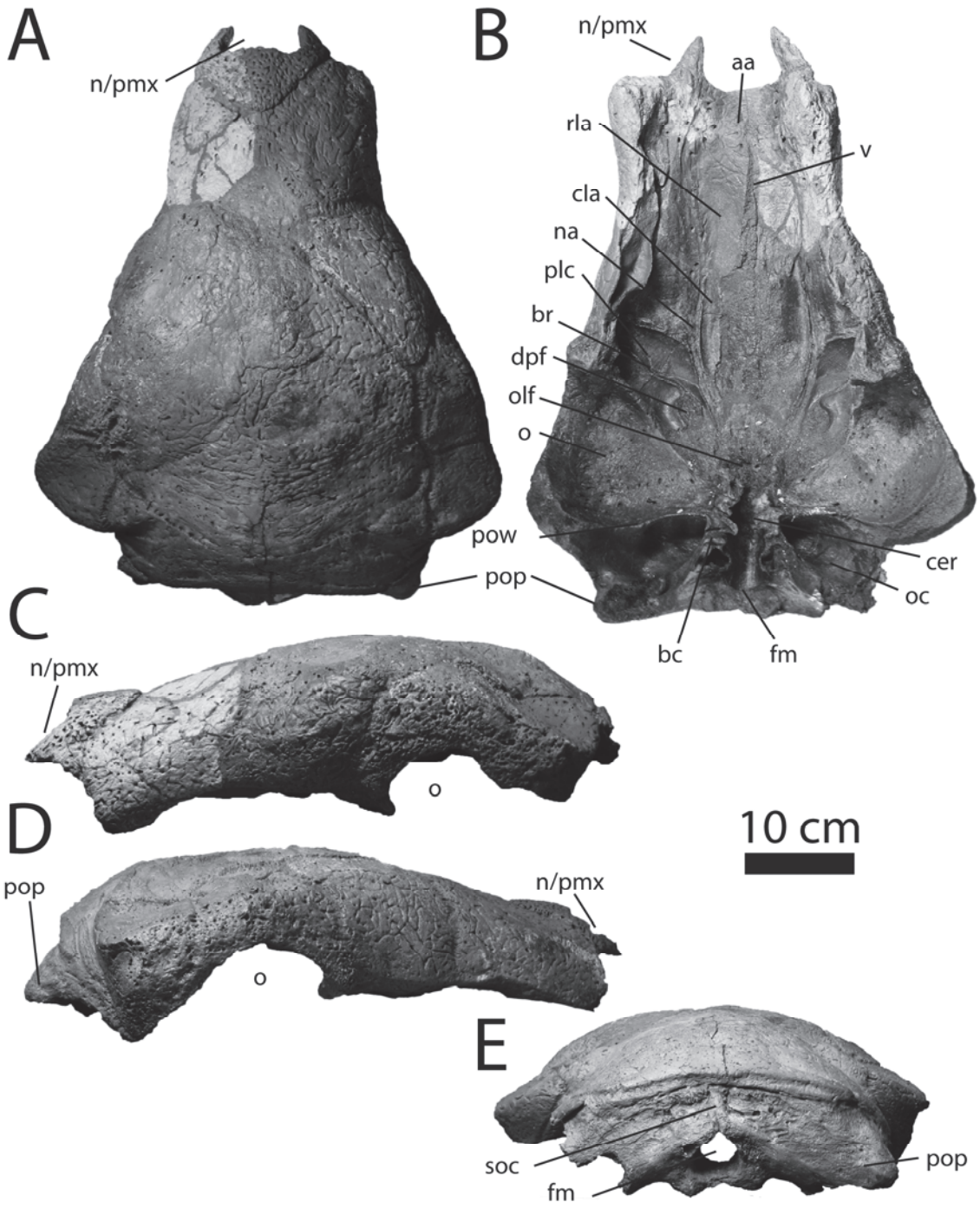

FIGURE 4.9. Skull roof of *Denversaurus schlessmani* (BHI 6225) in dorsal (A), ventral (B), left lateral (C), right lateral (D), and posterior (E) views.

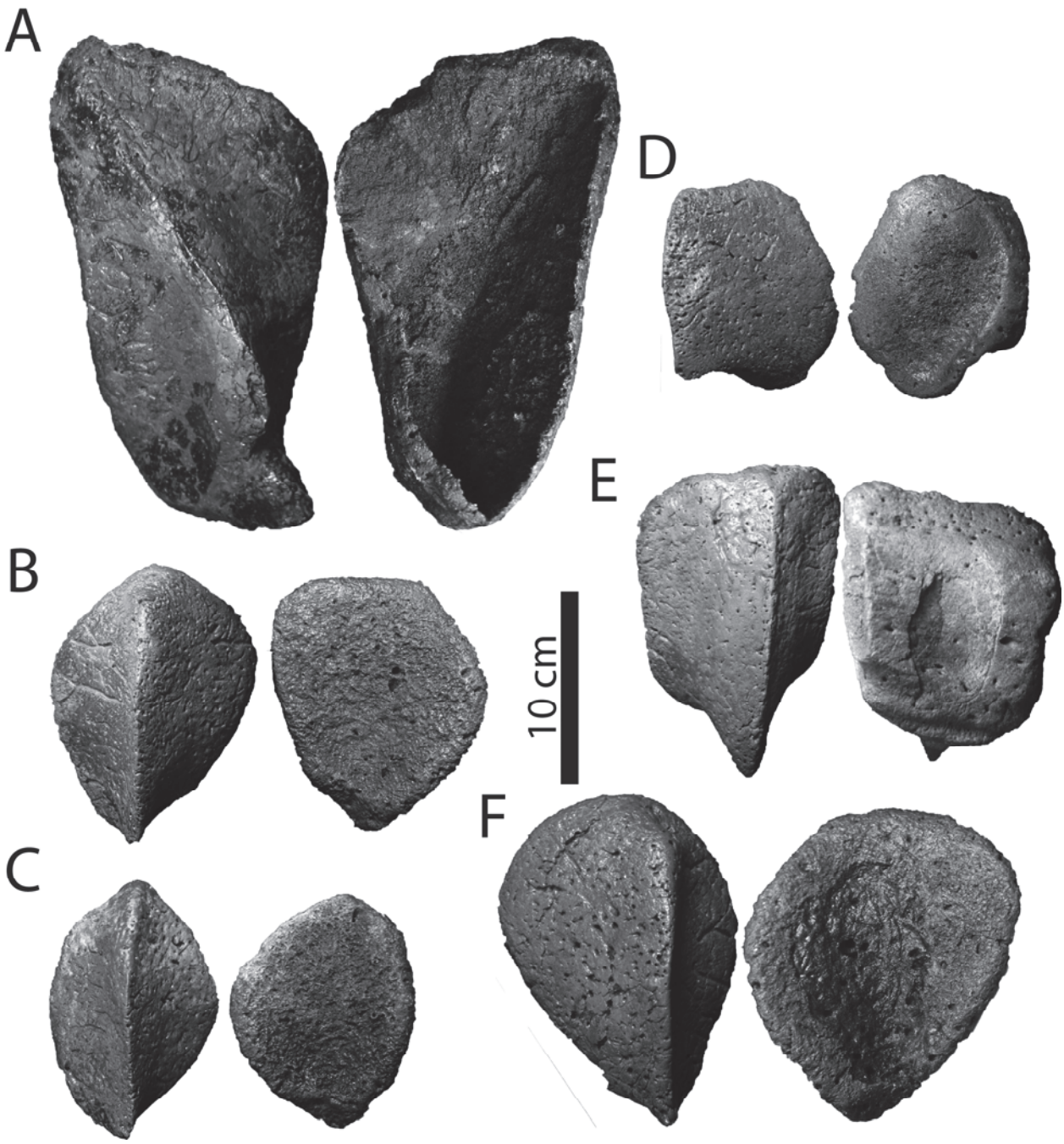

FIGURE 4.10. Osteoderms of *Denversaurus schlessmani* (BHI 6225) in external and basal views. Anterior is up.

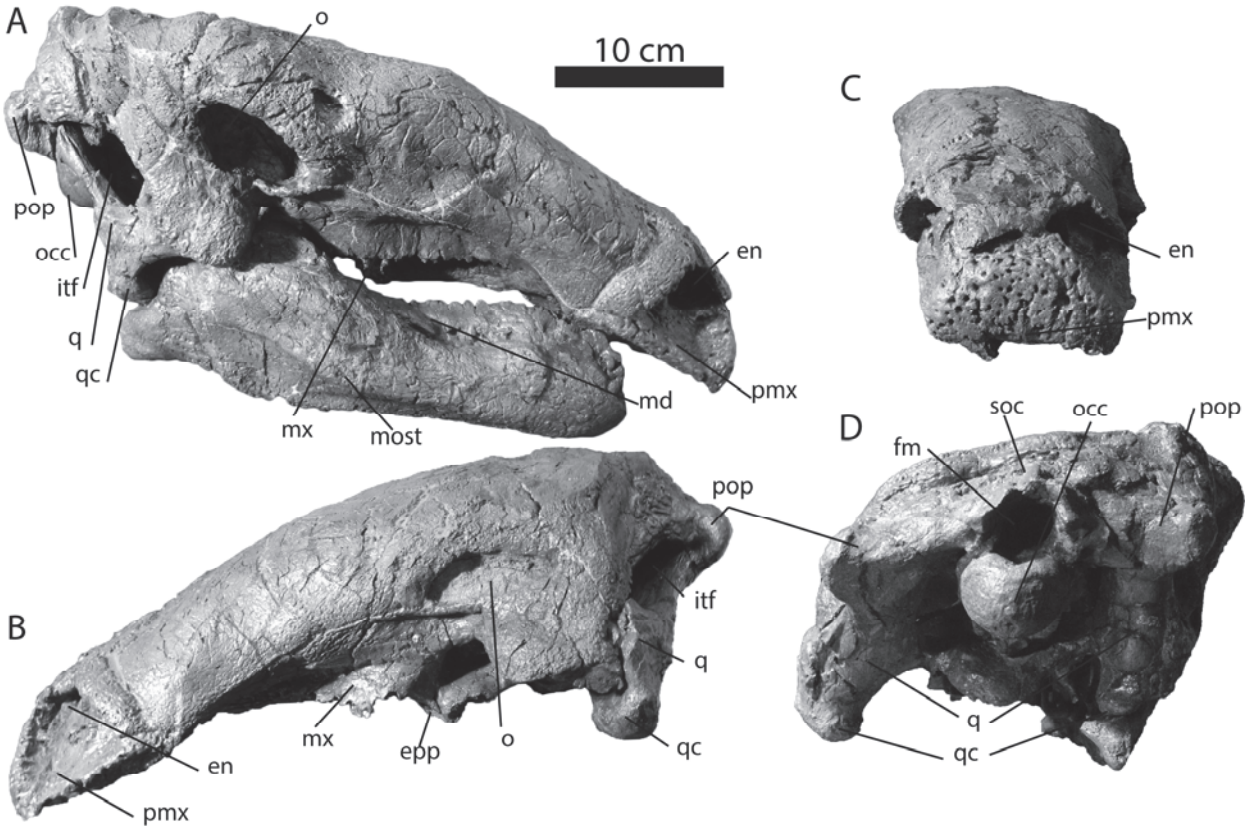

FIGURE 4.11. Skull and articulated right mandible of *Edmontonia longiceps* (CMN 8351, holotype) in right lateral (A), left lateral (B), anterior (C), and posterior (D) views.

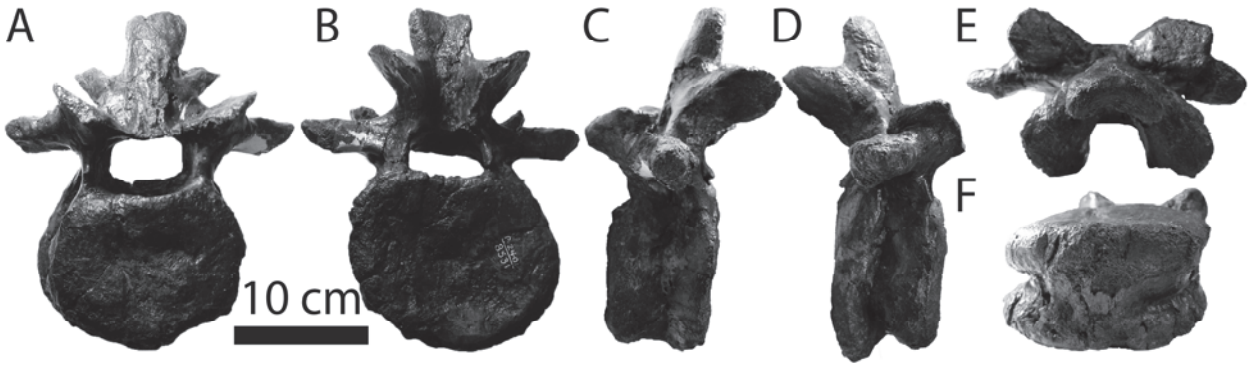

FIGURE 4.12. Cervical vertebra of *Edmontonia longiceps* (CMN 8351, holotype) in anterior (A), posterior (B), left lateral (C), right lateral (D), dorsal (E), and ventral (F) views. Dorsal is up in A–D and anterior is up in E–F.

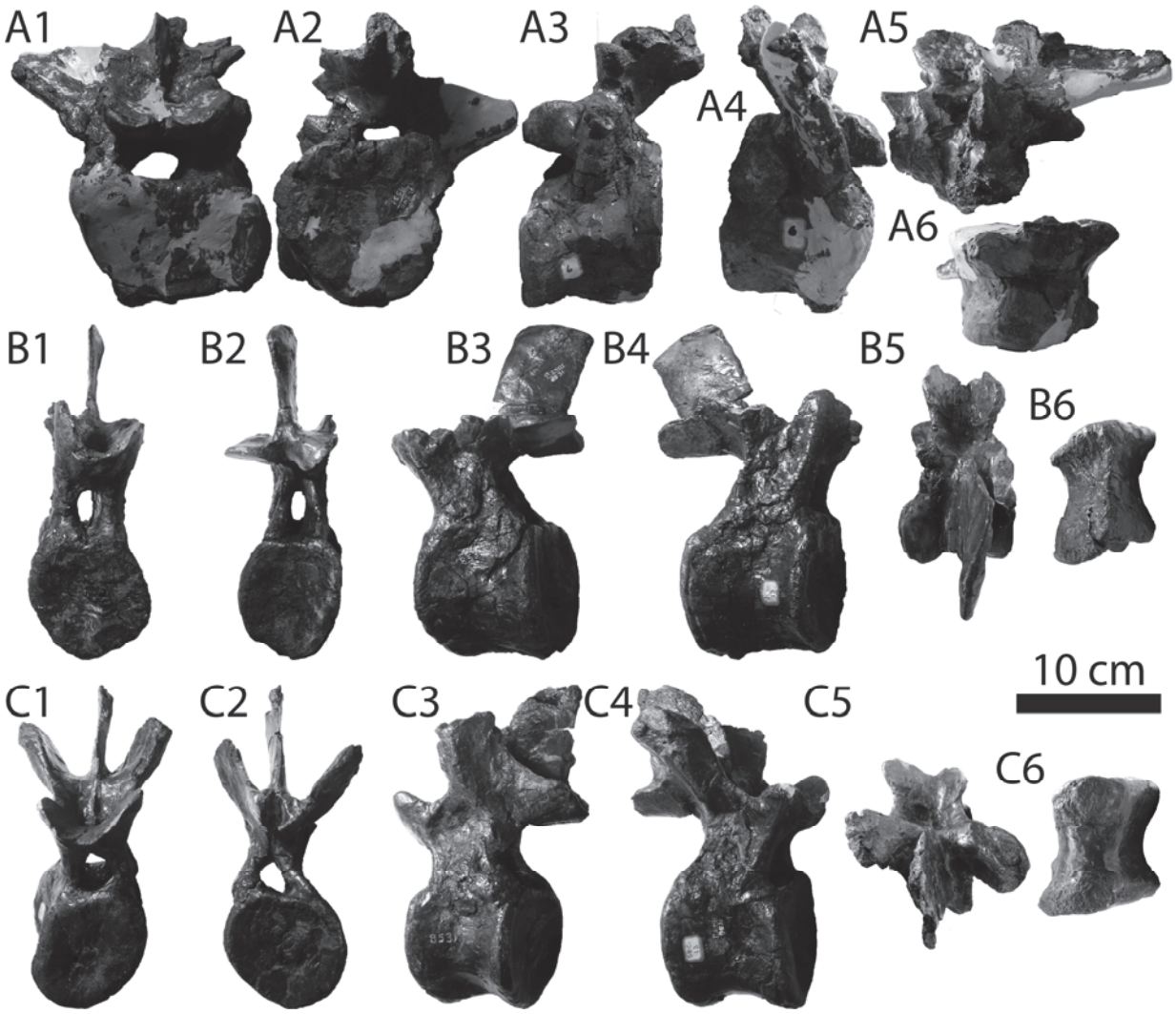

FIGURE 4.13. Dorsal vertebrae of *Edmontonia longiceps* (CMN 8351, holotype) in anterior (1), posterior (2), left lateral (3), right lateral (4), dorsal (5), and ventral (6) views. Dorsal is up in 1–4 and anterior is up in 5–6.

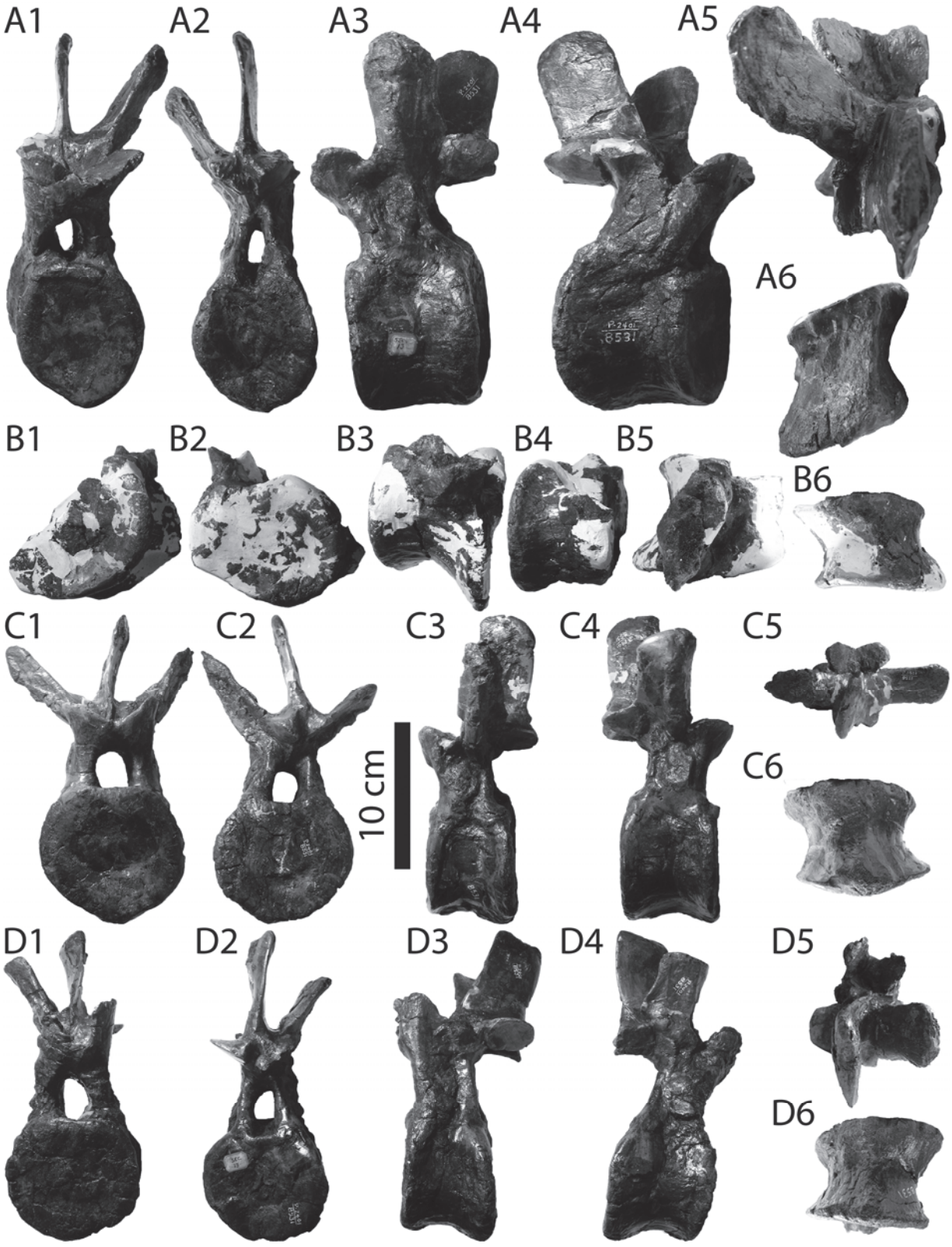
A1
A2
A3
A4
A5
A6
B1
B2
B3
B4
B5
B6
C1
C2
C3
C4
C5
C6
10 cm
D1
D2
D3
D4
D5
D6

FIGURE 4.14 (previous page). Dorsal vertebrae of *Edmontonia longiceps* (CMN 8351, holotype) in anterior (1), posterior (2), left lateral (3), right lateral (4), dorsal (5), and ventral (6) views. Dorsal is up in 1–4 and anterior is up in 5–6.

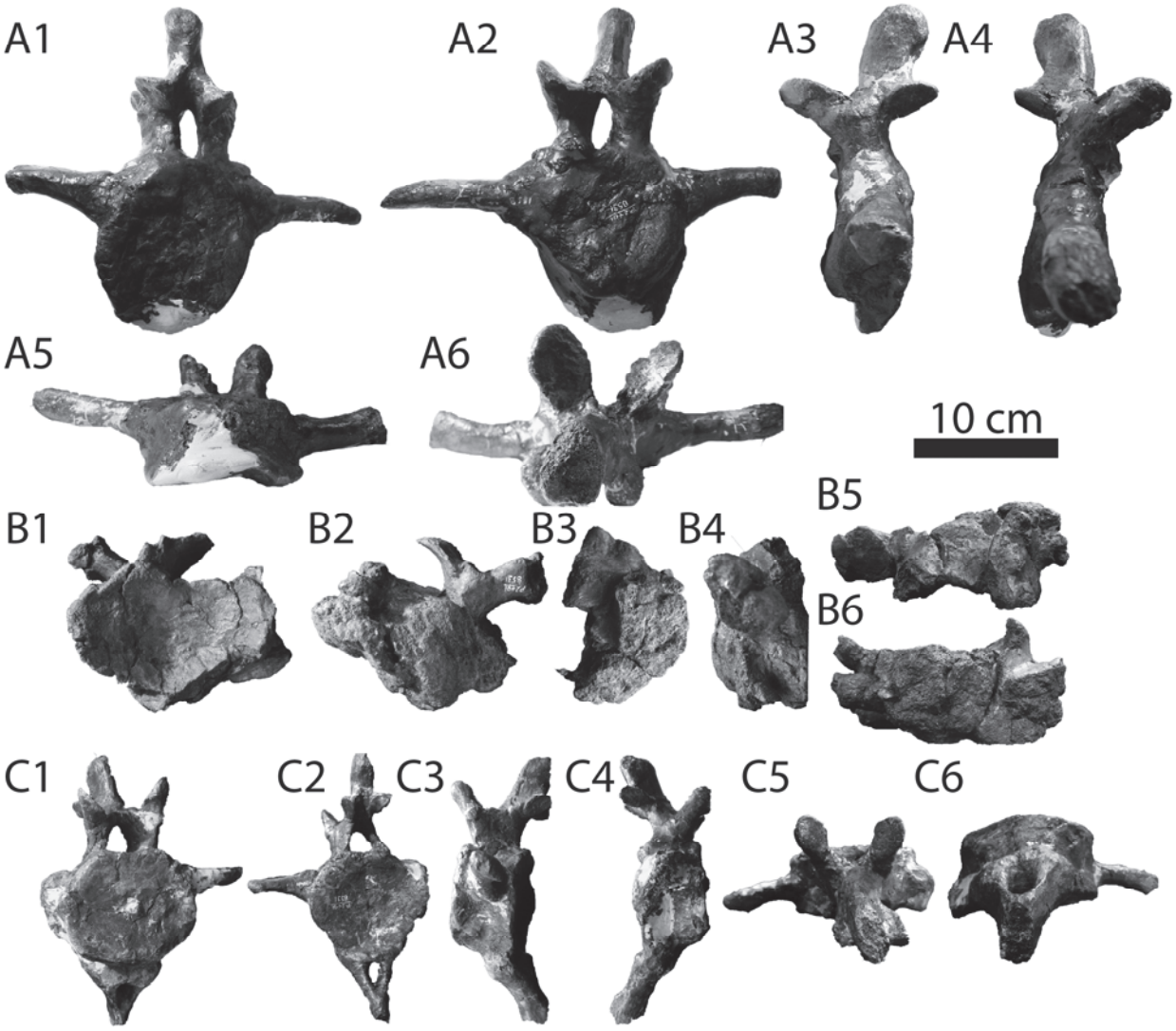

FIGURE 4.15. Caudal vertebrae of *Edmontonia longiceps* (CMN 8351, holotype) in anterior (1), posterior (2), left lateral (3), right lateral (4), dorsal (5), and ventral (6) views. Dorsal is up in 1–4 and anterior is up in 5–6.

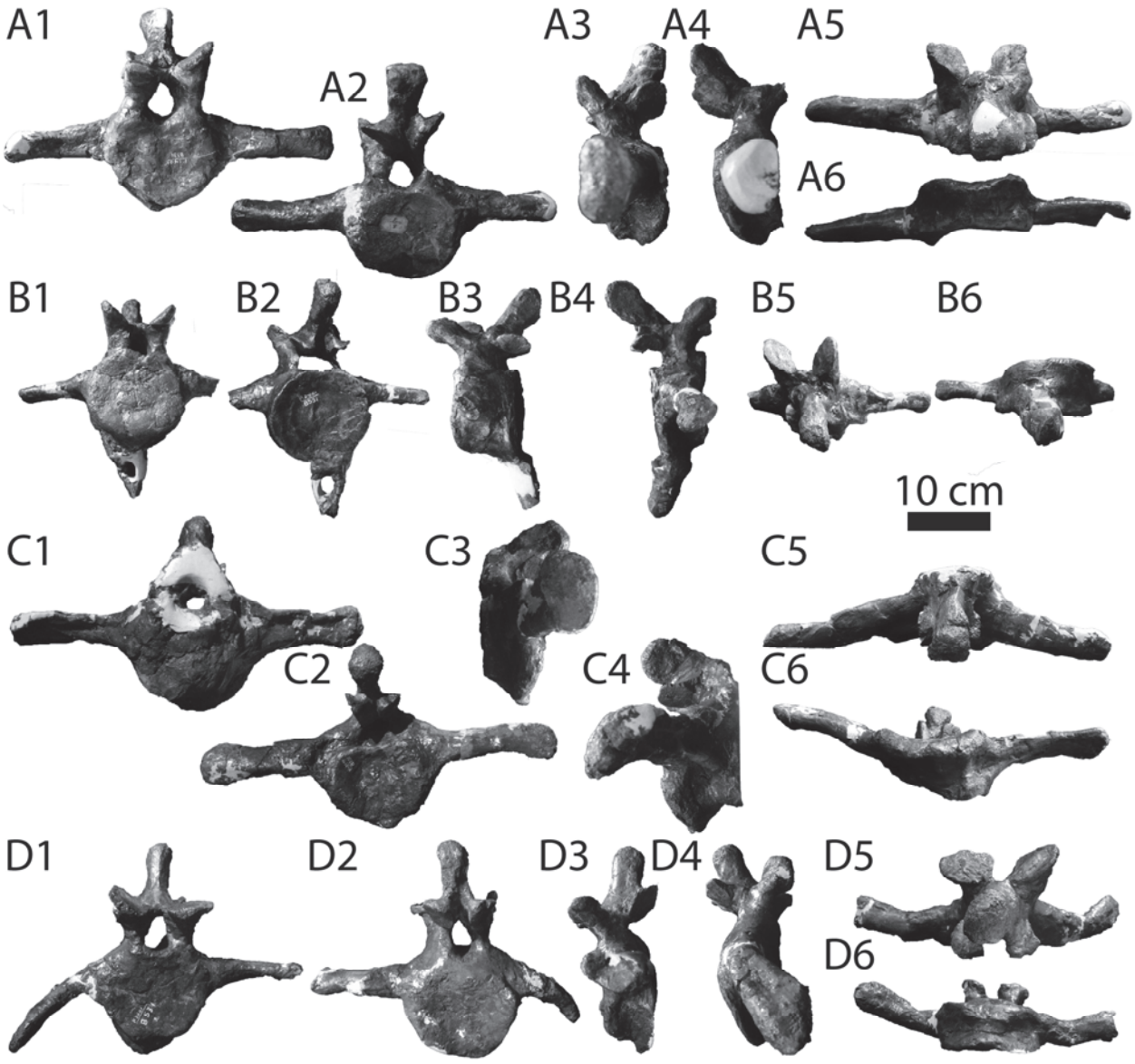

FIGURE 4.16. Caudal vertebrae of *Edmontonia longiceps* (CMN 8351, holotype) in anterior (1), posterior (2), left lateral (3), right lateral (4), dorsal (5), and ventral (6) views. Dorsal is up in 1–4 and anterior is up in 5–6.

FIGURE 4.17. Sternal elements of *Edmontonia longiceps* (CMN 8351, holotype) in superficial and deep views: left (A) and right (B) sternal plates (medial is up), left (C) and right (D) xiphisternal plates (anterior is up), and left (E) and right (F) internal plates (anterior is up).

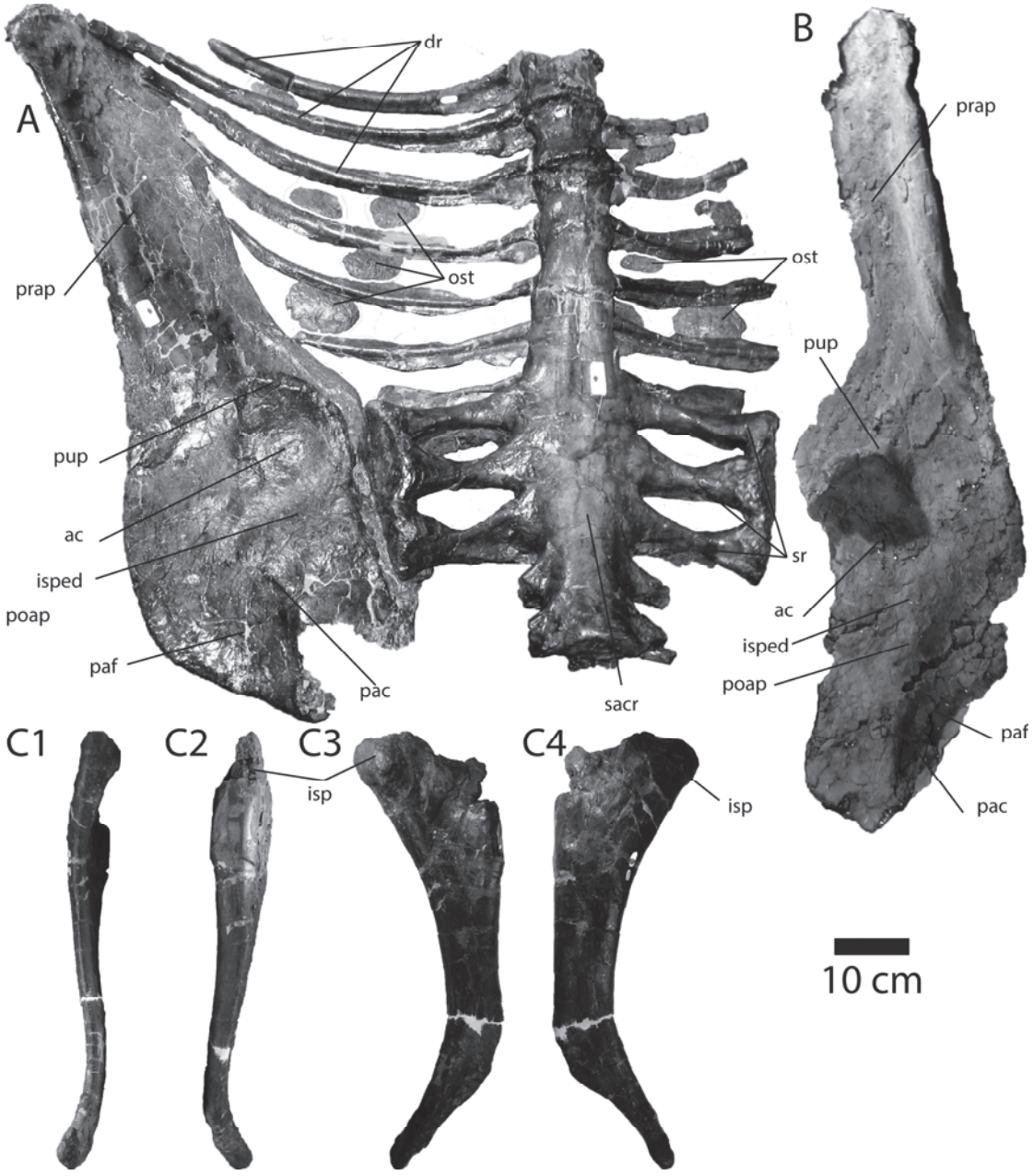

FIGURE 4.18. Pelvic elements of *Edmontonia longiceps* (CMN 8351, holotype): (A) articulated right ilium and synsacrum and associated osteoderms in ventral view, amnteior is up; (B) associated left ilium in ventral view, anterior is up; (C) left ischium in anterior (C1), posterior (C2), lateral (C3), and medial (C4) views.

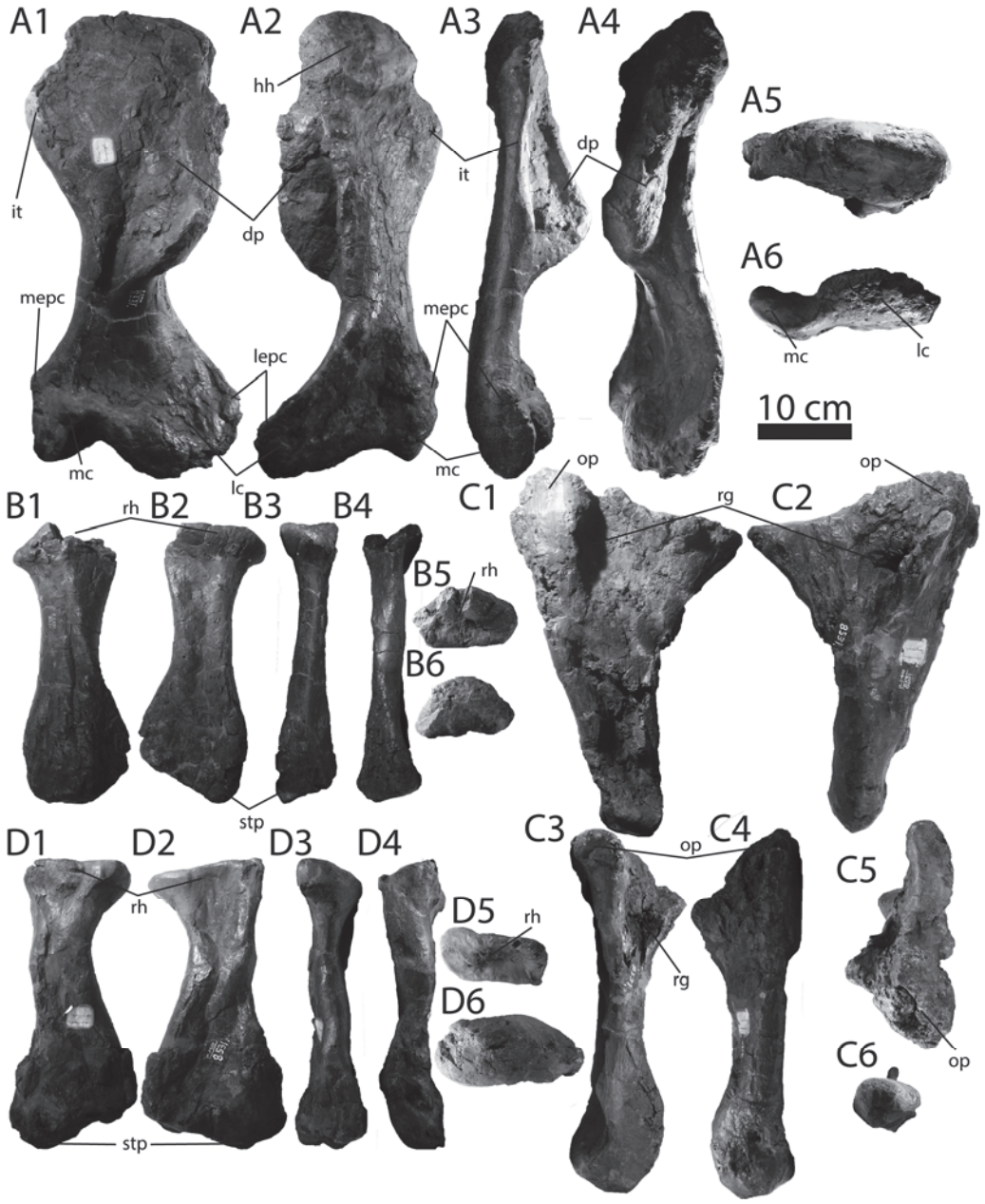

FIGURE 4.19. Forelimb elements of *Edmontonia longiceps* (CMN 8351, holotype) in anterior (1), posterior (2), medial (3), lateral (4), proximal (5) and distal (6) views. Proximal is up in 1–4 and anterior is up in 5–6. Left humerus (A), radius (B), and ulna (C), and right radius (D).

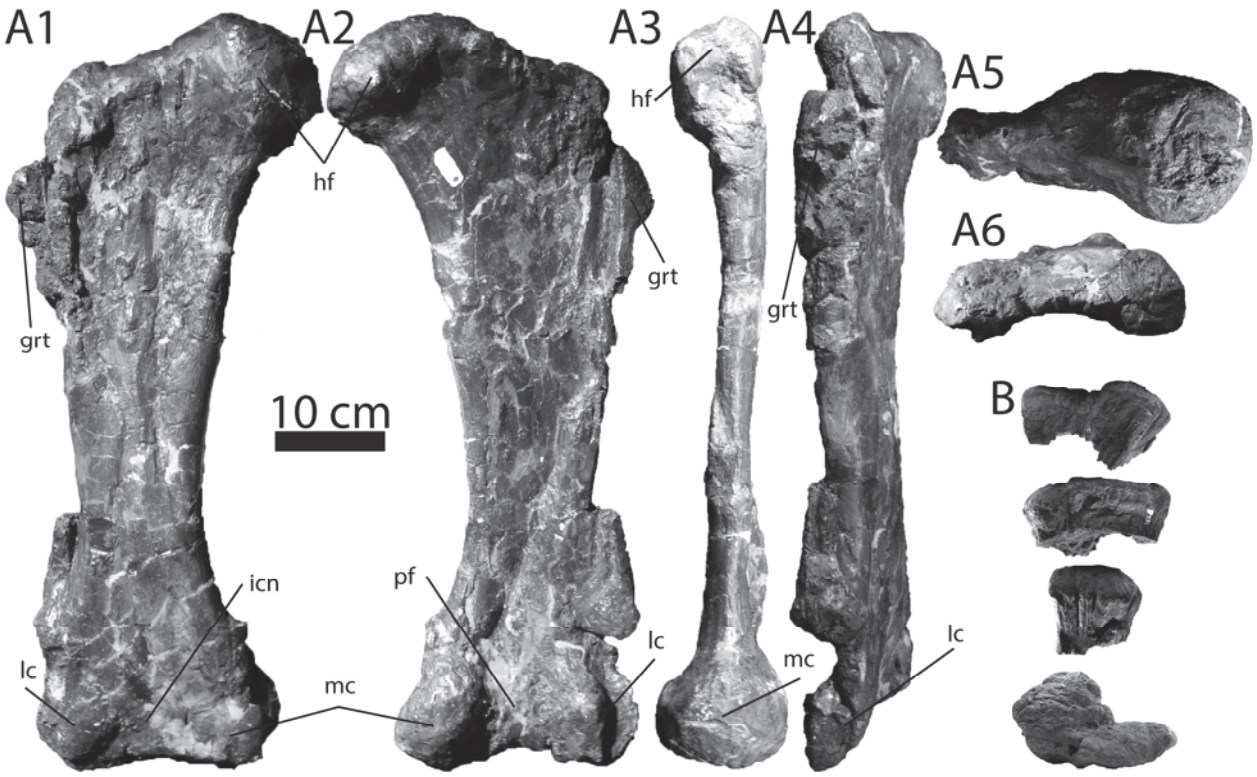

FIGURE 4.20. Hind limb elements of *Edmontonia longiceps* (CMN 8351, holotype) Right femur (A) in anterior (1), posterior (2), medial (3), lateral (4), proximal (5) and distal (6) views (proximal is up in 1–4 and anterior is up in 5–6). Left tibial plateau (B) in anterior, posterior, lateral (proximal is up), and proximal (anterior is up) views.

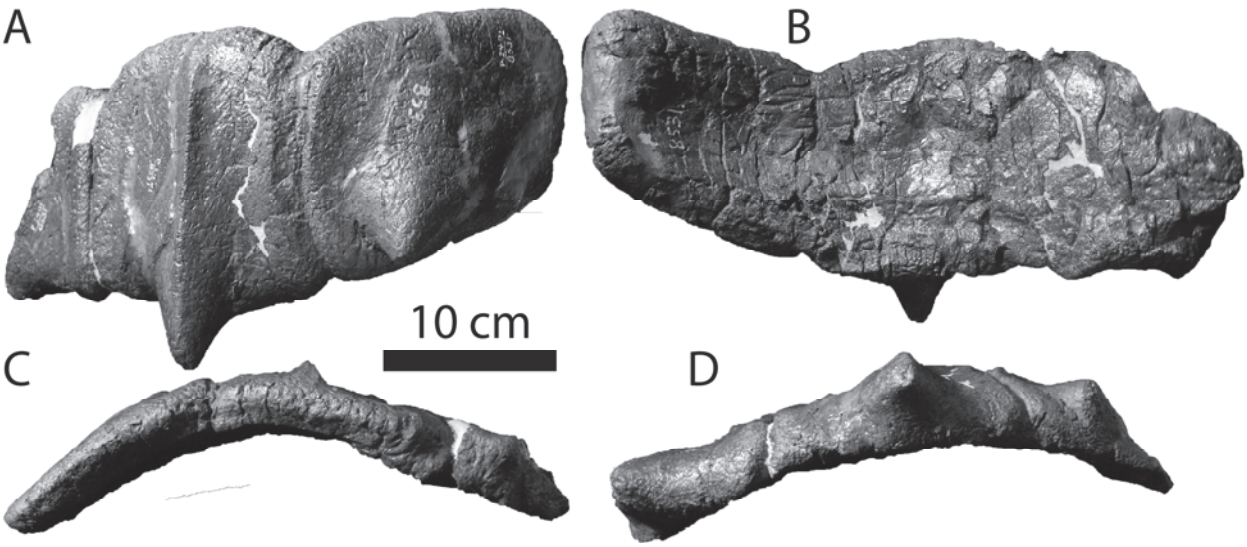

FIGURE 4.21. Left first cervical half ring of *Edmontonia longiceps* (CMN 8351, holotype) in external (A), basal (B), anterior (C), and posterior (D) views. Anterior is up in A–B and external is up in C–D.

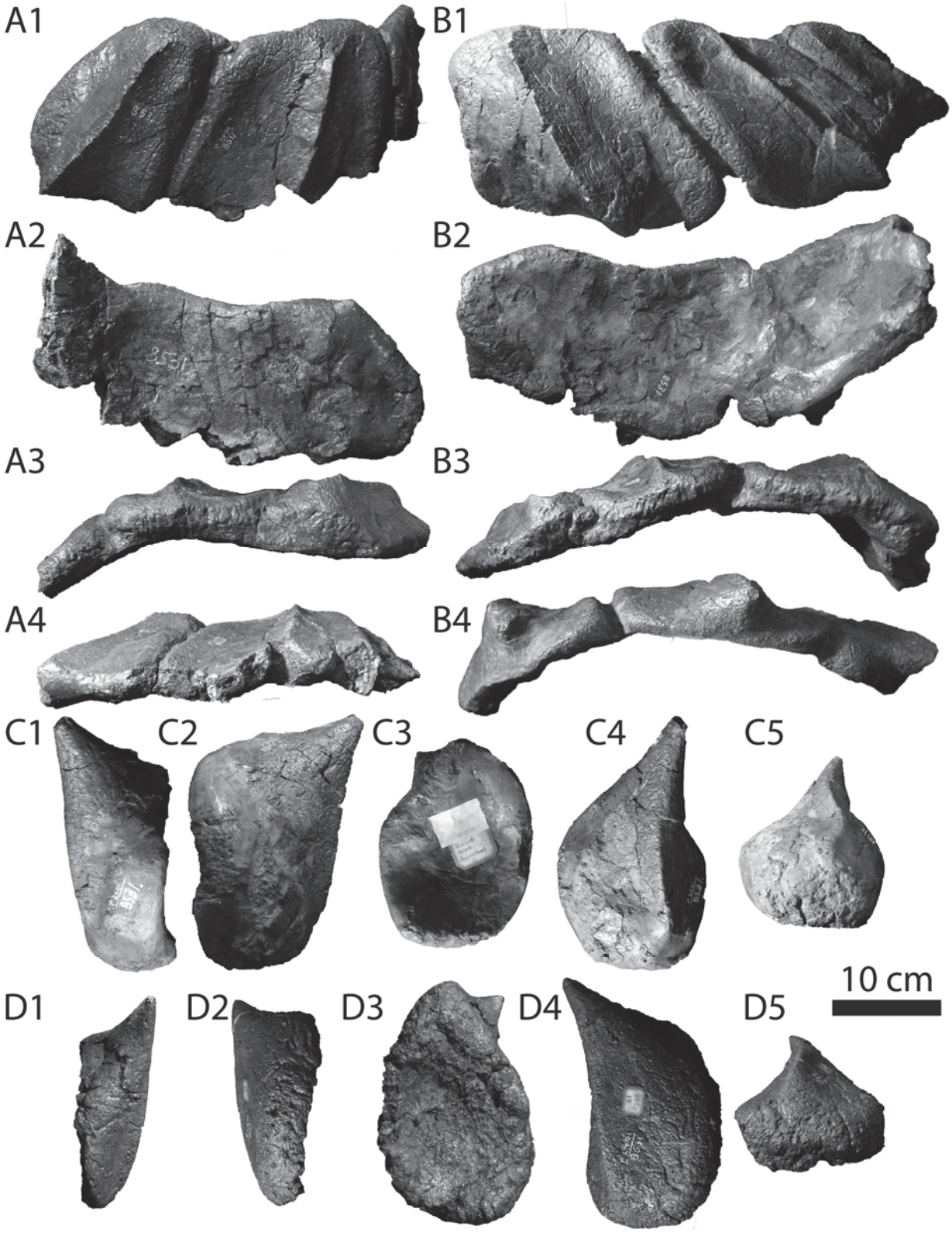
A1
B1
A2
B2
A3
B3
A4
B4
C1
C2
C3
C4
C5
D1
D2
D3
D4
D5
10 cm

FIGURE 4.22 (previous page). Second cervical half ring of *Edmontonia longiceps* (CMN 8351, holotype). Medial, lateral, and distal osteoderms from the left (A) and right (B) sides in external (1), basal (2), anterior (3), and posterior (4) views (anterior is up in 1–2 and external is up in 3–4). Cervical spines from left (C) and right (D) sides in anterior (1), posterior (2), basal (3), external (4), and dorsal (5) views (ventral is up in 1–4 and external is up in 3).

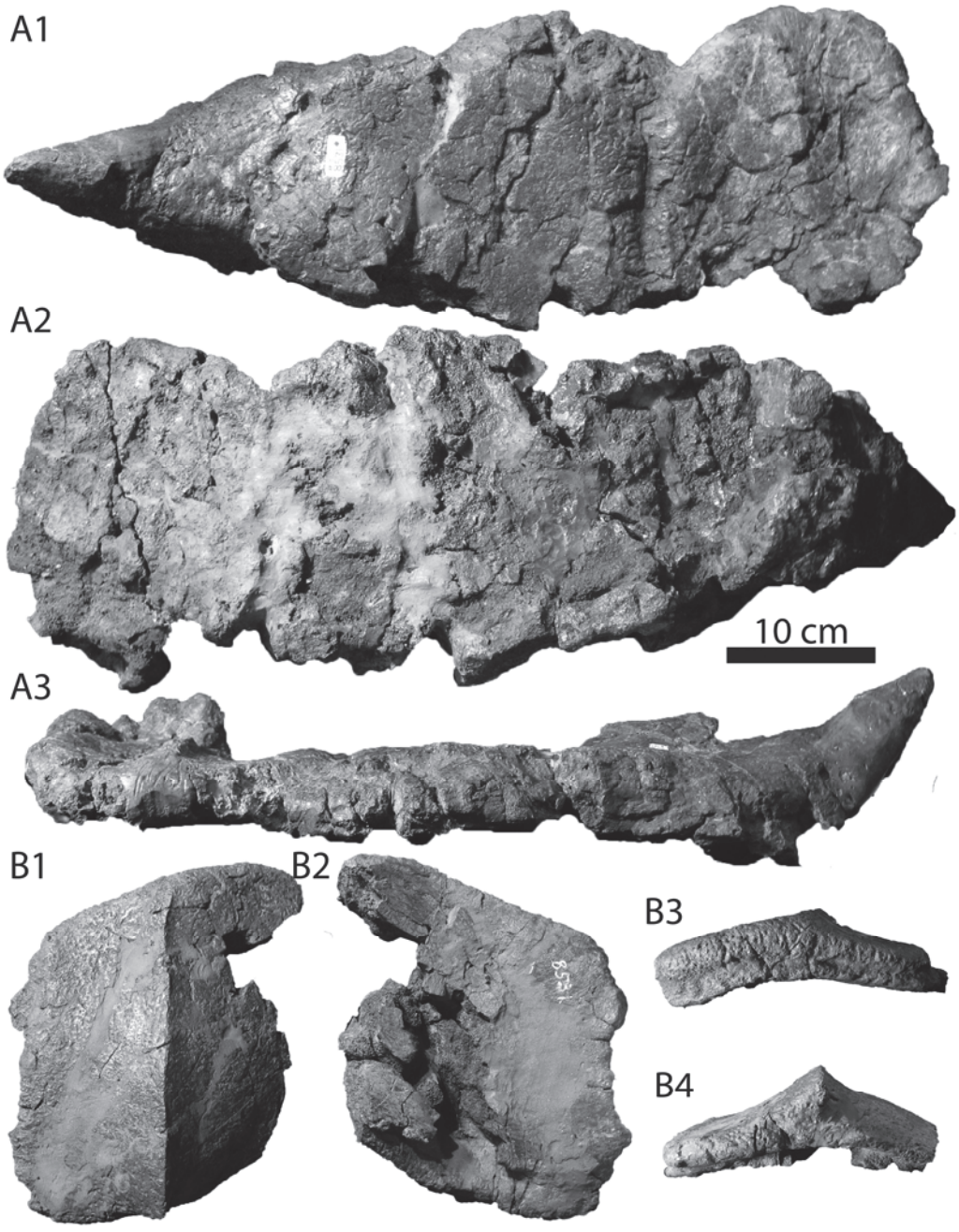

FIGURE 4.23. Left pectoral half ring of *Edmontonia longiceps* (CMN 8351, holotype). Lateral osteoderm and distal spine (A) in external (1), basal (2), and anterior (3) views. Medial osteoderm (B) in external (1), basal (2), anterior (3), and posterior (4) views.

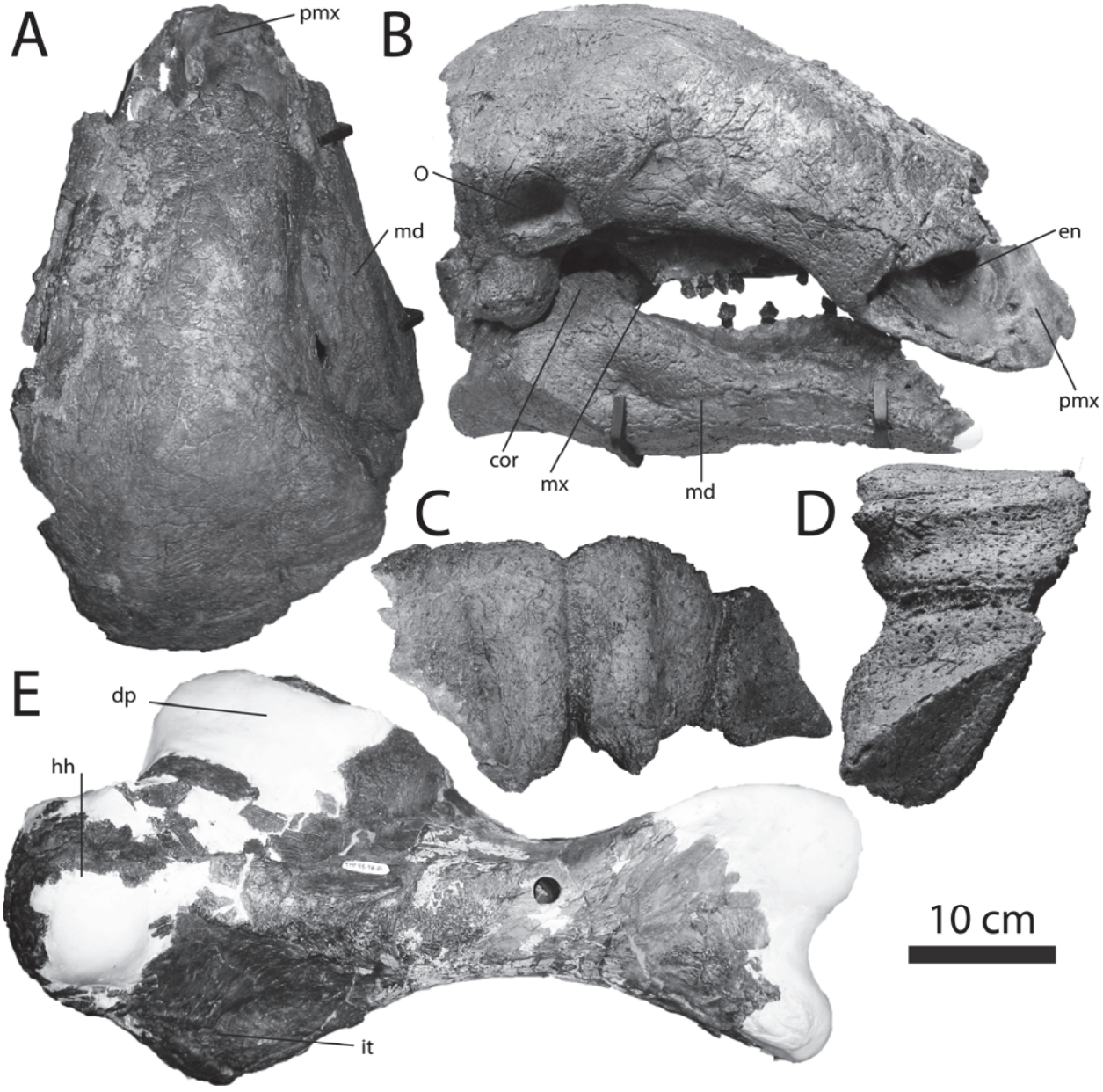

FIGURE 4.24. Elements of *Edmontonia longiceps* (TPM 98.98.1). Skull and right mandible in dorsal (A) and right lateral (B) views. Right first cervical half ring in external (C, anterior is up) and right lateral (views). Right humerus € in posterior view.

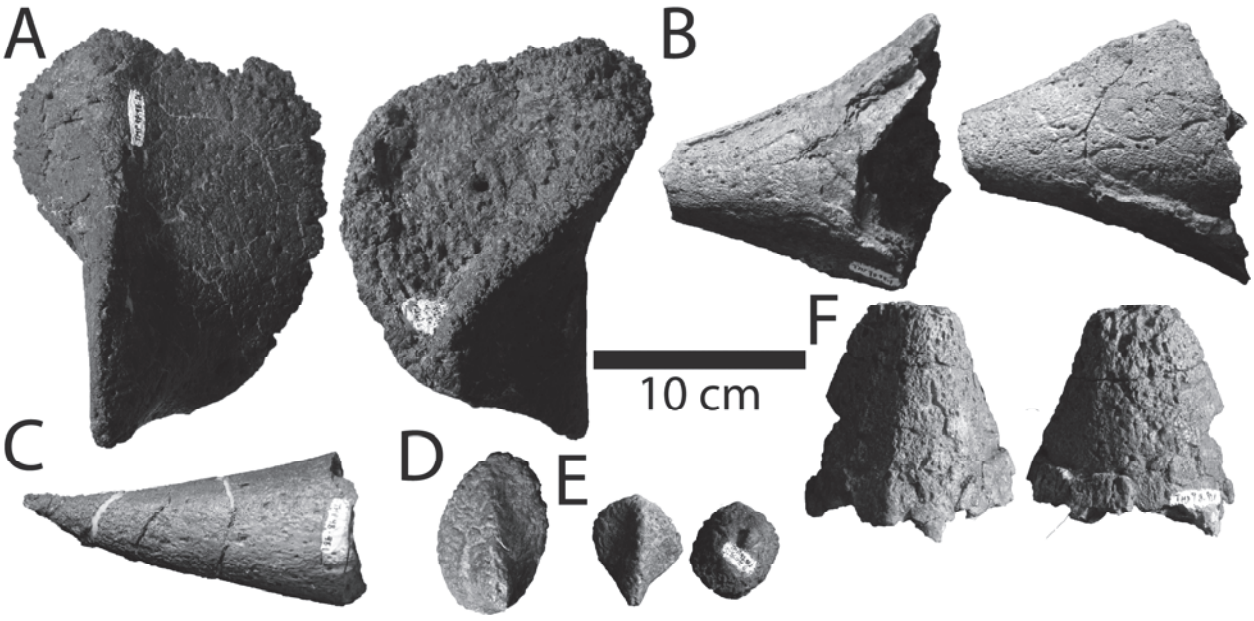

FIGURE 4.25. Osteoderms of *Edmontonia longiceps* (TPM 98.98.1). A,E in external and basal views. D in external view. Orientation uncertain in B,C.

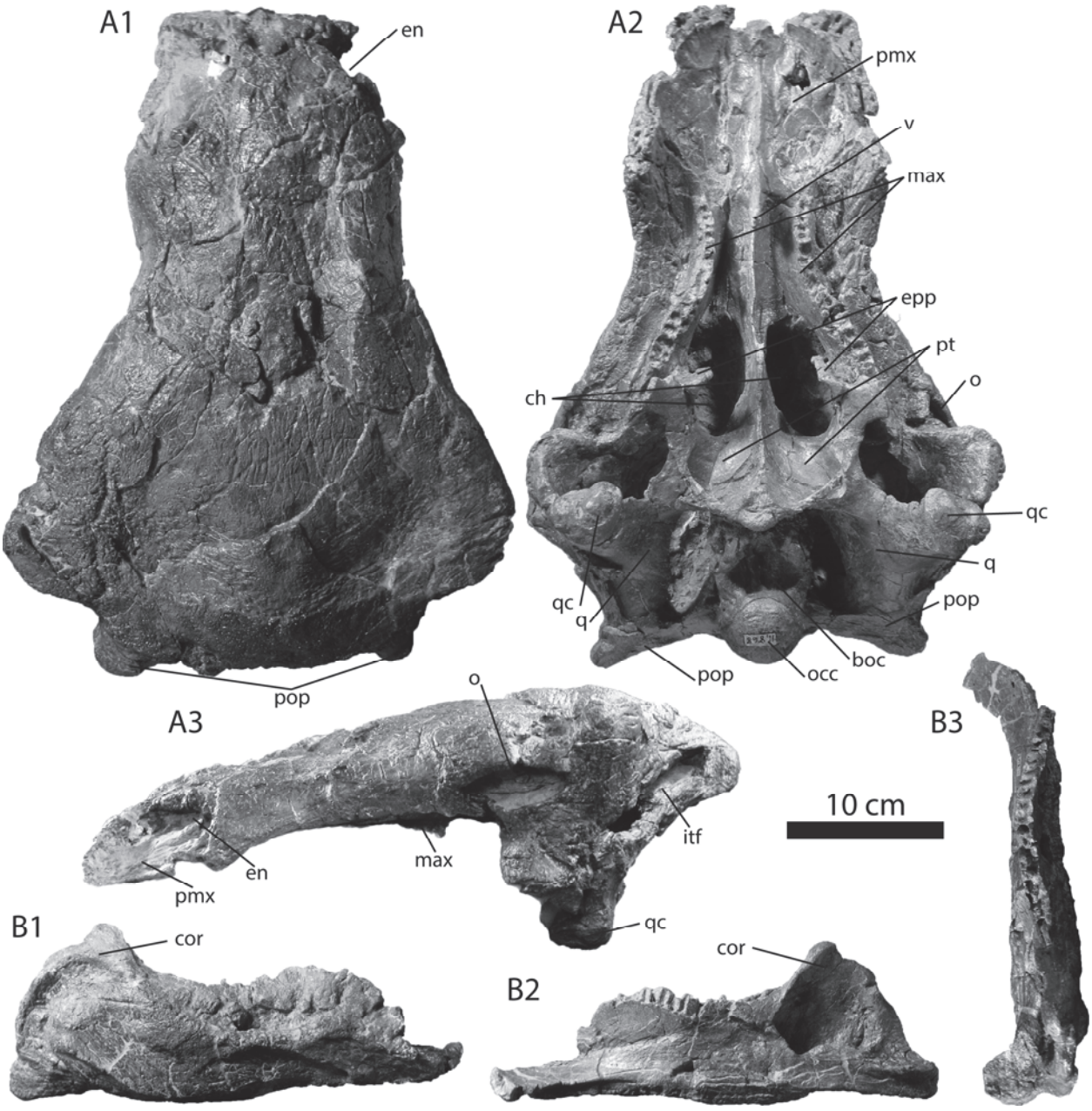

FIGURE 4.26. Skull (A) of *Edmontonia rugosidens* (USNM 11868, holotype) in dorsal (1), ventral (2), and left lateral (3) views. Right mandible (B) in lateral (1), medial (2), and dorsal (3) views.

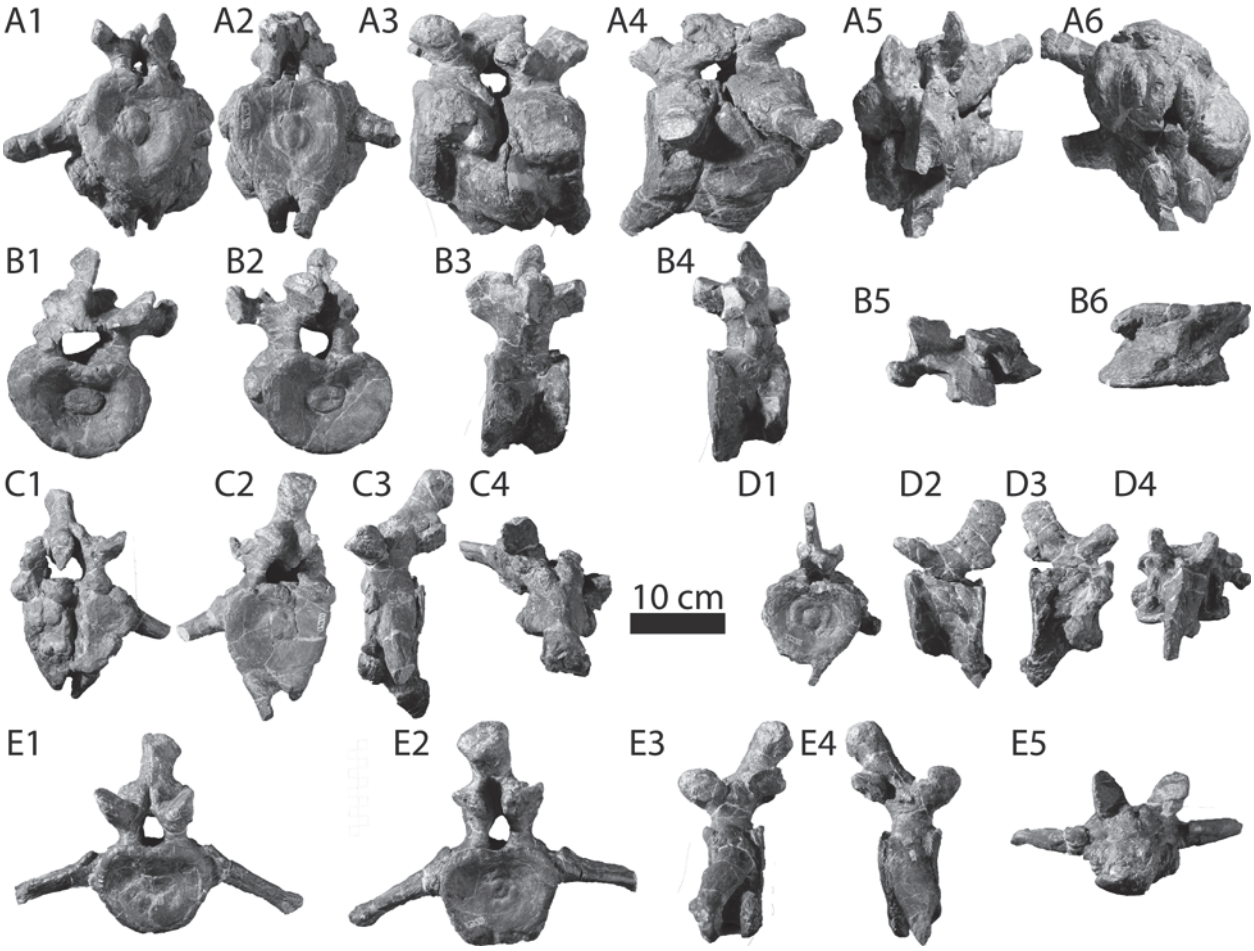

FIGURE 4.27. Caudal vertebrae of *Edmontonia rugosidens* (USNM 11868, holotype). A includes two articulated vertebrae. A and B are in in anterior (1), posterior (2), left lateral (3), right lateral (4), dorsal (5), and ventral (6) views. C is in anterior (1), posterior (2), left lateral (3), and dorsal (4) views. D is in posterior (1), left lateral (2), right lateral (3), and dorsal (4) views. E is in anterior (1), posterior (2), left lateral (3), right lateral (4), and dorsal (5) views. Dorsal is up in anteroposterior and lateral views. Anterior is up in dorsoventral views.

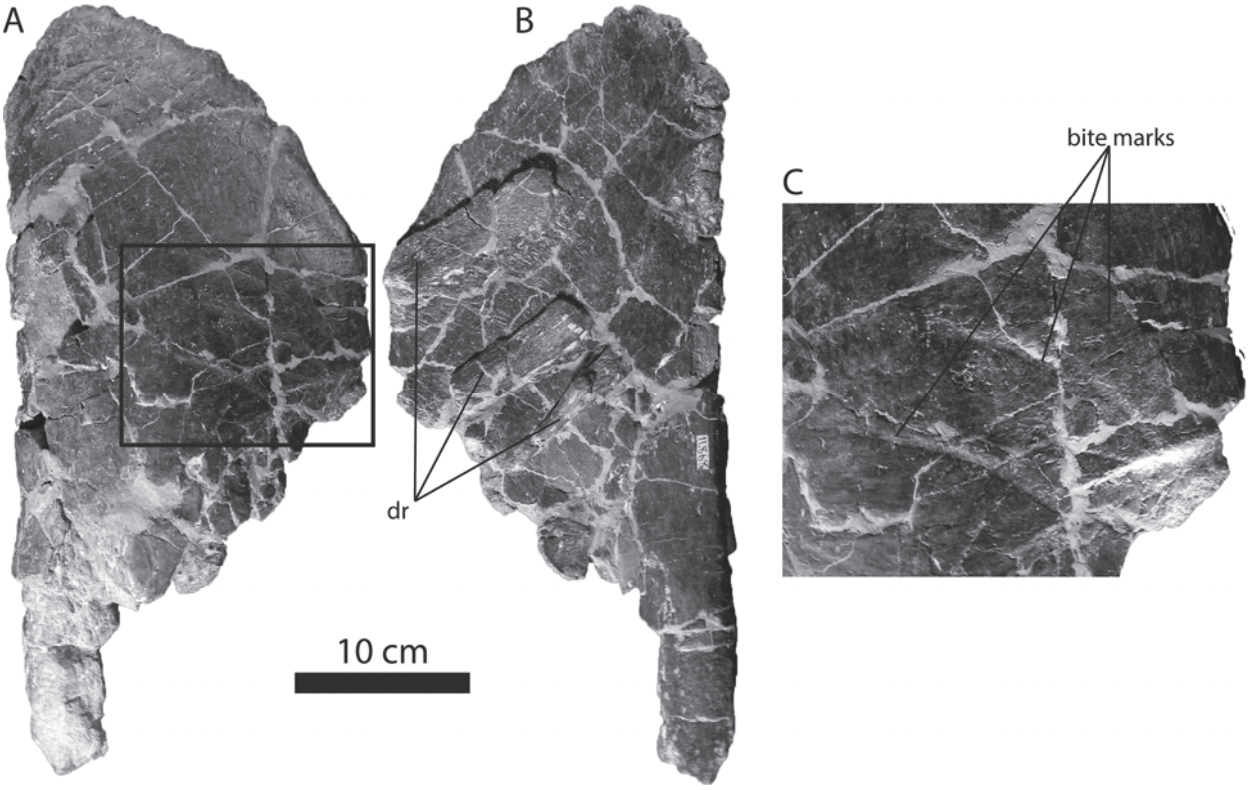

FIGURE 4.28. Partial ilium of *Edmontonia rugosidens* (USNM 11868, holotype) in dorsal (A) and ventral (B) views, with rib fragments coossified to the ventral side. Orientation uncertain. Box in A corresponds to C: detail of peri- or postmortem bite marks.

FIGURE 4.29. Right (A) and left (B) ischia of *Edmontonia rugosidens* (USNM 11868, holotype) in anterior (1), posterior (2), medial (3) and lateral (4) views. Proximal is up.

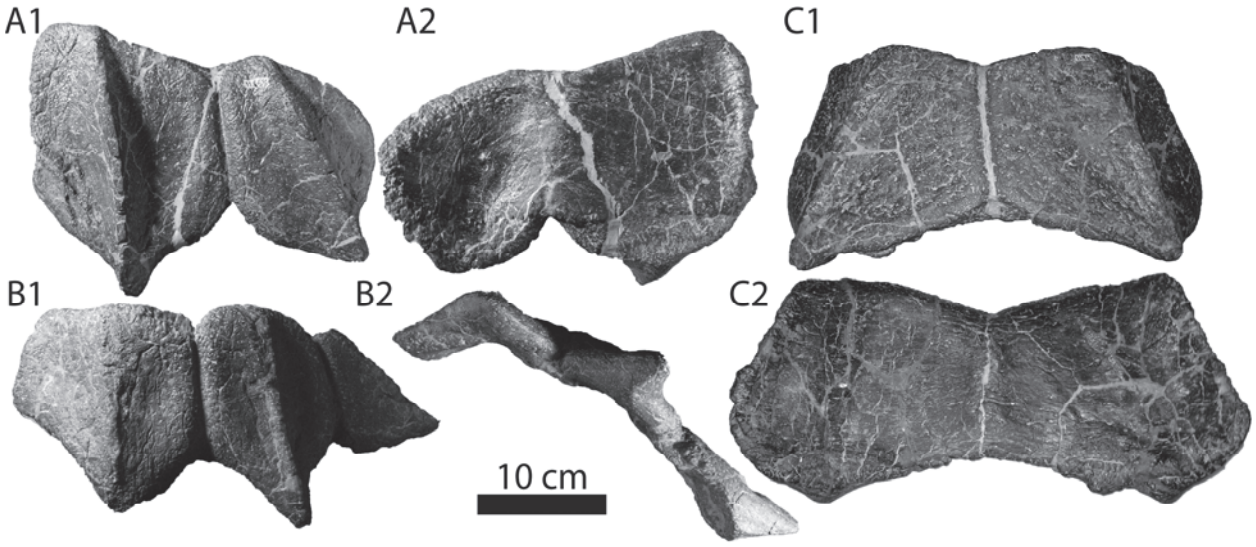

FIGURE 4.30. Cervical and pectoral osteoderms of *Edmontonia rugosidens* (USNM 11868, holotype): A, right first cervical half ring in external (1) and basal (2) views; B, right second cervical half ring in external (1) and posterior (2) views; C, coossified medial osteoderms of the pectoral half ring in external (1) and basal (2) views. External is up in B2. Anterior is up in all others.

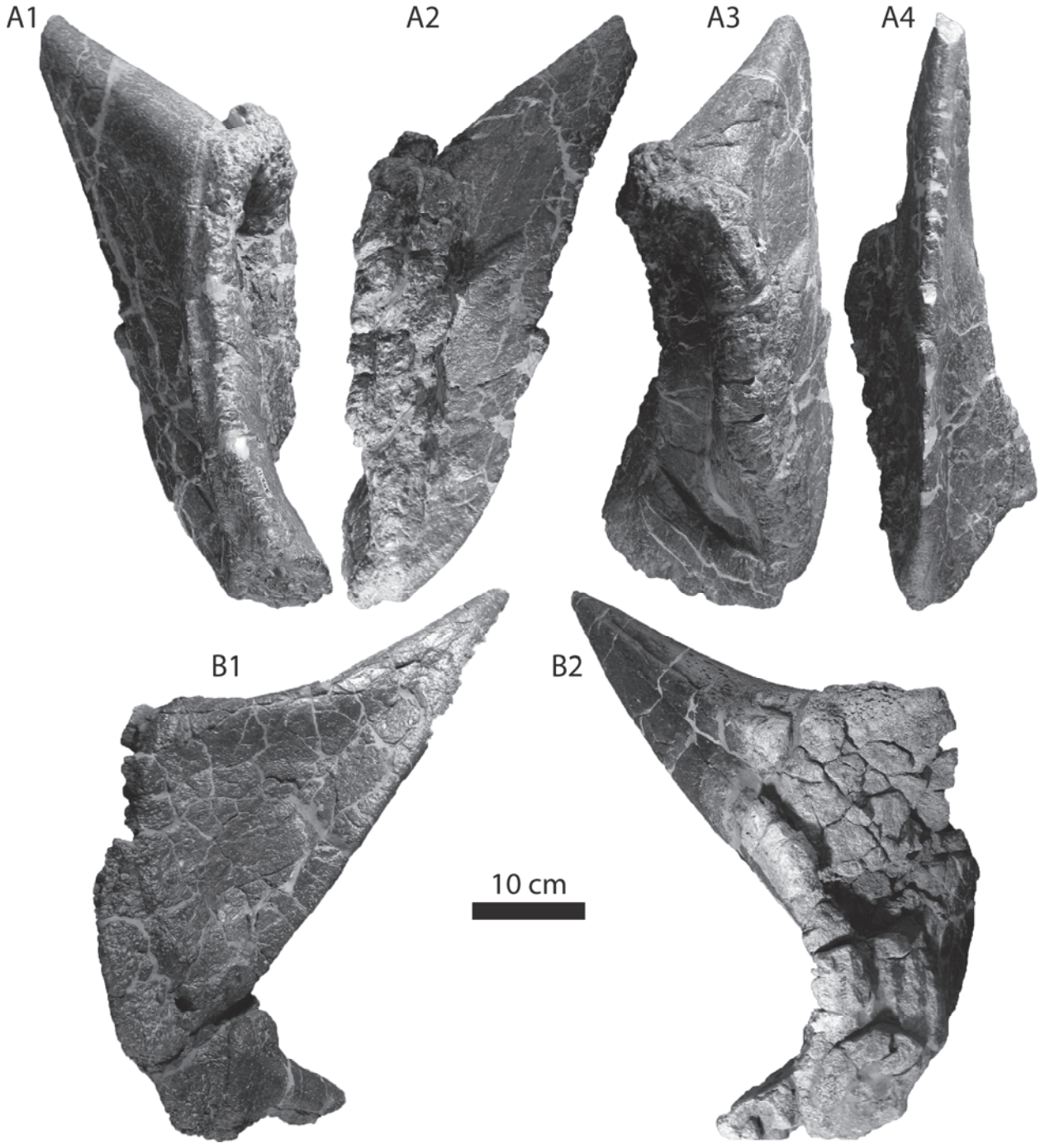

FIGURE 4.31. Right osteodermal spines of *Edmontonia rugosidens* (USNM 11868, holotype). Distal pectoral spine (A) in ventral (1), dorsal (2), basal (3), and external (4) views. Articulated distal thoracic spines (B) in dorsal (1) and ventral (2) views. Anterior is up.

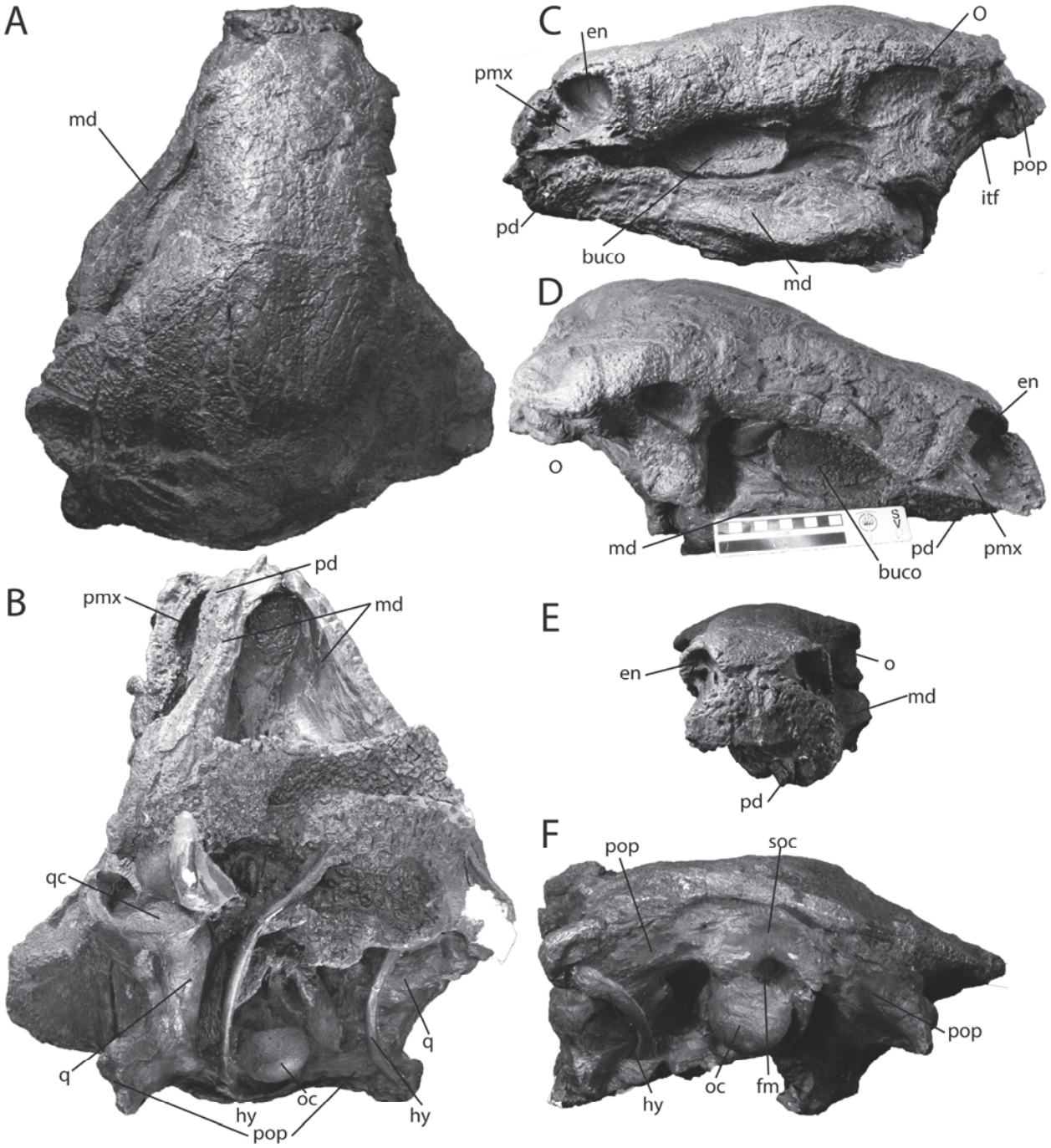

FIGURE 4.32. Skull, lower jaw, and hyoids of *Edmontonia rugosidens* (AMNH 5381) in dorsal (A), ventral (B), left lateral (C), right lateral (D), anterior (E), and posterior (F) views. Anterior is up in A–B, dorsal is up in C–F. Scale bar (D) equals 10 cm.

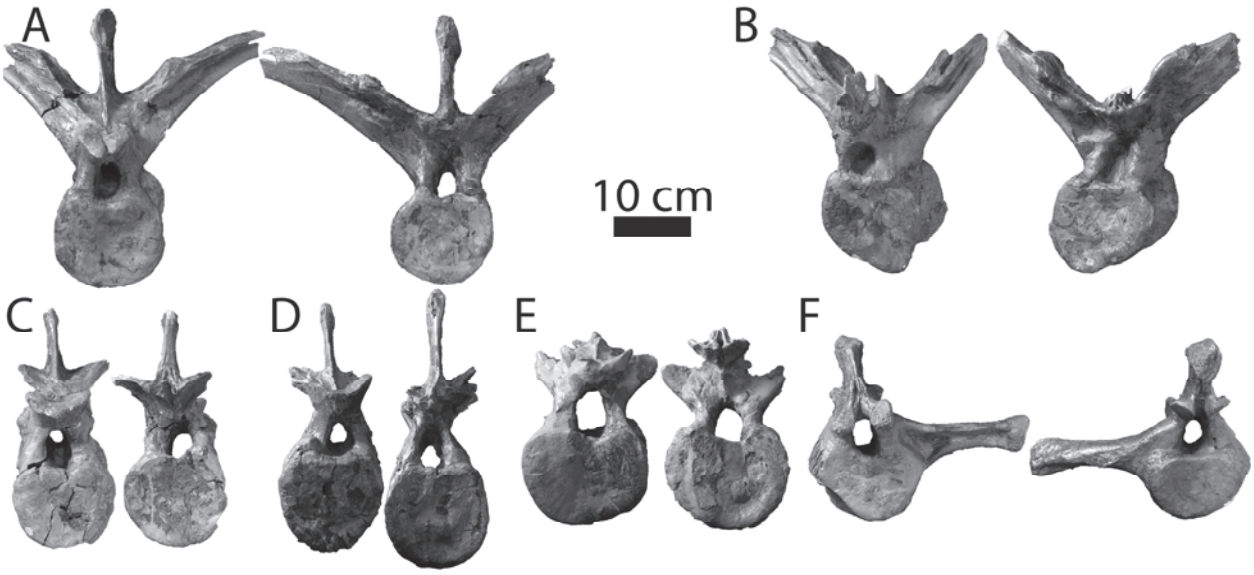

FIGURE 4.33. Vertebrae of *Edmontonia rugosidens* (AMNH 5381) in anterior an posterior views: A–B, dorsal vertebrae; C–F, caudal vertebrae.

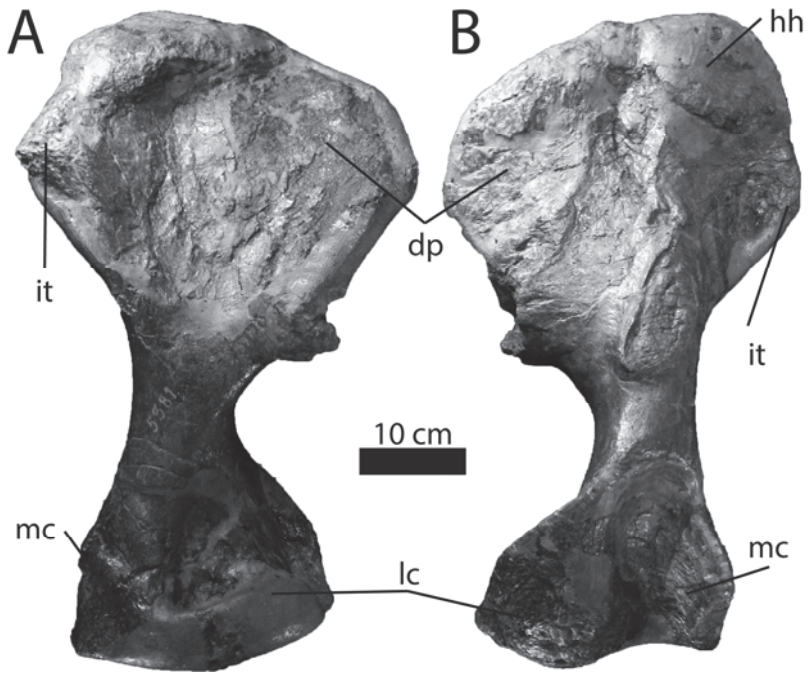

FIGURE 4.34. Left humerus of *Edmontonia rugosidens* (AMNH 5381) in anterior (A) and posterior (B) views.

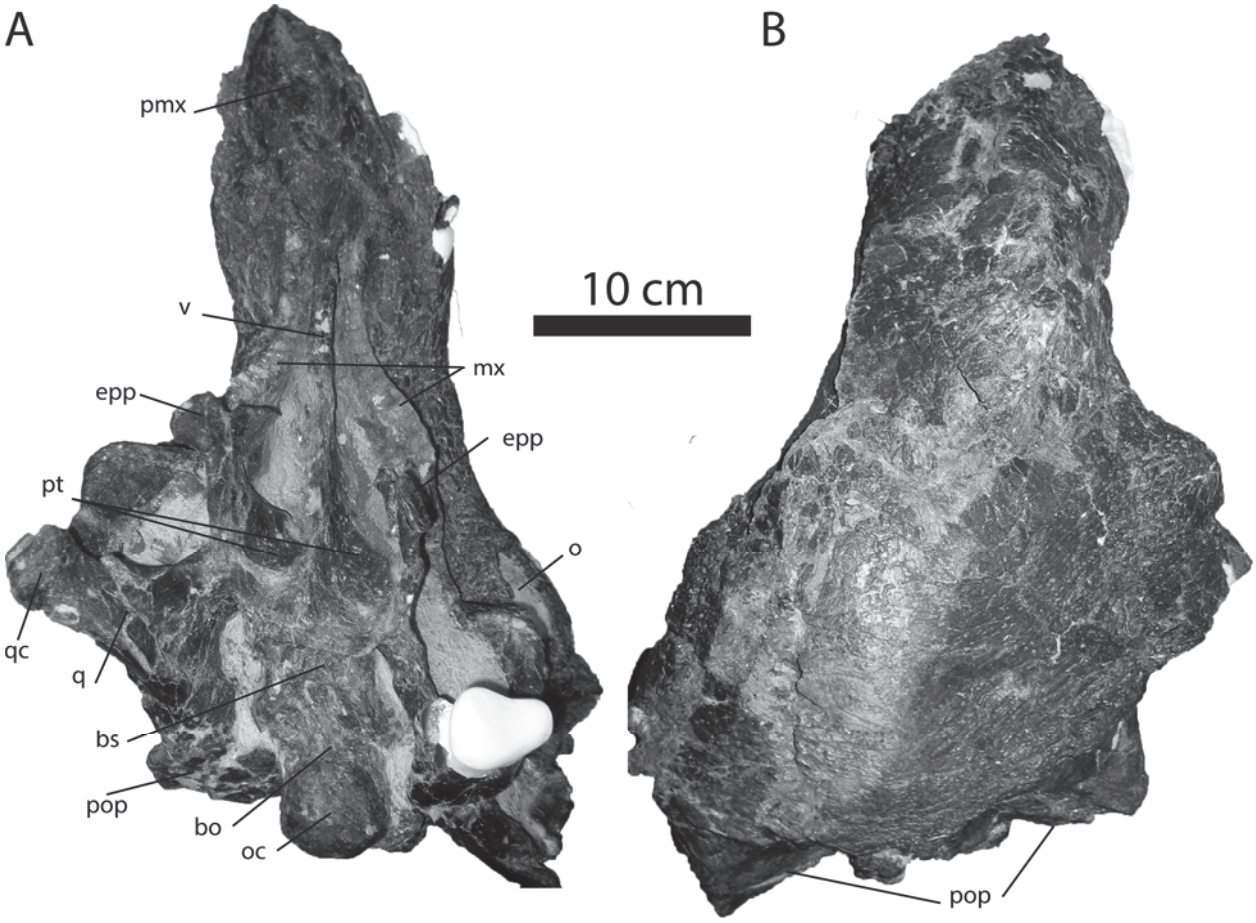

FIGURE 4.35. Skull of *Edmontonia rugosidens* (TMP 2000.12.158) in ventral (A) and dorsal (B) views.

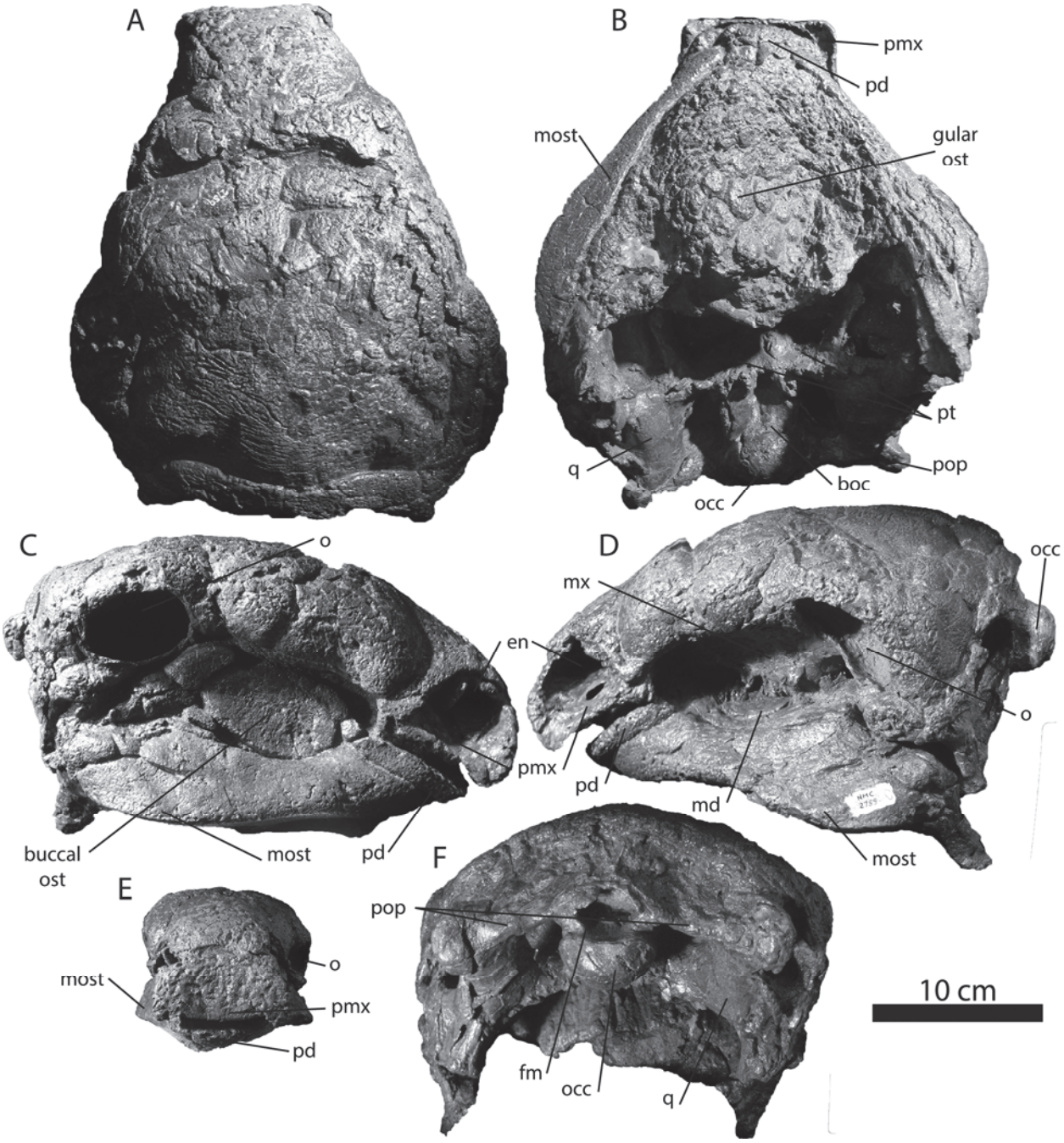

FIGURE 4.36. Skull and mandibles of *Panoplosaurus mirus* (CMN 2759, holotype) in dorsal (A), ventral (B), right lateral (C), left lateral (D), anterior (E), and posterior (F) views. Anterior is up in A–B, dorsal is up in C–F.

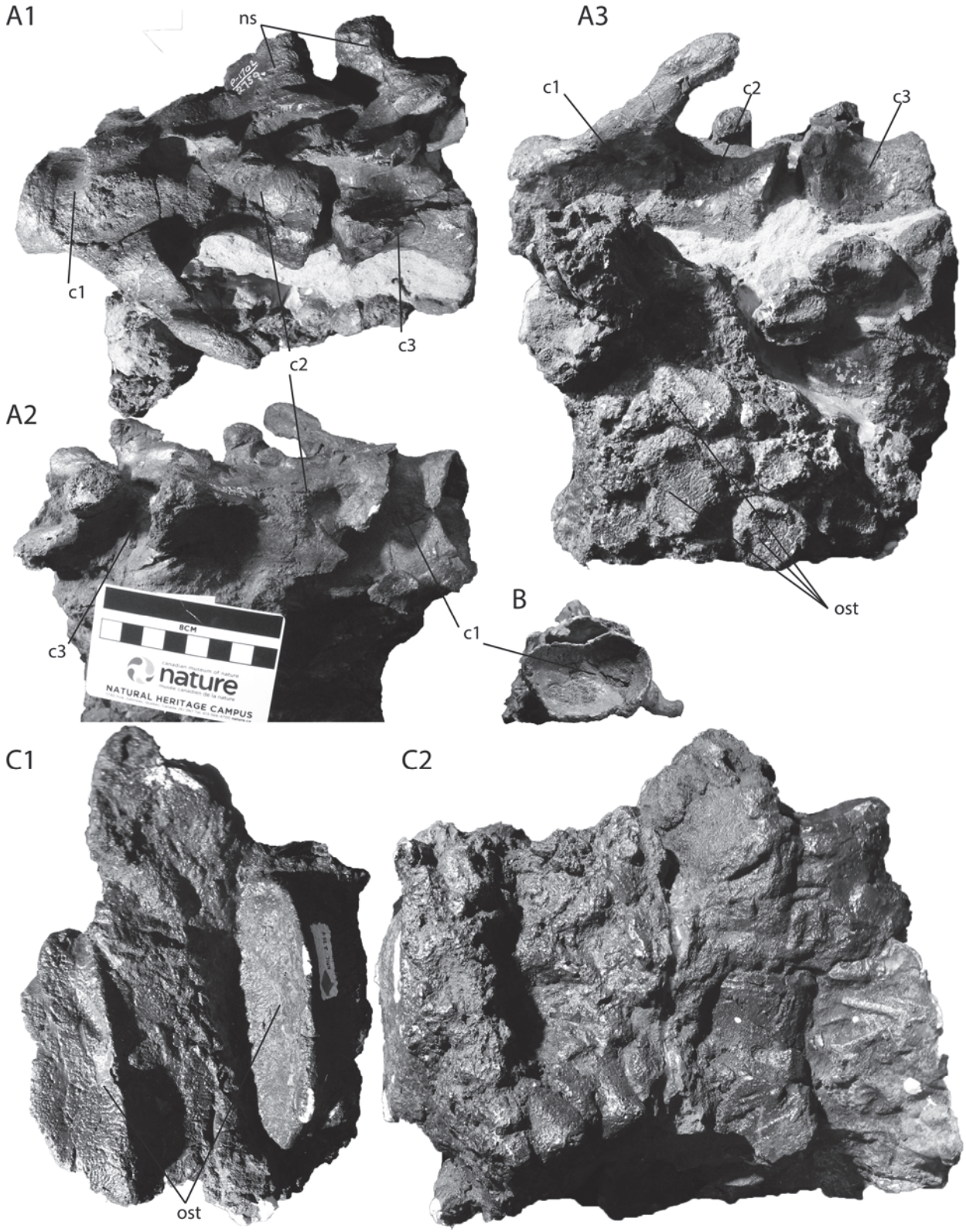
A1
ns
c1
c2
c3
A2
c1
c2
c3
8CM
canadian museum of nature
nature
NATURAL HERITAGE CAMPUS
A3
c1
c2
c3
ost
B
c1
C1
ost
C2

FIGURE 4.37 (previous page). Blocks of articulated syncervical, cervical vertebrae, and osteoderms of *Panoplosaurus mirus* (CMN 2759, holotype). A, anterior block in left lateral (1, dorsal is up), dorsal (2, anterior is to the right), and ventral (3, anterior is to the right) views; B, anteriormost cervical vertebra in anterior block in anterior view (dorsal is up); C, posterior block in right lateral (1) and ventral (2) views (anterior is up). Scale bar (A2) equals 8 cm.

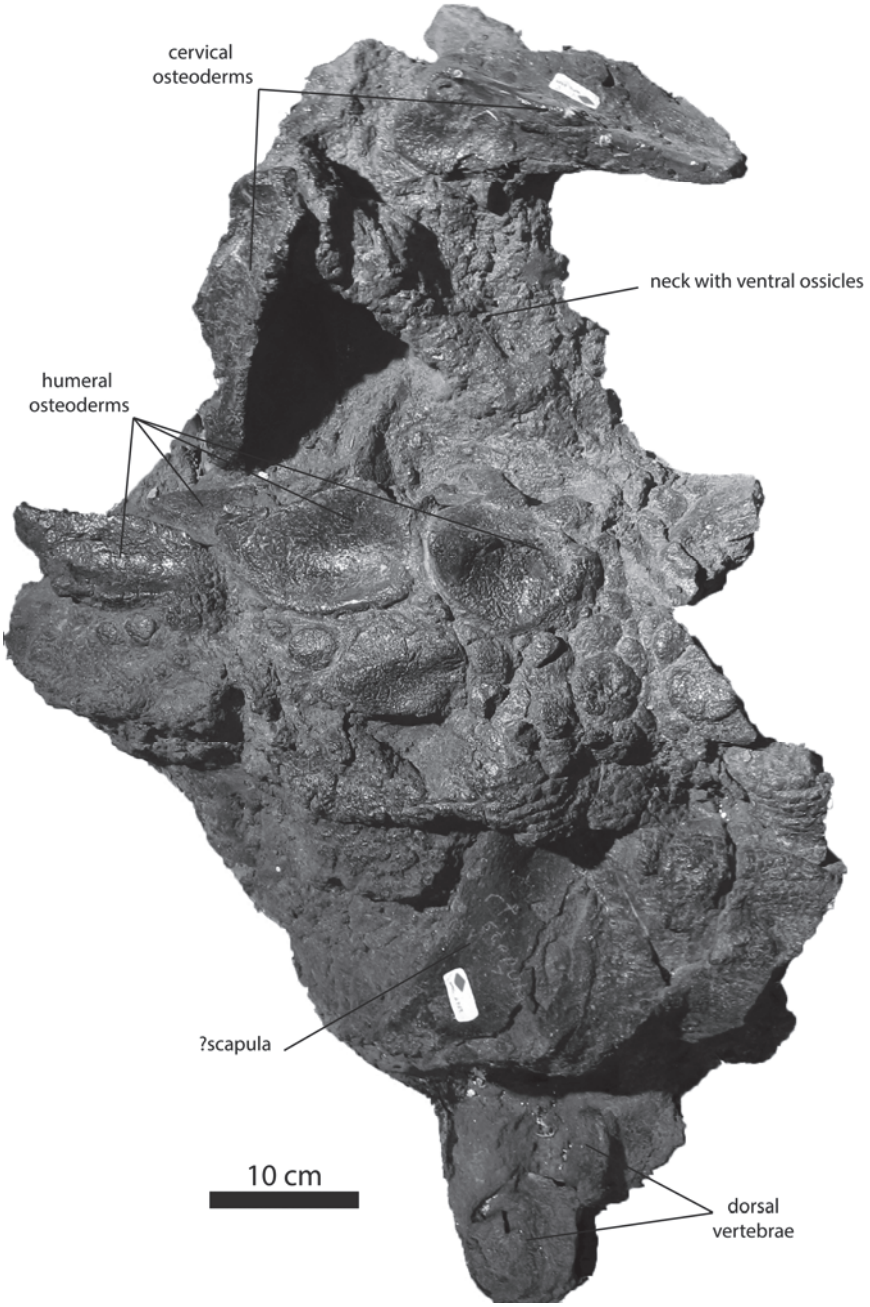

FIGURE 4.38. Block of in situ posterior cervical and thoracic osteoderms and skin impressions of *Panoplosaurus mirus* (CMN 2759, holotype) in ventral view, anterior is up. Humeral osteoderms indicate that the right forelimb is preserved as folded underneath the body.

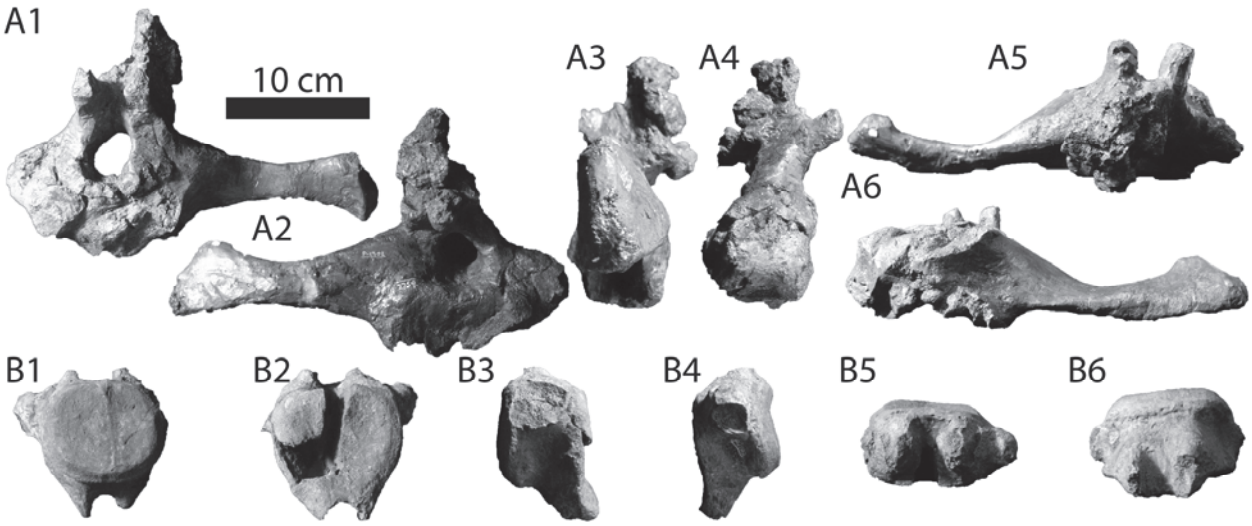

FIGURE 4.39. Caudal vertebrae (A, B) of *Panoplosaurus mirus* (CMN 2759, holotype) in anterior (1), posterior (2), left lateral (3), right lateral (4), dorsal (5), and ventral (6) views.

FIGURE 4.40. Articulated left manus of *Panoplosaurus mirus* (CMN 2759, holotype) in dorsal view. Proximal is up.

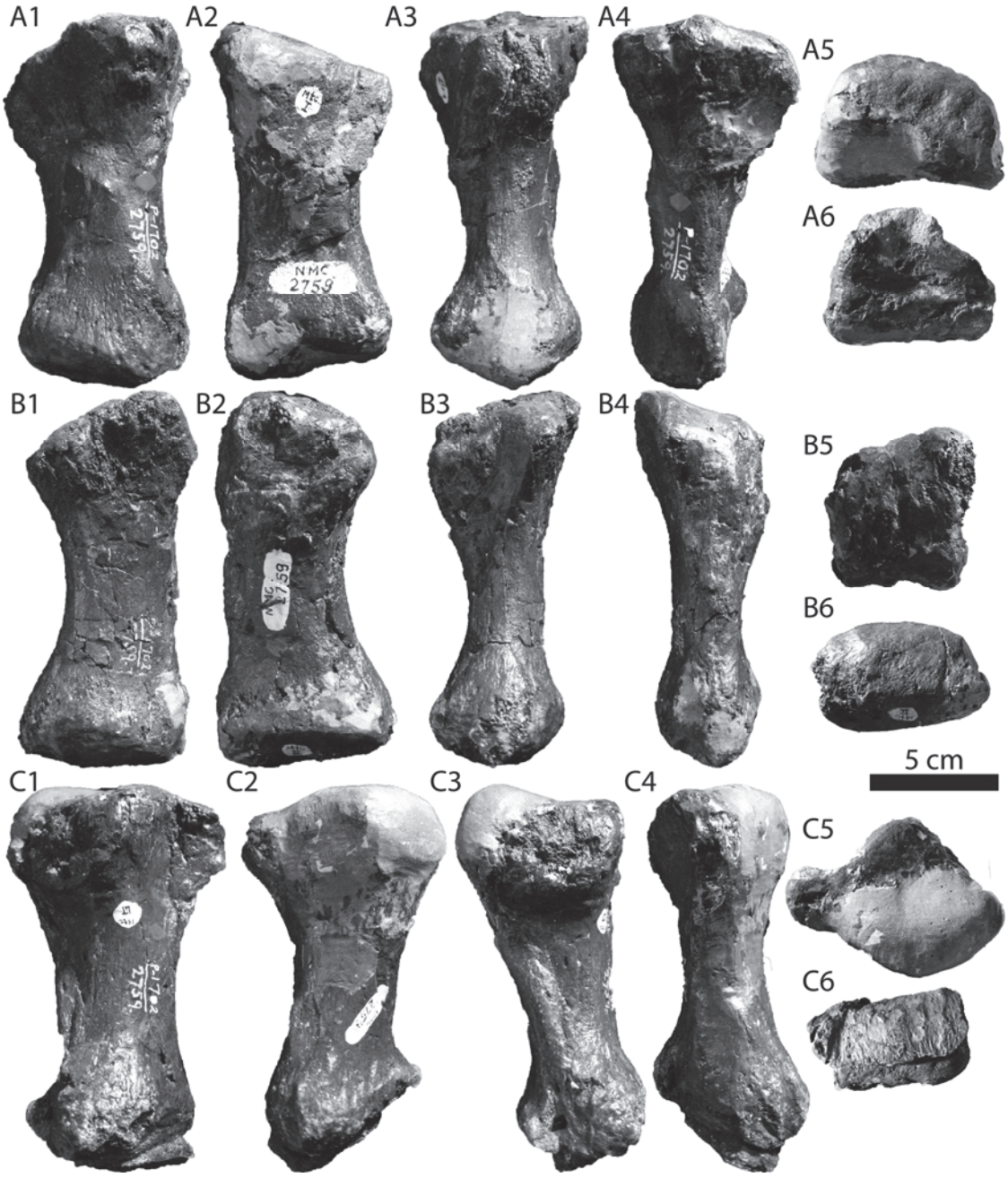

FIGURE 4.41. Metacarpals, MC I (A), MC II (B), and MC III (C) of *Panoplosaurus mirus* (CMN 2759, holotype) in dorsal (1), ventral (2), medial (3), lateral (4), proximal (5), and distal (6) views. Proximal is up in 1–4, dorsal is up in 5–6.

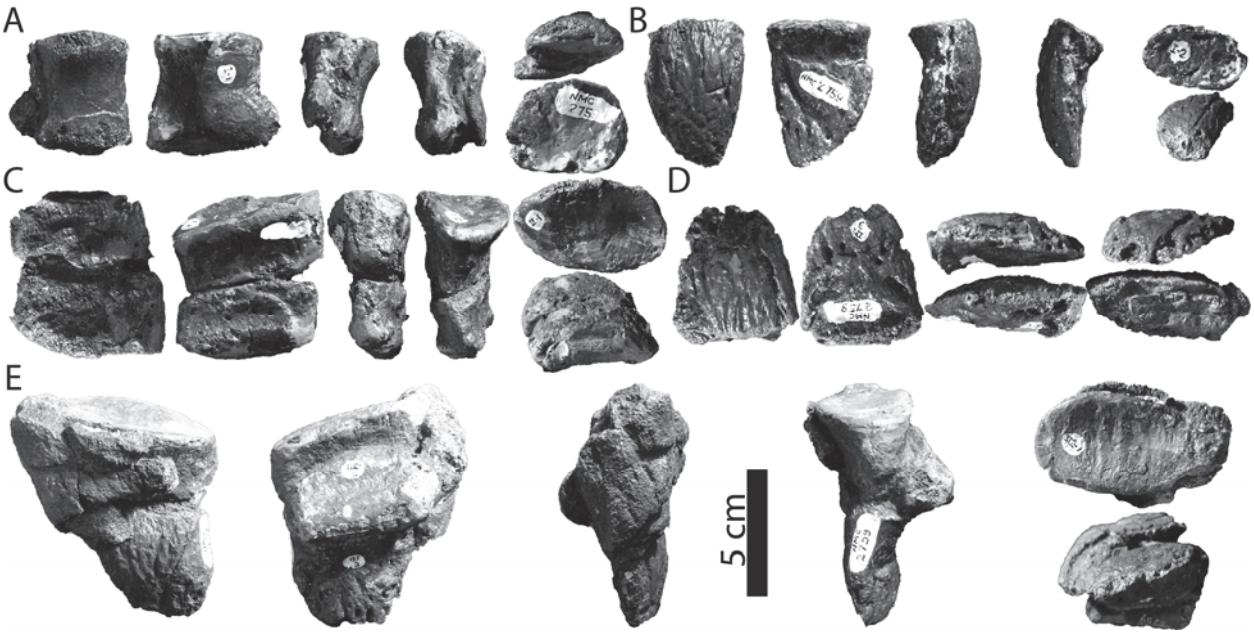

FIGURE 4.42. Manual phalanges and unguals of *Panoplosaurus mirus* (CMN 2759, holotype) in dorsal, ventral, medial, lateral, proximal, and distal views. Proximal is up in dorsoventral and mediolateral views, dorsal is up in proximodistal views. C represents coossified phalanges II-1 and II-2. D represents coossified phalanx III-1 and ungual III-2.

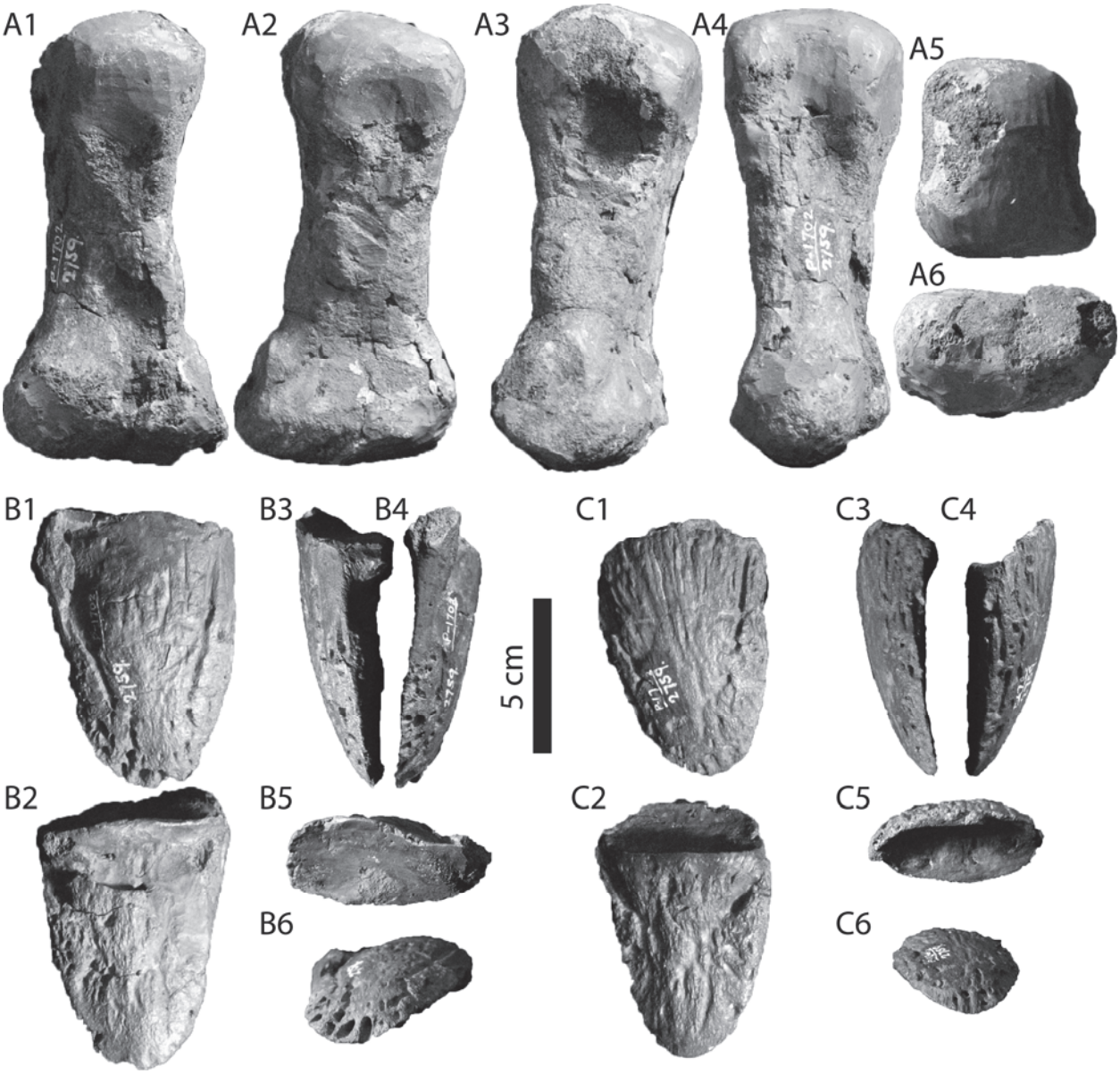

FIGURE 4.43. Metatarsal (A) and pedal unguals (B, C) of *Panoplosaurus mirus* (CMN 2759, holotype) in dorsal (1), ventral (2), medial (3), lateral (4), proximal (5), and distal (6) views. Proximal is up in 1–4, dorsal is up in 5–6.

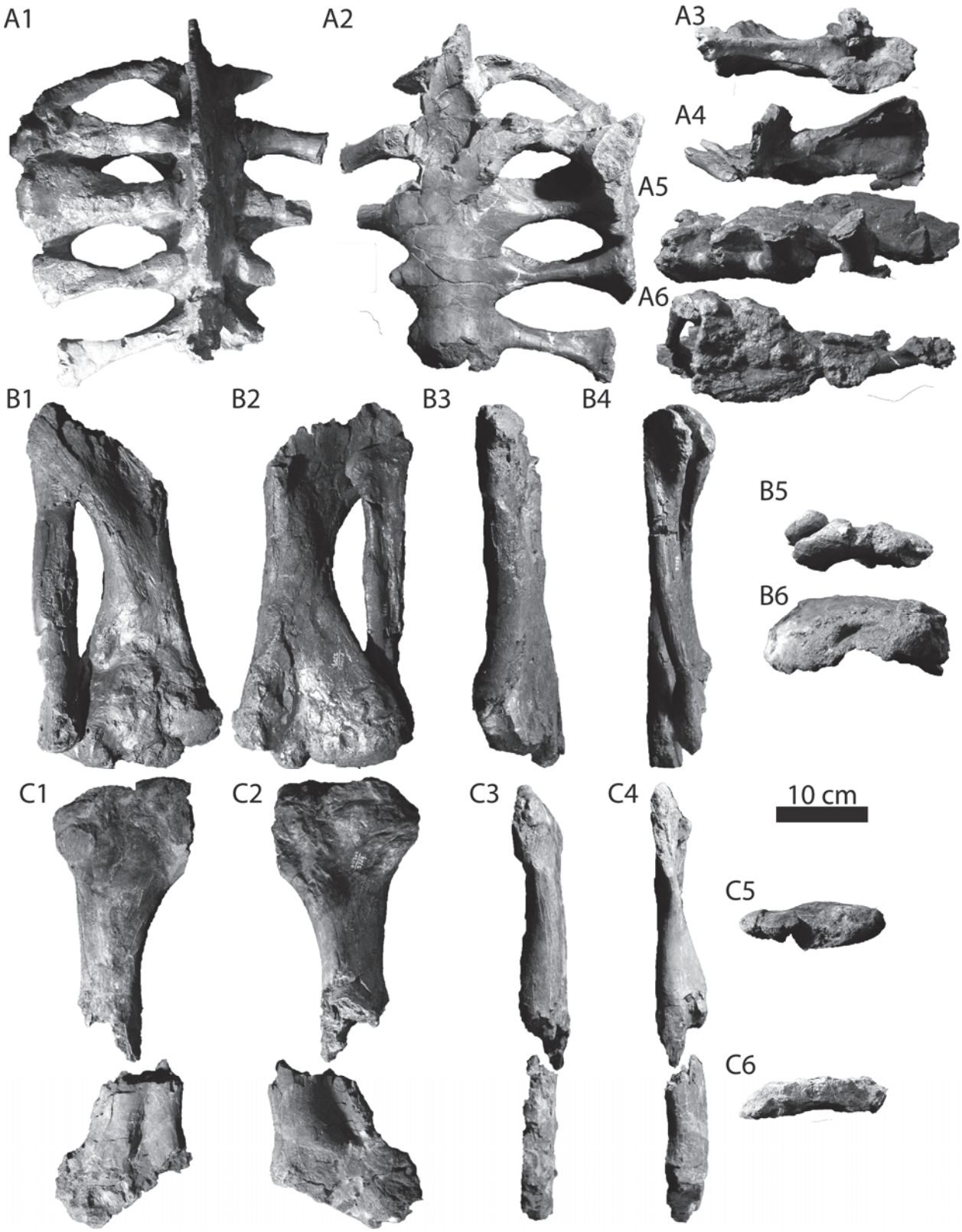
A1
A2
A3
A4
A5
A6
B1
B2
B3
B4
B5
B6
C1
C2
C3
C4
C5
C6
10 cm

FIGURE 4.44 (previous page). Pelvic girdle and hind limb elements of *Panoplosaurus mirus* (CMN 2759, holotype). A, synsacrum in dorsal (1), ventral (2), anterior (3), posterior (4), right lateral (5), and left lateral (6) views; B, articulated right tibia and fibula, and C, broken left tibia, in anterior (1), posterior (2), medial (3), lateral (4), proximal (5), and distal (6) views. For A, anterior is up in 1–2 and dorsal is up in 3–6. For the B–C, proximal is up in 1–4 and anterior is up in 5–6.

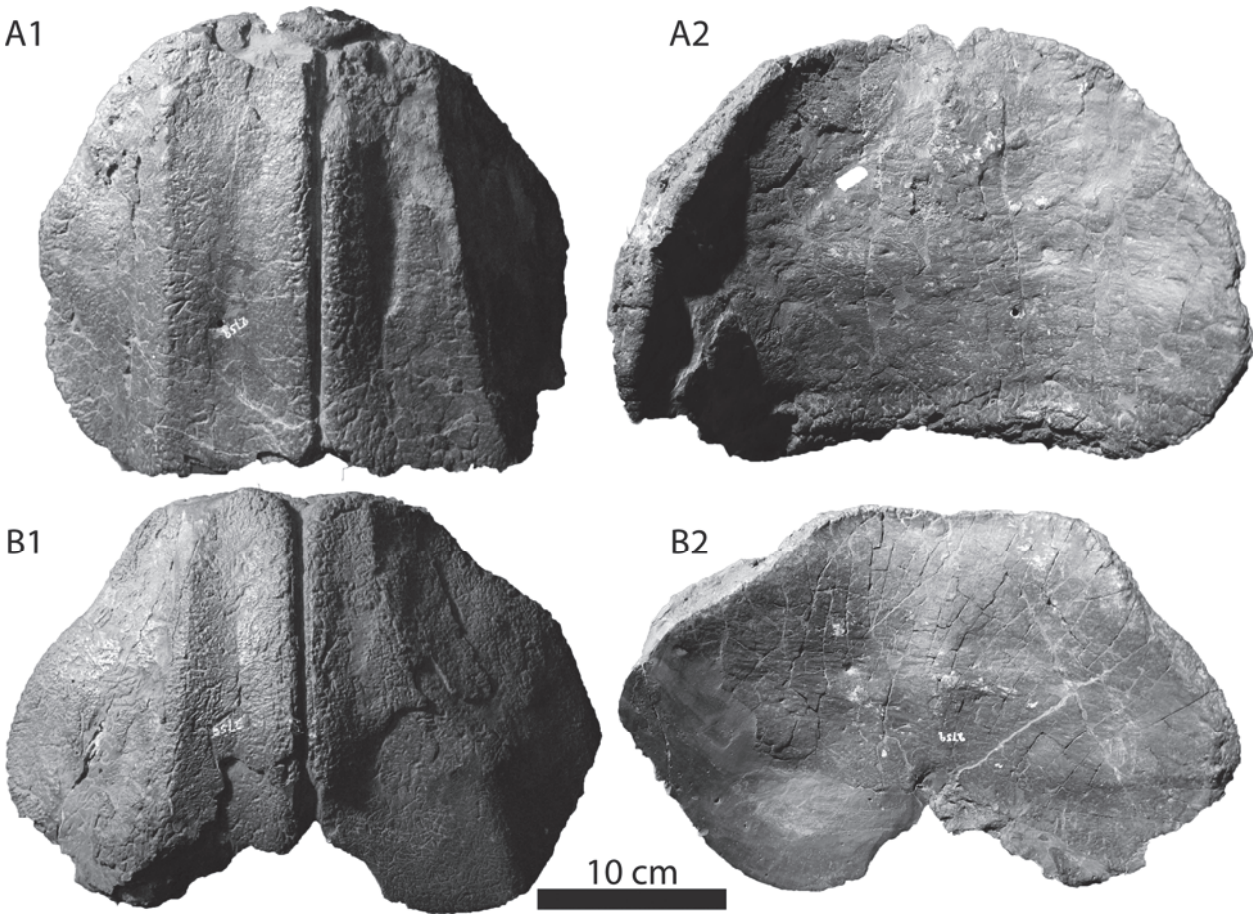

FIGURE 4.45. Coossified medial osteoderms of the first (A) and second (B) cervical half rings of *Panoplosaurus mirus* (CMN 2759, holotype) in external (1) and basal (2) views. Anterior is up.

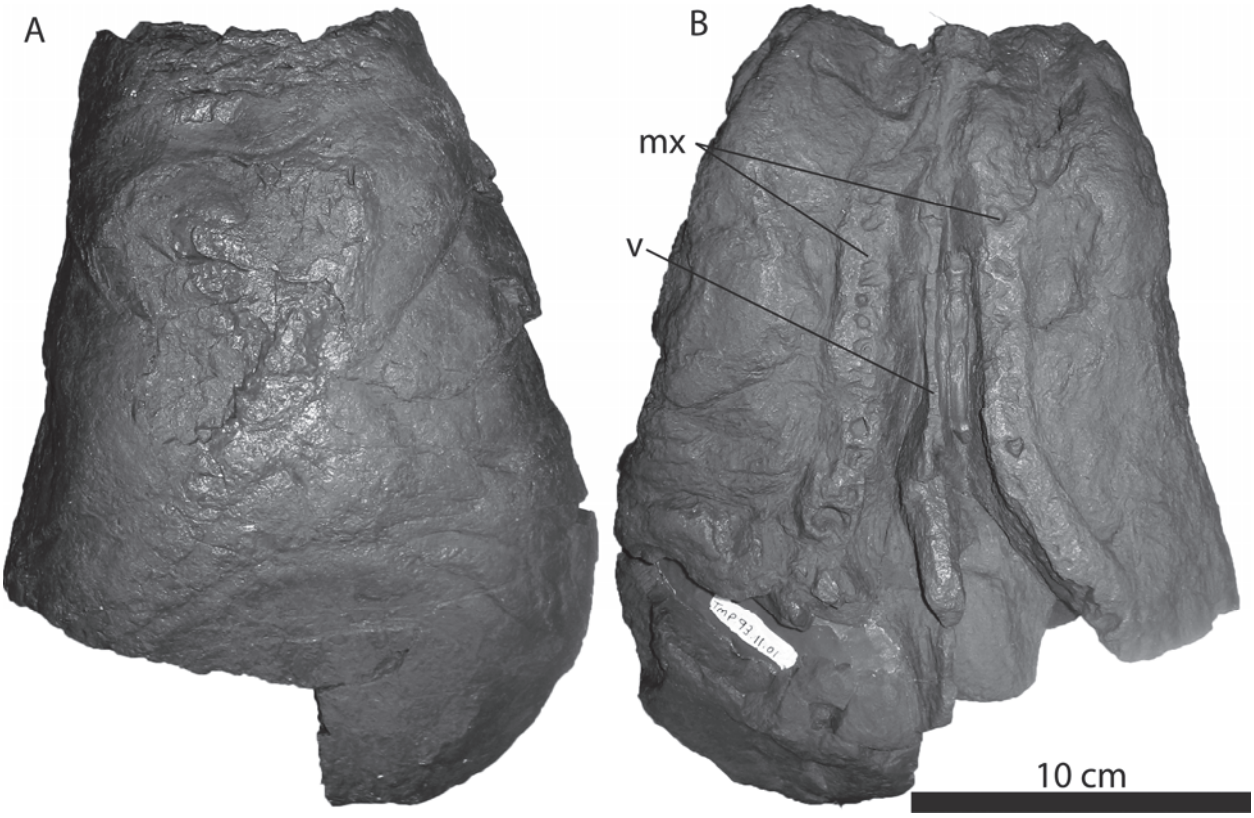

FIGURE 4.46. Partial skull of *Panoplosaurus mirus* (DPMWA 90-25) in dorsal (A) and ventral (B) views. Anterior is up.

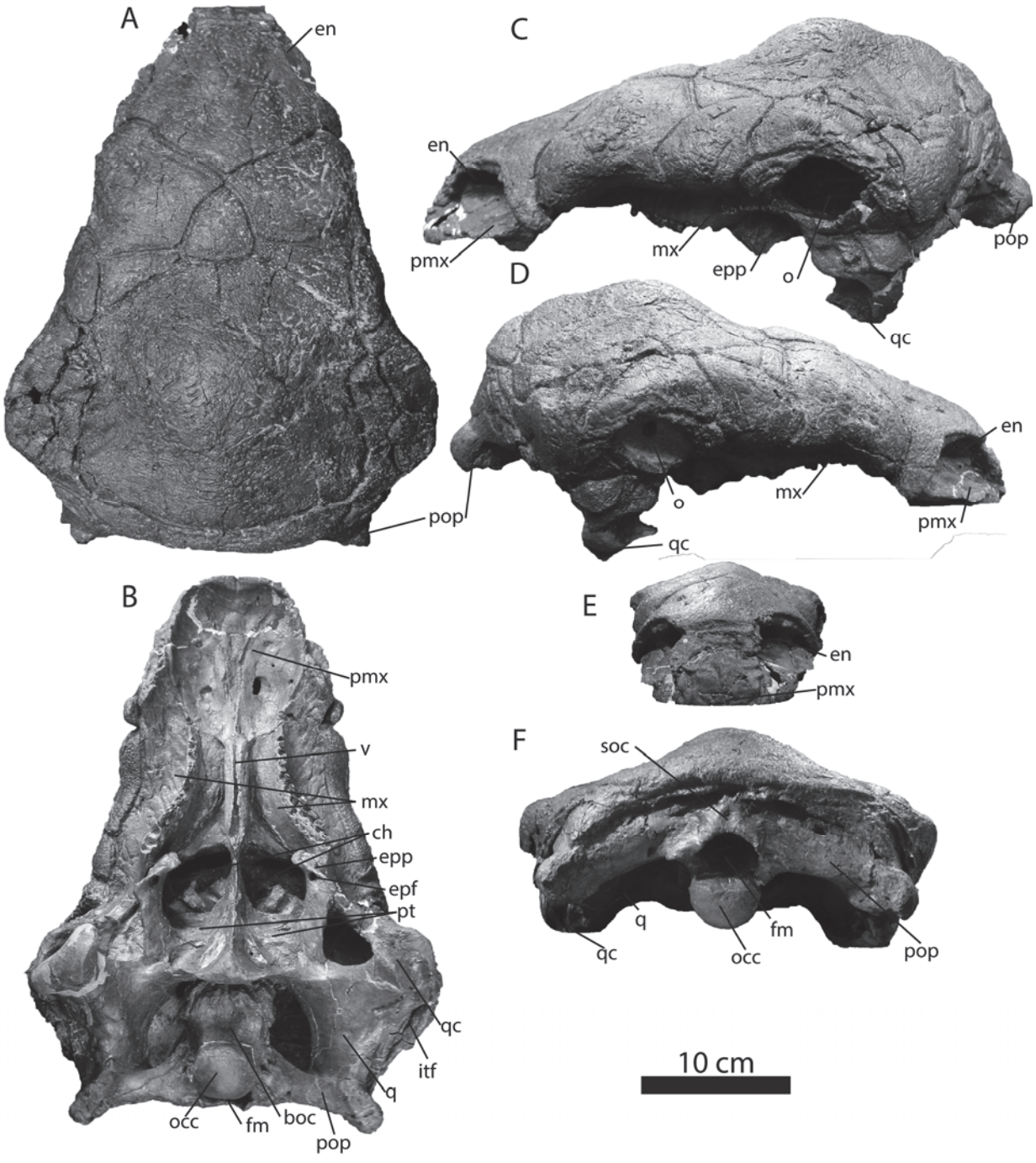

FIGURE 4.47. Skull of *Panoplosaurus mirus* (ROM 1215) in dorsal (A), ventral (B), left lateral (C), right lateral (D), anterior (E), and posterior (F). Anterior is up in A–B, dorsal is up in C–F.

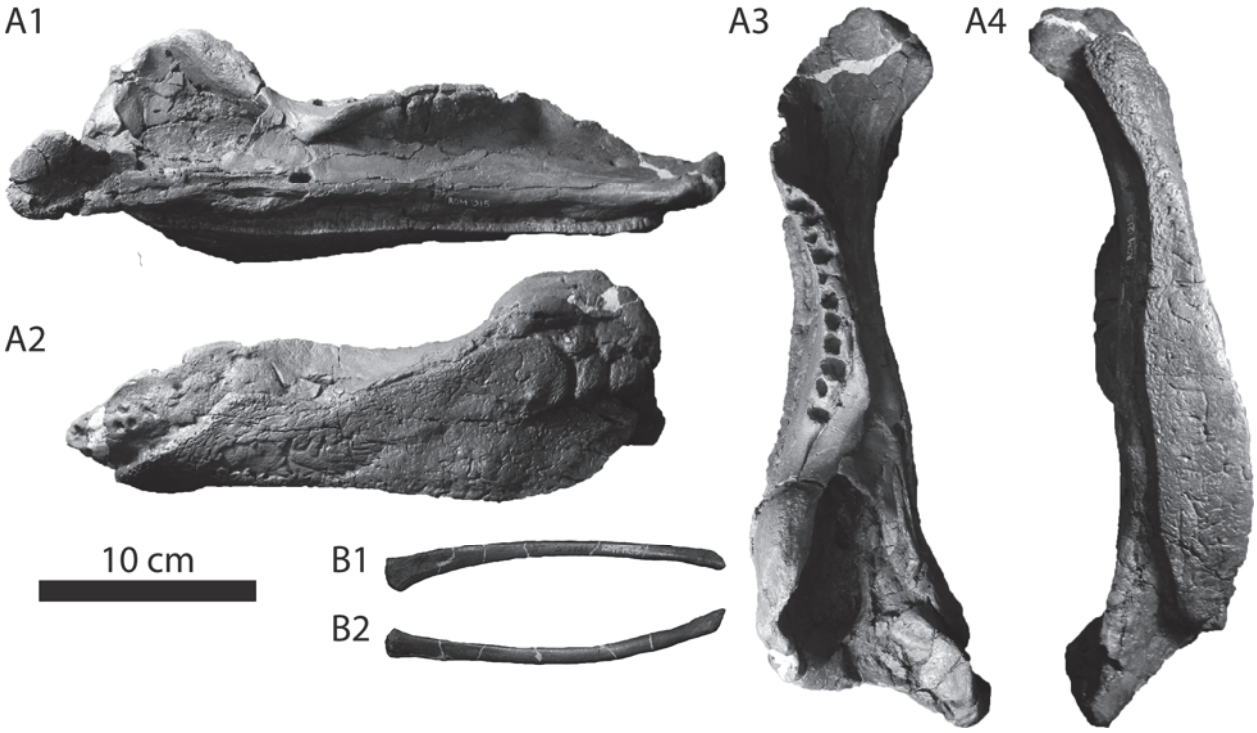

FIGURE 4.48. Left mandible (A) and hyoid (B) of *Panoplosaurus mirus* (ROM 1215). Mandible (A) in medial (1), lateral (2), dorsal (3), and ventral (4) views. Dorsal is up in A1–2, anterior is up in A3–4.

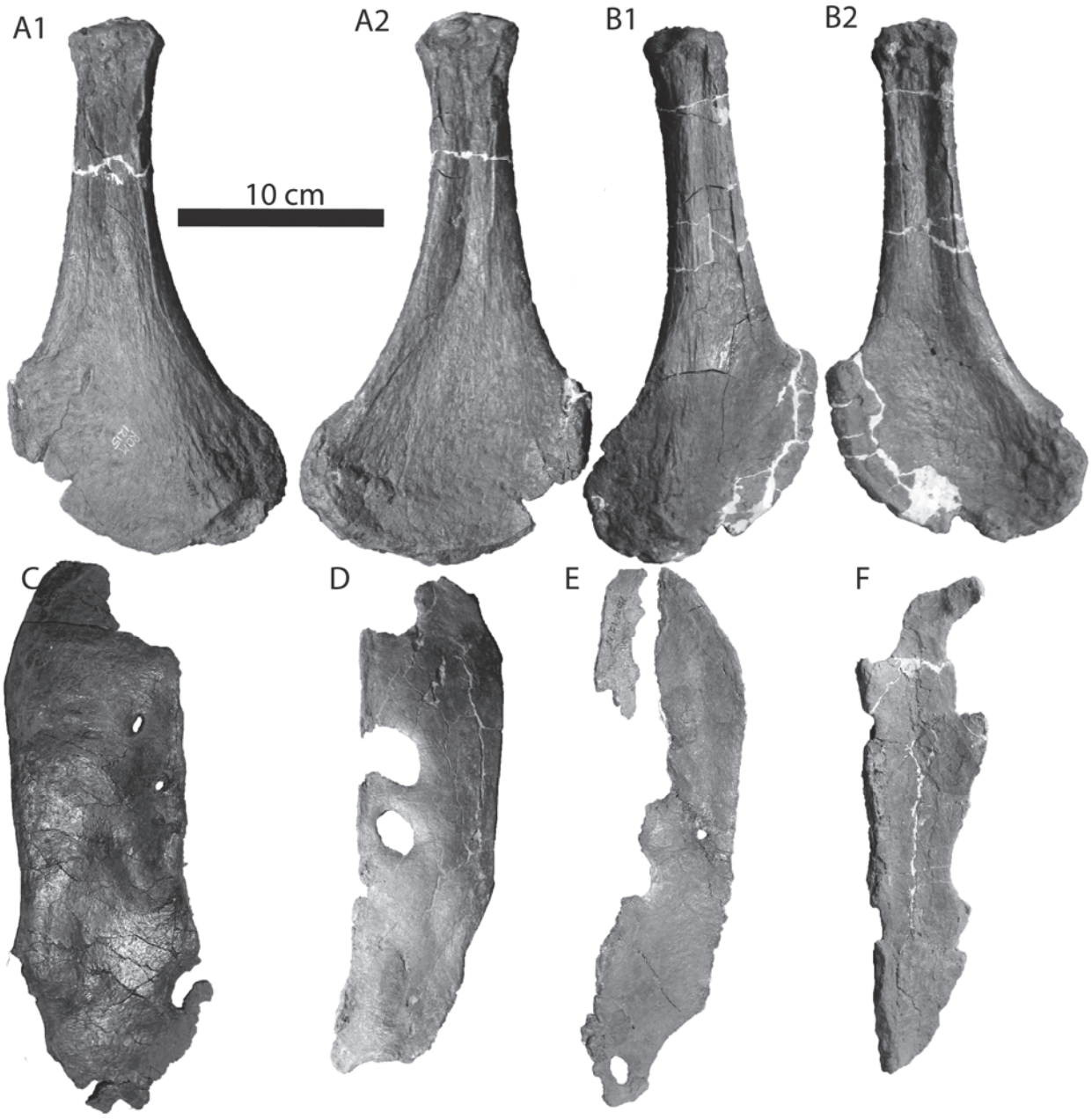

FIGURE 4.49. Sternal elements of *Panoplosaurus mirus* (ROM 1215). Sternal plates (A–B) in superficial (1) and deep (2) views, and xiphisternal plates (C–F).

FIGURE 4.50. Shoulder girdle and forelimb elements of *Panoplosaurus mirus* (ROM 1215). A, right scapulocoracoid in lateral and medial views; B, right humerus in anterior and posterior views; C, left humerus in anterior and posterior views; D, left ulna in anterior and posterior views. Dorsal is up in A, proximal is up in B–D.

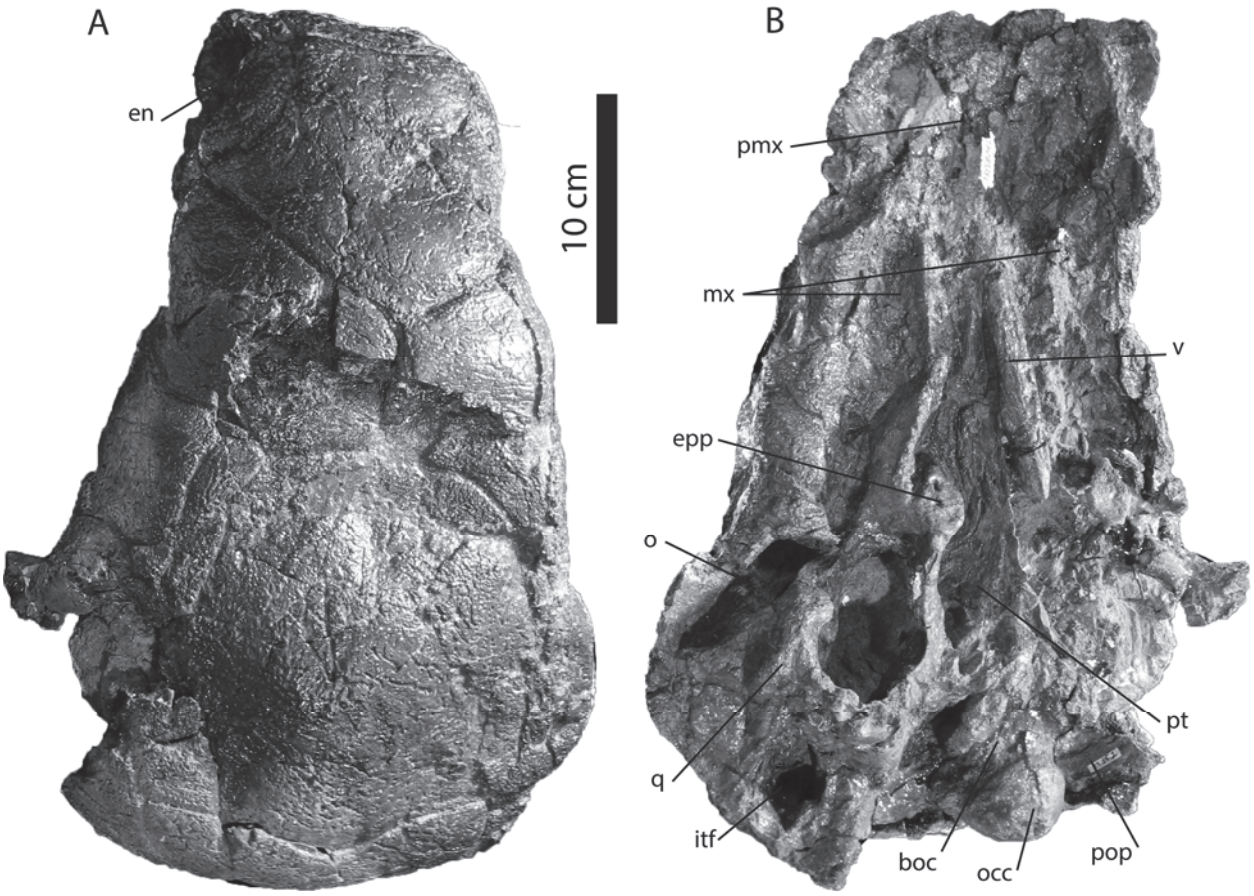

FIGURE 4.51. Skull of *Panoplosaurus mirus* (TMP 83.25.2) in dorsal (A) and ventral (B) views. Anterior is up.

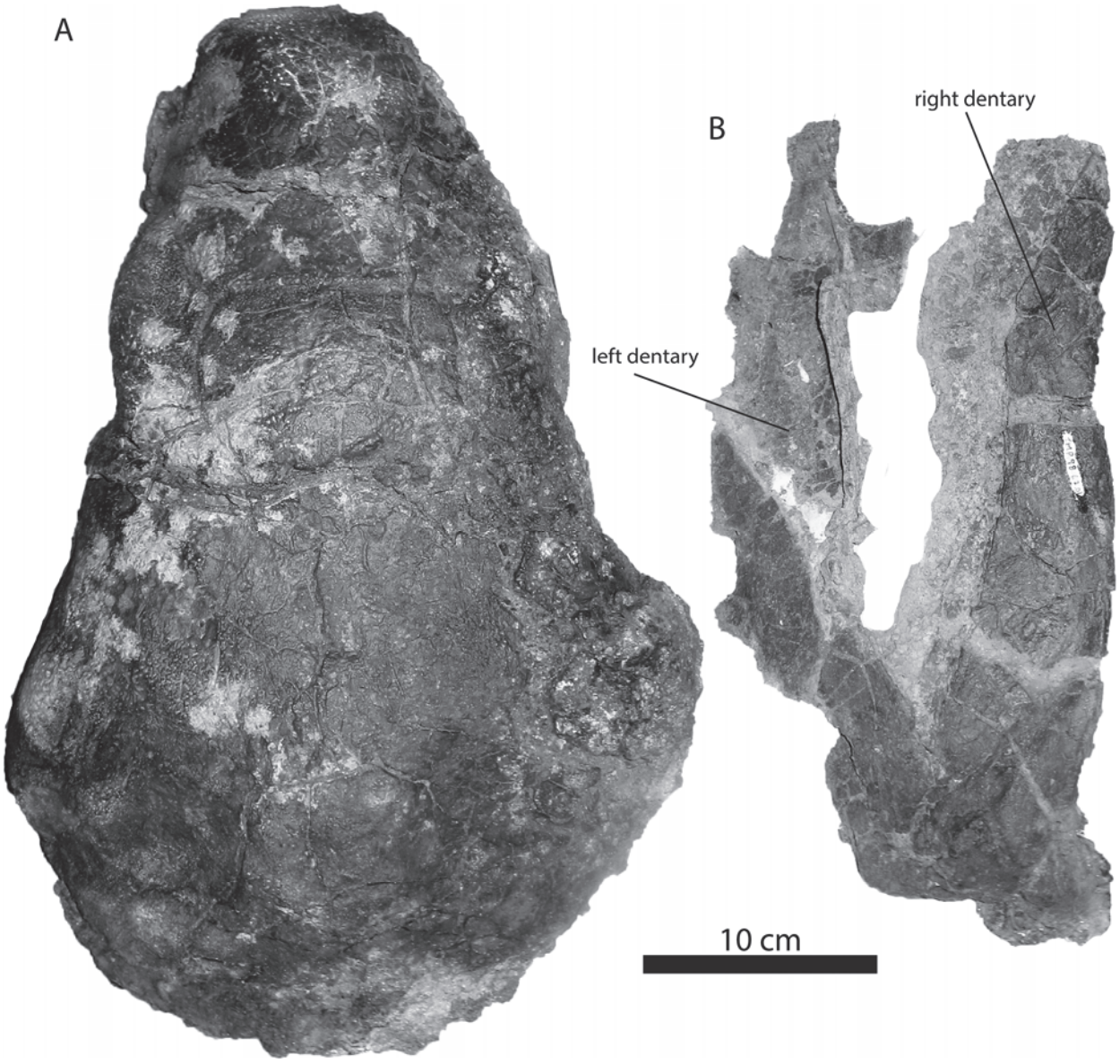

FIGURE 4.52. Skull (A, in dorsal view) and partially prepared mandibles (B, both in lateral view) of *Panoplosaurus mirus* (TMP 98.67.1). Anterior is up.

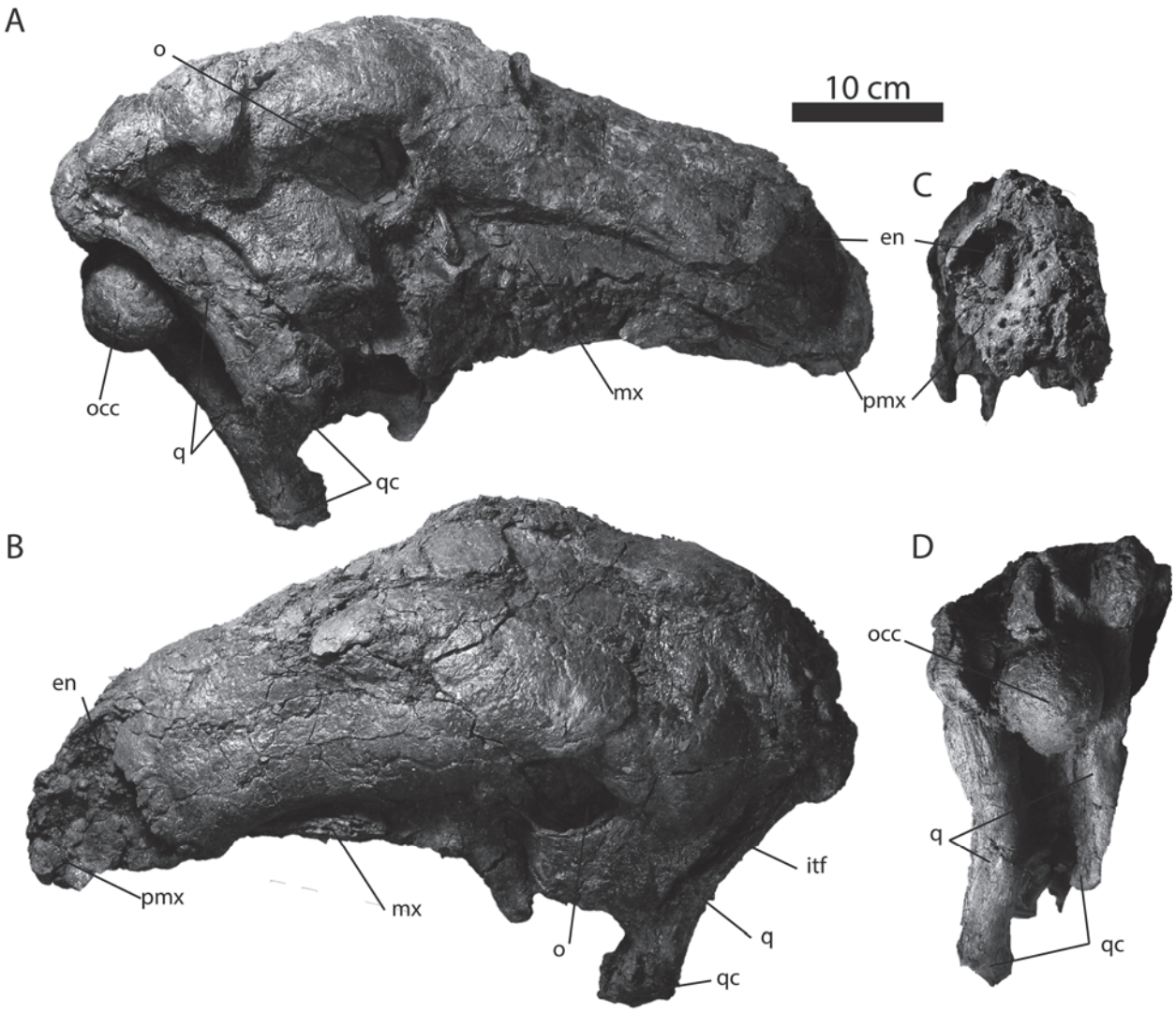

FIGURE 4.53. Skull of Panoplosaurinae indet. (BHI 6332) in right lateral (A), left lateral (B), anterior (C), and posterior (D) views. Dorsal is up.

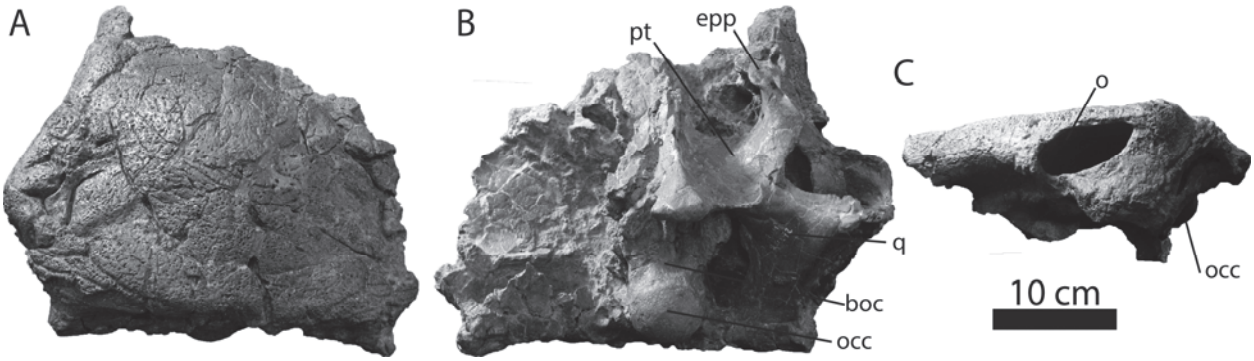

FIGURE 4.54. Partial skull of Panoplosaurinae indet. (ROM 20892) in dorsal (A), ventral (B), and left lateral (C) views. Anterior is up in A–B. Dorsal is up in C.

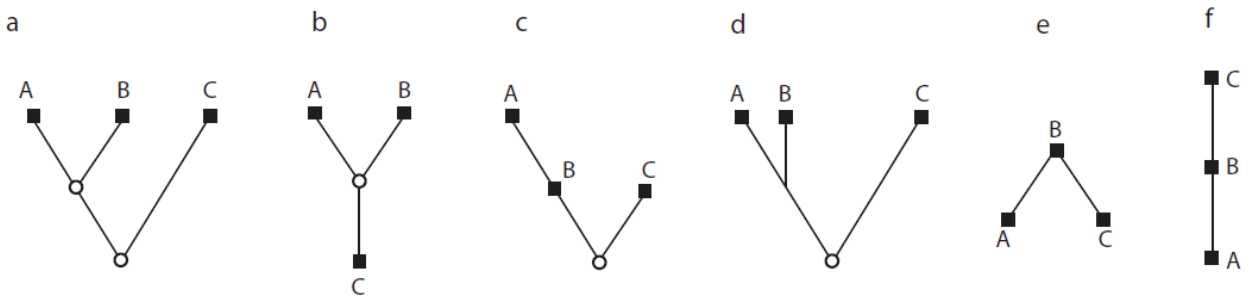

FIGURE 4.55. Six different depictions/hypotheses for the evolution of three taxa. A, B, and C. Hypothetical ancestors are pictured as circles. A represents the most commonly used cladogram. Modified from (Hörandl & Stuessy, 2010, fig. 4).

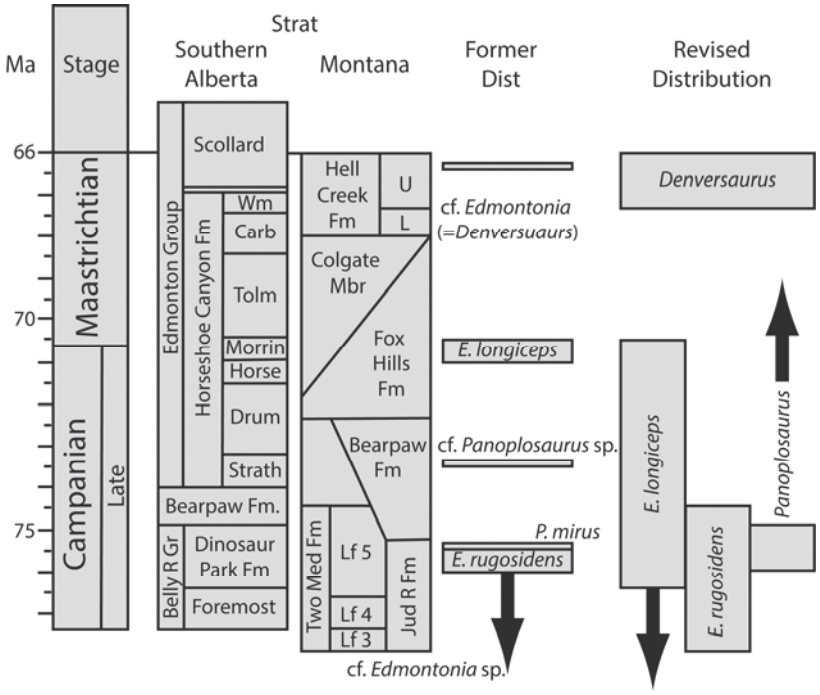

FIGURE 4.56. Hypothesized former and revised stratigraphic distribution of panoplosaurines based on addition of new specimens and revised taxonomy. Modified from Arbour et al. (2009; fig. 7) and Sullivan and Lucas (2006) with stratigraphic data from Currie and Russell (2005), Eberth and Braman (2012), and Eberth and Bell (2014).

CHAPTER 5

ENDOCRANIAL ANATOMY OF LATE CRETACEOUS NODOSAURID ANKYLOSAURS (NODOSAURIDAE: ANKYLOSAURIA)

5.1 INTRODUCTION

The braincase tends to be one of the most poorly understood pieces of anatomy in fossil vertebrates due to visual obstruction by other cranial bones, its fragility, and its complexity (Currie, 1997). Endocasts correspond to the dura mater, which includes underlying sinuses and blood vessels in addition to the brain (Hopson, 1979). As a result, endocasts are useful for researching the approximate overall size of the brain and the relative development of its different parts, including most cranial nerves and blood vessels and pneumatic diverticula associated with the inner and middle ear (Currie, 1997). Although the brain does not entirely fill the endocranial cavity in all vertebrates (it does in modern birds and mammals but not reptiles), endocasts of most fossil archosaurs closely resemble those of living crocodilians, indicating a high fidelity relationship between brain and endocranial morphology (Edinger, 1929; Hopson, 1979). Therefore, the size and shape of the endocranial cavity can yield useful information about the morphology of the brain and associated structures (Hopson, 1979).

This is especially true for ankylosaurs, a clade of heavily armoured ornithischian dinosaurs, in which extensive ossification of the skull obscures much of the internal cranial anatomy. This has led to varying identifications of foramina that perforate the braincase in studies that have dealt with braincases and/or endocasts (Maryańska, 1977; Coombs, 1978c;

Kurzanov and Tumanova, 1978; Carpenter et al., 2001; Averianov, 2002; Vickaryous and Russell, 2003; Hayakawa et al., 2005; Witmer and Ridgely, 2008; Parsons and Parsons, 2009; Miyashita et al., 2011). Although the portions of the clade's taxonomy and classification have been labile, a basic familial dichotomy (Ankylosauridae and Nodosauridae) has been widely accepted over the past 40 years (Coombs, 1971, 1978a; Vickaryous et al., 2004; Thompson et al., 2012). The endocranial anatomy of ankylosaurids has been studied more extensively. The first endocast description for ankylosaur was that of the nodosaurid *Struthiosaurus transylvanicus* by Nopsca (1929). The endocast of the Late Cretaceous North American ankylosaurid *Euoplocephalus* (American Museum of Natural History 5337) was described independently by Coombs (1978b) and Hopson (1979) at roughly the same time. Vickaryous and Russell (2003) would later revisit the braincase of *Euoplocephalus*, creating a composite schematic from several specimens. Kurzanov and Tumanova (1978) detailed and compared the endocranial anatomies of the Mongolian ankylosaurids *Amtosaurus magnus* and *Talarurus plicatospineus* without an endocast. *Amtosaurus magnus* has since, however, been reinterpreted as an indeterminate ornithischian by Parish and Barrett (2004). Parish and Barrett (2004) also reassessed a braincase described by Averianov (2002) as *Amtosaurus archibaldi*, reassigning it to the new genus *Bissektipelta*. Braincase anatomy was also included with the description of *Tatankacephalus* (Parsons and Parsons, 2008). The endocranial anatomy of *Euoplocephalus* has recently been explained in further detail via 3D reconstructions by Witmer and Ridgely (2008) and supported by comparison with direct morphology by Miyashita et al. (2011).

The literature on the nodosaurid endocranium is far sparser. A latex endocast for *Polacanthus* was described by Norman and Faiser (1996). This taxon has variously been considered a member of the "Polacanthidae" (Carpenter, 2001), "Polacanthinae" in either the

Ankylosauridae or Nodosauridae (Thompson et al., 2012), or as part of a basal grade within Ankylosauria or one of the two established families (Coombs, 1978a; Kirkland, 1998). The braincase and an endocast were described for the Early Cretaceous *Cedarpelta* by Carpenter et al. (2001). Currently considered a basal ankylosaurid, its familial placement has also been contentious (Carpenter et al., 2001; Vickaryous et al., 2004; Carpenter et al., 2008). In a description of a partial nodosaurid skull from the Cenomanian of Japan, Hayakawa et al. (2005) created an endocranial peel, although it lacked detail. The endocast of a Late Cretaceous nodosaurid also lacked detail in a digital reconstruction by Witmer and Ridgely (2008).

The nasal cavity of ankylosaurs has been studied less extensively than the braincase and associated endocasts (Maryańska, 1977; Coombs, 1978c; Witmer, 1997; Vickaryous and Russell, 2003; Vickaryous, 2006) and has only recently been three-dimensionally reconstructed using X-ray computed tomography (Witmer and Ridgeley, 2008; Miyashita et al., 2011). In ankylosaurids, the nasal passage is convoluted and occupies most of snout. The airway consists of two main loops, anterior and posterior. The anterior loop is subdivided into several more complex loops. The airway of derived nodosaurids also possess 360° anterior and posterior loops; however they are not as complex as in *Euoplocephalus*. The internal choanae were reconstructed as positioned just anteroventral to the olfactory region, with the inhaled air passing directly into the choanae from the posterior loop (Witmer and Ridgely, 2008).

The endocranial anatomy of derived Late Cretaceous nodosaurids will be described in this paper largely on the basis of a well-preserved, undeformed, incomplete cranial vault specimen from the Hell Creek Formation (Black Hills Institute (BHI) 6225). The description was aided by the creation of a physical artificial endocast and latex peel of the vascularity in the nasal cavity.

5.2 MATERIALS AND METHODS

A taxonomic revision of the Late Cretaceous Nodosauridae is in preparation elsewhere, and therefore taxonomic assignments for undescribed material is avoided, individual specimens are referred to by specimen number instead. The focal specimen for this manuscript (BHI 6225) is undeformed but incomplete. It is the cranial vault of a nodosaurid ankylosaur. Although cranial sutures are obscured by dermal sculpturing, the preserved cranium likely includes the nasals, frontals, parietals, prefrontals, postfrontals, postorbitals, squamosals, supraorbitals and associated dermal ornamentation. The specimen was collected from the upper Maastrichtian (Upper Cretaceous) Hell Creek Formation near Powderville, southeastern Montana, USA. Comparisons with other ankylosaurs are taken from the literature where noted. A cast (UALVP 54155) of the holotype skull (CEUM 1307) of *Gastonia* was used for comparison with that taxon because the braincase is not detailed in the original description for *Gastonia* (Kirkland, 1998). Other comparisons are made with descriptions from the literature where noted.

Herein, homologies and terminology in the antorbital region follow Witmer (1995, 1997), Evans (2006), Witmer and Ridgely (2008), and Miyashita et al. (2011). The term “nasal cavity” is used sensu Miyashita et al. (2011) and is divided into the non-olfactory “dorsomedial” passages and the olfactory “posteromedial” chambers.

5.3 DESCRIPTION

The premaxillae of BHI 6225 (Fig. 5.1) are taphonomically disarticulated along their contacts with the nasals. None of the elements of the palatal region are preserved. The braincase, as preserved, is separated along the contact for the basicranium (the basisphenoid and basioccipital are largely not preserved). Portions of the basioccipital and exoccipitals are preserved in part as a bony ring outlining the circumference of the foramen magnum.

5.3.1 Braincase and endocast

The supraoccipital is the only complete unpaired braincase element preserved in BHI 6225. The supraoccipital contacts the parietals dorsally and exoccipital-opisthotic complexes anterolaterally. Paired braincase elements (Fig. 5.2) preserved include the exoccipital-opisthotic complex, interorbital elements, laterosphenoid, and prootics. The exoccipitals, along with the opisthotics, form the paroccipital processes that extend between the foramen magnum and quadrates. Where the exoccipitals form the ventrolateral walls of the foramen magnum, they extend ventrally as paired protuberances. Only a portion of the basioccipital is preserved where it forms the floor of the foramen magnum between the exoccipital ventrolateral protuberances.

The otic elements, the opisthotic and prootic, form the lateral bony walls of the dorsal part of the braincase. Although no sutural contact between these elements remains in BHI 6225, their position may be estimated by the position of the fenestra ovalis, which is bisected by the contact. The jugular foramen occurs between the basioccipital and the exoccipital-opisthotic. Similarly, the laterosphenoid-prootic contact includes the foramen for the maxillomandibular trunk of the trigeminal nerve (CN $V_{2,3}$). The laterosphenoid encases the cerebral hemispheres and contributes to the bony postocular wall. It, along with the interorbital elements, also includes the

foramen for the ophthalmic trunk of the trigeminal nerve (CN V_1) and the common foramen for the oculomotor and trochlear nerves (CN III/IV).

Overall, the endocast (Fig. 5.3) from BHI 6225 preserves fine (< 1 mm in diameter) blood vessel casts on its surface (mostly visible on the hindbrain), indicating a high fidelity relationship between endocast and brain morphology. The cerebrum, the widest and deepest part of the endocast, bulges to a maximum mediolateral width of 40 mm and dorsoventral height of 43 mm. The cerebral hemispheres are not distinct. Projecting from the lateral pole of the cerebrum, dorsal to the midpoint between the casts of the optic (CN II) and oculomotor (CN III) nerves, the cast of the orbitocerebral vein exits through the braincase ventrolaterally. Posteriorly, the midbrain occupies a narrow (16 mm) band between the cerebrum and hindbrain. A median epiphysis cerebri projects from the posterodorsal portion of the midbrain as in *Euoplocephalus* (Coombs, 1978c). The hindbrain measures 65 mm from the posterior extent of the midbrain to the foramen magnum. It has a dorsoventral constriction along its midlength that is more similar to *Cedarpelta* than *Euoplocephalus* (Coombs, 1978c; Carpenter et al., 2001; Miyashita et al., 2011) or *Polacanthus* (Norman and Faiers, 1996), although these differences may be preservational or produced by the method by which the endocasts were produced. A cast of the root of the posterior middle cerebral vein is preserved laterally on the anterior swelling of the hindbrain dorsal to the root of the trigeminal nerve (CN V) in the same relative position as on the Hokkaido nodosaurid (Hayakawa et al., 2005). A cast of the anterior cerebral vein may be preserved as a swelling just dorsal to the trunk of the trigeminal nerve (CN V), as expected based on its position in *Euoplocephalus* (Miyashita et al., 2011); however, this feature is too indistinct in the endocast of BHI 6225 to be certain.

The olfactory bulbs form two spherical structures, each of which is 23 mm in diameter. The olfactory stalk (diameter = 14 mm), which connects the olfactory bulbs with the cerebral hemispheres posteriorly. The distinction between the cerebrum and olfactory bulbs (i.e., a more prominent constriction of the olfactory stalk) is more similar to the condition in *Polacanthus* (Norman and Faiers, 1996) than in other ankylosaur endocasts (Coombs, 1978c; Carpenter et al., 2001; Hayakawa, 2005; Miyashita, 2011). The impressions of the olfactory nerves (CN I), whereas not well-preserved, are visible as smooth impressions on the internal surface of the skull roof. They indicate that the olfactory nerves (CN I) exit the bulbs and extend anterolaterally, entering the posterolateral chambers of the nasal cavity just anterior to their posteromedial corners. They diverge at an angle of 80°, similar to the 80–100º reported for *Euoplocephalus* (Miyashita et al., 2011). The divergence angle of the olfactory nerves is unknown for *Cedarpelta* and *Polacanthus* (Norman and Faiers, 1996; Carpenter et al., 2001).

At the posterior end of the optic lobes, the optic nerves (CN II) extend anterolaterally into the apices of the pear-shaped orbits. The optic nerves exit the braincase at an angle of 158° relative to one another, similar to the 150–176° divergence seen in *Euoplocephalus* (Coombs, 1978c, text-fig. 1; Miyashita et al., 2011, fig. 7d). The common trunk for the oculomotor (CN III) and trochlear (CN IV) nerves is preserved between those for the optic and trigeminal nerves. This nerve trunk extends anterolaterally through the braincase, entering the apex of the orbit just posterior to the entrance for the optic nerve. Although BHI 6225 is not preserved far enough ventrally to demonstrate a common opening for these nerves, comparison with other nodosaurid skulls (UALVP 55668) in which a common foramen for both nerves can be confirmed. *Gastonia* shows a common foramen for these nerves as do other ankylosaurids (Miyashita et al., 2011).

The trigeminal nerve (CN V) exits the midbrain and extends through the braincase laterally. As better preserved on the right side, the nerve splits as it passed through the wall of the braincase into an anterior ophthalmic nerve (CN V_1) and posterior branch that forms the common maxillomandibular trunk for the maxillary (CN V_2) and mandibular (CN V_3) nerves. The ophthalmic nerve converges with the CN III/IV trunk as it traverses the braincase and enters the apex of the orbit just posterolateral to the CN III/IV trunk. The stapedial artery can also be seen on the right side of BHI 6225, exiting the endocast just anterior to the root of the trigeminal nerve and extending laterally, crossing the ophthalmic nerve and following the maxillomandibular trunk out of the braincase. The braincase is not preserved ventrally far enough to show an opening for the abducens nerve (CN VI).

The facial nerve (CN VII) exits the midbrain just anteroventral to the inner ear, extending laterally prior to changing course, arcing posteriorly around the inner ear, to exit the braincase posterolaterally. It is only well-preserved on the right side. Its position, relative to the trigeminal nerve and inner ear labyrinth, and extent are similar to *Euoplocephalus* (Coombs, 1978c; Miyashita et al., 2011).

The jugular foramen extends posteroventrally from the posterior part of the hindbrain cavity to open just lateral to the exoccipital protuberance that forms its ventral contribution to the foramen magnum. Except for the middle ear labyrinth and root of the trigeminal nerve, the cast of the jugular foramen is the largest structure extending from the endocast, encompassing the glossopharyngeal (CN IX), vagus (CN X), and accessory (CN XI) nerves as well as the jugular vein.

The lateral wall of the exoccipital protuberance is pierced by an opening for the posterior trunk of hypoglossal nerve (CN XII) anteriorly. The anterior trunk extends through the braincase

just posterior to the jugular foramen. The number of trunks for the hypoglossal, however, is variable. In *Polacanthus*, the hypoglossal nerve trunks enter and exit the bony wall of the braincase via two fenestrae on each side posterior to the jugular foramen (Norman and Faiers, 1996). Coombs (1978b) reconstructed three distinct branches for the hypoglossal nerve for *Euoplocephalus*, with the anterior two (both the entrance and exit in the bony wall of the braincase) situated ventromedial to the jugular foramen. Miyashita et al. (2011) reconstruct two branches for this nerve in AMNH 5405, but note that it may be variable within *Euoplocephalus*. *Cedarpelta*, in two specimens with the basioccipital preserved, showed only one trunk and opening for the hypoglossal (Carpenter et al., 2001). In *Gastonia*, three trunks exit the braincase posterior to the jugular foramen. In BHI 6225, the endocast is not be preserved ventrally enough to assess whether or not a third hypoglossal trunk existed in vivo ventromedial to the jugular foramen. In no ankylosaur has bilateral asymmetry been reported in the number or position of the hypoglossal trunks.

Within the foramen magnum, visible as grooves in occipital view, are two paired endolymphatic ducts. They do not appear on the endocast, potentially because the silicone used was too viscous to pick up these small features. To date, these ducts have not been reported in any ankylosaur braincase or endocast.

The vestibular system of the inner ear (Fig. 5.4) is partially preserved on both sides just posterior to the foramen for the facial nerve (CN VII), although it is more complete on the left side where the fenestra ovalis opens into the medial wall of the otic capsule. In the endocast, on the dorsal side of the vestibule, the ampulla for the dorsal canal extends dorsoposterolaterally. Just anterior to it, the ampulla for the lateral canal extends anterolaterally. The common crux for the dorsal and posterior canals extends from the posterior side of the vestibule and bifurcates into

the dorsal and posterior canals. Preserved only on the left side, the ampulla for the posterior canal extends posterolaterally from the ventral portion of the vestibule. Also on the left side, the cochlear fenestra is preserved at the posteroventral corner of the vestibule. There is no floccular recess preserved on the endocast, although this does not mean it was absent. Coombs (1978b) did not reconstruct a flocculus in *Euoplocephalus*, although it was identified in the same specimen (AMNH 5337) by Hopson (1979). Miyashita et al. (2011) were able to recover the flocculus on a digital endocast of *Euoplocephalus* (AMNH 5405) even though it did not appear in a physical endocast (UALVP 47977).

5.3.2 Nasal cavity

The nasal cavity is preserved anterior to the sutural butt joint between the maxillae and premaxillae, the latter of which are not preserved. On the medial walls of the nasals in this region (better preserved on the right side), are a series of large (up to 13 mm diameter) vascular impressions (Fig. 5.5A) that branch anteriorly multiple times. A latex peel shows that the main vessel has three major branches, one of which originates about 43 mm posterior to the premaxillary contact. Anterior to this (by 13 mm) the main vessel bifurcates into the other two major branches. All three branches send off a series of smaller vessels into the maxilla and extend anteriorly past the premaxillary contact. In addition several small branches arch posteroventrally into the nasal cavity. Furthermore, a series of even smaller vessels extends medially to form an anastomosing network with the contralateral vessels anterior to the origin of the vomerine keel (Fig. 5.5A).

At the posterolateral corners of the nasal cavity, just anterior to the orbits, are the bilateral posterolateral chambers (Fig. 5.5B, C). They are roughly triangular in ventral view, with the longest axis (15 cm) extending anterolaterally. The anterior walls separate them from the maxillary sinuses, the medial walls contact the nasal cavity, and posterior wall contacts the orbit. The posterolateral chamber is subdivided by a bony ridge that extends along the long axis of the chamber from the descending process of the frontal (sensu Miyashita et al., 2011). The descending process, although somewhat weathered, shows a scroll-like morphology.

The dorsal impressions of both nasal cavities on the skull roof are roughly straight anteroposteriorly until they converge toward the midline posteriorly (82% of the length from the premaxillary contact). Nevertheless, there are several bony correlates that correspond to the morphology of the double looping airway as reconstructed by Witmer and Ridgely (2008). There is a small (2 cm) mediolateral ridge in the middle (54% of the length from the premaxillary contact) of the nasal cavity. This ridge is u-shaped (concave posteriorly) and preserved on both sides and likely corresponds to the most posterior extent of the anterior loop

Although some vascular impressions are present in the more posterior nasal cavity roof, nowhere are they as prominent as in the anterior portion. Although somewhat weathered, the posterior extent of the nasal cavity (a total of 33 cm long) is at least in line with the midpoint of the orbits.

5.4 DISCUSSION

The occiput is normally formed by four bones (supraoccipital, basioccipital, and a pair of exoccipitals), all contributing to the margin of the foramen magnum (Currie, 1997). In stegosaurs, among other taxa, the supraoccipital forms the entire dorsal margin of the foramen magnum by excluding the exoccipitals (Gilmore, 1914; Currie, 1997) in posterior view. The opposite condition is seen in ceratopsids and hadrosaurs (Hatcher et al., 1907; Langston, 1960; Taquet, 1976; Norman, 1986; Galton, 1989; Weishampel and Horner, 1990; Currie, 1997). Epiotics are unknown in ankylosaurs, as is the case for most adult dinosaur specimens, due to coalescence early in ontogeny with the supraoccipital that obliterates any sutural evidence of discrete, independent ossification centers (Currie, 1997; Vickaryous et al., 2004). In juvenile *Pinacosaurus*, the exoccipitals form a significant component of at least the floor of the foramen magnum, although they are generally excluded from its margin in adults of *Pinacosaurus* and other ankylosaurid taxa (Burns et al., 2011)

Overall, BHI 6225 demonstrates the typical nodosaurid endocranial morphology. Ankylosaurs in general retain a fairly primitive archosaurian endocast with little cerebral expansion. The high fidelity of the endocast relative to true brain morphology, as indicated by the preservation of fine vasculature on the surface of the endocast, has been noted in the nodosaur *Struthiosaurus* and suggests a more complete filling of the endocranial cavity than in ankylosaurids (Buchholtz, 2012). Features of the endocast and braincase of ankylosaurs have been in the past interpreted differently (Maryańska, 1977; Coombs, 1978c; Kurzanov and Tumanova, 1978; Carpenter et al., 2001; Averianov, 2002; Vickaryous and Russell, 2003; Hayakawa et al., 2005; Witmer and Ridgely, 2008; Parsons and Parsons, 2009; Miyashita et al., 2011). Several confusing structures will therefore be discussed further.

The identification of the orbitocerebral vein here is based on its identification in *Euoplocephalus* by Miyashita et al. (2011). They interpreted CN III and CN IV as passing through a common foramen in the braincase. The orbitocerebral vein was reconstructed as exiting the braincase dorsal to the midpoint between the CN II/IV and CN V foramina, whereas the anterior cerebral vein exited just anterodorsal to the CN V exit. The orbitocerebral vein had been interpreted as the trochlear nerve in previous descriptions of ankylosaur endocrania (Coombs, 1978c; Maryańska, 1977; Averianov, 2002; Parsons and Parsons, 2009). As noted by Miyashita et al. (2011), this interpretation is more consistent with the situation in other dinosaurs for which the endocast is known (Sampson and Witmer, 2007; Sereno et al., 2007; Witmer et al., 2008; Witmer and Ridgely, 2008).

The identification of the ophthalmic (CN V_1) and common maxillary/mandibular (CN $V_{2,3}$) nerves is based on comparison with other published dinosaur endocasts. In most theropods (Currie 1985, 2003), *Hypacrosaurus* (Evans, 2010) and lambeosaurines (Evans et al., 2009; Lauters et al., 2013) the ophthalmic nerve can be seen as an anteriorly projecting groove in lateral view along the lateral wall of the laterosphenoid. No similar groove was observed in BHI 6225, however. A common trunk and separate opening for the ophthalmic and maxillary/mandibular branches is common in tyrannosaurs (Bakker et al., 1988; Brochu, 2000; Currie, 2003). In some theropod taxa, though, (e.g., *Giganotosaurus*; Paulina Carabajal and Canal, 2010) the trigeminal exits the braincase via a common foramen. Some, though not all, tetanurans (Larsson, 2001; Coria and Currie, 2002), among tyrannosaurs and other theropods (Witmer and Ridgley, 2008) exhibit the condition seen in BHI 6225, in which a common trunk for CN V bifurcates within the braincase and exits via separate foramina.

The trigeminal nerve exits the braincase via common foramen in all other ankylosaurs for which endocasts have been described (Coombs, 1978c; Norman and Faiers, 1996; Carpenter et al., 2001; Miyashita et al., 2011). In *Gastonia*, however, this is less clear and it is possible that (at least as preserved on the left side) the trigeminal bifurcated proximal to exiting the braincase. In *Polacanthus*, the trigeminal nerve appears to have a more anteriorly-directed course as it exits the braincase (Norman and Faiers, 1996). The condition of the trigeminal nerve in this sense may prove a systematically useful character. If it suggests a nodosaurid affinity for *Gastonia*, such a character may diminish some support for a Polacanthine as currently understood (Burns and Currie, 2014). It may also, however, be indicative of plasticity in the thickness of the bony wall of braincase and suggest no more than individual variation. More attention to the endocranial morphology of basal ankylosaurs may aid in resolving some of the deeper evolutionary relationships among ankylosaurs.

5.4.1 Airway

Witmer and Ridgley (2008) reconstructed, using three-dimensional modeling based on CT data, the same double-looping airway in ROM 1215 that appears to be present in BHI 6225. Previous to that study, Vickaryous (2006) reconstructed a simple airway for AMNH 3076 due to the lack of any visible bony subdivisions within the nasal cavity. Upon revisiting the specimen, Witmer and Ridgely (2008) noted laminae within the nasal cavity. In the present study, osteological correlates are visible on the internal skull roof of BHI 6225 that correspond to the anterior and posterior loops of the airway as well as a bony ridge that demarcates the border between them.

Witmer and Ridgely (2008) reconstructed the olfactory region of nodosaurids as encompassing the entire posterior region of the nasal passages. In ankylosaurids, however, the olfactory region is restricted to posterolateral chambers of the nasal cavity according to Miyashita et al (2011) and supported by the reconstructions of AMNH 5405 by Witmer and Ridgely (2008). The similarly wide divergence angle of the olfactory nerves in BHI 6225, which enter the posteromedial corners of the posterolateral chambers, indicates that in the ankylosaurid condition olfaction was limited to this portion of the nasal cavity; this is true for derived nodosaurids, as well. Because, among known archosaurs, this is only seen in nodosaurids and ankylosaurids, this may prove an important phylogenetic character for reconstructing basal ankylosaurian and polacanthine relationships.

The extensive blood supply to the anterior nasal cavity roof is interpreted as originating from the nasal artery, a branch of the anterior ethmoidal artery. The artery courses along the roof of the nasal cavity, through the bony wall dividing the dorsomedial and olfactory regions of the nasal cavity. No other major blood vessels that might supply this region of the nasal cavity are apparent as impressions on the skull roof.

The posterior region of the airway (including the posterior portion of the posterior loop and posterolateral chambers) is more complex in nodosaurs than previously thought. It is more similar, in fact, to this region as reconstructed for *Euoplocephalus* (Witmer and Ridgley, 2008). Air would have to have entered the posterolateral chamber near the descending process of the frontal. The scroll-like morphology of this process may have acted as a turbinate or concha, diverting inspired air from the posterior loop of the main airway. The bony ridge extending laterally from the descending process and bisecting the chamber may have also aided in the smooth and/or unidirectional flow of air through the posterolateral chamber. This ridge is also

present in *Euoplocephalus* (Miyashita et al., 2011; fig. 2). The well-vascularized groove on the anterior wall of the posterolateral chamber, described in *Euoplocephalus* (Miyashita et al., 2011), is absent in BHI 6225. The posterior loop itself would have extended farther posteriorly than reconstructed for ROM 1215. Witmer and Ridgely (2008) reconstructed the internal choanae anteroventral to the posterolateral chambers. If this is the case, inspired air in the posterior loop would have passed medial to the posterolateral chamber before coursing anteroventrally towards the internal choanae.

FIGURES

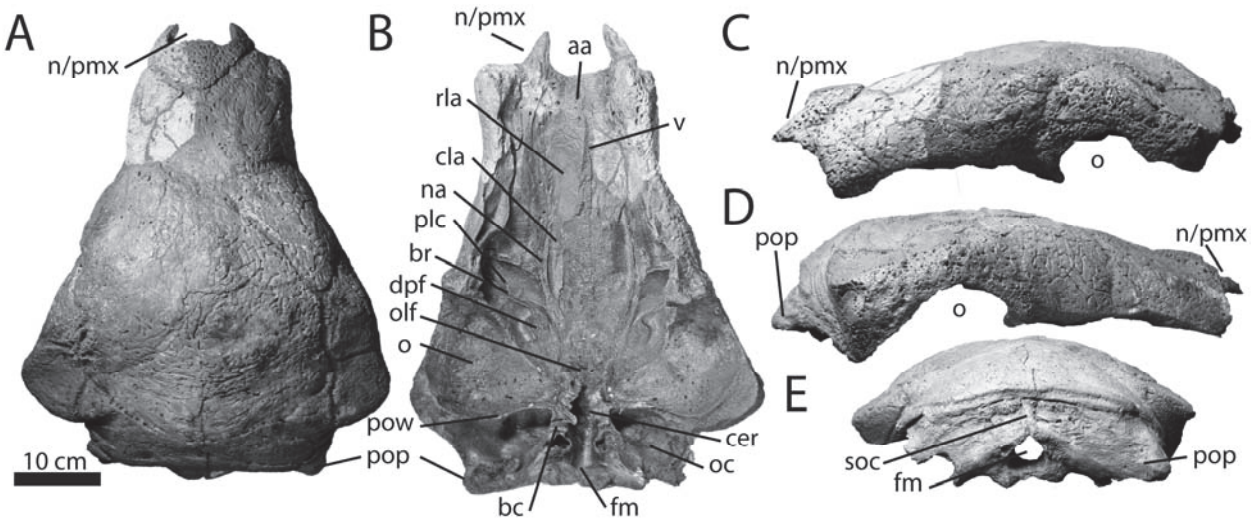

FIGURE 5.1 Preserved skull roof of BHI 6225 in (A) dorsal, (B) ventral, (C) left lateral, (D) right lateral, and (E) posterior views.

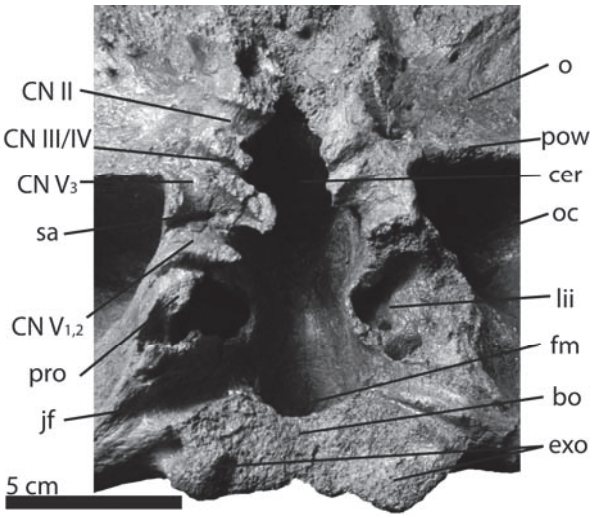

FIGURE 5.2 Detail of braincase of BHI 6225 in ventral view. Anterior is up.

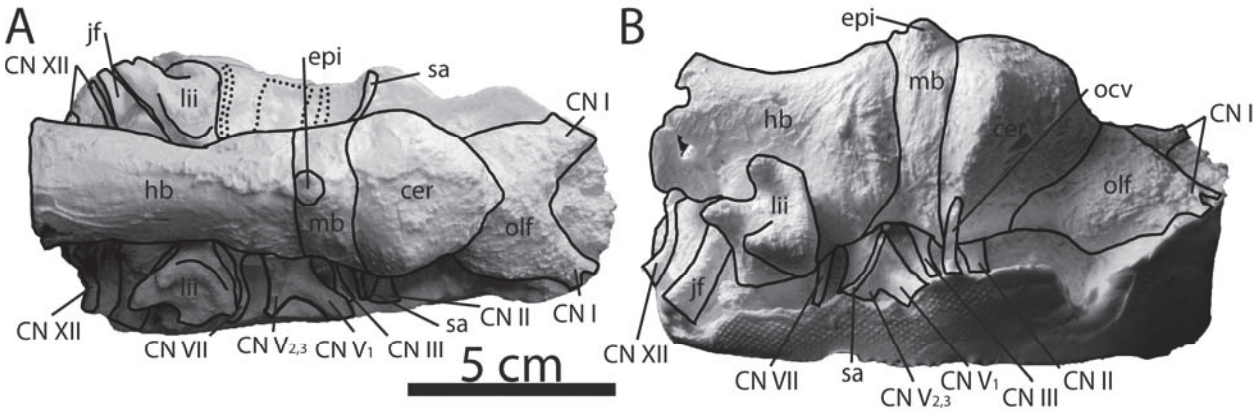

FIGURE 5.3 Physical endocast of BHI 6225 in (A) dorsal and (B) right lateral views. Anterior is to the right.

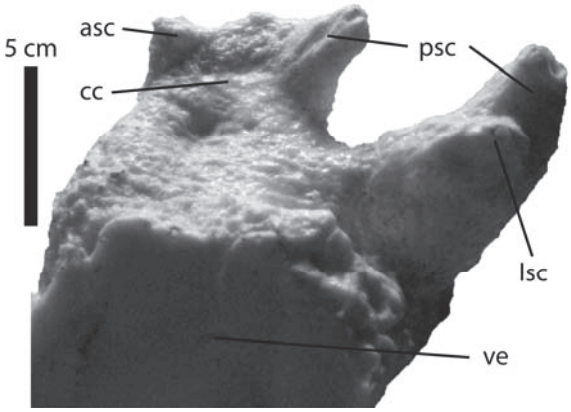

FIGURE 5.4 Detail of right inner ear labyrinth (=vestibular apparatus) of BHI 6225 in lateral view. Anterior is to the left.

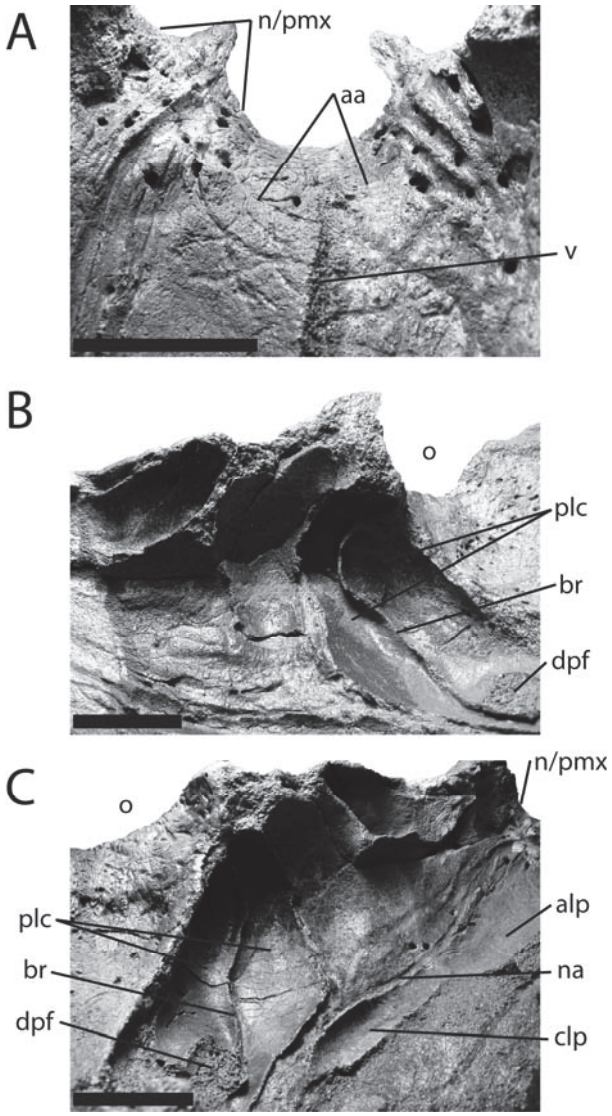

FIGURE 5.5 Detail of preserved airway of BHI 6225. (A) Anterior airway in posteroventral view (anterior is up). (B) Left and (C) right posterolateral chambers in ventromedial oblique view. Anterior is to the left in B and to the upper right in C. Scale bars (lower left of each pane) equal 5 cm.

CHAPTER 6

6.1 CONCLUSIONS

Sources of intraspecific variability include individual variation, sexual dimorphism, and ontogeny. The degree of observable morphological intraspecific variation is itself taxon-dependent. Therefore, a sound understanding of intraspecific variation ideally involves a taxon-specific approach.

With respect to the armoured dinosaurs (Dinosauria, Ankylosauria), the majority of the currently-valid 61 species (Appendix 1) are represented by single specimens. Ankylosaurs show considerable differences in terms of absolute size, from *Liaoningosaurus* (body length < 34 cm; Xu et al., 2001) to *Ankylosaurus* (body length ≤ 6.25 m; Carpenter, 2004). The ankylosaurids *Liaoningosaurus* and *Pinacosaurus*, and the nodosaurid *Propanoplosaurus* are examples known almost entirely from juvenile specimens (Burns et al., 2011; 2014; Currie et al., 2011; Stanford et al., 2011; Xu et al., 2001). Others, such as *Ahshislepelta*, have been considered relatively small-bodied adults (Burns and Sullivan, 2011). Sexual dimorphism has not played a large part in discussion of morphological variation in ankylosaurs, although it has been hypothesized for *Edmontonia* (Carpenter, 1990).

This thesis tests for intraspecific variation, in terms of ontogenetic and individual variability, in ankylosaurs using several approaches. First (Chapter 2), the postcrania was assessed in an assemblage of juvenile to ?subadult *Pinacosaurus* and across other ankylosaur taxa to test for differences in ontogenetic versus taxonomic allometry. Samples from the *Pinacosaurus* assemblage as well as an assemblage of subadult *Gastonia* were examined

histologically (Chapter 3) to describe ontogenetic differences in the microstructure of postcranial bones. Finally, to investigate individual versus taxonomic variation, I examined Late Cretaceous specimens referable to the Nodosauridae (Chapter 4). Characters were tested via a specimen-specific parsimony analysis to determine which, if any, supported species-level groups. In addition, the endocranial anatomy of these nodosaurids was described (Chapter 5), which can prove useful for providing characters for deeper-level phylogenetic hypotheses for ankylosaurs.

All ankylosaurine material from Alag Teeg and ZPAL MgD II/1 are referable to *Pinacosaurus grangeri*. The assignment of PIN 614 to *Pinacosaurus* is equivocal, currently based on provenance, and requires the collection of adult postcranial material definitively referable to the genus. One individual from Alag Teeg has a significantly larger body size than the rest of the population. The large specimen indicates a delayed onset of postcranial fusion. This adds support to the validity of ankylosaur taxa erected using specimens of relatively small body size, but whose postcrania show a high degree of skeletal fusion. Relative to other ankylosaurines, the average body size of *Pinacosaurus* at Alag Teeg is small. At least at early stages of growth, the element widths of the shoulder girdle and forelimb are strongly correlated with the lengths of these elements, suggesting a weight-bearing origin for their robust morphology. The scapula becomes allometrically taller as its length increases, with the highest allometric coefficients occurring proximally. Humeral width shows the highest positive allometry at its distal end. Although zeugopodial elements exhibit positive allometry along their lengths, the allometric coefficient increases proximally for the ulna and distally for the radius. The hind limb does not show similar significant allometric trends. Future studies should expand upon this by testing for these allometric trends are also observable in assemblages of larger

ankylosaurs, such as *Peloroplites* (Carpenter et al., 2008), or small-bodied adult ankylosaurs, such as *Hungarosaurus* (Ősi, 2005).

An understanding of the growth dynamics in ankylosaurs allows for an examination of the morphological allometry (Chapter 2), and has possible implications for the use of element size and/or robustness in some ankylosaurian taxa (Chapters 2, 4). Juvenile ankylosaur elements are characterized by well-vascularized FLB and few to no CGMs. Subadult ankylosaur elements preserve primary bone that shows varying degrees of preservation of CGMs, some of which may be identified as LAGs. Whereas the growth rates of juveniles are likely as fast as other dinosaurs of comparable body size, subadults show a prolonged period of slowing growth and heavy secondary remodeling. This is possibly associated with the mineralization of the pervasive system of armour during this stage of ontogeny. Ideally, the relationship between ontogeny and bone histology should be tested using an assemblage representing a broad size range of individuals from a single species, as had been done, for example, with *Maiasaura peeblesorum* (Horner et al., 2000), although such an assemblage is currently unknown for ankylosaurs. Nevertheless, the preliminary description presented in this thesis can serve as a framework for identifying the rough ontogenetic stage of ankylosaurs at various body sizes.

A specimen-by-specimen parsimony analysis is a useful tool for making taxonomic delineations for cases in which specimens show a high degree of morphological variability. This method uses explicit character weighting for alpha taxonomy and, as a result, taxonomic hypotheses are more easily tested with the addition of new anatomical information. A revision of Upper Cretaceous nodosaurids reveals that, in addition to the widely-accepted *Edmontonia* and *Panoplosaurus*, *Denversaurus* is also likely valid; all three may be considered members of the Panoplosaurinae, with *Edmontonia* as the more basal genus. This analysis provides a method for

distinguishing intraspecifically variable characters, such as the development and thickening of the vomer, from taxonomically-informative characters, such as the relative development of ornamentation over the skull roof.

The preservation of BHI 6225 (*Denversaurus schlessmani*) also allows for the detailed description of the endocranial anatomy for a derived nodosaurid. Although generally morphologically conservative, the endocast may provide some taxonomically useful characters for ankylosaurs. For example, the bifurcation of the trigeminal nerve (CN V) within the bony wall of the braincase has not been observed in other ankylosaur taxa. The extent to which this is simply individual variation (i.e., dependent solely on the thickness of the braincase wall) is unknown at present. The airway of derived nodosaurids is more similar than previously thought to the complex system known in ankylosaurids, and olfaction was similarly restricted to posterolateral chambers. It is unknown, however, whether or not these convoluted airways are independently derived or shared due to common ancestry. Because it is generally evolutionarily conservative, endocranial anatomy holds potential for determining some of the deeper relationships within ankylosaurian phylogeny. In light of ever-increasing comparative data on ankylosaur endocrania, some basal taxa require more detailed reanalysis, including, among others, the endocast of *Polacanthus* and the braincase of *Gastonia*.

This thesis provides a framework for assessing intraspecific (ontogenetic and/or individual) variation in the armoured dinosaurs. Although postcrania can provide useful taxonomic characters, the effects of ontogenetic allometry (e.g., more pronounced development of forelimb as opposed to hind limb features) should be considered. When possible, the rough ontogenetic stage of an individual may be assessed histologically. The process of delimiting species can be improved by employing a specimen-based parsimony analysis in cases where the

degree of intraspecific morphological diversity may be difficult to distinguish from taxonomic variation. This allows for explicit *a priori* character weighting and a more easily falsifiable alpha taxonomic hypothesis.

REFERENCES CITED

Abel, O. 1919. Die Stämme der Wirbeltiere. Walter de Gruyter, Berlin, Leipzig. 914 p.

Amprino, R. 1947. La structure du tissu osseux envisagée comme expression de différences dans la vitesse de l'accroissement. Archives of Biology 58:315–330.

Arbour, V. M., and P. J. Currie. 2011. Taphonomic filters of age groups of the ankylosaurid dinosaur *Pinacosaurus*. Journal of Vertebrate Paleontology 31:64.

Arbour, V. M., and P. J. Currie. 2013. The taxonomic identity of a nearly complete ankylosaurid dinosaur skeleton from the Gobi Desert of Mongolia. Cretaceous Research 46:24–30.

Arbour, V. M., M. E. Burns, and R. L. Sissons. 2009. A redescription of the ankylosaurid dinosaur *Dyoplosaurus acutosquameus* Parks, 1924 (Ornithischia: Ankylosauria) and a revision of the genus. Journal of Vertebrate Paleontology 29:1117–1135.

Arbour, V. M., M. E. Burns, R. M. Sullivan, S. G. Lucas, A. K. Cantrell, J. Fry, and T. L. Suazo. 2014. A new ankylosaurid dinosaur from the Upper Cretaceous (Kirtlandian) of New Mexico with implications for ankylosaurid diversity in the Upper Cretaceous of western North America. PLoS ONE 9:e108804. doi:10.1371/journal.pone.0108804

Arbour, V. M., P. J. Currie, and D. Badamgarav. 2014. The ankylosaurid dinosaurs of the Upper Cretaceous Baruungoyot and Nemegt formations of Mongolia. Zoological Journal of the Linnean Society 172:631–652.

Arbour, V. M., and E. Snively. 2009. Finite element analyses of ankylosaurid dinosaur tail club impacts. Anatomical Record 292:1412–1426.

Arbour, V. M., M. E. Burns, and P. J. Currie. 2013. A review of pelvic shield morphology in ankylosaurs (Dinosauria: Ornithischia). Journal of Paleontology. 85:298–302.

Averianov, A. O. 2002. An ankylosaurid (Ornithischia: Ankylosauria) from the Upper Cretaceous Bissekty Formation of Uzbekistan. Bulletin de l'Institut royal des Sciences naturelles de Belgique, Sciences de la Terre 72:97–110.

Bakker, R. T. 1988. Review of the Late Cretaceous nodosaurid Dinosauria: *Denversaurus schlessmani*, a new armor-plated dinosaur from the latest Cretaceous of South Dakota, the last survivor of the nodosaurians, with comments on stegosaur-nodosaur relationships. Hunteria 1:1–23.

Barrett, P. M., H. You, P. Upchurch and A. C. Burton. 1998. A new ankylosaurian dinosaur (Ornithischia: Ankylosauria) from the Upper Cretaceous of Shanxi Province, People's Republic of China. Journal of Vertebrate Paleontology 18:376–384.

Befus, K. S., Hanson, R. E., Lehman, T. M., and Griffin, W. R. 2008. Cretaceous basaltic phreatomagmatic volcanism in west Texas: maar complex at Pena Mountain, Big Bend National park. Journal of Volcanology and Geothermal Research 173: 245–264.

Blows, W. T. 1996. A new species of *Polacanthus* (Ornithischia: Ankylosauria) from the Lower Cretaceous of Sussex, England. Geological Magazine 133:671–682.

Bohlin, B. 1953. Fossil reptiles from Mongolia and Kansu. Paleontologia Sinica, unnumbered volume, the Sino-Swedish Expedition 37:1–113.

Breyer, J. A., Busbey III, A. B., Hanson, R. E., Befus, K. E., Griffin, W. R., Hargrove, U. S., and Bergman, S. C.2007. Evidence for Late Cretaceous volcanism in Trans-Pecos Texas. The Journal of geology 115:243–251.

Brochu, C. A. 2000 A digitally-rendered endocast for *Tyrannosaurus rex*. Journal of Vertebrate Paleontology 20:1–6

Broom, R. 1912. Observations on some specimens of South African fossil reptiles preserved in the British Museum. Transactions of the Royal Society of South Africa 2:19–25.

Brown, B., and E. M. Schlaikjer. 1940. The structure and relationships of *Protoceratops.* Annals of the New York Academy of Sciences 40:133–265.

Brown, B. 1908. The Ankylosauridae, a new family of armored dinosaurs from the Upper Cretaceous. Bulletin of the American Museum of Natural History 24:187–201.

Buchholtz, E. 2012. Dinosaur paleoneurology. Pp. 191–208 *in* Brett-Surman, M. K., T. R. Holtz Jr., and J. O. Farlow (eds.). The Complete Dinosaur. Second Edition. Indiana University Press: Bloomington.

Bufrénil, V. de, and J. Castanet. 2000. Age estimation by skeletochronology in the Nile monitor lizard (*Varanus niloticus*), a highly exploited species. Journal of Herpetology 34:414–424.

Bunzel, E. 1870. Notice of a fragment of a reptilian skull from the Upper Cretaceous of Grünbach. Quarterly Review of the Geological Society of London 26:394.

Bunzel, E. 1871. Die reptilfauna der Goasu-Formation in der neuen Welt bei Wiener-Neustadt. Abhandlungen der Geologischen Bundesanstalt 5:7–18.

Burns, M. E., and R. M. Sullivan. 2011. A new ankylosaurid from the Upper Cretaceous Kirtland Formation, San Juan Basin, with comments on the diversity of ankylosaurids in New Mexico. New Mexico Museum of Natural History Bulletin 53:169–178.

Burns, M. E., P. J. Currie, R. L. Sissons, and V. M. Arbour. 2011. Juvenile specimens of *Pinacosaurus grangeri* Gilmore, 1933 (Ornithischia: Ankylosauria) from the Late Cretaceous of China, with comments on the specific taxonomy of *Pinacosaurus*. Cretaceous Research 32:174–186.

Burns, M.E. 2008. Taxonomic utility of ankylosaur (Dinosauria: Ornithischia) osteoderms: *Glyptodontopelta mimus* Ford, 2000—a test case. Journal of Vertebrate Paleontology 28:1102–1109.

Burns, M. E., and M. J. Vavrek. 2014. Probable ankylosaur ossicles from the middle Cenomanian Dunvegan Formation of northwestern Alberta, Canada. PLoS ONE 9(5): e96075. doi:10.1371/journal.pone.0096075

Burns, M. E., and P. J. Currie. 2014. External and internal structure of ankylosaur (Dinosauria, Ornithischia) osteoderms and their systematic relevance, Journal of Vertebrate Paleontology 34:835–851.

Burns, M. E., M. K. Vickaryous, and P. J. Currie. 2013. Histological Variability in Fossil and Recent Alligatoroid Osteoderms: Systematic and Functional Implications. Journal of Morphology 274:676–686.

Campione, N. E., and D. C. Evans. 2012. A universal scaling relationship between body mass and proximal limb bone dimensions in quadrupedal terrestrial tetrapods. BMC Biology, 10:60.

Carpenter, K. 1990. Ankylosaur systematics: examples using *Panoplosaurus* and *Edmontonia* (Ankylosauria: Nodosauridae); Pp. 281–298 *in* Carpenter, K., and P. J. Currie (eds.), Dinosaur Systematics: Approaches and Perspectives. Cambridge University Press, Cambridge, U.K.

Carpenter, K. 2001. Phylogenetic analysis of the Ankylosauria. Pp.455–483 *in* K. Carpenter (ed.), The Armored Dinosaurs. Indiana University Press, Bloomington and Indianapolis, Indiana.

Carpenter, K. 2004. Redescription of *Ankylosaurus magniventris* Brown 1908 (Ankylosauridae) from the Upper Cretaceous of the Western Interior of North America. Canadian Journal of Earth Sciences 41:961–986.

Carpenter, K. 2012. Ankylosaurs. Pp. 505-526 *in* Brett-Surman, M. K., T. R. Holtz Jr., and J. O. Farlow (eds.). The Complete Dinosaur. Second Edition. Indiana University Press: Bloomington.

Carpenter, K., and B. Breithaupt. 1996. Latest Cretaceous occurrence of nodosaurid ankylosaurs. Journal of Vertebrate Paleontology 6:251–257.

Carpenter, K., C. Miles, and K. Cloward, 1998. Skull of a Jurassic ankylosaur Dinosauria). Nature 393:782–783.

Carpenter, K., D. W., Dilkes, and D. P. Weishampel, 1995. The dinosaurs of the Niobrara Chalk Formation (Upper Cretaceous, Kansas). Journal of Vertebrate Paleontology 15:275–297.

Carpenter, K., Dilkes, D., and Weishampel, D. B. 1995. The dinosaurs of the Niobrara Chalk Formation (Upper Cretaceous, Kansas). Journal of Vertebrate Paleontology 15:275–297.

Carpenter, K., J. I., Kirkland, D. L. Burge, and J. Bird, 2001. Disarticulated skull of a new primitive ankylosaurid from the Lower Cretaceous of eastern Utah. Pp. 211–238 *in* Carpenter, K. (ed.), The Armored Dinosaurs. Indiana University Press, Bloomington.

Carpenter, K., J. Bartlett, J. Bird, and R. Barrick, 2008. Ankylosaurs from the Price River Quarries, Cedar Mountain Formation (Lower Cretaceous), east-central Utah. Journal of Vertebrate Paleontology 28:1089–1101.

Carpenter, K., T. DiCroce, B. Kinneer, and R. Simon R. 2013. Pelvis of *Gargoyleosaurus* (Dinosauria: Ankylosauria) and the origin and evolution of the ankylosaur pelvis. PLoS ONE 8(11): e79887. doi:10.1371/journal.pone.0079887.

Carpenter, K; S. Hayashi, Y. Kobayashi, T. Maryańska, R. Barsbold, K. Sato, and I. Obata. 2011. *Saichania chulsanensis* (Ornithischia, Ankylosauridae) from the Upper Cretaceous of Mongolia. Palaeontographica Abteilung A Band 294 Lieferung 1-3 (2011):1–61.

Castanet, J., A. Grandin, A. Abourachid, and A. de Ricqlès. 1996. Expression de la dynamique de croissance dans la structure de l'os périostique chez *Anas plathyrhynchos*. Comptes Rendus de l'Académie des sciences—Series III—Sciences de la Vie 319:301–308.

Castanet, J., H. Francillon-Vieillot, P. J. Meunier, and A. de Ricqlès. 1993. Bone and individual aging. Pp. 245–283 *in* Hall, B.K., (ed.). Bone. London: CRC Press.

Castanet, J., S. Croci, F. Aujard, M. Perret, J. Cubo, and E. de Margerie. 2004. Lines of arrested growth in bone and age estimation in a small primate: *Microcebus murinus*. Journal of Zoology 263:31–39.

Chakravarti, D. K. 1934. On a stegosaurian humerus from the Lameta beds of Jubbulpore. Quarterly Journal of the Geological, Mining and Metallurgical Society of India 6:75–79.

Chinsamy, A. 1990. Physiological implications of the bone histology of *Syntarsus rhodesiensis* (Saurischia: Theropoda) Paleontologica Africana 27:77–82.

Chinsamy, A. 1993. Bone histology and growth trajectory of the prosauropod dinosaur *Massospondylus carinatus* Owen. Modern Geology 18:319–321.

Chinsamy-Turan, A. 2005. The Microstructure of Dinosaur Bone. The Johns Hopkins University Press, Baltimore. 216 p.

Colbert, E. H. 1981. A primitive ornithischian dinosaur from the Kayenta Formation of Northern Arizona. Museum of Northern Arizona Press Bulletin 53:1–61.

Coombs W. P., Jr. 1979. Osteology and myology of the hindlimb in the Ankylosauria (Reptilia, Ornithischia). Journal of Paleontology 53:666–684.

Coombs W. P., Jr. 1990. Teeth and taxonomy in ankylosaurs. Pp. 269–279 *in* Carpenter, K., and P.J. Currie (eds.). Dinosaur Systematics: Perspectives and Approaches. Cambridge: Cambridge University Press.

Coombs, W. P., Jr. 1971. The Ankylosauria. Ph.D. dissertation, Columbia University, New York, 487 pp.

Coombs, W. P., Jr. 1978a. The families of the ornithischian dinosaur order Ankylosauria. Palaeontology 21:143–170.

Coombs, W. P., Jr. 1978b. Forelimb muscles of the Ankylosauria (Reptilia, Ornithischia). Journal of Paleontology 52:642–657.

Coombs, W. P., Jr. 1978c. An endocranial cast of *Euoplocephalus* (Reptilia, Ornithischia). Palaeontographica Abteilung A 161:176–182.

Coombs, W. P., Jr. 1995. A new nodosaurid ankylosaur (Dinosauria: Ornithischia) from the Lower Cretaceous of Texas. Journal of Vertebrate Paleontology 15:298–312.

Cope, E. D. 1876. Description of some new vertebrate remains from the Fort Union beds of Montana. Proceedings of the Academy of Natural Sciences of Philadelphia 28:248–261.

Currie, P. J. 1985. Cranial anatomy of *Stenonychosaurus inequalis* (Saurischia, Theropoda) and its bearing on the origin of birds. Canadian Journal of Earth Sciences 22:1643–1658.

Currie, P. J. 1997. Braincase anatomy. pp. 81–85 *in* Encyclopedia of Dinosaurs. Currie, P. J., and K. Padian (eds.). San Diego: Academic Press.

Currie, P. J. 2003. Cranial anatomy of tyrannosaurid dinosaurs from the Late Cretaceous of Alberta, Canada. Acta Palaeontolia Polonica 48:191–226.

Currie, P. J., and E. B. Koppelhus, eds. 2005. Dinosaur Provincial Park: A Spectacular Ancient Ecosystem Revealed. Indiana University Press, Bloomington, 648 p..

Currie, P. J., D. Badamgarav, E. B. Koppelhus, R. Sissons, and M. K. Vickaryous. 2011. Hands, feet, and behaviour in *Pinacosaurus* (Dinosauria: Ankylosauridae). Acta Palaeontologica Polonica 56:489–504.

Curry, K. A. 1999. Ontogenetic histology of *Apatosaurus* (Dinosauria: Sauropoda): new insights on growth rates and longevity. Journal of Vertebrate Paleontology 19:654–665.

Dashzeveg, D., L. Dingus, D. B. Loope, C. C. Swisher, III, T. Dulam, and M. R. Sweeney. 2005. New stratigraphic subdivision, depositional environment, and age estimate for the Upper Cretaceous Djadokhta Formation, southern Ulan Nur Basin, Mongolia. American Museum Novitates 3498:1–31.

Delair, J. B. 1982. Notes on an armoured dinosaur from Barnes High, Isle of Wight. Proceedings of the Isle of Wight Natural History and Archaeological Society 7:297–302.

DiCroce, T., K. Carpenter, and B. Kinneer. 2005. Reconstruction of the pelvic and hind limb musculature in the ankylosaur *Gastonia.* Journal of Vertebrate Paleontology 25 (suppl. to 3):51A.

Dong, Z. –M. 1993. An ankylosaur (ornithischian dinosaur) from the Middle Jurassic of the Junggar Basin, China. Vertebrata PalAsiatica 31:257–266.

Dong, Z. –M. 2002. A new armored dinosaur (Ankylosauria) from Beipiao Basin, Liaoning Province, northeastern China. Vertebrata PalAsiatica 40:276–285.

Eaton, T. H., Jr. 1960. A new armored dinosaur from the Cretaceous of Kansas. The University of Kansas Paleontological Contributions 8:1–24.

Eberth, D. A. 2005. The geology. Pp. 54–82 *in* Currie, P. J., and E. B. Koppelhus (eds.). Dinosaur Provincial Park: A Spectacular Ancient Ecosystem Revealed. Indiana University Press, Bloomington.

Eberth, D. A., and M. A. Getty. 2005. Ceratopsian bonebeds: Occurrence, origins, and significance. Pp. 501–536 *in* Currie, P. J., and E. B. Koppelhus (eds.). Dinosaur Provincial Park: A Spectacular Ancient Ecosystem Revealed. Indiana University Press, Bloomington.

Edinger, T. 1929. Die fossilen Gehirne. Erg Anat Entw Gesch 28:1–249.

Erickson, G. M., and T. A. Tumanova. 2000. Growth curve of *Psittacosaurus mongoliensis* Osborn (Ceratopsia: Psittacosauridae) inferred from long bone histology. Zoological Journal of the Linnean Society 130:551–566.

Erickson, G. M., P. J. Makovicky, P. J. Currie, M. A. Norell, S. A. Yerby, and C. A. Brochu. 2004. Gigantism and comparative life-history parameters of tyrannosaurid dinosaurs. Nature, 430:772–775.

Evans, D. C. 2006. Nasal cavity homologies and cranial crest function in lambeosaurine dinosaurs. Paleobiology 32:109–125.

Evans, D. C. 2010. Cranial anatomy and systematics of *Hypacrosaurus altispinus*, and a comparative analysis of skull growth in lambeosaurine hadrosaurids (Dinosauria: Ornithischia). Zoological Journal of the Linnaean Society of London 159:398–434.

Evans, D. C., R. Ridgely, and L. M. Witmer. 2009. Endocranial anatomy of lambeosaurine hadrosaurids (Dinosauria: Ornithischia): a sensorineural perspective on cranial crest function. Anatomical Record 292:1315–1337.

Fastovsky, D. E, and M. Watabe. 2000. Sedimentary environment of Alag Teg (Djadochta Age), central Gobi, Mongolia. Hayashibara Museum of Natural Sciences Research Bulletin 1:137.

Fastovsky, D. E. 2000. Short summary of the geology of some selected dinosaur-bearing localities in the western Gobi Desert, Mongolia. Hayashibara Museum of Natural Sciences Research Bulletin 1:132–133.

Ford, T. L. 2000. A review of ankylosaur osteoderms from New Mexico and a preliminary review of ankylosaur armor. Dinosaurs of New Mexico. New Mexico Museum of Natural History and Science Bulletin 17:157–176.

Ford, T. L. 2003. A new look at the armor of *Ankylosaurus*, just how did it look? Pp. 48–68 *in* The Mesozoic in Wyoming, Tate 2002, Casper. The Geological Museum, Casper College, Casper, Wyoming.

Ford, T. L., and J. I. Kirkland, 2001. Carlsbad ankylosaur (Ornithischia, Ankylosauria): an ankylosaurid and not a nodosaurid. Pp.239–260 *in* K. Carpenter, K. (ed.), The Armored Dinosaurs. Indiana University Press, Bloomington and Indianapolis, Indiana.

Frylestam, B., and T. von Schantz. 1977. Age determination of European hares based on periosteal growth lines. Mammal Review 7:151–154.

Galton, P. M. 1989. Crania and endocranial casts from ornithopod dinosaurs of the families Dryosauridae and Hypsilophodontidae (Reptilia: Ornithischia). Geologica et Palaeontologica 23:217–239.

Galton, P. M. 1980. Partial skeleton of *Dracopelta zbyszewskii* n. gen. and n. sp., an ankylosaurian dinosaur from the Upper Jurassic of Portugal. Géobios 13:451–457.

Gangloff, R. A. 1995. *Edmontonia* sp., the first record of an ankylosaur from Alaska. Journal of Vertebrate Paleontology 15:195–200.

Garcia, G., and X. Pereda-Suberbiola, 2003. A new species of *Struthiosaurus* (Dinosauria: Ankylosauria) from the Upper Cretaceous of Villeveyrac (southern France). Journal of Vertebrate Paleontology 23:156–165.

Gilmore, C. W. 1914. Osteology of the armored Dinosauria in the United States National museum: with special reference to the genus *Stegosaurus*. Bulletin (United States National Museum) 89:1–143.

Gilmore, C. W. 1933. Two new dinosaurian reptiles from Mongolia with notes on some fragmentary specimens. American Museum Novitates 679:1–20.

Gilmore, C. W. 1930. On dinosaurian reptiles from the Two Medicine Formation of Montana. Proceedings of the United States National Museum 77:1–39.

Godefroit, P., X. P. Suberbiola, H. Li, and Z. –M. Dong. 1999. A new species of the ankylosaurid dinosaur *Pinacosaurus* from the Late Cretaceous of Inner Mongolia (P.R. China). Bulletin - Institut royal des sciences naturelles de Belgique. Sciences de la terre 69(Supplement):17–36.

Hammer, Ø., D. A. T. Harper, and P. D. Ryan. 2001. PAST: Paleontological Statistics software package for education and data analysis. Palaetonologia Electronica 4.

Hart, D. R. 1982. Growth of painted turtles, *Chrysemys picta,* in Manitoba and Louisiana. The Canadian Field-Naturalist 96:127–130.

Hatcher, J. B, O. C. Marsh, and R. S. Lull. 1907 The Ceratopsia. US Geological Survey Monograph 49:1–198.

Hayakawa, H., M. Manabe, and K. Carpenter. 2005. Nodosaurid ankylosaur from the Cenomanian of Japan. Journal of Vertebrate Paleontology 25:240–245.

Hayashi, S., K. Carpenter, and D. Suzuki. 2009. Different growth patterns between the skeleton and osteoderms of Stegosaurus (Ornithischia: Thyreophora). Journal of Vertebrate Paleontology 29:123–131.

Hayashi, S., K. Carpenter, T. M. Scheyer, M. Watabe, and D. Suzuki. 2010. Function and evolution of ankylosaur dermal armor. Acta Palaeontologica Polonica 55:213–228.

Hayashi, S., M. E. Burns, M. Watabe, and K. Carpenter. 2012. Different developmental patterns between ankylosaur and stegosaur osteoderms: implications for the behavior variations among thyreophoran dinosaurs. Centenary Meeting of the Paläontologische Gesellschaft.

Henning, E. 1915. Stegosauria: Fossilium Catalogus I, Animalia pars 9:1–16.

Henning, E. 1924. *Kentrurosaurus aethiopicus* die Stegosaurier-Funde vom Tendaguru, Deutsch-Ostafrika. Palaeontographica, supplement 7:103–253.

Hill, R. V., L. M. Witmer, and M. A. Norell. 2003. A new specimen of *Pinacosaurus grangeri* (Dinosauria: Ornithischia) from the Late Cretaceous of Mongolia: ontogeny and phylogeny of ankylosaurs. American Museum Novitates 3395:1–29.

Hopson, J.A. 1979. Paleoneurology. Pp. 39–146 *in* Biology of the Reptilia, Vol. 9. Gans C, R. G. Northcutt, and P. Ulinski (eds). New York: Academic Press.

Horner, J. R., A. de Ricqlès, and K. Padian. 2000. Long bone histology of the hadrosaurid dinosaur *Maiasaura peeblesorum*: growth dynamics and physiology based on an ontogenetic series of skeletal elements. Journal of Vertebrate Paleontology, 20:115–129.

Horner, J. R., A. de Ricqlès, K. Padian, and R. D. Scheetz, R. D. 2009. Comparative long bone histology and growth of the “hypsilophodontid” dinosaurs *Orodromeus*

makelai, *Dryosaurus altus*, and *Tenontosaurus tillettii* (Ornithischia: Euornithopoda). Journal of Vertebrate Paleontology 29:734–747.

Horner, J. R., and K. Padian. 2004. Age and growth dynamics of *Tyrannosaurus rex*. Proceedings of the Royal Society of London. Series B: Biological Sciences 271:1875–1880.

Horner, J. R., K. Padian, and A. de Ricqlès. 2001. Comparative osteohistology of some embryonic and perinatal archosaurs: developmental and behavioral implications for dinosaurs. Paleobiology 27:39–58.

Horner, J. R., K. Padian, and A.de Ricqlès. 1999. Osteohistology of some embryonic and perinatal archosaurs: phylogenetic and behavioral implications for dinosaurs. Journal of Vertebrate Paleontology, 19(3, suppl.):53A.

Hou, L. –H. 1977. A new primitive Pachycephalosauria from Anhui, China. Vertebrata PalAsiatica 15:198–202.

Huene, F. von. 1909. Skizze zu einer Systematik und Stammesgeschichte der Dinosaurier [Sketch of the systematics and origins of the dinosaurs]. Centralblatt für Mineralogie, Geologie und Paläontologie. 1909:12–22.

Huene, F. von. 1914. Über die Zweistämmigkeit der Dinosaurier, mit Beträgen zur Kenntnis einiger Schädel. Neues Jahrbuch für Mineralogie, Geologie und Paläontologie 37:577–589.

Huene, F. von. 1948. Short review of lower tetrapods. Royal Society of South Africa, Special Publication (Robert Broom Commemorative Volume):65–106.

Huene, F. von. 1956. Paläontologie und Phylogenie der Niederen Tetrapoden [Paleontology and Phylogeny of the Lower Tetrapods]. VEB Gustav Fischer Verlang, Jena:1–716.

Hulke, J. W. 1881. *Polacanthus foxi*, a large undescribed dinosaur from the Wealden Formation in the Isle of Wight. Philosophical Transactions of the Royal Society of London 172:653–662.

Hunt, A. P., and S. G. Lucas. 1992. Stratigraphy, paleontology, and age of the Fruitland and Kirtland Formations (Upper Cretaceous) San Juan Basin, New Mexico. New Mexico Geological Society Guidebook 43:217–239.

Huttenlocker, H. K., H. N. Woodward, and B. K. Hall. 2013. The biology of bone. Pp. 13-34 *in* Padian, K., and E.-T. Lamm (eds.). Bone Histology of Fossil Tetrapods. Berkeley, University of California Press.

Hutton, J. M. 1986. Age determination of living Nile crocodiles from the cortical stratification of bone. Copeia 2:332–341.

Huxley, T. H. 1867. On *Acanthopholis horridus*, a new reptile from the Chalk Marl. Geological Magazine 4:65–67.

Kirkland, J. I. 1998. A polacanthine ankylosaur (Ornithischia: Dinosauria) from the Early Cretaceous (Barremian) of eastern Utah. New Mexico Museum of Natural History and Science Bulletin 14:271–281.

Kirkland, J. I., and K. Carpenter. 1994. North America's first pre-Cretaceous ankylosaur (Dinosauria) from the Upper Jurassic Morrison Formation of western Colorado. Brigham Young University Geology Studies 40:25–42.

Kirkland, J. I., and S. K. Madsen. 2007. The Lower Cretaceous Cedar Mountain Formation, eastern Utah: the view up an always interesting learning curve: Utah Geological Association, Publication 35 (Field trip guide for 2007 Geological Society of America, Rocky Mountain Section, Annual Meeting, St. George, Utah, May 4–6, 2007.):1–108.

Kirkland, J. I., L. Alcalá, M. A. Loewen, E. Espílez, L. Mampel, and J. P. Wiersma, 2013. The Basal Nodosaurid Ankylosaur *Europelta carbonensis* n. gen., n. sp. From the Lower Cretaceous (Lower Albian) Escucha Formation of Northeastern Spain. PLoS ONE 8: e80405.

Klein, N., T. Scheyer, and T. Tütken. 2009. Skeletochronology and isotopic analysis of a captive individual of *Alligator mississippiensis* Daudin, 1802. Fossil Record 12:121–131.

Klevezal, G. A. 1996. Recording Structures of Mammals: Determination of Age and Reconstruction of Life History. A. A. Balkema Publishers, Brookfield, 274 pp.

Köhler, M., N. Marin-Moratalla, X. Jordana, and R. Aanes. 2012. Seasonal bone growth and physiology in endotherms shed light on dinosaur physiology. Nature 487:358–61.

Kurzanov, S. M, and T. A. Tumanova. 1978. [On the structure on the endocranium in some ankylosaurs from Mongolia]. Paleontogicheskii Zhurnal. 1978:90–96.

Lambe, L. M. 1902. New genera and species from the Belly River Series (mid-Cretaceous). Geological Survey of Canada Contributions to Canadian Palaeontology 3:25–81.

Lambe, L. M. 1902. On Vertebrata of the mid-Cretaceous of the Northwest Territory. 2. New genera and species from the Belly River Series (mid-Cretaceous). Contributions to Canadian Paleontology 3:25–81.

Lambe, L. M. 1910. Note on the parietal crest of *Centrosaurus apertus*, and a proposed new generic name for *Stereocephalus tutus*. The Ottawa Naturalist 14:149–151.

Lambe, L. M. 1919. Description of a new genus and species (*Panoplosaurus mirus*) of armored dinosaur from the Belly River Beds of Alberta. Transactions of the Royal Society of Canada, series 3, 13:39–50.

Lambe, L. M. 1920. The hadrosaur *Edmontosaurus* from the Upper Cretaceous of Alberta. Department of Mines, Geological Survey of Canada, Memoir 120:1–79.

Langston, W. 1960. The vertebrate fauna of the Selma Formation of Alabama. VI. The dinosaurs. Fieldiana Geological Memoirs 3:313–361.

Lapparent, F., de, and R. Lavocat. 1955. Dinosauriens. Pp. 783–962 *in* Piveteau, J. (ed.). Traite de Paleontologie. Paris.

Larsson, H. C. E. 2001. The endocranial anatomy of *Carcharodontosaurus saharicus* (Theropoda: Allosauroidea) and its implications for theropod brain evolution. pp. 19–33 *in* Mesozoic Vertebrate Life. Tanke D, and K. Carpenter. (eds.). Bloomington: Indiana University Press.

Lauters, P., M. Vercauteren, Y. L. Bolotsky, and P. Godefroit. 2013. Cranial Endocast of the lambeosaurine hadrosaurid *Amurosaurus riabinini* from the Amur Region, Russia. PLoS ONE 8: 1–7 (e78899).

Lee, A. H., and S. Werning. 2008. Sexual maturity in growing dinosaurs does not fit reptilian growth models. Proceedings of the National Academy of Sciences 105:582–587.

Lee, Y. –N. 1996. A new nodosaurid ankylosaur (Dinosauria: Ornithschia) from the Paw Paw Formation (late Albian) of Texas. Journal of Vertebrate Paleontology 16:232–245.

Leidy, J. 1856. Notice of the remains of extinct reptiles and fishes discovered by Dr. F. V. Hayden in the Badlands of the Judith River, Nebraska Territory. Proceedings of the Academy of Natural Sciences of Philadelphia 8:72.

Li, X., J. Lü, X. Zhang, S. Jia, W. Hu, J. Zhang, Y. Wu and Q. Ji. 2007. [A new nodosaurid dinosaur fossil from the Cretaceous Period of Ruyang, Henan]. Acta Geologica Sinica 81:433–438.

Lü J., Q. Ji, Y. Gao, and Z. Li. 2007. A new species of the ankylosaurid dinosaur *Crichtonsaurus* (Ankylosauridae:Ankylosauria) from the Cretaceous of Liaoning Province, China. Acta Geologica Sinica (English edition) 81:883–897.

Lü J., X. Jin, Y. Sheng, and Y. Li. 2007. New nodosaurid dinosaur from the Late Cretaceous of Lishui, Zhejiang Province, China. Acta Geologica Sinica (English edition) 81:344–350.

Lucas, F. A. 1901. A new dinosaur, *Stegosaurus marshi*, from the Lower Cretaceous of South Dakota. Proceedings of the United States National Museum 23:591–592.

Lucas, F. A. 1902. Paleontological notes. The generic name *Omosaurus*. A new generic name for *Stegosaurus marshi*. Science, new series 16:435.

Lydekker, R. 1893. On the jaw of a new carnivorous dinosaur from the Oxford Clay of Peterborough. Quarterly Journal of the Geological Society of London 49:284–287.

Main, R. P., A. de Ricqles, J. R. Horner, and K. Padian. 2005. The evolution and function of thyreophoran dinosaur scutes; implications for plate function in stegosaurs Paleobiology 31:291–314.

Maleev, E. A. 1954. Pantsyrnye dinosavry verchnego mela Mongolii (Semeustvo Syrmosauridae). Trudy Paleontologicheskogo Instituta Akademiy Nauk SSSR 48:142–170.

Maleev, E. A. 1952a. Noviy ankilosavr is verchnego mela Mongolii [A new ankylosaur from the Upper Cretaceous of Mongolia]. Doklady Akademii Nauk SSSR 87:273–276.

Maleev, E. A. 1952b. Novoe semeystvo pantsirnich dinosavrov is verchnego mela Mongolii [A new family of armored dinosaurs from the Upper Cretaceous of Mongolia]. Doklady Akademii Nauk SSSR 87:131–134.

Maleev, E. A. 1956. [Armored dinosaurs from the Upper Cretaceous of Mongolia]. Trudy Paleontologicheskogo Instituta Akademiy Nauk USSR 6+2:51–91. (In Russian.)

Mallon, J. C, D. C. Evans, M. J. Ryan, and J. S. Anderson. 2013. Feeding height stratification among the herbivorous dinosaurs from the Dinosaur Park Formation (upper Campanian) of Alberta, Canada. BMC Ecology 13:14.

Mantell, G. A. 1833. Geology of the South-East of England. Longman, Rees, Orme, Brown, Green, & Longman, London. 415 pp.

Mantell, G. A. 1844. Medals of creation; or first lessons in geology and in the study of organic remains. H. G. Bohn, London, 930 pp.

Mantell, G. A. 1848. On the structure of the jaws and teeth of the *Iguanodon.* Philosophical Transactions of the Royal Society of London 1848:183–202.

Marangoni, F., E. Schaefer, R. Cajade, and M. Tejedo. 2009. Growth-mark formation and chronology of two neotropical anuran species. Journal of Herpetology 43:546–550.

Marsh, O. C. 1888. Notice of a new genus of Sauropoda and other new dinosaurs from the Potomac Formation. American Journal of Science 35:89–94.

Marsh, O. C. 1889. Notice of gigantic horned dinosauria from the Cretaceous. American Journal of Science 38:173–175.

Marsh, O. C. 1890. Additional characters of the Ceratopsidae, with notice of new Cretaceous dinosaurs. American Journal of Science 39:418–426.

Marsh, O. C. 1892. Notes on Mesozoic vertebrate fossils. American Journal of Science 44:170–176.

Maryańska, T. 1977. Ankylosauridae (Dinosauria) from Mongolia. Palaeontologia Polonica 37:85–151.

Matley, C. A. 1923. Note on an armoured dinosaur from the Lameta Beds of Jubbulpore. Records of the Geological Survey of India 55:105–109.

Matthew, W. D. 1922. A super-dreadnaught of the animal world, the armored dinosaur *Paleoscincus*. Natural History 22:333–342.

Mehl, M. G. 1936. *Hierosaurus coleii*; a new aquatic dinosaur from the Niobrara Cretaceous of Kansas. Denison University Bulletin, Journal of the Scientific Laboratory 31:1–20.

Miles, C. A., and C. J. Miles. 2009. Skull of *Minotaurasaurus ramachandrani*, a new Cretaceous ankylosaur from the Gobi Desert. Current Science 96:65–70.

Miyashita, T., V. M. Arbour, L. M. Witmer, and P. J. Currie. 2011. The internal cranial morphology of an armoured dinosaur *Euoplocephalus* corroborated by X-ray computed tomographic reconstruction. Journal of Anatomy 219:661–675.

Molnar, R. E. 1980. An ankylosaur (Ornithischia, Reptilia) from the Lower Cretaceous of southern Queensland. Memoirs of the Queensland Museum 20:77–87.

Molnar, R. E., and H. T. Clifford. 2000. Gut contents of a small ankylosaur. Journal of Vertebrate Paleontology 20:194–196.

Nopsca, F. B., von. 1902a. Notizen uber Cretacische Dinosaurier [Notes on Cretaceous dinosaurs]. Sitzungsberichte der Mathematisch-Naturwissenschaftlichen Classe der Kaiserlichen Akademie der Wissenschaften 111:93–114.

Nopsca, F. B., von. 1902b. Dinosaurierreste aus Siebenburgen. II. Schadelreste von Mochlodon.

Nopsca, F. B., von. 1915. Die dinosaurier der Siebenbürgischen landesteile Ungarns [Dinosaurs of the Siebenberger regions of Hungary]. Mitteilungen aus dem Jahrbuche der Kgl. Ungarischen Geologischen Reichsanstalt 23:1–24.

Nopsca, F. B., von. 1918. *Leipsanosaurus* n. gen. in neuer thyreophore aus der Gosau [*Leipsanosaurus* n. gen. a new thyreophoran from the Gosau]. Földtani Közlöny 48:324–328.

Nopsca, F. B., von. 1923. Die Familien der Reptilien [The families of reptiles]. Forschritte der Geologie und Palaeontologie. Verlag von Gebrüder Borntraeger, Berlin 2:1–210.

Nopsca, F. B., von. 1928. Palaeontological notes on reptiles. V. On the skull of the Upper Cretaceous dinosaur *Euoplocephalus*. Geologica Hungarica, Series Palaeontologica 1:1–84.

Nopsca, F. B. von**.** 1929. Dinosaur remains from Siebenbürgen V. Geologica Hungarica, Series Palaeontologica 4:1–72. (In Hungarian)

Norman, D. B. 1986. On the anatomy of Iguanodon atherfieldensis (Ornithischia: Ornithopoda). Bulletin Institut Royale d'Histoire Naturelle de Belgique 56:281–372.

Norman, D. B., and T. Faiers. 1996. On the first partial skull of an ankylosaurian dinosaur from the Lower Cretaceous of the Isle of Wight, southern England. Geological magazine 133:299–310.

Norman, D. B. 1985. The illustrated encyclopedia of dinosaurs. Salamander Books, London, 208 p.

Olshevsky, G. 1991. A revision of the parainfraclass Archosauria Cope, 1869, excluding the advanced Crocodylia. Mesozoic Meanderings 2:1–196.

Osborn, H. F. 1923. Two Lower Cretaceous dinosaurs of Mongolia. American Museum Novitates 95:1-10.

Ősi, A. 2005. *Hungarosaurus tormai*, a new ankylosaur (Dinosauria) from the Upper Cretaceous of Hungary. Journal of Vertebrate Paleontology 25:370–383.

Ősi, A., P. M. Barrett, T. Földes, and R. Tokai. 2014. Wear pattern, dental function, and jaw mechanism in the Late Cretaceous ankylosaur *Hungarosaurus*. The Anatomical Record: 297:1165–1180.

Ostrom, J. H. 1970. Stratigraphy and paleontology of the Cloverly Formation (Lower Cretaceous) of the Bighorn Basin area, Wyoming and Montana. Peabody Museum Bulletin 35:1–234.

Ostrom, J. H., and J. McIntosh. 1966. Marsh's dinosaurs: the collections from Como Bluff. Yale University Press, New Haven, 416 p.

Owen, R. 1842. Report on British fossil reptiles, part II. Report of the British Association for the Advancement of Science 11:60–204.

Owen, R. 1865. A monograph of the fossil Reptilia of the Liassic formations. Part I, Sauropterygia. Palaeontographical Society Monographs 17:1–40.

Padian, K. Why study the bone microstructure of fossil tetrapods?. Pp. 1-12 *in* Padian, K., and E.-T. Lamm (eds.). Bone Histology of Fossil Tetrapods. Berkeley, University of California Press.

Padian, K., and J. R. Horner. 2011. The evolution of 'bizarre structures' in dinosaurs: biomechanics, sexual selection, social selection or species recognition?. Journal of Zoology 283:3–17.

Padian, K., J. R. Horner, and A. de Ricqlès. 2004. Growth in small dinosaurs and pterosaurs: the evolution of archosaurian growth strategies. Journal of Vertebrate Paleontology 24:555–571.

Pang, Q., and Z. Cheng, 1998. A new ankylosaur of Late Cretaceous from Tianzhen, Shanxi. Progress in Natural Science 8:326–334.

Parish, J. C., and P. M. Barrett. 2004. A reappraisal of the ornithischian dinosaur *Amtosaurus magnus* Kurzanov and Tumanova 1978, with comments on the status of *A. archibaldi* Averianov 2002. Canadian Journal of Earth Sciences 41:299–306.

Parks, W. A. 1924. *Dyoplosaurus acutosquameus*, a new genus and species of armoured dinosaur; and notes on a skeleton of *Prosaurolophus maximus*. University of Toronto Studies, Geological Series 18:1–35.

Parsons, W. L., and K. M. Parsons, 2009. A new ankylosaur (Dinosauria: Ankylosauria) from the Lower Cretaceous Cloverly Formation of central Montana. Canadian Journal of Earth Sciences 46:721–738.

Paulina Carabajal, A., and J. I. Canale. 2010. Cranial endocast of the carcharodontosaurid theropod *Giganotosaurus carolinii* Coria & Salgado, 1995. Neues Jahrbuch für Geologie und Paläontologie-Abhandlungen 258:249–256.

Peabody, F. E. 1961. Annual growth zones in living and fossil vertebrates. Journal of Morphology 108:11–62.

Penkalski, P. 2014. A new ankylosaurid from the late Cretaceous Two Medicine Formation of Montana, USA. Acta Palaeontologica Polonica 59:617–634.

Penkalski, P. 2001. Variation in specimens referred to *Euoplocephalus tutus*. Pp. 363–385 *in* Carpenter, K (ed.), The Armored Dinosaurs, Indiana University Press, Bloomington.

Penkalski, P., and W. T. Blows. 2013. *Scolosaurus cutleri* (Ornithischia: Ankylosauria) from the Upper Cretaceous Dinosaur Park Formation of Alberta, Canada. Canadian Journal of Earth Sciences 50:171–182.

Ricqlés, A. de. 1980. Tissue structures of dinosaur bone: functional significance and possible relation to dinosaur physiology. *In* A Cold Look at the Warm-Blooded Dinosaurs. AAAS Selected Symposium 28.

Rozhdestvensky, A. K. 1965. [Growth changes in Asian dinosaurs and some problems of their taxonomy]. Paleontologicheskii Zhurnal 1965:95–109. (In Russian)

Russell, L. S. 1940. *Edmontonia rugosidens* (Gilmore), an armored dinosaur from the Belly River Series of Alberta. University of Toronto Studies, Geology Series 43:3–27.

Ryan, M. J., and D. C. Evans. 2005. Ornithischian dinosaurs. PP. 312–348 *in* Currie, P. J., and E. B. Koppelhus (eds.). Dinosaur Provincial Park: A Spectacular Ancient Ecosystem Revealed. Indiana University Press, Bloomington.

Rybczynski, N, and M. K. Vickaryous. 2001. Evidence of complex jaw movement in the Late Cretaceous ankylosaurid *Euoplocephalus tutus* (Dinosauria: Thyreophora). Pp. 299–317 *in* Carpenter, K., (ed.). The Armored Dinosaurs. Bloomington, Indiana University Press.

Salgado, L., and Z. Gasparini. 2006. Reappraisal of an ankylosaurian dinosaur from the Upper Cretaceous of James Ross Island (Antarctica). Geodiversitas 28:119–135.

Sampson, S. D., and L. D. Witmer. 2007. Craniofacial anatomy of *Majungasaurus crenatissimus* (Theropoda: Abelisauridae) from the Late Cretaceous of Madagascar. Society of Vertebrate Paleontology Memoir 8:32–102.

Sander, P. M., and C. Tückmantel. 2003 Bone lamina thickness, bone apposition rates, and age estimates in sauropod humeri and femora. Paläontologische Zeitschrift, 77:161–172.

Sander, P.M. 2000. Longbone histology of the Tendaguru sauropods: implications for growth and biology. Paleobiology 26:466–488.

Sankey, J. 2010. Faunal composition and significance of high–diversity, mixed bonebeds containing *Agujaceratops mariscalensis* and other dinosaurs, Aguja Formation (Upper Cretaceous), Big Bend, Texas. In New Perspectives on Horned Dinosaurs: The Royal Tyrrell Museum Ceratopsian Symposium:520–537.

Scheyer, T. M., and P. M. Sander. 2004. Histology of ankylosaur osteoderms: implications for systematics and function. Journal of Vertebrate Paleontology 24:874–893.

Schweitzer, M. H., R. M. Elsey, C. G. Dacke, J. R. Horner, and E. –T. Lamm, 2007. Do egg-laying crocodilian (*Alligator mississippiensis*) archosaurs form medullary bone?. Bone 40:1152–1158.

Seeley, H. G. 1869. Index to the Fossil Remains of Aves, Ornithosauria, and Reptilia, from the Secondary System of Strata, Arranged in the Woodwardian Museum of the University of Cambridge. Deighton, Bell, and Co, Cambridge:1–143.

Seeley, H. G. 1875. On the maxillary bone of a new dinosaur (*Priodontognathus phillipsii*), contained in the Woodwardian Museum of the University of Cambridge. Quarterly Journal of the Geological Society of London 31:439–443.

Seeley, H. G. 1879. On the Dinosauria of the Cambridge Greensand. Quarterly Journal of the Geological Society of London 35:591–636.

Seeley, H. G. 1881. The reptile fauna of the Gosau Formation preserved in the Geological Museum of the University of Vienna. Quarterly Journal of the Geological Society of London 37:620–707.

Seeley, H. G. 1887. On the classification of the fossil animals commonly named Dinosauria. Proceedings of the Royal Society of London 43:165–171.

Sereno, P. C., J. A. Wilson, L. M. Witmer, J. A.Whitlock, A. Maga, O. Ide, and T. A. Rowe. 2007. Structural extremes in a Cretaceous dinosaur. PLoS ONE 2:1–9 (e1230).

Sereno, P. C. 1999. The evolution of dinosaurs. Science 5423:2137–2147.

Sereno, P. C. 1986. Phylogeny of the bird-hipped dinosaurs (Order Ornithischia).National Geographic Research 2:234–256.

Snover, M. L., and A. A. Hohn. 2004. Validation and interpretation of annual skeletal marks in loggerhead (*Caretta caretta*) and Kemp's ridley (*Lepidochelys kempii*) sea turtles. Fishery Bulletin 102:682–692.

Stanford, R., D. B. Wesihampel, and V. B. DeLeon, 2011. The first hatchling dinosaur reported from the eastern United States: *Propanoplosaurus marylandicus* (Dinosauria: Ankylosauria) from the Early Cretaceous of Maryland, U.S.A. Journal of Paleontology 85:916–924.

Stein, M., S. Hayashi, and P.M. Sander. 2013. Long bone histology and growth patterns in ankylosaurs: Implications for life history and evolution. PloS one 8: e68590.

Sternberg, C. H. 1915. Evidence proving that the Belly River beds of Alberta are equivalent with the Judith River beds of Montana. Science 42:131–133.

Sternberg, C. H. 1917. Five years' explorations in the fossil beds of Alberta. Transactions of the Kansas Academy of Science 28:205–211.

Sternberg, C. M. 1928. A new armored dinosaur from the Edmonton Formation of Alberta. Transactions of the Royal Society of Canada, series 3 22:93–106.

Sternberg, C. M. 1929. A toothless armoured dinosaur from the Upper Cretaceous of Alberta. Canada Department of Mines Geological Survey Bulletin (Geological Series) 54:28–33.

Sternberg, C. M. 1950. Steveville–West of the Fourth Meridian, Alberta. Geological Survey of Canada Topographic Map 969A. 1/31,680 scale (1 inch to ½ mile).

Sullivan, R. M. 1999. *Nodocephalosaurus kirtlandensis*, gen. et sp. nov., a new ankylosaurid dinosaur (Ornithischia: Ankylosauria) from the Upper Cretaceous Kirtland Formation (Upper Campanian) San Juan Basin, New Mexico. Journal of Vertebrate Paleontology 19:126–139.

Sullivan, R. M., and S. G. Lucas. 2006. The Kirtlandian land-vertebrate "age"—faunal composition, temporal position and biostratigraphic correlation in the nonmarine Upper Cretaceous of western North America. New Mexico Museum of Natural History and Science Bulletin 35:7–29.

Taquet, P. 1976. Geology and Paleontology of the Gadoufaoua Locality (Aptian of Niger). Cahiers de Paléontologie, Centre National de la Recherche Scientifique, Paris 1–191. (In French)

Tennyson, H. 1897. Alfred Lord Tennyson: A memoir, by his son, 1st ed. Mac-Millan and Company, London and New York.

Thompson, R. S., J. C. Parish, S. C. R. Maidment, and P. M. Barrett. 2012. Phylogeny of the ankylosaurian dinosaurs (Ornithischia: Thyreophora). Journal of Systematic Palaeontology 10:301–312.

Tucker, A. D. 1997. Validation of skeletochronology to determine age of freshwater crocodiles (Crocodylus johnstoni) Australian Journal of Marine and Freshwater Research 48:343–351.

Tumanova, T. A. 1977. New data about *Tarchia gigantea*. Paleontological Journal 4:92–100. (in Russian).

Tumanova, T. A. 1983. Pervyy ankilozavr iz nizhnego mela Mongolii [The first ankylosaurs from the Lower Cretaceous of Mongolia]. In Tatarinov, L. P., R. Barsbold, E. Vorobyeva, B. Luvsandanzan, B. A. Trofimov, Yu. A. Reshetov, & M. A. Shishkin (eds.), Iskopayemyye reptilii mongolii [Fossil Reptiles of Mongolia]. Trudy Sovmestnaya Sovetsko-Mongol'skaya Paleontologicheskaya Ekspeditsiya 24:110–118.

Tumanova, T. A. 1987 Armored Dinosaurs of Mongolia. Proceedings of Paleontological Institute, 80 pp.

Tumanova, T. A. 1993. A new armored dinosaur from southeastern Gobi. Paleontological Journal 27:119–125.

Tverdochlebov, V. P., and J. I. Zybin. 1974. Genesis of the Upper Cretaceous sediments with dinosaur remains at Tugrikin-us and Alag-Taag localities. Sovmestnaâ Sovetsko-Mongolskaâ Paleontologiceskaâ Ekspediciâ, Trudy 1:314–319. (In Russian)

Varricchio, D. J. 1993. Bone microstructure of the Upper Cretaceous theropod dinosaur *Troodon formosus*. Journal of Vertebrate Paleontology 13:99–104.

Vickaryous, M. K. 2006. New information on the cranial anatomy of *Edmontonia rugosidens* Gilmore, a Late Cretaceous nodosaurid dinosaur from Dinosaur Provincial Park, Alberta. Journal of Vertebrate Paleontology 26:1011–1013.

Vickaryous, M. K., A. P. Russell, P. J. Currie, and X. –J. Zhao. 2001. A new ankylosaurid (Dinosauria: Ankylosauria) from the Lower Cretaceous of China, with comments on ankylosaurian relationships. Canadian Journal of Earth Sciences 38:1767–1780.

Vickaryous, M. K., and A. P. Russell. 2003. A redescription of the skull of *Euoplocephalus tutus* (Archosauria: Ornithischia): a foundation for comparative and systematic studies of ankylosaurian dinosaurs. Zoological Journal of the Linnean Society 137:157–186.

Watabe, M., and S. Suzuki. 2000. Report on the Japan-Mongolia Joint Paleontological expedition to the Gobi desert, 1996. Hayashibara Museum of Natural Sciences Research Bulletin 1:58–68.

Wieland, G. R. 1909. A new armored saurian from the Niobrara. American Journal of Science 27:250–252.

Wieland, G. R. 1911. Notes on the armored Dinosauria. The American Journal of Science, series 4 31:112–124.

Wilkinson, M. 2001. *TAXEQ3.* Software and documentation London: The Department of Zoology, Natural History Museum.

Williston, S. W. 1905. A new armored dinosaur from the Upper Cretaceous of Wyoming. Science 22:503.

Witmer, L. M. 1995. Homology of facial structures in extant archosaurs (birds and crocodilians), with special reference to paranasal pneumaticity and nasal conchae. Journal of Morphology 225:269–327.

Witmer, L. M. 1997. The evolution of the antorbital cavity of archosaurs: a study in soft-tissue reconstruction in the fossil record with an analysis of the function of pneumaticity. Society of Vertebrate Paleontology Memoir 3:1–73.

Witmer, L. M., and R. C. Ridgely. 2008. The paranasal air sinuses of predatory and armored dinosaurs (Archosauria: Theropoda and Ankylosauria) and their contribution to cephalic structure. Anatomical Record 291:1362–1388.

Witmer, L. M., and R. C. Ridgely. 2009. New insights into the brain, braincase, and ear region of tyrannosaurs (Dinosauria, Theropoda), with implications for sensory organization and behavior. Anatomical Record 292:1266–1296.

Witmer, L. M., R. C. Ridgely, D. L. Dufeau, and M.C. Semones. 2008. Using CT to peer into the past: 3D visualization of the brain and ear regions of birds, crocodiles, and nonavian dinosaurs. Pp 67–87*in* Endo, H., and R Frey (eds.). Anatomical Imaging: Towards a New Morphology. Tokyo, Springer.

Woodward, H. N. 2005. Bone histology of the sauropod dinosaur *Alamosaurus sanjuanensis* from the Javelina Formation, Big Bend National Park, Texas. M.Sc. thesis, 225 p.

Woodward, H. N., J. R. Horner, and J. O. Farlow. 2014. Quantification of intraskeletal histovariability in *Alligator mississippiensis* and implications for vertebrate osteohistology. PeerJ 2:e422.

Xu, X., X. –L. Wang, and H. L. You. 2001. A juvenile ankylosaur from China. Naturwissenschaften 88:297–300.

Young, C. –C. 1935. On a new nodosaurid from Ninghsia. Palaeontologia Sinica, Series C 11:1–28.

Zug, G. R., A. H. Wynn, and C. Ruckdeschel. 1986. Age determination of loggerhead sea turtles, *Caretta caretta*, by incremental growth marks in the skeleton. Smithsonian Contributions to Zoology 427:1–34.

APPENDIX 1. Current classification of Ankylosauria including authorities, synonymies, and nomina dubia. Type taxa are indicated and currently valid species are in bold. For currently valid species, holotype information includes current specimen number, stratigraphic occurrence, and type locality. GPS coordinates are relative to the WGS84 datum. Estimated GPS coordinates (designated by "est.") have been calculated based on published locality information and may not correspond to exact type localities.

SUBORDER ANKYLOSAURIA Osborn, 1923

- = Ancylosauria Huene, 1914
- = Thyreophora Nopsca, 1915
- = Apraedentalia Huene, 1948
- = Apraedentalidae Huene, 1956
- FAMILY ANKYLOSAURIDAE Brown, 1908
    - = Ancylosauridae Huene, 1909
    - = Ankylosuauridae Nopsca, 1918
    - = Ankylosaurinae Nopsca, 1923
    - = Syrmosauridae Maleev, 1952
    - *Aletopelta* Ford and Kirkland, 2001
        - ***Aletopelta coombsi*** Ford and Kirkland, 2001, type species
        - SDNHM 33909; Late Cretaceous (late Campanian), Point Loma Formation, 11S 475390E 3667693N est. (SDNHM Locality 3392),

College Blvd. between El Camino Real and Palomar Airport Rd, NW of Palomar McClellan Airport, Carlsbad California.

- *Cedarpelta* Carpenter, Kirkland, Burge, and Bird, 2001
  - ***Cedarpelta bilbeyhallorum*** Carpenter, Kirkland, Burge, and Bird, 2001, type species
    - CEUM 12360; Early Cretaceous (Aptian-Albian boundary), Cedar Mountain Formation (base of Mussentuchit Member), CEM locality number EM 419, Carbon County, Utah, USA
- *Gobisaurus* Vickaryous, Russell, Currie, and Zhao, 2001
  - ***Gobisaurus domoculus*** Vickaryous, Russell, Currie, and Zhao, 2001, type species
    - IVPP V12563; Early Cretaceous (Aptian–?Albian), Ulanhushao (Suhongtu) Formation, 60 km N of Chilantai (Jilantai; 39 45 N, 105 45E), on the east side of Chilantai Salt Lake (Chilantaiyen Chih), Maortu, Alashan Desert, Nei Mongol Zizhique (Inner Mongolia), People's Republic of China
- *Liaoningosaurus*
  - ***Liaoningosaurus paradoxus*** Xu, Wang, and You, 2001, type species

- IVPP V12560; Early Cretaceous (Barremian), Yixian Formation, WangJiagou, Yixian, Liaoning Province, China People's Republic of China

- *Minmi* Molnar, 1980
  - ***Minmi paravertebra*** Molnar, 1980, type species
    - QM F10329; Early Cretaceous (Aptian) Bungil Formation, southeastern Queensland, Australia
- *Shamosaurus* Tumanova, 1983
  - ***Shamosaurus scutatus*** Tumanova, 1983, type species
    - PIN N 3779/2; Early Cretaceous (Aptian–Albian), Dzun Bayn Formation, Hühteeg Svita (Övörkhangai), Mongolia
- SUBFAMILY ANKYLOSAURINAE
  - *Ankylosaurus* Brown, 1908, type genus
    - = *Ancylosaurus* Huene, 1909
    - = *Anchylosaurus* Sternberg, 1917
    - ***Ankylosaurus magniventris*** Brown, 1908, type species
      - AMNH 5895; Late Cretaceous (late Maastrichtian), 61–67 m below the K–T boundary, Hell Creek Formation, 120 miles N of Miles City, upper end of Gilbert Creek, probably somewhere in Section (Sec.) 27 or 28, Township (T) 22N, Range (R) 40E, Garfield County, Montana, USA
  - *Anodontosaurus* Sternberg, 1929

- ***Anodontosaurus lambei*** Sternberg, 1929, type species
    - CMN 8530; Late Cretaceous (late Campanian), Horseshoe Canyon Formation (Horsethief Member), sec. 3 tp. 21 range 31 W. 4th prin. mer., Red Deer River, 8km SW of Morrin, Alberta, Canada

- *Chritonsaurus* Dong, 2002
    - ***Chrichtonsaurus benxiensis*** Lu, Ji, Gao, and Li, 2007
        - BXGMV0012; Late Cretaceous (Cenomanian–Turonian), Sunjiawan Formation, Beipiao, Liaoning Province, People's Republic of China
    - ***Chrichtonsaurus bohlini*** Dong, 2002, type species
        - IVPP V 12745; Late Cretaceous (Cenomanian–Turonian), Sunjiawan Formation, Liaoning, People's Republic of China

- *Dyoplosaurus* Parks, 1924
    - ***Dyoplosaurus acutosquameus*** Parks, 1924, type species
        - ROM 784; Late Cretaceous (late Campanian), lower Dinosaur Park Formation, Quarry Q002, 12U 466787E 5622422N est., Dinosaur Provincial Park, Alberta, Canada

- *Euoplocephalus* Lambe, 1910
    - = *Europlocephalus* Sternberg, 1915
    - = *Euplocephalus* Lambe, 1920

- = *Euplocephalus* (Hunt and Lucas, 1992)
- = *Euoploceplhalus* Hou, 1977
- = *Euoplosaurus* Nopsca, 1928
- = *Erroplocephalus* Nopsca, 1928
- = *Stereocpehalus* Lambe, 1902
- ***Euoplocephalus tutus*** Lambe, 1910, type species
    - CMN 2010; Late Cretaceous (late Campanian), lower Dinosaur Park Formation, ¾ mi SE of Steveville, Dinosaur Provincial Park, Alberta, Canada
    - = *Stereocephalus tutus* Lambe, 1902
    - = *Paleoscincus tutus* (Lambe, 1902)
    - = *Paleoscincus asper* Lambe, 1902

▪ *Maleevus* Tumanova, 1987

- = *Syrmosaurus* Maleev, 1952
- = *Talarurus* Maryańska, 1977 (partim)
- ***Maleevus disparoserratus*** Tumanova, 1987, type species
    - PIN 554/1; Late Cretaceous Batanshiree Svita, Shiregin Gashoon, eastern Gobi, Mongolia
    - = *Syrmosaurus disparoserratus* Maleev, 1952
    - = *Pinacosaurus disparoserratus* (Maleev, 1952)
    - = *Talarurus disparoserratus* (Maleev, 1952)

▪ *Nodocephalosaurus* Sullivan, 1999

- ***Nodocephalosaurus kirtlandensis*** Sullivan, 1999, type species
    - SMP VP-900; Late Cretaceous (late Campanian), Lower Kirtland Formation (De-na-zin Member), 12S 750178E 4025677N ets., SMP locality 319, west of Willow Wash, San Juan Basin, New Mexico, USA

- *Pinacosaurus* Gilmore, 1933
    - = *Syrmosaurus* Maleev, 1952
    - ***Pinacosaurus grangeri*** Gilmore, 1933, type species
        - AMNH 6523; Late Cretaceous (Campanian), Djadokhta Formation, Bayan Dzak, Shabarakh Usu, Gobi Desert, Mongolia
        - = *Heishansaurus pachycephalus* Bohlin, 1953
        - = *Pinacosaurus ninghsiensis* Young, 1935
        - = *Syrmosaurus disparoserratus* Maleev, 1952
        - = *Syrmosaurus viminocaudus* Maleev, 1952
        - = *Syrmosaurus viminicaudus* Maleev, 1954
    - ***Pinacosaurus mephistocephalus*** Godefroit, Pereda-Suberbiola, Li, and Dong, 1999
        - IMM 96BM3/1; Late Cretaceous (Campanian), Bayan Mandahu Formation, Quarry SBDE 96BM3 (48T 643438E 4627658N elevation 1239 m), Bayan

Mandahu, Urad Houqi Banner, Bayan Nur, Inner Mongolia Autonomous Region, People's Republic of China

- *Saichania* Maryańska, 1977
  - ***Saichania chulsanensis*** Maryańska, 1977, type species
    - MPC 101/151; Late Cretaceous (?middle Campanian), Barungoyot Formation, Red Beds of Hermiin Tsav (Ömnögovi), Mongolia
- *Scolosaurus* Nopsca, 1928
  - = *Oohkotokia* Penkalski, 2013
  - = *Scalosaurus* Mehl, 1936
  - ***Scolosaurus cutleri*** Nopsca, 1928, type species
    - NHMUK R5161; Late Cretaceous (late Campanian), lower Dinosaur Park Formation; Quarry Q080,12U 471365.051E 5622321.978N, Dinosaur Provincial Park, Alberta, Canada
    - = *Oohkotokia horneri* Penkalski, 2013
- *Shanxia* Barrett, You, Upchurch, and Burton, 1998
  - ***Shanxia tianzhenensis*** Barrett, You, Upchurch, and Burton, 1998, type species
    - IVPP V11276; Late Cretaceous, Huiquanpu Formation, 50T 267003E 4462783N est., ~270km

NW of Beijing, Wu Valley, Tian Zhen County, Shanxi Province, People's Republic of China

- *Tarchia* Maryańska, 1977
    - ***Tarchia gigantea*** (Maleev, 1956), type species
        - PIN N 551/29; Late Cretaceous (?late Campanian–early Maastrichtian), Baruungoyot Svita, Nemegt Formation, White Beds of Hermiin Tsav (Ömnögovi), Mongolia
        - = *Dyoplosaurus giganteus* Maleev, 1956
        - = *Euoplocephalus giganteus* Maleev, 1956
    - ***Tarchia kielanae*** Maryańska, 1977
        - ZPAL MgD I/111; Late Cretaceous (late Campanian), Baruungoyot Formation, Khulsan (Ömnögovi), Mongolia
        - = *Minotaurasaurus ramachandrani* Miles and Miles, 2009
- *Talarurus* Maleev, 1952
    - ***Talarurus plicatospineus*** Maleev, 1952, type species
        - PIN 557/91; Late Cretaceous (Cenomanian–Campanian), Bayanshiree Svita (Dornogovi), Batanshiree Svita (Ömnögovi), Mongolia
- *Tianzhenosaurus* Pang and Cheng, 1998

- ***Tianzhenosaurus youngi*** Pang and Cheng, 1998, type species
    - HBV 10001; Late Cretaceous, Huiquanpu Formation (Shanxi), Kangdailiang near Zhaojiagou Village, Tianzhen County, Shanxi Province, People's Republic of China

- *Tsagantegia* Tumanova, 1993
    - ***Tsagantegia longicranialis*** Tumanova, 1993, type species
        - MPC N 700/17; Late Cretaceous (Cenomanian–Turonian), Bayanshiree Svita (Dornogovi), Tsagaan Teeg, southeastern Gobi Desert, Mongolia
- *Zaraapelta* Arbour, Currie, and Badamgarav, 2014
    - ***Zaraapelta nomadis*** Arbour, Currie, and Badamgarav, 2014
        - MPC D100/1338; Late Cretaceous (late Campanian), 47T 568792E 4813630N, Baruungoyot Formation, Hermiin Tsav, Gobi Desert, Mongolia
- *Ziapelta* Arbour, Burns, Sullivan, Lucas, Cantrell, Fry, and Suazo, 2014
    - ***Ziapelta sanjuanensis*** Arbour, Burns, Sullivan, Lucas, Cantrell, Fry, and Suazo, 2014

        - NMMNH P-64484; Late Cretaceous (late Campanian), Lower Kirtland Formation (De-na-zin Member); East branch of Hunter Wash, Bisti/De-na-zin Wilderness, San Juan County, New Mexico, USA
    - *Zhongyuanosaurus* Zu, Lu, Zhang, Jia, Hu, Zhang, Wu, and Ji, 2007
        - ***Zhongyuanosaurus luoyangensis*** Zu, Lu, Zhang, Jia, Hu, Zhang, Wu, and Ji, 2007
            - HGM 41HIII-0002; Late Cretaceous, Sichuan Group, Liu Dianxiang, Ruyang County, Henan Province, People's Republic of China
- FAMILY NODOSAURIDAE
    - = Acanthopholidae Marsh, 1890
    - = Acanthopholididae Nopsca, 1902
    - = Acanthopholinidae von Huene, 1956
    - = Acanthopholinae Nopsca, 1923
    - = Edmontoniidae Bakker, 1988
    - = Edmontoniinae Russell, 1940
    - = Hylaeosauridae Nopsca, 1917
    - = Hylaeosauridae Nopcsa, 1917
    - = Nodosaurinae Abel, 1919 (Nopsca, 1923)
    - = Palaeoscincidae Nopsca, 1918

- = Panoplosaurinae Nopsca, 1929
- = Polacanthidae Wieland, 1911
- = Polacanthinae Lapparent and Lavocat, 1955
- *Animantarx* Carpenter, Kirkland, Burge, and Bird, 1999
    - ***Animantarx ramaljonesi*** Carpenter, Kirkland, Burge, and Bird, 1999, type species
        - CEUM 6228R; middle Cretaceous (Albian–early Cenomanian), Upper Cedar Mountain Formation (just above base of Mussentuchit Member), Carol Site (42EM366V), Utah, USA
- *Antarctopelta* Salgado and Gasparini, 2006
    - ***Antarctopelta oliveroi*** Salgado and Gasparini, 2006, type species
        - MLP 86-X-28-1; Late Cretaceous (late Campanian), Marambio Group (Santa Marta Formation, lower part of the Gamma Member) of the Santa Marta Formation, 21E 457251E 2914683S est., locality D6-1, Santa Marta Cove, North James Ross Island, Antarctica
- *Denversaurus* Bakker, 1988
    - ***Denversaurus schlessmani*** Bakker, 1988, type species
        - DMNH 468; Late Cretaceous (Maastrichtian), Lower Hell Creek Formation, Corson Coounty, South Dakota, USA.
- *Edmontonia* Sternberg, 1928
    - = *Chassternbergia* (Bakker, 1988) Olshevsky, 1991

        - = *Denversaurus* Bakker, 1988
        - = *Edmontia* (Hunt and Lucas, 1992)
        - = *Panoplosaurus* (Lambe, 1919) (partim)
        - ***Edmontonia longiceps*** Sternberg, 1928, type species
            - CMN 8531; Late Cretaceous, Horseshoe Canyon Formation, UTM 12U 367696E 5727158N est., Red Deer River, Alberta, Canada
            - = *Panoplosaurus longiceps* (Sternberg, 1928)
        - ***Edmontonia rugosidens*** (Gilmore, 1930) Russell, 1940
            - USNM 11868; Late Cretaceous, Two Medicine Formation, 12U 378177E 5424854N est., Milk River, Blackfeet Indian Reservation, Glacier County, Montana
            - = *Chassternbergia rugosidens* (Bakker, 1988) Olshevsky, 1991
            - = *Paleoscincus* sp. Matthew, 1922
            - = *Paleoscincus rugosidens* Gilmore, 1930
            - = *Panoplosaurus rugosidens* (Gilmore, 1930)
    - *Gargoyleosaurus* Carpenter, Miles, and Cloward, 1998
        - ***Gargoyleosaurus parkpinorum*** Carpenter, Miles, and Cloward, 1998 type species
            - DMNH 27726; Late Jurassic (Kimmeridgian-Tithonian), Upper Morrison Formation, Bone Cabin Quarry, Albany County, Wyoming

        - = *Gargoyleosaurus parkpini* (spelling amended)
- *Gastonia* Kirkland, 1998
    - ***Gastonia burgei*** Kirkland, 1998, type species
        - CEUM 1307; Early Cretaceous (Berremian), Lower Cedar Mountain Formation (Yellow Cat Member), Township 14S Range 21E, Grand County, Utah, USA
- *Glyptodontopelta* Ford, 2000
    - ***Glyptodontopelta mimus*** Ford, 2000, type species
        - USNM 8610; Late Cretaceous (early Maastrichtian), Ojo Alamo Formation (Naashoibito Member), Barrel Springs Arroyo (=De-na-zin Wash), about 1.5 km southwest of Ojo Alamo Store, San Juan County, New Mexico, USA
        - = *Edmontonia australis* Ford, 2000
- *Mymoorapelta* Kirkland and Carpenter, 1994
    - ***Mymoorapelta maysi*** Kirkland and Carpenter, 1994, type species
        - MWC 1815; Late Jurassic (Kimmeridgian–Tithonian) Morrison Formation (middle Brushy Basin Member),MEC Loc. 1.05.86, Mygatt-Moore Quarry, Mesa County, western Colorado, USA
- *Niobrarasaurus* Carpenter, Dilkes, and Weishampel, 1995
    - ***Niobrarasaurus coleii*** (Mehl, 1936), type species
        - MU 650 VP; Late Cretaceous (Coniacian–early Campanian), Niobrara Chalk Formation (Smoky Hill Chalk

Member), 14S 394197E 4289588N est., Gove County, Kansas, USA

- = *Hierosaurus coleii* Mehl, 1936
- = *Nodosaurus coleii* (Mehl, 1936)

- *Nodosaurus* Marsh, 1889, type genus
  - ***Nodosaurus textilis*** Marsh, 1889, type species
    - YPM 1815; Late Cretaceous, Frontier Formation (Mowry or Thermopolis Shale), 1.5 mi SE of Quarry 13, Como Bluff, Wyoming, USA
- *Panoplosaurus* Lambe, 1919
  - = *Edmontonia* Russell, 1940 (partim)
  - = *Edmontonia rugosidens* (Gilmore, 1930) (partim)
  - ***Panoplosaurus mirus*** Lambe, 1919, type species
    - CMN 2759; Late Cretaceous (late Campanian), lower Dinosaur Park Formation, Quarry Q008 (#69, Sternberg, 1950; GSC 2), 12U 463938E 5620734N, Dinosaur Provincial Park, Alberta, Canada
- *Pawpawsaurus* Lee, 1996
  - ***Pawpawsaurus campbelli*** Lee, 1996, type species
    - SMU 73203; Early Cretaceous (late Albian), Paw Paw Formation, 14S 659055E 3637787N est., SMU locality 263, Tarrant County, Texas, USA
- *Peloroplites* Carpenter, Bartlett, Bird, and Barrick, 2008

        - ***Peloroplites cedrimontanus*** Carpenter, Bartlett, Bird, and Barrick, 2008, type species
            - CEUM 26331; Early Cretaceous (Aptian-Albian boundary), Cedar Mountain Formation (base of Mussentuchit Member), ~24.5km SE of Price, Price River II Quarry (Locality number EM 372), Emery County, Utah, USA
    - *Polacanthus* Owen, 1865 (Huxley, 1867)
        - ***Polacanthus foxii*** Owen, 1865 (Hulke, 1881), type species
            - NHMUK R175; Early Cretaceous (Barremian), Wealden Group (Upper part of Wessex Formation), Barnes High, northwest of Cowleaze China, Isle of Wight, England
            - = *Euacanthus* Tennyson, 1897 (nomen nudum)
            - = *Hylaeosaurus foxii* (Hulke, 1881)
            - = *Polacanthoides ponderosus* Nopsca, 1929 (partim)
            - = *Polacanthus becklesi* Henning, 1924
            - = *Polacanthus foxi* Seeley, 1891 non Hulke, 1881
            - = *Vectensia* Delair, 1982
        - ***Polacanthus rudgwickensis*** Blows, 1996
            - HORSM 1988.1546; Early Cretaceous (Hauterivian–Barremian), Wessesx Formation (Weald Clay Formation), locality N.G.R.TQ085 343, Rudgwick Brickworks Company quarry, Rudgwick, Sussex, England
    - *Propanoplosaurus* Stanford, Wesihampel, and Deleon, 2011

        - ***Propanoplosaurus marylandicus*** Stanford, Wesihampel, and Deleon, 2011, type species
            - USNM 540686; Early Cretaceous (early Aptian), Potomac Group (lower Patuxent Formation), Prince Georges County, Maryland, USA
    - *Sauropelta* Ostrom, 1970
        - ***Sauropelta edwardsorum*** Ostrom, 1970, type species
            - AMNH 3032; Early Cretaceous (late Aptian), Cloverly Formation, 12T 712519E 5028809 N est., Montana, USA
            - = *Sauropelta edwardsi* Ostrom, 1970 (spelling amended)
    - *Silvisaurus* Eaton, 1960
        - ***Silvisaurus condrayi*** Eaton, 1960, type species
            - UK 10296; Early Cretaceous (Albian), Dakota Group (Terra Cotta Member), 14S 632985E 4339558N est., Oattawa County, Kansas, USA
    - *Tatankacephalus* Parsons and Parsons, 2009
        - ***Tatankacephalus cooneyorum*** Parsons and Parsons, 2009, type species
            - MOR 1073; Early Cretaceous (late Aptian–early Albian), Cloverly Formation, 12T 600138E 5123720N est., ~1km W of AMNH locality 33-1, Middle Dome region, Harlowtown, Wheatland County, Montana, USA
    - *Stegopelta* Williston, 1905

        - ***Stegopelta landernensis*** Williston, 1905, type species
            - FMNH UR88; middle Cretaceous (latest Albian or early Cenomanian), Frontier Formation (base of Belle Fourche Member), near Conant Creek, Fremont County, Wyoming, USA
            - = *Nodosaurus landernensis* (Williston, 1905)
    - *Zhejiangosaurus* Lü, Jin, Sheng, and Li, 2007
    - ***Zhejiangosaurus lishuiensis*** Lü, Jin, Sheng, and Li, 2007, type species
        - ZMNH M8718; 50R 780517E 3153365N, Liancheng, Lishui of Zhejiang Province, People's Republic of China
    - STRUTHIOSAURINAE NOPCSA, 1923
        - *Anoplosaurus* Seeley, 1879
            - ***Anoplosaurus curtonotus*** Seeley, 1879, type species
                - SMC B55731 (lectoype); Early Cretaceous (late Albian), Upper Gault Clay or Cambridge Greensand, near Reach, Cambridgeshire, England
                - = *Acanthopholis curtonotus (*Seeley, 1879) Nopsca, 1902
        - *Europelta* Kirkland, Alcalá, Loewen, Espílez, Mampel, and Wiersma, 2013
            - ***Europelta carbonensis*** Kirkland, Alcala´, Loewen, Espílez, Mampel, and Wiersma, 2013, type species

        - AR-1/10; Early Cretaceous (early Albian), lower Escucha Formation, Fundación Conjunto Paleontológico of Teruel-Dinópolis locality AR-1, Sociedad Anónima Minera Catalano-Aragonesa Group's Ariño coal mine, east of Ariño, Teruel Province, Spain
- *Hungarosaurus* Ősi, 2005
    - ***Hungarosaurus tormai*** Ősi, 2005, type species
        - MTM 2007.26.1–2007.26.34, 2007.89.1, 2007.89.2; Late Cretaceous (Santonian), Csehbánya Formation, 33T 700782E 5234326N est., Iharkút, Veszprém County, Bakony Mountains, Transdanubian Range, western Hungary
- *Struthiosaurus* Bunzel, 1870, type genus
    - = *Crataeomus* Seeley, 1881
    - = *Danubiosaurus* Bunzel, 1871
    - = *Hoplosaurus* Seeley, 1881
    - = *Leipsanosaurus* Nopsca, 1918
    - = *Pleuropeltis* Seeley, 1881 (partim)
    - = *Rhodanosaurus* Nopsca, 1929
    - ***Struthiosaurus austriacus*** Bunzel, 1871, type species
        - PIUW 2349/6; Late Cretaceous (lower Campanian), Gosau Formation (Grünbach Basin), Gute Hoffnung

coal mine, Muthmannsdorf, Wiener Neustad-Land, Niederösterreich (= Lower Austria), Austria

- = *Crataeomus lepiodphorus* Seeley, 1881
- = *Crataeomus powlowitschii* (Seeley, 1881)
- = *Danubiosaurus anceps* Bunzel, 1871
- = *Hoplosaurus ischyrus* Seeley, 1881
- = *Hoplosaurus powlowitschii* (Seeley, 1881)
- = *Hylaeosaurus* sp. Bunzel, 1871
- = *Leipsanosaurus noricus* Nopsca, 1918
- = *Nodosaurus ischyrus* (Seeley, 1881)
- = *Pleuropeltis suessi* Seeley, 1881
- = *Rhodanosaurus alcimus* Seeley, 1881 (partim)
- = *Scelidosaurus* sp. Bunzel, 1871
- = *Struthiosaurus lepidophorus* (Seeley, 1881)

- ***Struthiosaurus transilvanicus*** Nopsca, 1915
  - NHMUK 4966; Late Cretaceous (late Maastrichtian), Sânpetru Formation, Hunedoara, Romania
  - = *Struthiosaurus noricus* (Nopsca, 1918)
- ***Struthiosaurus languedocensis*** Garcia and Pereda-Suberbiola, 2003
  - UM2 OLV-D50 A–G CV; Late Cretaceous (Campanian), Unnamed unit, Hérault, France

- Ankylosauria incertae sedis
    - *Amtosaurus* Kurzanov and Tumanova, 1978
        - ***Amtosaurus magnus*** Kurzanov and Tumanova, 1978, type species
            - PIN 3780/2; Late Cretaceous (Santonian–Cenomanian), Bayanshiree Svita, Ömnögovi, Amtgai, Mongolia
    - *Dracopelta*
        - ***Dracopelta zbyszewskii*** Galton, 1980, type species
            - SGP unnumbered; Late Jurassic (Kimmeridgian), Unnamed unit, Ribamar, near Lourinhã Municipality, District of Lisbon, Portugal
    - *Hoplitosaurus* Lucas, 1902
        - ***Hoplitosaurus marshi*** Lucas, 1902, type species
            - USNM 4752; Early Cretaceous (?Barremian), Lakota Formation, 13T 633211E 4819178N est., Calico Canyon, Custer County, South Dakota, USA
            - = *Stegosaurus marshi* Lucas, 1901
            - = *Polacanthoides ponderosus* Nopsca, 1929 (partim)
            - = *Polacanthus marshi* (Lucas, 1901)
    - *Hylaeosaurus* Mantell, 1833
        - ***Hylaeosaurus armatus*** Mantell, 1833, type species
            - NHMUK 3775; Early Cretaceous (middle-late Valanginian), Wealden Group (Hastings subgroup, Tunbridge Wells Sand Formation, Grinstead Clay

Member), Tilgate Forest, near Cuckfield, West Sussex, England

- = *Hylaeosaurus oweni* Mantell, 1844
- = *Polacanthoides ponderosus* Nopsca, 1929 (partim)

- *Sarcolestes* Lydekker, 1893
  - ***Sarcolestes leedsi*** Lydekker, 1893, type species
    - NHMUK 2682; Middle Jurassic (middle Callovian), Lower Oxford Clay (probably *Kosmoceras jason* Zone), brick pit at Fletton, Cambridgeshire, England
- *Texasetes* Coombs, 1995
  - ***Texasetes pleurohalio*** Coombs, 1995, type species
    - USNM 337987; Early Cretaceous (late Albian), Paw Paw Formation, 14S 655819E 3645129N est.,Tarrant County, Texas, USA

In addition to synonymized taxa, there are a number of **nomina dubia** which have been found to represent material of indeterminate taxonomic assignment either within or outside of Ankylosauria. These include:

Acanthopholis eucerus Seeley, 1869

Acanthopholis horridus Huxley, 1867

Acanthopholis macrocercus Seeley, 1869

Acanthopholis platypus Seeley, 1869 (partim)

Acanthopholis stereocercus Seeley, 1869 (partim)

Anoplosaurus major Seeley, 1869 (partim)

Brachypodosaurus gravis Chakravarti, 1934

Cryptodraco eumerus (Seeley, 1869)

Cryptosaurus eumerus Seeley, 1869

Dysganus bicraniatus Cope, 1876

Dysganus encaustus Cope, 1876

Dysganus naydenianus Cope, 1876

Dysganus peiganus Cope, 1876

Eucercosaurus tanyspondylus Seeley, 1879

Hierosaurus sternbergii Wieland, 1909

Iguanodon phillipsii Seeley, 1875

Lametasaurus indicus Matley, 1923 (partim)

Onychosaurus hungaricus Nopsca, 1902

Paleoscincus africanus Broom, 1912

Paleoscincus costatus Leidy, 1856

Paleoscincus latus Marsh, 1892

Paleoscincus magoder Henning, 1915 (nomen nudum)

Paranthodon oweni Nopsca, 1929

Peishansaurus philemys Bohlin, 1953

Priconodon crassus Marsh, 1888

Priodontognathus phillipsii (Seeley, 1875)

Regnosaurus northamptoni Mantell, 1848

Rhadinosaurus alcinus Seeley, 1881

Sauroplites scutiger Bohlin, 1953

Stegasauroides excavatus Bohlin, 1953

Sygnosaurus macrocercus Seeley, 1879

Tianchisaurus nedegoaperfermia Dong, 1993

APPENDIX 2. Morphological character and character state descriptions used in parsimony analysis of Upper Cretaceous panoplosaurines (Chapter 4).

1. Highest point of skull roof: caudal to orbits (1), anterior to orbits (2).
2. Premaxillary palate wider than long: absent (0); present (1)
3. Premaxillary teeth: present (0); absent (1)
4. Fused osteoderm(s) on premaxilla: absent (0); present (1)
5. Anterior edge of premaxilla with ventrally concave notch in rostral view: absent (0); present (1)
6. Maxillary tooth rows deeply inset from lateral edge of skull: absent (0); present (1)
7. Maxillary tooth rows deeply concave laterally, outlining an hourglass shape: absent (0); present (1)
8. Nasal septum dividing the respiratory passage into two separate bony canals: absent (0); present (1)
9. Closure of antorbital fenestra: absent (0); present (1)
10. Accessory antorbital ossification(s) completely separating orbit and antorbital cavity: absent (0); present (1)
11. Median palatal keel composed of the vomer and pterygoid: absent or weakly developed (0); extending ventrally to level of maxillary tooth crowns (1)
12. Extension of the vomerine septum: incomplete (0); extending to palatal shelves (1); extending to skull roof (2)

13. Secondary palate: incomplete or absent (0); present and flat, reaching as far as the second or third maxillary tooth (1); present and composed of two palatal shelves, describing S-shaped respiratory route (2)
14. Quadrate shaft angled strongly anteroventrally: absent (0); present (1)
15. Paroccipital processes projecting posterolaterally: absent (0); present (1)
16. Occiput wider than high: absent (0); present (1)
17. Occipital condyle set off from the ventral braincase by a distinct neck: absent (0); present (1)
18. Closure of supratemporal fenestra: absent (0); present (1)
19. Obliteration of cranial sutures in adults, involving fusion and dermal sculpturing of the outer surface of most of the dermal skull roof: absent (0); present (1)
20. Large subcircular dermal ossification covering most of the skull roof between the orbits: absent (0); present (1)
21. Anteroposteriorly narrow dermal ossification along the posterior border of the skull roof: absent (0); present (1)
22. Secondary dermal ossification, projecting ventrolaterally from the quadratojugal region: absent (0); present and rounded (1); present and wedge-shaped (2)
23. Median dermal ossification overlying dorsum of nasal region: absent (0); present (1)
24. Tooth crowns with cingulum: absent (0); present (1)
25. Closure of external mandibular fenestra: absent (0); present (1)
26. Coronoid process low and rounded, projecting only slightly above the level of the dentary tooth row: absent (0); present (1)

27. Osteoderm fused to the ventrolateral aspect of the mandible in adults: absent (0); present (1)
28. Sinuous ventral margin of mandible, which parallels the sinuosity of the dorsal margin in lateral view: absent (0); present (1)
29. Groove on ventral margin of vomer: absent (0), present (1)
30. Anterior rim of lateral temporal fenestra obscured completely in lateral view by osteodermal encroachment: absent=completely visible (0); at least partially visible (1); not visible (2)
31. Ectopterygoid-pterygoid foramen: absent (0); on medial surface of ectopterygoids (1); on anteroventral surface od ectopterygoid pad (2)
32. Maximum adult skull width: less than or equal to 302 mm (0); greater than 302 mm (1).
33. The lateral edge of the snout in dorsal view, between the postorbital prominence and anterolateral corner of the premaxillary beak: concave (0); flat or convex (1).
34. Keeled postcranial osteoderms: absent (0), longer than wide (1), wider than long (2).
35. Lateral margin of medial cervical/pectoral osteoderms: rounded (0), angular (1).
36. Projection of distal pectoral spines: absent (0), anteriorly (1), anterolaterally (2).
37. Triangular osteoderm on dorsum of rostral region posterior to nasal osteoderm: absent (0), present (1).
38. Cranial osteoderms over rostral region: absent (0), bulbous to polygonal (1), flat, separated by distinct (3-10 mm wide) grooves (2),flat, expanded to cover grooves,

although they are still discernible (3), flat, completely fused, not separated by grooves (4).

39. 3), flat, completely fused, not separated by grooves (4).
40. Anterior maxillary tooth rows: nearly parallel (<10°) to convergent; strongly divergent (>20°).
41. Posterior displacement of orbit: ratio antoribital to postorbital skull length less than (0) greater than (1) 2.
42. Oval-shaped prevomer foramen: absent (0); present (1).
43. Ratio of the width of the anterior end of the snout to maximum skull width: less than (0), greater than (1) 46%.